

DISS. ETH Nr. 25222

Peptide Catalyzed Conjugate Addition Reactions of Aldehydes to Nitroolefins - Mechanistic Insights and Transformation of Bifunctional Substrates

A thesis submitted to attain the degree of
DOCTOR OF SCIENCES of ETH ZÜRICH
(Dr. sc. ETH Zürich)

presented by

Patrick Hilpert

Master of Science, University of Basel
born on 14.07.1988
citizen of Winterthur (ZH), Switzerland

Accepted on the recommendation of

Prof. Dr. Helma B. Wennemers, examiner
Prof. Dr. Jeffrey W. Bode, co-examiner

2018

“We choose to go to the moon in this decade and do the other things, not because they are easy, but because they are hard”

John Fitzgerald Kennedy

This thesis was carried out under the supervision of Prof. Dr. Helma Wennemers between June 2013 and June 2018 at the Laboratory of Organic Chemistry at the ETH Zürich.

Parts of this thesis have been presented at the following events:

Poster Presentation:

Fall Meeting of the Swiss Chemical Society Zürich (Switzerland), September 2016 "*Organocatalyzed 1,4-addition reactions of aldehydes to nitroolefins – Mechanistic studies*"

Acknowledgment

First, I want to thank Prof. Dr. Helma Wennemers for giving me the opportunity to work in her group and discover the exciting field of peptide catalysis. I am grateful for all the helpful discussions and advice throughout my research in her group.

I want to thank also Prof. Dr. Jeffrey Bode for accepting to co-examine my thesis.

A big thanks goes to all former and present group members for the great time in- and outside of the lab. In particular, my gratitude goes to my colleagues from the peptide catalysis subgroup, for all the helpful discussions about reaction mechanisms and reactivities of catalysts.

In the course of this research I was fortunate to work with great collaborators. I would like to thank Prof. Dr. Markus Reiher, Dr. Thomas Weymuth, Dr. Reinhard Kissner, as well as my talented master and exchange-PhD students Andreas Kaspar and Marco Emma.

Many thanks go to Dr. Rüdiger Borrmann, Tobias Schnitzer, Dr. Oliver Engl and Dr. Matthew Aronoff for proofreading this thesis.

My deepest gratitude goes to my family Karin, Kurt, Nicole and Fabienne Hilpert for their continuous support throughout this journey and the motivating words when needed.

For her love and being at my side in good and bad times, I am wholeheartedly grateful to Mandy Widmer.

II - Acknowledgment

Abstract

The conjugate addition reaction between aldehydes and nitroolefins belongs to an active field of organocatalyzed reactions. Accordingly, highly enantio- and diastereoselective methodologies relying on secondary amine organocatalysts have been established.

In the context of this thesis we investigated the secondary amine-catalyzed conjugate addition reaction of aldehydes to nitroolefins. Despite intensive research on the mechanism, the role of the intermediate generated by the carbon-carbon formation is still under debate. The structure of such an intermediate is thought to be either an iminium nitronate- or a 1,2-oxazine *N*-oxide species. We show in Chapter 3 that a nitronate model system allows identification of nitronates by UV/Vis spectroscopy. Under preparative conditions, a novel characteristic band was identified alongside established ones. By computational studies we demonstrated that the newly observed excitation belongs to the intermediate formed by the carbon-carbon bond formation. We monitored this intermediate *in situ* and showed that the structure of the secondary amine catalyst as well as the nature of the solvent significantly influence its stabilization.

Since alkylating substrates are prone to deactivate secondary amine catalysts, the application of these substrates is a major challenge in the field. In Chapter 4 we address this issue and show that in the secondary amine-catalyzed conjugate addition reaction of aldehydes to nitroolefins nitroacrylates alkylate the catalyst reversibly. We demonstrate that the release of the alkylated catalyst becomes rate limiting and a complementary mechanistic scenario is observed when using nitroacrylates. Further we show how sterically demanding nitroacrylates reduce the alkylation rate of the catalyst, and then use such bulky substrates to achieve faster reaction rates. We identified a cocatalyst that led to even faster reaction rates and allowed use of only 500 ppm of a peptidic catalyst to prepare various substrates in good yields, diastereoselectivities and enantiomeric excesses.

Further we demonstrate in Chapter 5 that combining the peptide-catalyzed conjugate addition reactions of aldehydes to nitroacrylates with subsequent cinchona-catalyzed additions of thioenolates allows the synthesis of tricyclic natural product derivatives (tetraponerines). We developed a synthetic route for the transformation of ester-substituted γ -nitroaldehydes formed in peptide-catalyzed conjugate addition of aldehydes to nitroacrylates to a chiral imine building block. We demonstrate that this imine reacts with thioenolates in the presence of a cinchona alkaloid catalyst to form a tetraponerine core structure (annulated 5-6-5 ring), which bears up to seven stereogenic centers.

Zusammenfassung

Die konjugierte Additionsreaktion von Aldehyden an Nitroolefine gehört zu einem sehr aktiv bearbeiteten Forschungsgebiet. Dabei wurden enantio- und diastereoselective Synthesen mittels sekundären Aminkatalysatoren entwickelt.

In der vorliegenden Arbeit haben wir, die von sekundären Aminen katalysierte konjugierte Additionsreaktion von Aldehyden an Nitroolefinen untersucht. Trotz intensiver Forschung zum Mechanismus dieser Reaktion konnte die Rolle und die Struktur des Intermediats, welches in der Kohlenstoff-Kohlenstoff Bindungsknüpfung generiert wird, nicht abschliessend geklärt werden. Es wird momentan vermutend, dass dieses Intermediat entweder als Iminiumnitronat oder als 1,2-Oxazin *N*-Oxid vorliegt. In Kapitel 3 zeigen wir anhand eines Nitronat-Modellsystems, dass eine Nitronatdetektion mittels UV/Vis-Spektroskopie möglich ist. Unter präparativen Bedingungen haben wir eine neue charakteristische UV/Vis Bande des Nitronats gefunden. Mittels computergestützten Untersuchungen konnten wir zeigen, dass diese neue Bande zu dem durch die Kohlenstoff-Kohlenstoffbindung generierten Intermediat gehört. Wir haben ein solches Intermediat unter Reaktionsbedingungen beobachtet und zeigten, dass dessen Stabilisierung durch die Katalysatorstruktur sowie der Art des Lösungsmittels abhängen.

Da alkylierende Substrate dazu tendieren den sekundären Aminkatalysator zu deaktivieren, ist die Verwendung solcher Substrate besonders anspruchsvoll. In Kapitel 4 haben wir uns diesem Problem angenommen und gezeigt, dass Nitroacrylate in einer durch sekundäre Amine katalysierte Additionsreaktion von Aldehyden an Nitroolefine zu einer reversiblen Alkylierung des Katalysators führen. Wir zeigten auch, dass die Rückreaktion des Katalysatoradduktes und somit die Freisetzung des Katalysators zum geschwindigkeitsbestimmenden Schritt in der Reaktion wird und dass deshalb ein komplementärer katalytischer Zyklus bei der Verwendung von Nitroacrylaten vorhanden ist. Wir konnten zeigen, dass je sterisch anspruchsvoller das Nitroacrylate ist, desto langsamer findet die Alkylierungsreaktion statt, was zu einer Beschleunigung der Gesamtreaktion führt. Im Verlauf dieser Untersuchungen fanden wir einen Cokatalysator,

welcher es uns ermöglichte mit nur 500 ppm Katalysatorbeladung eine signifikant schnellere Reaktionsgeschwindigkeit zu erreichen. Dies ermöglichte uns mit einer so tiefen Katalysatorbeladung verschiedene Substrate mit guter Ausbeute in guter Enantio- und Diastereoselektivität zu synthetisieren.

Des Weiteren konnten wir in Kapitel 5 zeigen, dass die Peptid katalysierte Additionsreaktion von Aldehyden an Nitroacrylate in Kombination mit der Cinchona Alkaloid katalysierten Addition von Thioesterenolaten die Synthese eines Naturproduktderivats (Tetraonerine) ermöglicht. Wir haben dafür eine Synthese von chiralen, zyklischen Iminen aus γ -Nitroaldehyden entwickelt. Diese Imine reagierten in Gegenwart von Thioesterenolaten und Cinchona Alkaloid Katalysatoren zur Tetraonerin Struktur (annulierter 5-6-5 Ring) mit bis zu sieben stereogenen Zentren.

List of Abbreviations, Acronyms and Symbols

°C	degrees centigrade
Å	Ångstrom
abs.	absorption
Abs.	absorption
Ac	acetyl
ACN	acetonitrile
AcOH	acetic acid
Ahx	6-aminohexanoic acid
aq.	aqueous
Ar	aryl
BMIMCl	1-Butyl-3-methylimidazolium chloride
BMIMPF ₆	1-Butyl-3-methylimidazolium hexafluorophosphate
Bn	benzyl
Boc	<i>tert</i> -butyloxycarbonyl
Bu	butyl
cat.	catalytic, catalyst
conv.	conversion
d	doublet
DCM	dichloromethane
DFT	density functional theory
DIC	<i>N,N'</i> -diisopropylcarbodiimide
DMAP	4-(dimethylamino)-pyridin
DMF	dimethylformamide
DMSO	dimethylsulfoxide
dr	diastereomeric ratio
e.g.	exempli gratia, for example
ee	enantiomeric excess
equiv	equivalents
Et	ethyl
EtOAc	ethyl acetate
EWG	electron withdrawing group
FT	Fourier transformed
h	hours

VIII - List of Abbreviations, Acronyms and Symbols

HOBt	<i>N</i> -hydroxybenzotriazole
HOMO	highest occupied molecular orbital
HPLC	high-performance liquid chromatography
<i>i</i> Pr	<i>iso</i> -propyl
<i>i</i> Pr-OH	<i>iso</i> -propanol
<i>J</i>	coupling constant
k	kilo
LUMO	lowest unoccupied molecular orbital
m	multiplett
MAHO	malonic acid half oxoester
MAHT	malonic acid half thioester
maj.	major
Me	methyl
MIDA	<i>N</i> -methyliminodiacetic acid
min	minutes
MTBE	methy <i>tert</i> -butyl ether
MTM	monothiomalonate
n.d.	not determined
nACHR	nicotinic acetylcholine receptors
NMM	<i>N</i> -methylmorpholine
NMR	nuclear magnetic resonance
p-TSA	<i>para</i> -toluol sulfonic acid
PMB	<i>para</i> -methoxy benzyl
PMP	<i>para</i> -methoxy phenyl
ppm	parts per million
Pr	propyl
quant	quantitative
rac.	racemic
rt.	room temperature
s	singlett
SAR	structure-activity relationship
sat.	saturated
SFC	supercritical fluid chromatography
SOMO	single occupied molecular orbital
SOMO	single occupied molecular orbital
SPPS	solid phase peptide synthesis

^t Bu	<i>tert</i> -butyl
TC	thiophene 2-carboxylate
TFA	trifluoroacetic acid
THF	tetrahydrofuran
TLC	thin layer chromatograph
TMS	trimethylsilane
TOF	turn over frequency
TON	turn over number
Tosyl	4-toluenesulfonyl
Ts	4-toluenesulfonyl
UV	ultraviolet
Vis	visible light
vs.	versus
Xaa	any amino acid residue
δ	chemical shift in ppm

Table of Contents

Acknowledgment	I
Abstract	III
Zusammenfassung	V
List of Abbreviations, Acronyms and Symbols	VII
Table of Contents	1
1 Introduction	5
1.1 <i>Organocatalysis</i>	7
1.2 <i>Conjugate Addition Reactions of Aldehydes to Nitroolefins</i>	8
1.2.1 A Short Historical Perspective	8
1.2.2 Asymmetric Catalytic Applications: Substrate and Catalyst Scope	8
1.2.2.1 General	8
1.2.2.2 β -Alkyl- or Aryl- Substituted Nitroolefins	9
1.2.2.3 α,β -Disubstituted Nitroolefins	10
1.2.2.4 β,β -Disubstituted Nitroolefins	11
1.2.2.5 Electron Deficient Nitroolefins: Nitroacrylates	11
1.3 <i>Mechanistic Studies on Michael Reactions</i>	13
1.3.1 Catalysts with an Internal Acid	14
1.3.2 Catalysts Lacking an Internal Acid	15
1.3.3 Iminium Nitronate and 1,2-Oxazine N-Oxide Intermediates	17
2 Objectives	21
3 Mechanistic Investigations on the Nitronate Intermediate	25
3.1 <i>Background</i>	27
3.2 <i>Determination of Characteristic UV-Band for Nitronate Model System</i>	29
3.3 <i>Nitronate Species under Reaction Conditions</i>	33
3.4 <i>Conclusion</i>	38
4 Catalyst Deactivation by Electron Deficient Nitroolefins	41
4.1 <i>Background</i>	43
4.2 <i>Initial Experiments</i>	45
4.3 <i>Reversible Catalyst Alkylation</i>	47
4.3.1 Alkylation of the Peptidic Catalyst by Different Nitroalkenes	47

4.3.2	Tuning the Reactivity by Exploring the Alkylation Process	48
4.3.3	Catalytic Cycle: Kinetic vs. Thermodynamic Control	51
4.3.4	Steady State and Identification of an Aldol Cocatalyst	53
4.3.5	Revised Catalytic Cycle and ppm-Level Catalysis	57
4.3.6	Substrate Scope	59
4.4	<i>Irreversible Catalyst Alkylation</i>	61
4.5	<i>Conclusion</i>	62
5	Bioinspired Synthesis of the Tetraponerine Cores	65
5.1	<i>Background</i>	67
5.2	<i>Synthesis of the Cyclic Imine</i>	69
5.3	<i>Tetraponerine Core Structure Synthesis</i>	71
5.4	<i>Conclusion</i>	76
6	Summary and Outlook	79
7	Experimental Part	85
7.1	<i>General Aspects and Materials</i>	87
7.2	<i>General Protocols</i>	88
7.3	<i>Stopped-Flow UV/Vis Measurements</i>	90
7.4	<i>Computational Studies</i>	94
7.4.1	<i>Structural Analysis</i>	94
7.5	<i>NMR Experiments on Catalyst Alkylation:</i>	95
7.6	<i>Synthesis of Nitroolefins</i>	98
7.7	<i>Analytical Data of Catalysis Products</i>	105
7.8	<i>Analytical Data of Catalysis Product Derivatives</i>	117
7.9	<i>Towards Tetraponerine Structure</i>	125
7.10	<i>Other Compounds</i>	138
7.11	<i>X-Ray Crystal Structures</i>	139
8	References	147
9	Appendix	157
9.1	<i>Additional Experiments</i>	159
9.1.1	<i>Stopped-Flow Experiments Using Acetic Acid</i>	159
9.1.2	<i>Time Dependent Adduct Preformation</i>	161
9.1.3	<i>Time Dependent Enamine Formation</i>	162
9.1.3.1	<i>Increased Aldehyde Concentration</i>	162
9.1.3.2	<i>Aldol Addition Product Additive for Nitrostyrene</i>	162
9.1.3.3	<i>Aldol Addition Additive in Conjugate Additions to CF₃-Nitroolefins</i>	163

9.1.4 Stereochemistry Determination of Tetraponerines by NMR Spectroscopy	164
9.2 <i>Curriculum Vitae</i>	167

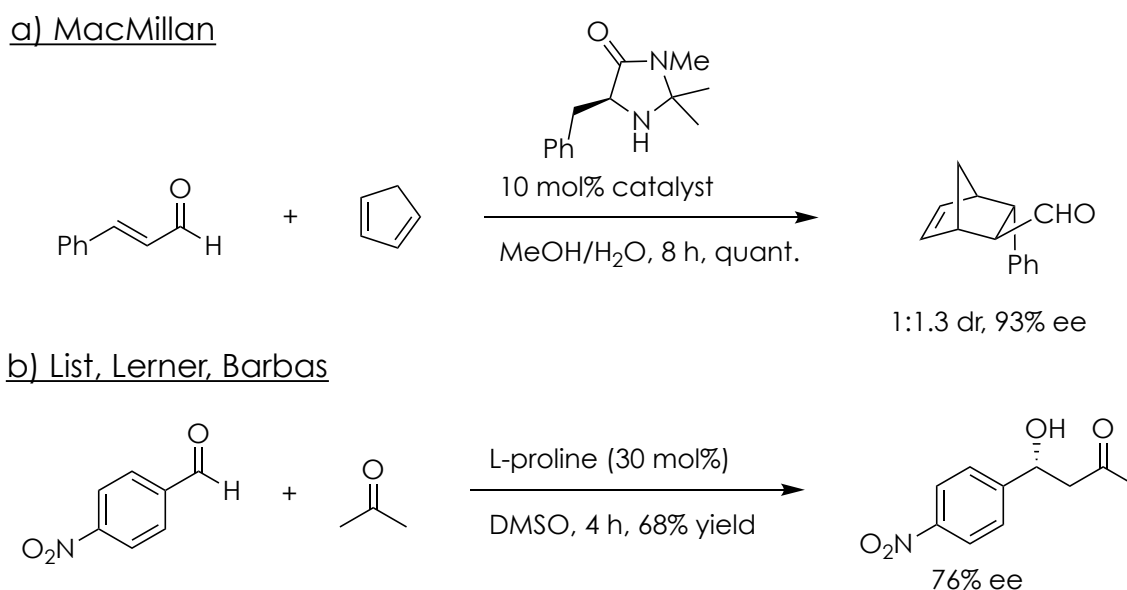
1

Introduction

1.1 Organocatalysis

Organocatalysis describes accelerated chemical reactions by metal-free organic molecules.^[1] Today, organocatalysis belongs among the most popular fields in modern organic chemistry and organocatalysts developed into one pillar in asymmetric synthesis besides metal and enzyme catalysts, providing a methodology that is mostly robust towards air and mostly non-toxic.^[1-3]

At the beginning of this millennium two highly influential articles were published, triggering a focus on enamine and iminium-based organocatalysis. First MacMillan and coworkers developed chiral imidazolidinone catalysts for asymmetric Diels-Alder reactions (Scheme 1-1a).^[4] Simultaneously List, Lerner and Barbas were inspired by class II aldolases and catalytic antibodies and rediscovered proline-catalyzed aldol reactions (Scheme 1-1b).^[5]



Scheme 1-1: Initial developments in secondary amine based organocatalysis: a) Imidazolidinone catalyzed Diels-Alder reaction; b) Proline catalyzed aldol addition reaction.

1.2 Conjugate Addition Reactions of Aldehydes to Nitroolefins

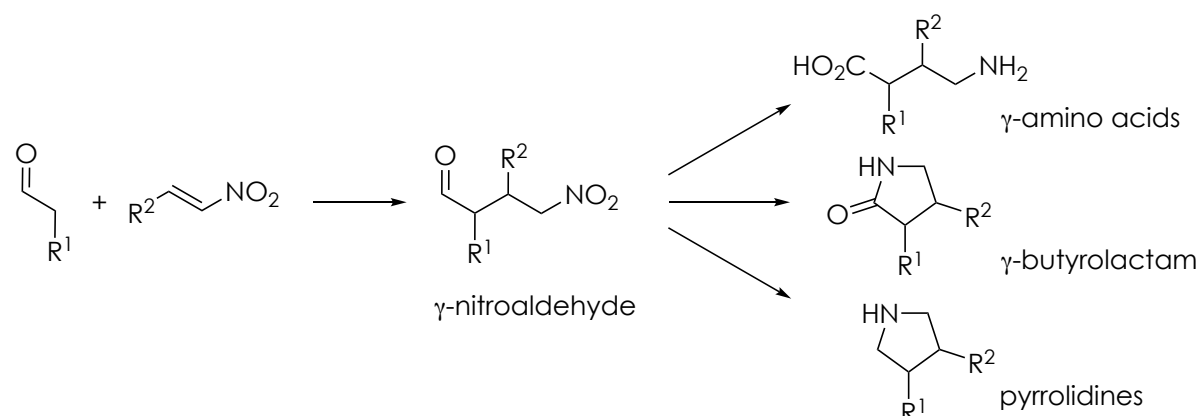
1.2.1 A Short Historical Perspective

The beginning of the stoichiometric use of enamines as nucleophiles was the development of reactive enamine intermediates for carbon-carbon bond formations by Stork in the 1960s.^[6] Later, enamines were established for addition reactions to nitroolefins by Kuehne and Foley.^[7] Due to the strong electron withdrawing character of the nitro group, nitroolefins are good Michael acceptors for nucleophiles such as enamines.^[8] An asymmetric addition reaction was established by addition of chiral enamines to achiral nitroolefins by Seebach.^[9,10]

1.2.2 Asymmetric Catalytic Applications: Substrate and Catalyst Scope

1.2.2.1 General

Today, an important carbon-carbon bond forming methodology is the amine catalyzed asymmetric addition of aldehydes to nitroolefins.^[11] In the last two decades many catalysts to synthesize different γ -nitroaldehydes with high stereo- and enantioselectivity have been developed. γ -Nitroaldehydes are highly valuable building blocks for subsequent transformations towards chiral pyrrolidines^[12-16], γ -butyrolactones^[17], γ -amino acids^[15,18] and tetrahydropyrans^[19] (Scheme 1-2).



Scheme 1-2: Michael addition reaction of aldehydes to nitroolefins.

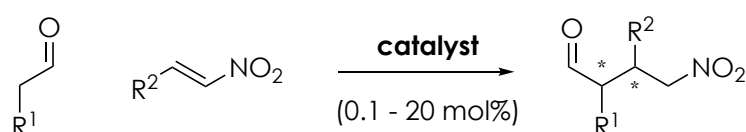
The effective and selective formation of γ -nitroaldehydes by organocatalyzed conjugate addition reactions was found to be strongly

dependent on the catalyst structure. The addition of α -branched aldehydes to nitroolefins is mostly performed using primary amine catalysts (often derived from a cinchona alkaloid^[20-22] or amino acids^[23,24]). In contrast, secondary amine catalysts are usually used to perform the addition of linear aldehydes and ketones to nitroolefins.^[3,11,14,15,18,19,25-32] Within this work we focus on the conjugate addition of linear aldehydes to nitroolefins.

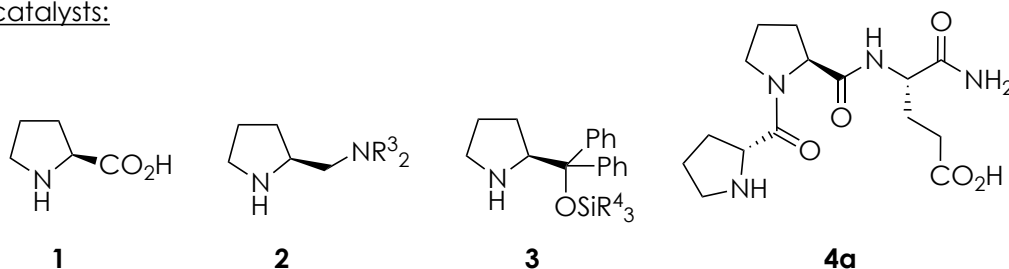
1.2.2.2 β -Alkyl- or Aryl- Substituted Nitroolefins

The organocatalyzed conjugate addition reaction of linear aldehydes to nitroolefins—bearing an alkyl- or an aryl-moiety in the β -position—belongs to the most widely investigated reactions in organocatalysis and many different catalysts have been developed (Scheme 1-3).^[2,3,11] Although L-proline (**1**) is a widely used secondary amine based catalyst, an effective and selective conjugate addition reaction of aldehydes to nitroolefins to γ -nitroaldehydes was not achieved.^[33] Therefore, more reactive derivatives have been developed, e.g. diamino pyrrolidines **2**. These catalysts were found to catalyze the conjugate addition reaction of most alkyl-substituted linear aldehydes to nitroolefins having differently substituted aromatic (e.g. $R^2 = \text{Ph}$, 4-MePh, 4-(OMe)Ph, 2-(CF₃)Ph, 2-thiophenyl) or aliphatic moieties ($R^2 = \text{butyl}$, cyclo-hexyl, CH(OMe)₂) with good enantio- and diastereoselectivity.^[26,34] Further, diamino pyrrolidines **2** allow the addition of β -branched aldehydes^[13] and are used as ionic liquids, where they serve as solvent and catalyst at the same time.^[35]

general reaction:



catalysts:



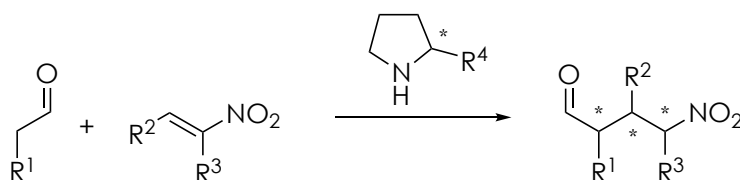
Scheme 1-3: Conjugate addition reaction of linear aldehydes to nitroolefins catalyzed by secondary amine catalysts.

Investigations towards more reactive proline-derived catalysts led to the identification of prolinol-silyl ethers **3** as catalysts, independently by Hayashi^[29] and Jørgensen.^[36-38] This catalyst motif became widely used for conjugate addition reactions of different linear aldehydes to various alkyl- or aryl-substituted nitroolefins.^[39]

A more reactive catalyst was obtained by our group, with the development of peptidic catalysts. H-DPro-Pro-Asp-NH₂^[40] and especially its congener H-DPro-Pro-Glu-NH₂ (**4a**)^[41,42] showed great enantio- and diastereoselectivity in conjugate addition reactions of aldehydes to nitroolefins even with very low catalyst loadings (down to 0.1 mol%).^[40-45] Further, the modularity of the H-Pro-Pro-Glu-NH₂ catalyst allowed C-terminal functionalization, which was used for immobilization on solid support^[46,47] and micelle formation for catalysis in water.^[48]

1.2.2.3 α,β -Disubstituted Nitroolefins

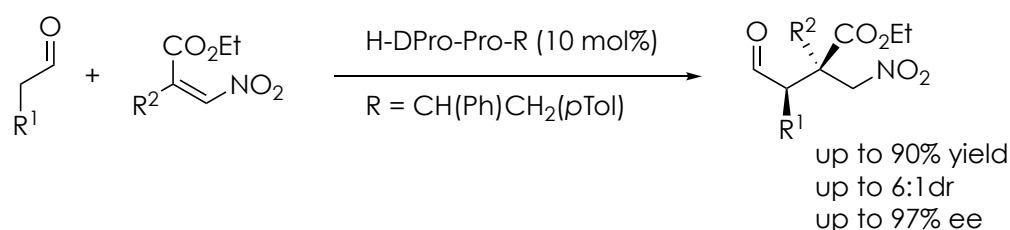
The catalysts developed for the conjugate addition reaction of linear aldehydes to β -substituted nitroolefins were reactive enough to address the more challenging α,β -disubstituted nitroolefins and to synthesize the highly desirable γ -nitroaldehydes with three consecutive stereogenic centers (Scheme 1-4). While proline (**1**) as a catalyst only showed limited reactivity,^[49] diamino pyrrolidine **2** catalysts have higher reactivity.^[50,51] A further increased reactivity was achieved using prolinol-silyl ether catalysts **3** for linear^[52-54] and cyclic^[55] α,β -disubstituted nitroolefins. Further, straightforward modifications on the peptidic catalyst **4a** to H-Pro-Pro-Asn-OH allowed an effective as well as an enantio- and diastereoselective transformation of numerous α,β -disubstituted nitroolefins.^[56]



Scheme 1-4: Conjugate addition reaction of linear aldehydes to α,β -disubstituted nitroolefins catalyzed by a secondary amine.

1.2.2.4 β,β -Disubstituted Nitroolefins

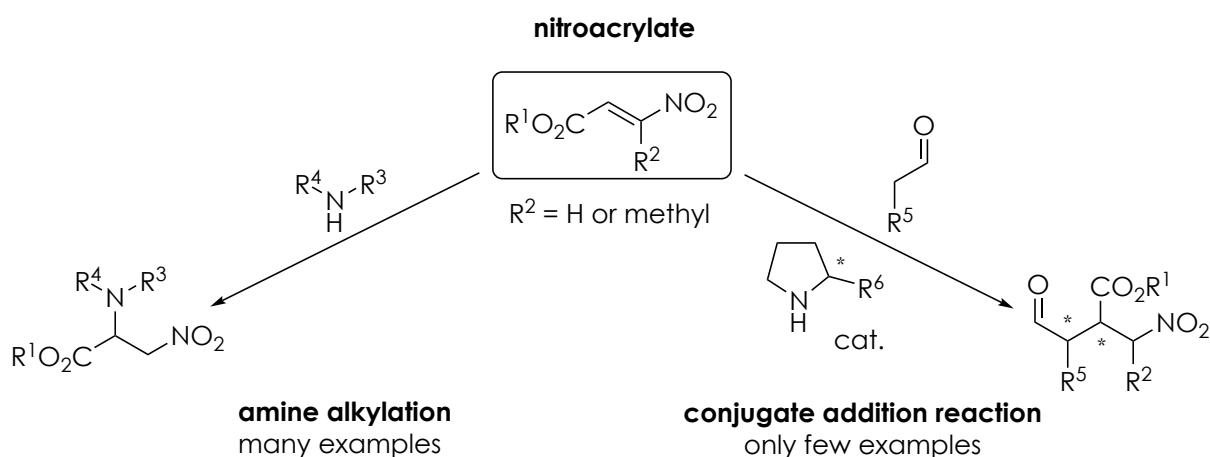
Among the most challenging tasks in the field is the addition of a linear aldehyde to a β,β -disubstituted nitroolefin for the formation of a γ -nitroaldehyde bearing an all carbon tetra-substituted stereogenic center. The only reported catalyst for this transformation is a tripeptide with a Pro-Pro-Xaa motive (Scheme 1-5).^[57] It was found that an ester substitution in one of the β -position is essential to obtain product. Therefore, the substrate scope is currently limited to these substituted nitroacrylates.^[57] In previous studies, we found the formation of catalyst-substrate adduct in combination with untypical reaction curves. Studies with different acidic additives suggested that the rate-determining step can differ depending on the additive and substrate.^[58]



Scheme 1-5: Peptide catalyzed conjugate addition reaction of aldehydes to β,β -disubstituted nitroolefins.

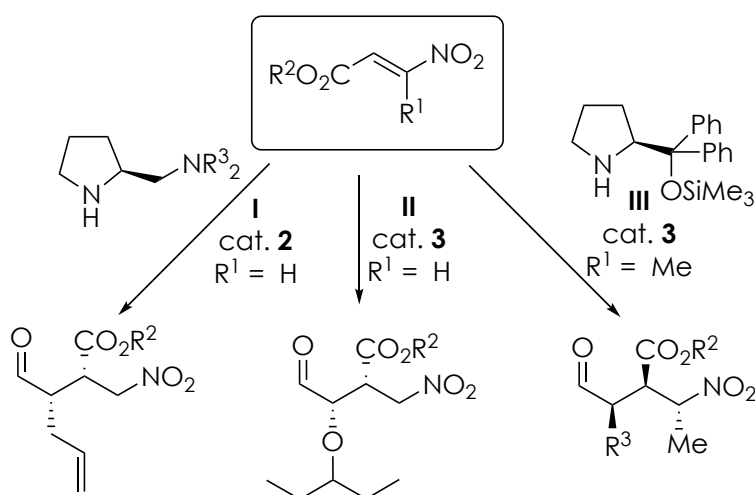
1.2.2.5 Electron Deficient Nitroolefins: Nitroacrylates

β -Ester-substituted nitroolefins, also known as nitroacrylates, are very reactive electrophiles. Hence, they react not only with enamines but also with secondary amines. This renders secondary amine catalyzed addition reactions of aldehydes or ketones to nitroacrylates difficult (Scheme 1-6).^[59,60]



Scheme 1-6: Reactivity of nitroacrylates in presence of aldehydes and/or secondary amines.

Today, most of the reported reactions of nitroacrylates include quantitative amine additions.^[59] Beside stoichiometric applications, nitroacrylates have been only successfully used in very few organocatalyzed transformations (Scheme 1-7).^[15,28,53,61-64] Secondary amine catalyzed conjugate addition reactions have been achieved for α -unsubstituted nitroacrylates ($R^1 = H$) with a pyrrolidine diamine catalyst **2** in one example in only moderate yields (reaction I).^[61] The more reactive prolinol-silyl ether catalysts **3** allowed a conjugate addition reaction in good yields in a key step in synthesis of the antiviral drug (-)-oseltamvir (Tamiflu)^[28,62-64] as well as for few aldehydes in water as solvent (reaction II).^[15] In addition, a prolinol-silyl ether **3** catalyzed the addition of few commercial available aldehydes to α -methylated nitroacrylates ($R^1 = Me$, reaction III).^[53] Despite the successful synthesis of γ -nitroaldehydes from nitroacrylates, alkylation of the catalyst has been observed in significant amounts as a side-reaction.^[65]

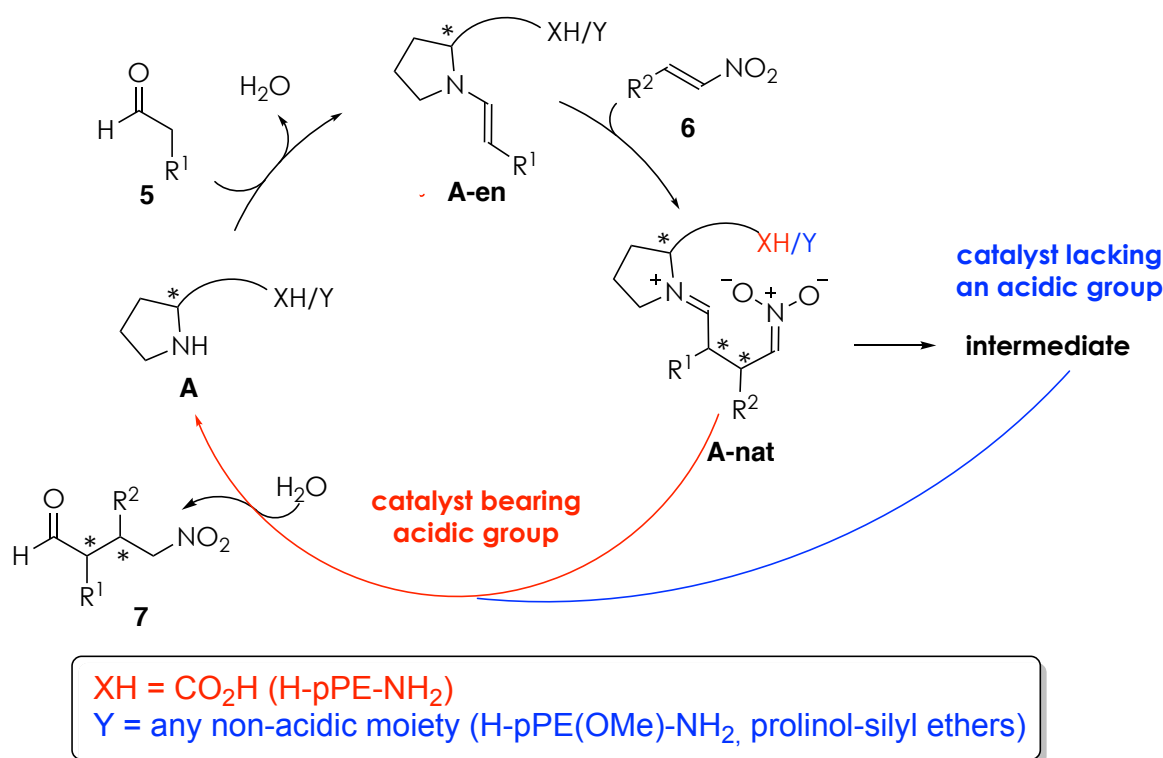


Scheme 1-7: Examples for conjugate addition reaction of aldehydes to nitroacrylates.

Alkylation reactions in the α -position of carbonyl compounds are challenging as the catalyst can react with the alkylating reagent. This phenomenon limits significantly a successful application of strong alkylating agents such as alkyl halides.^[66] To the best of our knowledge a mechanistic understanding of the role of a catalyst alkylation by nitroacrylates has not been achieved up to now. However, elucidating the mechanism when using alkylating substrates, might help to address the current challenges of secondary amine catalyzed addition using very reactive starting materials.

1.3 Mechanistic Studies on Michael Reactions

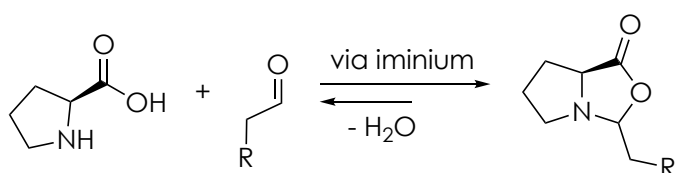
The stereoselective conjugate addition reaction of linear aldehydes to nitroolefins has received great attention and include detailed mechanistic studies.^[11,45,52,67-81] These studies have been performed mainly with two catalysts: prolinol-silyl ether **3** and the peptidic H-DPro-Pro-Glu-NH₂ (**4a**). They differ structurally and by the presence or lack of an intramolecular acid group. Both catalytic cycles share the initial condensation of a secondary amine **A** and an aldehyde **5** to form an enamine species **A-en** (Scheme 1-8). The enamine **A-en** attacks the nitroolefin **6** in a nucleophilic manner, forms a carbon-carbon bond and generates an iminium nitronate species **A-nat**.^[3,11] Subsequently, the nature of the catalyst determines the following pathway: either a catalyst contains an intramolecular acid (red pathway) or is lacking one (blue pathway).



Scheme 1-8: Catalytic cycle depending on the presence of an intramolecular acid in the catalyst.

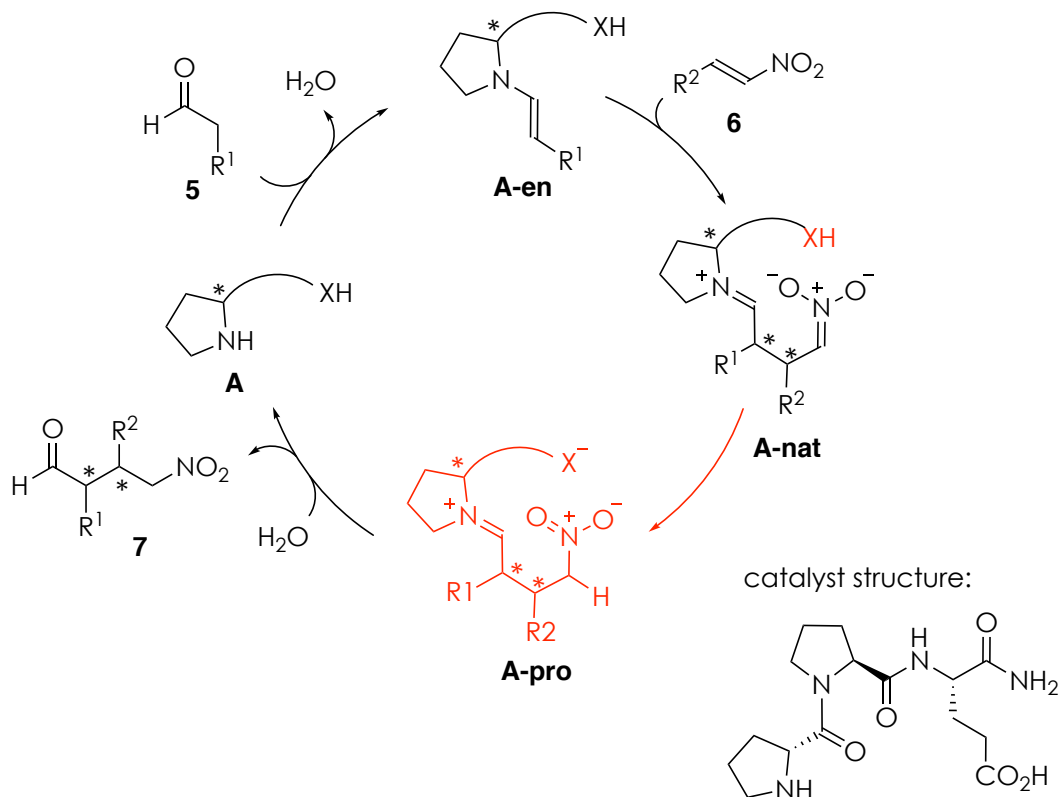
1.3.1 Catalysts with an Internal Acid

The group of catalysts for the conjugate addition reactions of linear aldehydes to nitroolefins bearing an intramolecular acidic moiety includes H-DPro-Pro-Glu-NH₂^[41,42] and its carboxylic acid containing derivatives.^[82-85] Despite the presence of an intramolecular acid, proline is not included in this group since the formation of an unproductive bicyclic oxazolidinone side-product limits its application as a catalyst for conjugated addition reactions of aldehydes to nitroolefins (Scheme 1-9).^[33,86-88]



Scheme 1-9: Oxazolidinone formation by proline and aldehyde.

The catalytic cycle is initiated when the secondary amine catalyst **A** reacts with aldehyde **5** to form the enamine **A-en** (Scheme 1-10). Subsequently **A-en** forms in a nucleophilic attack the carbon-carbon bond and **A-nat** is generated. By studies using quasi-enantiomers for the product back reactions

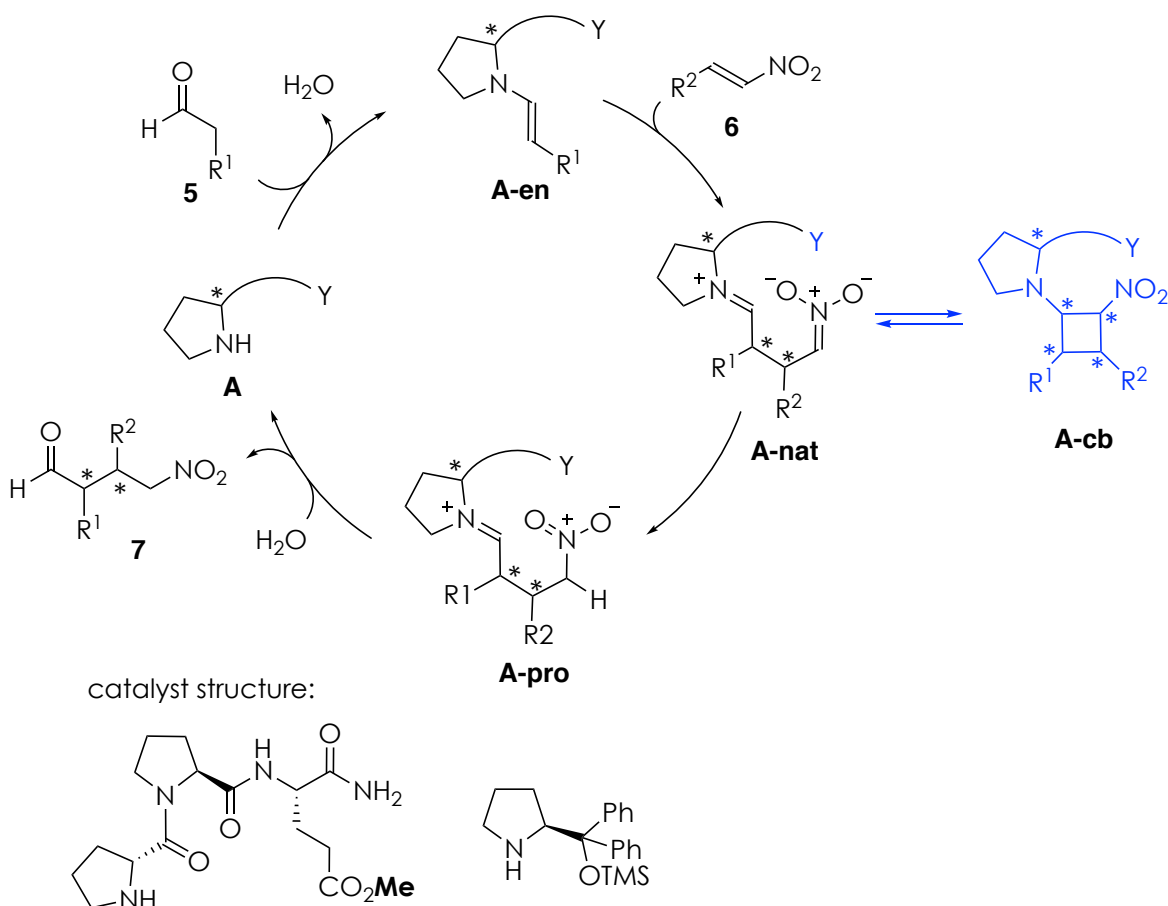


Scheme 1-10: Catalytic cycle of the conjugate addition reaction of aldehydes to nitroolefins for acid bearing catalyst. XH = carboxylic acid

monitored by ESI-MS we showed that this carbon-carbon bond formation is reversible and determines the enantioselectivity of the product.^[78] Further, kinetic studies using *in situ* IR-spectroscopy revealed that the carbon-carbon bond formation is the rate-limiting step.^[45,79] The resulting **A-nat** is then protonated by the intramolecular acid to give **A-pro**. Variation of linker length that connects the backbone with the acid revealed that if the side chain consists of more than four carbon atoms, the reaction profile of the catalyst is similar to catalysts lacking an intramolecular carboxylic acid.^[79] After release of the catalyst, it is available for a new catalytic cycle. For H-DPro-Pro-Glu-NH₂, the reaction orders for the conjugate addition reaction of a linear aldehyde to a β -substituted nitroolefin was determined by using initial rate measurements. It was found that the reaction is first order in the secondary amine catalyst. The rate order of the aldehyde is zero or close to zero, depending on the amount of water in the reaction. The order of the nitroolefin is in the range of 0.4-0.7, again depending on the amount of water in the reaction.^[45]

1.3.2 Catalysts Lacking an Internal Acid

The group of catalysts lacking an acidic moiety mainly consists of the pyrrolidine diamines, prolinol-silyl ethers, and the methylated congener of H-DPro-Pro-Glu-NH₂ (**4a**), H-DPro-Pro-Glu(OMe)-NH₂ (**4b**). Using these catalysts without an carboxylic acid, the secondary amine **A** and aldehyde **5** condense to form enamine **A-en**. After a nucleophilic attack at the nitroolefin, the carbon-carbon bond is formed often with *syn*-selectivity of R¹ and R² (when using prolinol silyl ether catalysts), resulting in **A-nat** (Scheme 1-11). Seebach and Golinski proposed that the *syn*-selectivity of this step is determined when **A-en** and **6** arrange in a quasi-chair conformation.^[29,76] However, later Blackmond proposed that this simple model can not explain the selectivity; a more complex Curtin-Hammond scenario is essential for the stereoselective formation of **A-nat**.^[70] Investigations by computational studies and time dependent back reaction studies by ESI-MS confirmed the presence of a Curtin-Hammond scenario for prolinol-silyl ether catalysts.^[72] The formation of an iminium nitronate **A-nat** species has been generally accepted for long time and **A-nat** was assumed to be key for the later reaction pathway by Seebach.^[65]

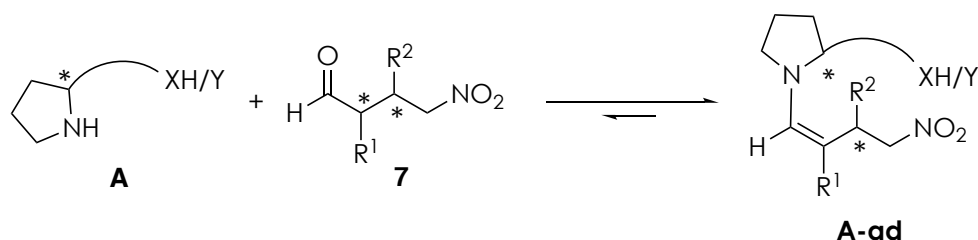


Scheme 1-11: Catalytic cycle of the conjugate addition reaction of aldehydes to nitroolefins for catalysts lacking an intramolecular carboxylic acid.

Acidic additives accelerate the reaction significantly in examples where the catalysts lack an acidic moiety.^[74,79] Closer investigations of this phenomenon with stoichiometric amounts of substrates by NMR-spectroscopy as a monitoring tool showed the formation of a cyclobutane off-cycle intermediate **A-cb**.^[74] Cyclobutanes have been known since 1982 to occur in non-catalytic additions of enamines derived from ketones to nitroolefins.^[76] It was proposed that the addition of an external acid favors the back reaction of the cyclobutane **A-cb** towards the iminium nitronate **A-nat**.^[74] The generation of cyclobutanes under catalytic conditions was found in NMR spectroscopic experiments by Blackmond, which led to a revised catalytic cycle including **A-cb**. Further, Blackmond suggested that the protonation of **A-nat** towards **A-pro** is irreversible and proposed the protonation as the rate limiting step.^[71] Subsequent to the protonation to form **A-pro**, the catalyst **A** and the product **7** are released. It was found that for prolinol-silyl ethers as catalysts in the conjugate addition reaction of linear aldehydes to

nitrostyrenes the reaction order of the aldehyde as well as for the nitroolefin is zero order. The rate limiting step of the reaction is the protonation, which is dependent on acidic additives. [71,74,79]

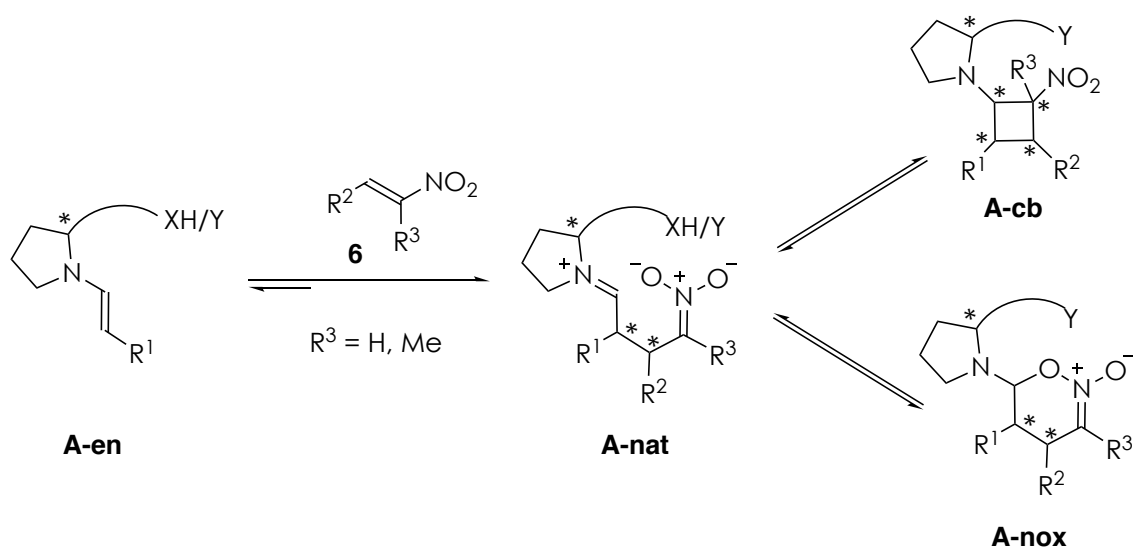
It is noteworthy to mention that in many experiments an enamine species of a product-catalyst adduct **A-ad** was reported (Scheme 1-12).^[52,71,74] Later computational investigations revealed that this adduct is of lower energy than **A** and **7**.^[81]



Scheme 1-12: Condensation of catalyst and product.

1.3.3 Iminium Nitronate and 1,2-Oxazine *N*-Oxide Intermediates

Mechanistic proposals rely on the occurrence of an iminium nitronate **A-nat** as product of the carbon-carbon bond formation by a nucleophilic addition of enamine **A-en** to nitroolefin **6**. For the conjugate addition reaction of aldehydes to nitroolefins with stoichiometric amounts of prolinol-silyl ethers, Seebach isolated a cyclic 1,2-oxazine *N*-oxides species **A-nox** (Scheme 1-13).^[74] Use of α -unsubstituted nitroolefins ($R^3 = H$) as substrates in absence of water led to an equilibrium of cyclobutane **A-cb** and 1,2-oxazine *N*-oxides **A-nox** (4:1). Switching the substrates to α -methylated nitroolefins ($R^3 = Me$) almost exclusively led to the formation of **A-nox**. However, the *in situ* formation of **A-nox** raised questions as the conversion to the observed **A-cb** would be energetically uphill and therefore should include a iminium nitronate species **A-nat**.^[74]

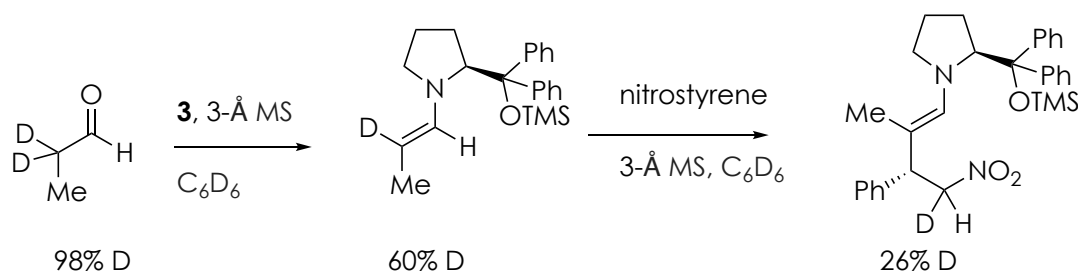


Scheme 1-13: Formation of iminium nitronate, cyclobutane and 1,2-oxazine *N*-oxide.

In later studies by Pikho & Papai, computational analyses indicated that the cyclic 1,2-oxazine *N*-oxide **A-nox** is of lower energy than the cyclobutane **A-cb**.^[52] This triggered NMR investigations of the conjugate addition reaction of linear aldehydes to α -substituted and unsubstituted nitrostyrenes catalyzed by prolinol-silyl ethers under conditions that differ from the original catalytic methodology (e.g. interruption of the reaction by addition of molecular sieve, quantitative catalyst loadings, ...). Herein, cyclic **A-nox** was identified for both nitroolefins. Investigating the equilibrium between the cyclobutane **A-cb** and **A-nox** showed for α -unsubstituted nitrostyrenes ($R^3 = \text{H}$) that only low amounts of **A-nox** occur while **A-cb** is present in up to six-fold higher concentrations. The α -substituted nitrostyrenes ($R^3 = \text{Me}$) formed the **A-nox** species to a large extent. Based on these experiments Pikho & Papai suggested a revised catalytic cycle where the direct formation of **A-nox** replaces the previously accepted iminium nitronate species **A-nat** and hypothesized that its decomposition is the rate limiting step of the reactions.^[52] Attempts to observe an iminium nitronate species in catalytic conditions by NMR was attempted by Blackmond, but turned out to be challenging.^[69,70]

Later, Seebach investigated whether the reaction is proceeding via an iminium nitronate species **A-nat** or whether a direct cyclisation from the nitroolefin **6** and the enamine **A-en** is occurring, using deuterated aldehydes (Scheme 1-14).^[65] This work underlined the occurrence of an iminium

nitronate **A-nat** species in the catalytic cycle, but could not answer the role of **A-nox**.^[65]



Scheme 1-14: Deuterium experiments by Seebach.

Recent computational studies further investigated this question and revealed that a direct [4+2] addition of **A-en** and **6** is unlikely but **A-nox** formation is likely to occur via a **A-nat** species.^[80]

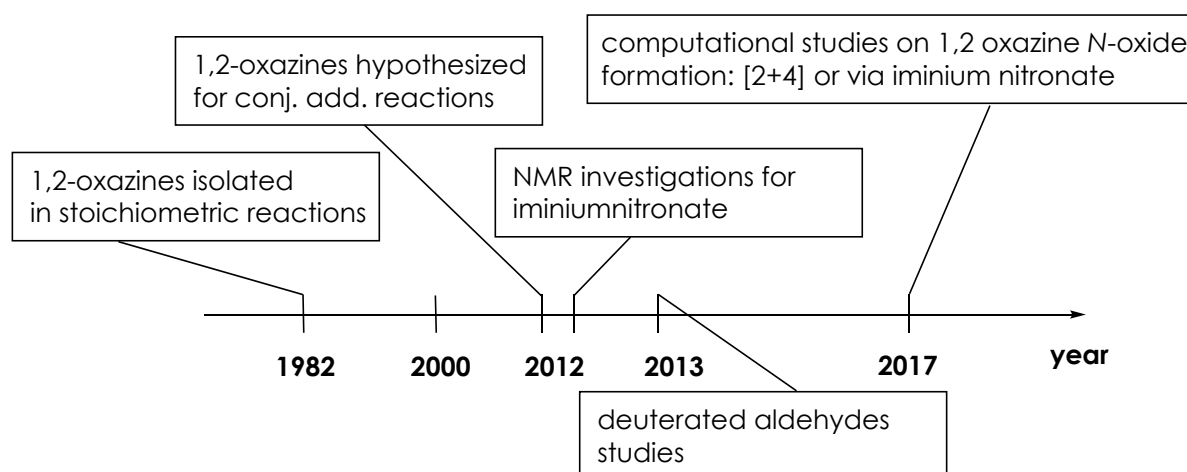


Figure 1-1: Time line of iminiumnitronate research.

Thus, despite intense research (Figure 1-1), the role of the iminium nitronate as a reactive intermediate in the conjugate addition reaction of linear aldehydes to nitroolefins is still under debate. Although there is *ex situ* indication on its formation, an *in situ* observation has not been possible up to now.

2

Objectives

In modern asymmetric organocatalysis, the conjugate addition reaction of aldehydes to nitroolefins provides a powerful tool to synthesize versatile, chiral building blocks,^[89] and many secondary amine catalysts have been developed for the addition of linear aldehydes.^[3] The development of new catalysts as well as mechanistic investigations have revealed a detailed but not fully understood mechanistic cycle.^[11]

1) Among the catalysts for conjugate addition reactions of linear aldehydes to nitroolefins only the peptidic catalyst H-DPro-Pro-Glu-NH₂ is known to avoid off-cycle intermediates via direct protonation of a nitronate species. We planned to investigate the previously elusive nitronate species^[52,65,70] under *in situ* conditions and to gain insights about how the catalyst structure influences its stabilization.

Aim 1: *Mechanistic investigations of the in situ nitronate intermediate structure and influence of the catalyst structure on its stabilization (Chapter 3).*

2) Organocatalytic transformations with substrates that also act as alkylating agents are known to be challenging. For such substrates, a productive catalytic cycle is in competition with catalyst deactivation by alkylation.^[66] Of particular interest are nitroacrylates that are known to alkylate secondary amines.^[59,65,90] Therefore, we planned to investigate the conjugate addition reaction of aldehydes to nitroacrylates, to obtain insights into catalyst deactivation pathways and to provide an improved reaction setup.

Aim 2: *Investigations of nitroolefins that alkylate the secondary amine catalyst to react in Michael additions (Chapter 4).*

3) With an optimized procedure for the transformation of nitroacrylates we planned to show applicability of the resulting γ -nitroaldehydes besides simple modifications e.g. in the synthesis of natural product derivatives.

Aim 3: *Synthesis of natural product derivatives from γ -nitroaldehydes (Chapter 5).*

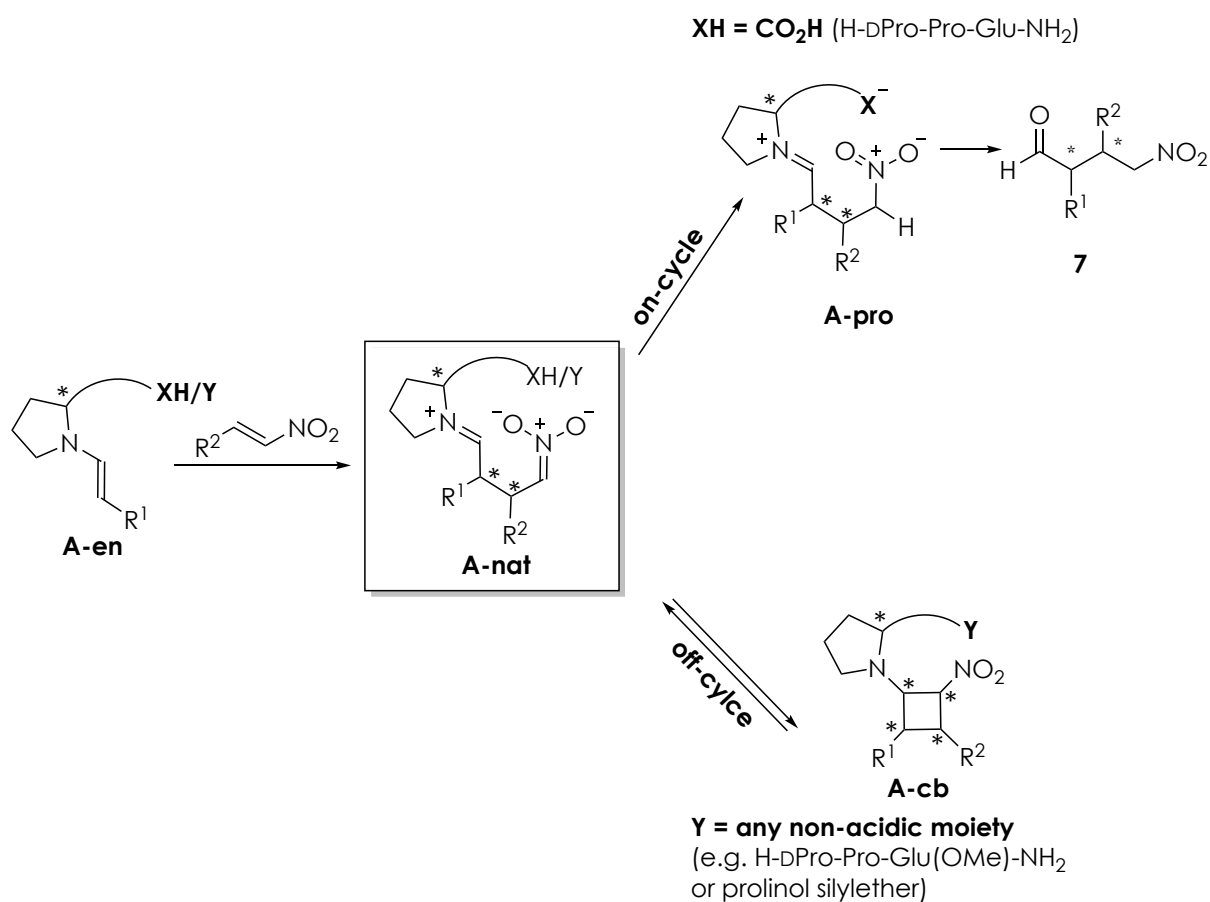
3

Mechanistic Investigations on the Nitronate Intermediate

Experiments within this chapter were performed in collaboration with Dr. Reinhard Kissner (UV/Vis stopped-flow experiments), Dr. Thomas Weymuth and Prof. Dr. Markus Reiher (computational studies).

3.1 Background

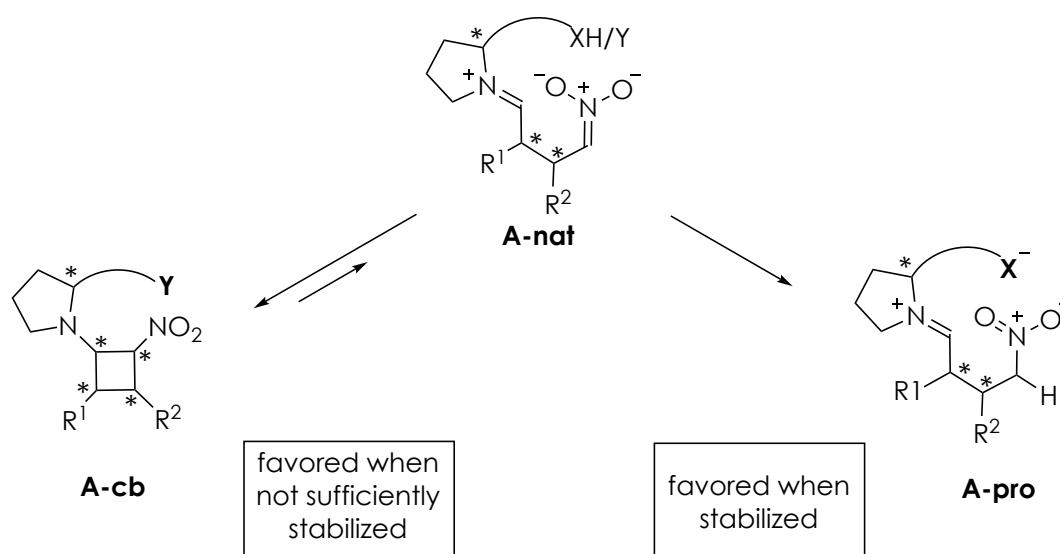
The conjugate addition reaction of aldehydes to nitroolefins catalyzed by secondary amines is amongst the most popular enantioselective synthetic strategies to form a carbon-carbon bond (Chapter 1.2).^[3,11] Its mechanism has also been thoroughly investigated (Chapter 1.3). Nevertheless, as described in Chapter 1.3 the intermediate that results from the carbon-carbon bond forming step is still under debate, as the most plausible iminium nitronate **A-nat** has never been observed *in situ* (Scheme 3-1). This intermediate is supposed to be key^[74] for the subsequent reaction pathway as it either undergoes a cyclisation towards the cyclobutane **A-cb** in the presence of non-acidic catalysts (e.g. prolinol-silyl ethers^[70] or H-DPro-Pro-Glu(OMe)-NH₂ **4b**;^[79] Chapter 1.3.2) or is directly protonated to **A-pro** in the presence of catalysts with a proton donor (e.g. H-DPro-Pro-Glu-NH₂ **4a**;^[79] Chapter 1.3.1).



Scheme 3-1: Nitronate intermediate as a central reactive species in the catalytic cycle of the conjugate addition reaction of aldehydes to nitroolefins.

The *in situ* observation of an iminium nitronate species has turned out to be extremely challenging due to its appearance in only low concentrations in the presence of the inevitably high quantities of the reactants during the reaction.^[69,70] We envisioned this challenge could be addressed using UV/Vis spectroscopy to detect nitronates under preparative conditions. This spectroscopic analysis of a nitronate species would be the first observation of this species under catalytic conditions. Further, UV/Vis spectroscopy would allow for a relative comparison of the **A-nat** absorbance, which is proportional to the nitronate concentrations, by different catalysts and therefore provide insights on the catalyst structure and its reactivity.

In previous mechanistic investigations of the organocatalyzed conjugate addition reaction of aldehydes to nitroolefins, our group showed that only the acid bearing catalysts of a Pro-Pro-Xaa motive (Xaa = any amino acid, e.g. H-DPro-Pro-Glu-NH₂, **4a**) avoid the formation of a significant amount of the cyclobutane species **A-cb** (see Chapter 1.3.1).^[79] The intermediate prior to the cyclobutane formation or the protonation, respectively, is proposed to be the iminium nitronate **A-nat**. Therefore, we hypothesized that the catalyst non-covalently interacts with the nitronate intermediate **A-nat** and the nature of this interaction determines the reaction pathway (Scheme 3-2). When a catalyst bears an acidic side chain, we hypothesized that it stabilizes the iminium nitronate **A-nat** by its carboxylic acid group.



Scheme 3-2: Reaction pathway dependent on catalyst stabilization of iminium nitronate.

The carboxylic sidechain hinders a cyclisation to the off-cycle intermediate **A-cb** when **A-nat** is directly protonated (on-cycle pathway). On the other hand, when a catalyst lacks an intramolecular acid the iminium nitronate **A-nat** should be insufficiently stabilized and a cyclisation towards **A-cb** becomes favored (off-cycle pathway). By using UV/Vis spectroscopy to observe the *situ* iminium nitronate **A-nat**, we envisioned on-sights into catalyst-nitronate stabilization by different secondary amine catalysts.

3.2 Determination of Characteristic UV-Band for Nitronate Model System

The iminium nitronate **A-nat** is a highly reactive, short-lived species and therefore only low amounts can be assumed to occur under catalytic conditions.^[69,74] As mentioned in the introduction NMR detection of the iminium nitronate species **A-nat** has been challenging.^[69,70] Therefore, we initiated our investigations using a different spectroscopic technique. Nitronates, however, show characteristic UV/Vis-bands with maxima around 260 nm.^[91,92] For the “benchmark reaction”,^[67] (addition of butanal (**5a**) to nitrostyrene (**6a**) to form the γ -nitroaldehyde (**7a**, Figure 3-1) a hypsochromic shift was observed over the course of the reaction under standard reaction conditions (aldehyde/nitroolefin 1.5:1.0, 0.5 M, room temperature). Control experiments underlined that the highest absorbing chromophores in the initial phase is nitroolefin **6a** and at the end product **7a**. Unfortunately, the starting materials as well as the products show a signal that’s absorbance is too strong to detect (detector oversaturation) at wavelengths lower than 440 nm or 390 nm, respectively. Therefore, the known nitronate specific UV absorption band at 260 nm is not visible for secondary amine catalyzed reactions that are performed at concentrations of around 0.5 M.

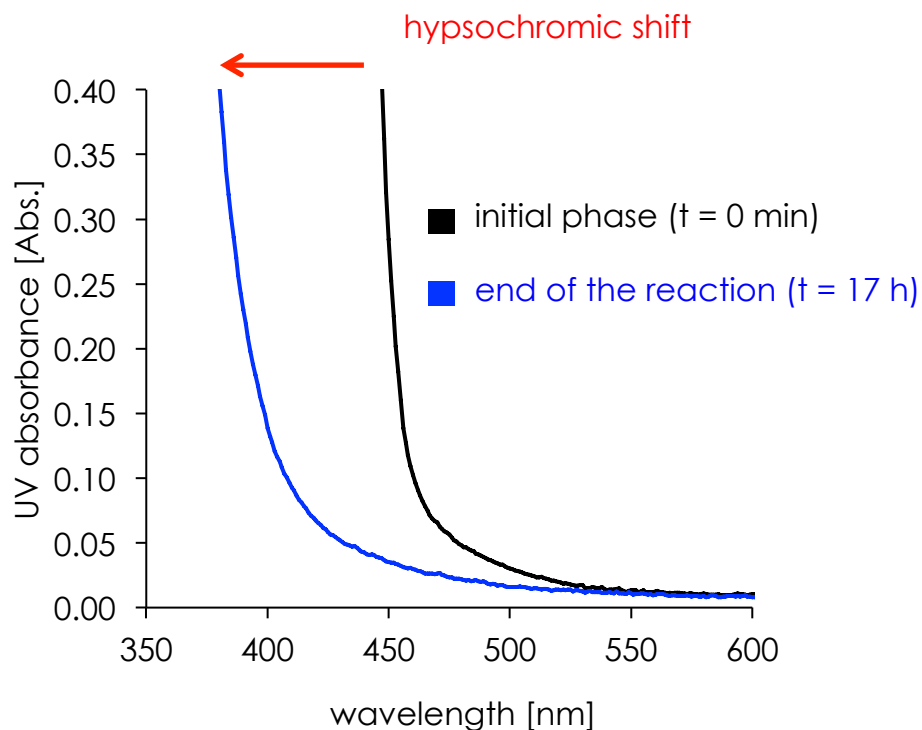
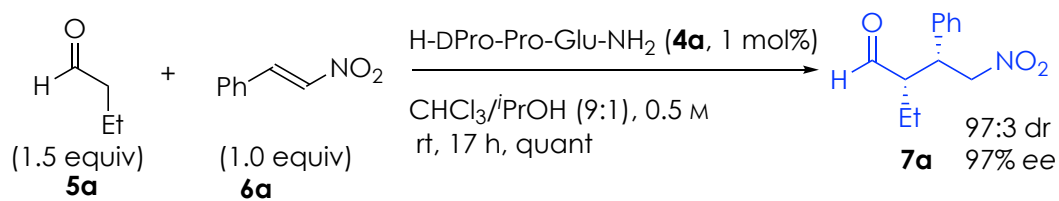


Figure 3-1: UV/Vis monitoring of the peptide catalyzed conjugate addition reaction of butanal to nitrostyrene. First spectrum was recorded in the initial phase (0 min, black), second spectrum recorded after full conversion (17 h, blue).

We therefore explored whether nitronates have other, so far unreported characteristic UV-bands. We synthesized a model nitronate **8a** derived from deprotonation of phenyl-nitroethane **8b** with CsOH (Figure 3-2).^[93] When monitored by UV/Vis, the starting material nitrostyrene **6a** as well as the product model phenyl-nitroethane **8b** did not show absorbance above 440 nm but the model nitronate compound **8a** showed an UV/Vis band with a maximum at 490 nm. This band of **8a** is of relative low intensity compared to the previously reported characteristic nitronate absorbance bands around 250 nm (only visible when **8a** was diluted to 0.5 mM).

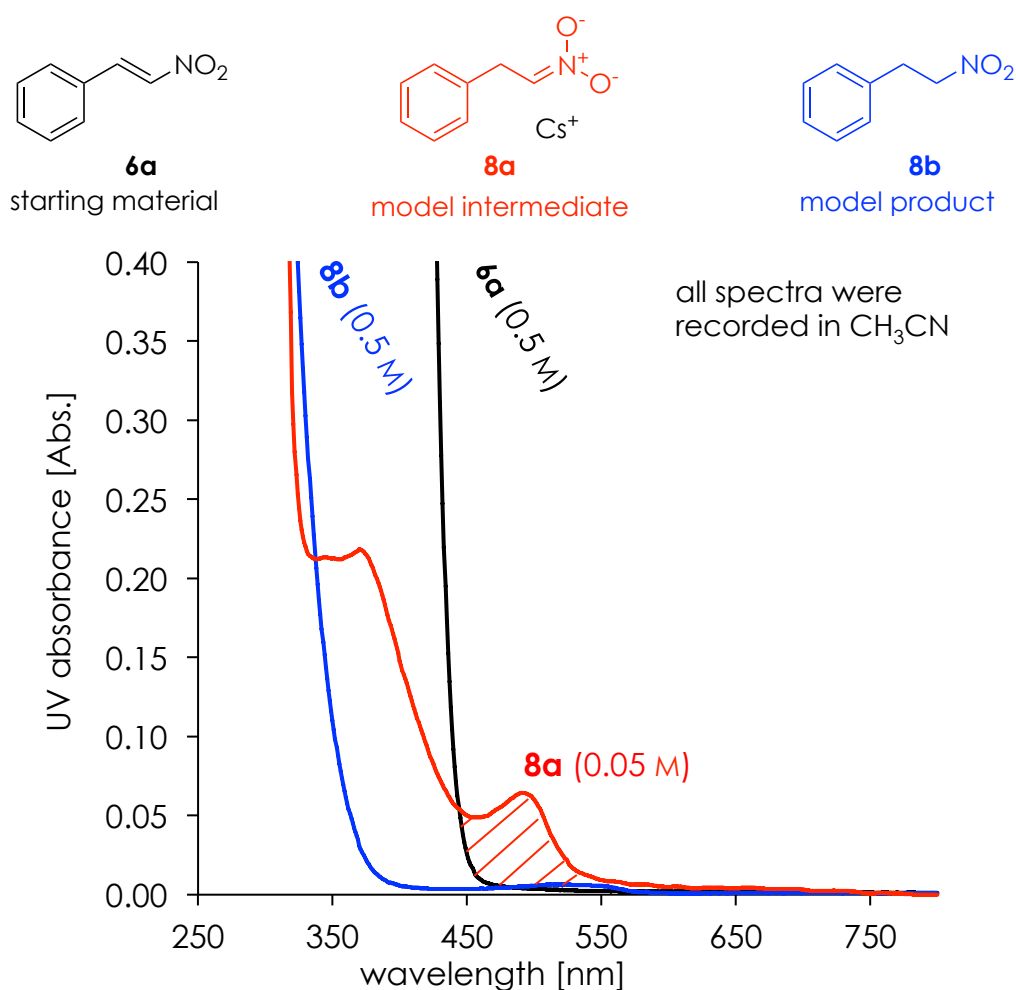


Figure 3-2: Overlay of the UV/Vis spectra in CH_3CN of the reactant **6a** (black), intermediate **8a** (red) and product model **8b** (blue). Red marked area = nitronate absorbance without overlay.

To further investigate the newly found UV/Vis band of the nitronate species, computational studies of the model system **8a** were conducted. Geometry optimizations by DFT (calculated in vacuum as well as in acetonitrile) provided four structures of comparable lowest energies (two in vacuum & two in acetonitrile). The visualization of the calculated HOMOs of the computed structures revealed that the orbitals are located at the nitronate residue (Figure 3-3). Electron excitation from the HOMOs to the excitation state revealed a UV/Vis transition between 501 nm and 507 nm. The calculations describe this excitation as spin-forbidden and therefore the excitation only obtains a nonzero intensity through spin-orbit couplings. This explains the weak intensities around 500 nm compared to the excitation around 250 nm that is spin-allowed. A second excitation was calculated to appear around 370 nm, which is also visible in the spectrum of model

compound **8a**. Supported by these computational studies we hypothesized the excitation band of low intensity around 490 nm to the nitronate species.

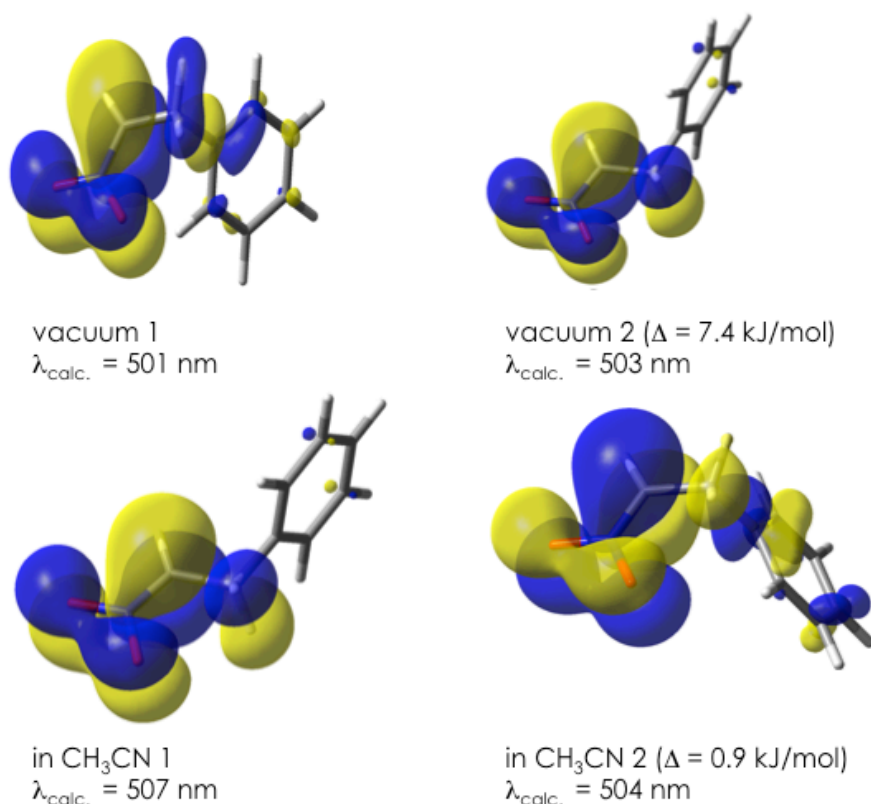


Figure 3-3: DFT-calculation of the HOMOs (visualized in yellow and blue) of two lowest energetic conformation of the nitronate model compound **8a** in vacuum and acetonitrile.

However, additional computational studies on cyclic 1,2-oxazine *N*-oxide **A-nox** structures and their excitation energies revealed a similar excitation around 500 nm. Thus, it is impossible to distinguish by UV/Vis spectroscopy between **A-nat** and **A-nox** and additional studies are ongoing in our laboratories to resolve this challenge. Computational studies^[80] and deuterium exchange experiments^[65] revealed that for the conjugate addition reaction an iminium nitronate species is likely to be included in the catalytic cycle. Although a distinguishability between the open and the cyclic structure was not possible, we showed that using the spectral window around 500 nm will allow exclusively monitoring the species after the carbon-carbon bond formation, independently of its exact structure.

3.3 Nitronate Species under Reaction Conditions

Having established a method to selectively detect the intermediate subsequent to the carbon-carbon-bond formation, we investigated its formation and steady-state absorbance in the presence of different secondary amine catalysts. Using the characteristic UV/Vis band at 490 nm to detect these intermediates we monitored its *in situ* absorbance that is proportional to its concentration during the conjugate addition reaction of butanal (**5a**) to β -nitrostyrene (**6a**) under preparative concentrations (0.5 M). Three different catalysts were evaluated: (I) acid containing peptide

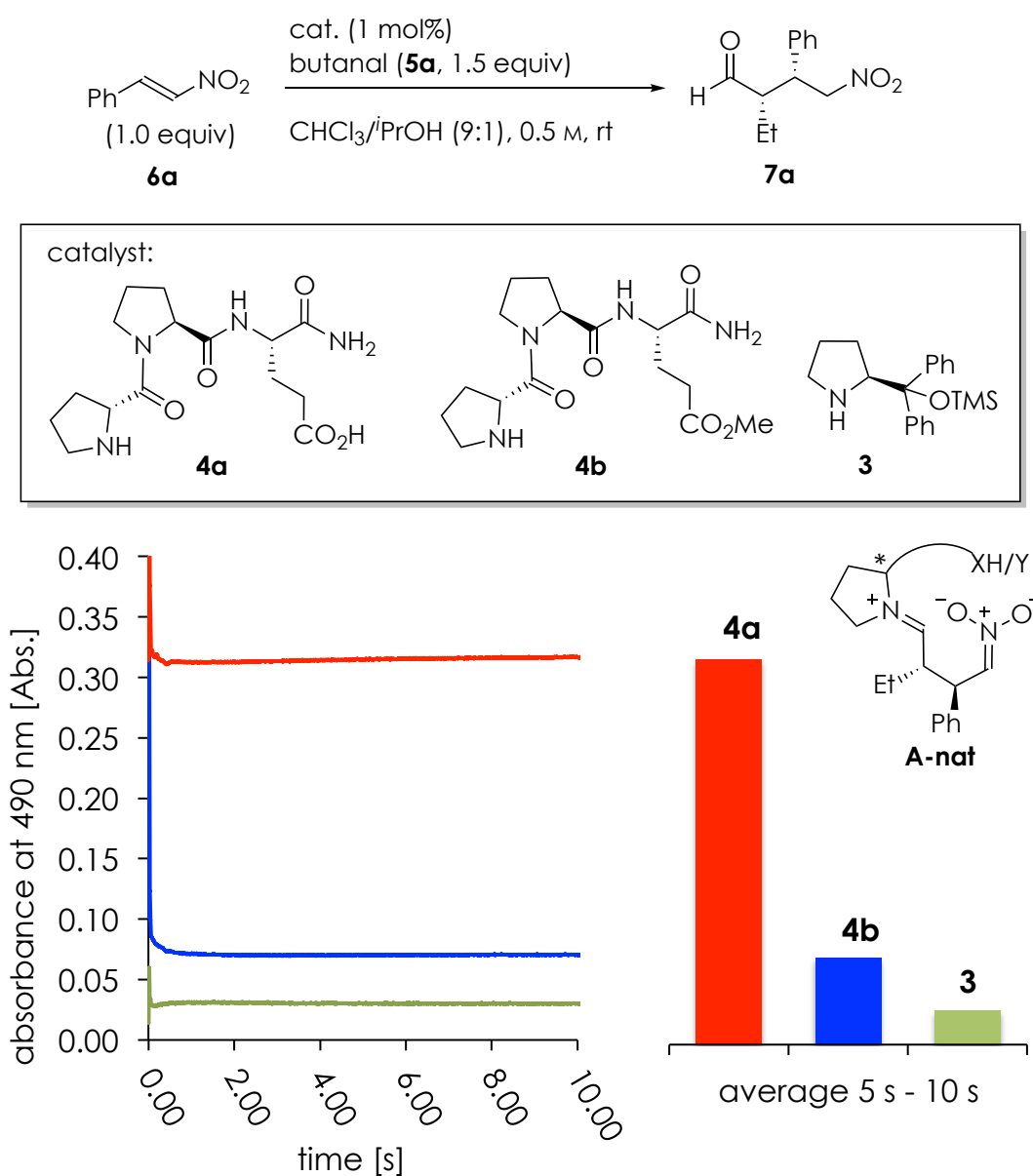


Figure 3-4: Comparison of *in situ* initial nitronate/oxazine *N*-oxide absorbances at 490 nm formed by different catalysts monitored by UV/Vis stopped flow spectroscopy.

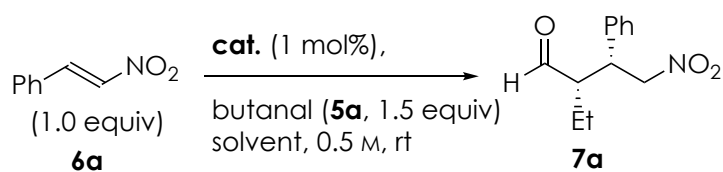
H-DPro-Pro-Glu-NH₂ (**4a**); (II) non-acid containing peptide H-DPro-Pro-Glu(OMe)-NH₂ (**4b**); (III) non-acid containing prolinol-silyl ether **3**. We hypothesized that the peptidic catalyst **4a** stabilizes the nitronate intermediate and therefore a higher nitronate absorbance should be observed than for catalysts **3** and **4b**. This scenario might explain the absence of an off-cycle cyclobutane intermediate **A-cb** caused by stabilization of the nitronate **A-nat**/oxazine *N*-oxide **A-nox** by **4a**. In contrast, a decreased stabilization effect by catalyst **3** and **4b** would potentially trigger the undesired cyclobutane formation.

In the initial phase of the reaction most of the catalyst is available for the first catalytic cycle, and the highest nitronate concentration is expected. A spectroscopic technique that provides good time resolution of the initial phase of a reaction is the stopped-flow technique. Time dependent UV/Vis spectroscopy by stopped-flow measurements of the Michael reaction in protic solvents with catalysts **4a**, **4b** and **3** showed in all cases absorbance at 490 nm (Figure 3-4). Since neither the product nor the starting materials absorb at this wavelength, this indicates that a nitronate/oxazine *N*-oxide species is formed by all catalysts. After a short initial phase (< 2 s) the nitronate absorbances and thus the concentrations became constant, indicating that a steady-state was reached. The acid containing catalyst **4a** led to a significantly higher nitronate/oxazine *N*-oxide absorbance in the steady-state compared to the non-acidic **3** and **4b**, the latter of which provided the lowest nitronate/oxazine *N*-oxide absorbance. This trend also reveals that a nitronate/oxazine *N*-oxide stabilization is increased for peptides compared to prolinol-silyl ethers (acid containing peptide **4a** > acid lacking peptide **4b** > acid lacking prolinol **3**). In the case of catalysts **3** and **4b**, the reaction accelerates upon addition of acid,^[71,79] so additional experiments with the addition of acetic acid (1 mol%) were performed. However, here the nitronate/oxazine *N*-oxide concentration did not increase to a comparable level as observed in reactions with catalyst **4a** (see appendix page 159). Therefore, we conclude that a carboxylic side chain of the catalyst provides an increased stabilization compared to ester side chains or silyl-ethers, the latter of which provided the lowest stabilization.

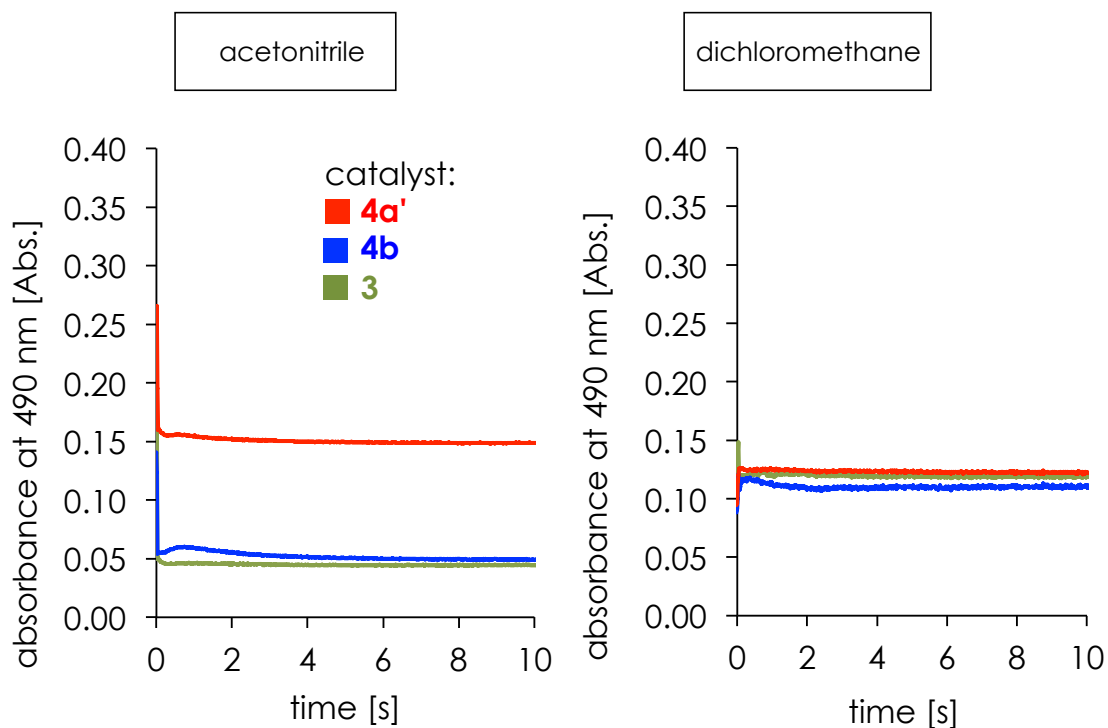
It has been shown in previous studies that protic solvents are beneficial for Pro-Pro-Xaa-type catalysts in conjugate addition reactions.^[40,77] Since the stability of isolated nitronates strongly depends on the availability of H-bonds by the solvent,^[94] we hypothesized that in non-protic solvents the overall stability of *in situ* formed nitronates/oxazine *N*-oxides will be lower. Thus, we anticipated that peptide **4a** stabilizes these species more than catalyst **3** and **4b**.

The stopped flow technique is limited to solvents that have a low compressibility, thus the aprotic solvents dichloromethane and acetonitrile were used to probe the role of solvent for the stabilization effect. The nitronate/oxazine *N*-oxide absorbance for the conjugate addition reaction of butanal (**5a**) to nitrostyrene (**6a**) was monitored in these solvents using catalyst **3** and **4b** as well as **4a'** (Figure 3-5). Catalyst **4a'** is an *N*-terminal alkylated congener of **4a** that has identical reactivity but better solubility in aprotic solvents.^[95] The obtained spectra showed formation of a constant absorbance and thus a constant concentration of a nitronate/oxazine *N*-oxide species after 5s. We assigned this to a formed steady-state, averaged the spectra from 5 s to 10 s, and then normalized the nitronate absorbance to the lowest concentration obtained. This excludes residual absorbance of the different backgrounds and therefore allows a better comparability of the relative values.

In acetonitrile as well as in dichloromethane the acid containing peptide **4a'** provided the highest nitronate absorbance compared to non-acid containing catalysts **4b** and **3**. The relative difference observed between **4a'** and **3/4b** was higher in the more polar acetonitrile than in dichloromethane, where nearly no difference was observed. Comparing the aprotic to the protic solvents, the differences between the catalyst with an intramolecular acid **4a** and the catalysts without an intramolecular acid **3/4b** were increased in the protic solvents. We assign this lower difference to a solvent assisted stabilization effect where polar solvents are involved in the coordination of the side chain to the nitronate. Here, H-bonds (by *i*PrOH) are favored over polar electrostatic interactions ($\text{CH}_3\text{CN} > \text{CH}_2\text{Cl}_2$). Further, control experiments with acetic acid as additive



4a' = H-DPro-Pro-Glu-NH(n-dodecyl)



Relative differences: (average from 5 to 10 s, lowest value set as 0):

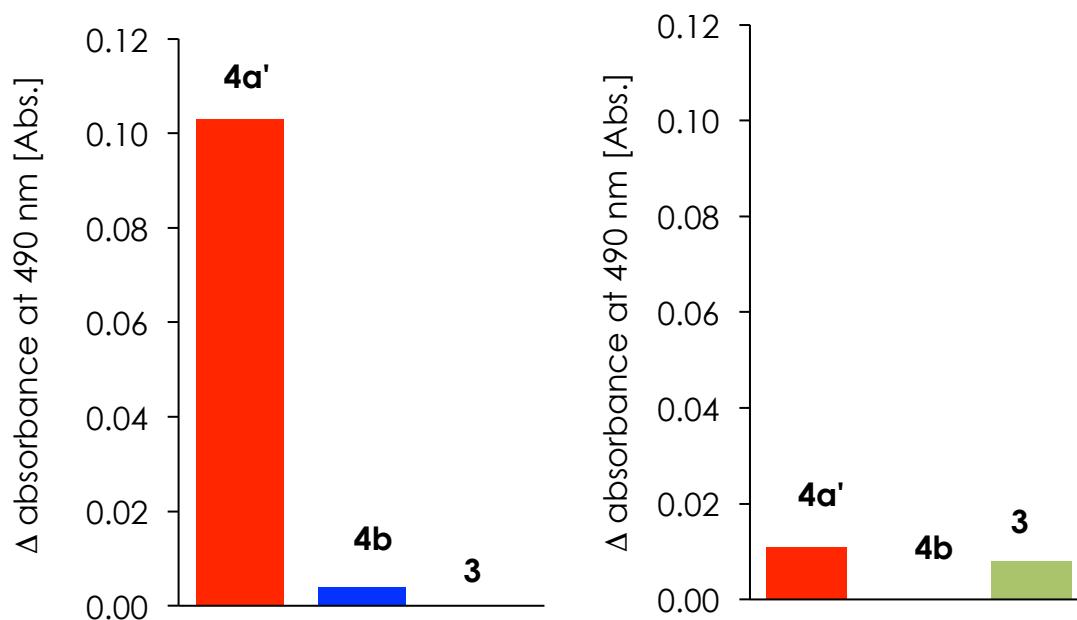


Figure 3-5: Comparison of the *in situ* initial nitronate/oxazine *N*-oxide absorbances at 490 nm in the non-protic solvents monitored by UV/Vis stopped-flow spectroscopy.

(1.0 mol%) were performed for catalysts **3** and **4b** but the nitronate/oxazine *N*-oxide concentration did not increase to a comparable level as with catalyst **4a** (see appendix page 159). Currently, additional *in silico* experiments are ongoing to further explain these findings.

Overall, our investigations revealed that in protic solvents the carboxylic acid bearing catalyst **4a** stabilizes a nitronate/oxazine *N*-oxide species in the conjugate addition reaction of aldehydes to nitrostyrenes to a larger extent than catalysts lacking an intramolecular acid **3/4b**. Since protic solvents increase this effect, we expect that H-bonding of the solvent is involved. In order to gain insights into the interaction between solvent and nitronate/oxazine *N*-oxide we recorded UV/Vis spectra in different solvents.

To get an UV/Vis spectrum exclusively of the nitronate/oxazine *N*-oxide, the difference spectrum (derived from a spectrum of the initial phase of the reaction with a higher concentration and of a spectrum of the steady state with constant concentration) was derived (Figure 3-6). A fundamental principle of electron excitation is that tighter coordination increases the required energy for a transition and therefore requires lower wavelength. Therefore a hypsochromic shift of the UV/Vis band is observed. Prominent examples are H-bonds that coordinate to a chromophore.^[96] The obtained difference spectra for the conjugate addition reaction catalyzed by **4a/4a'** in different solvents revealed that the absorbance maximum changes from 490 nm in aprotic solvents to 480 nm in protic solvents. Although the peak is of rather low intensity, such a shift indicates a coordination of the protic solvent to the nitronate species.

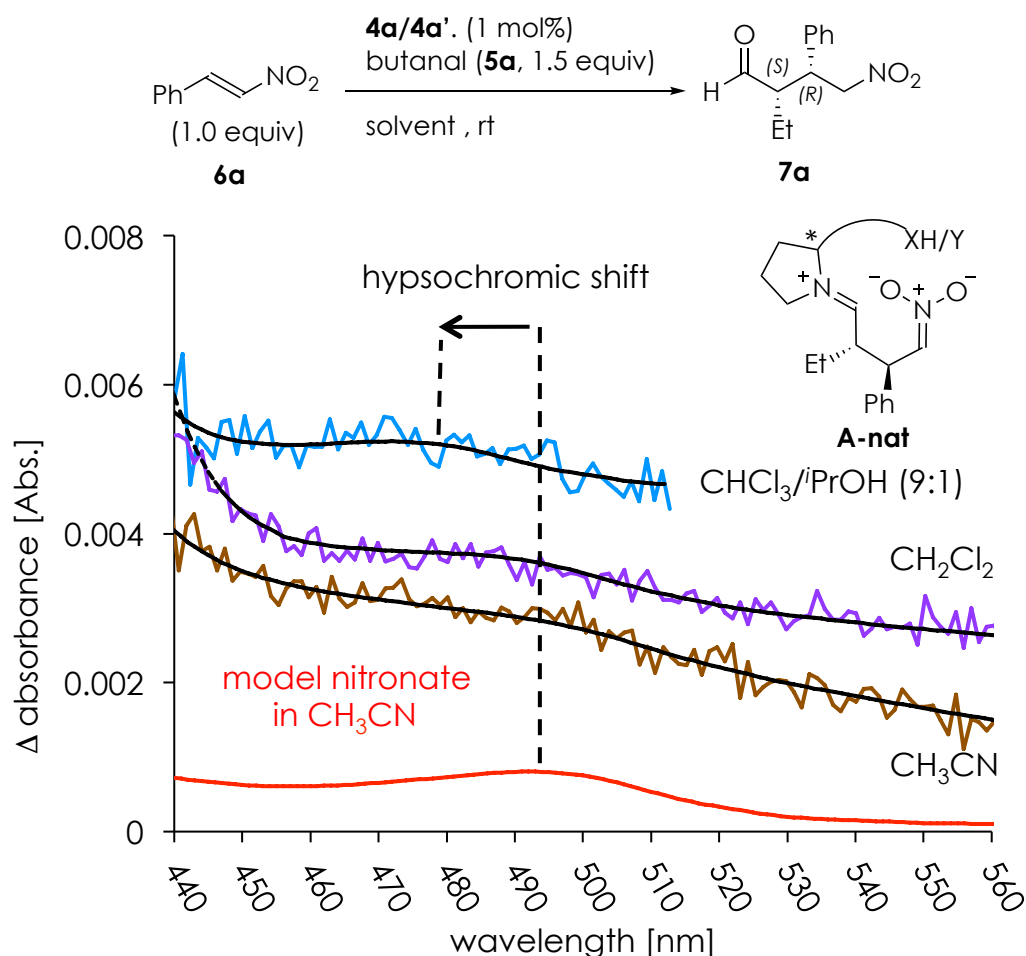


Figure 3-6: UV/Vis difference spectrum of the nitronate/oxazine *N*-oxide when using catalyst **4a/4a'**. The spectrum was obtained by subtraction of a spectrum after 5 s from a spectrum after 2 s. For a better comparison the spectrum of the nitronate model compound **8a** (red) was introduced with reduced intensity.

3.4 Conclusion

In this project we investigated the reaction mechanism of conjugate additions of aldehydes to nitroolefins with the structure of secondary amine-based catalysts. Although an iminium nitronate is widely accepted as the first reaction intermediate after the carbon-carbon bond formation, an *in situ* observation has remained elusive. Since detection via NMR spectroscopy has proven to be difficult, we focused our investigations on UV/Vis spectroscopic monitoring. Searching for isolated UV/Vis bands of nitronates, we found a previously unreported band around 500 nm. Computational studies assigned this wavelength to an excitation of a nitronate HOMO orbital, but also revealed that a cyclic oxazine *N*-oxide, which has been proposed as an alternative structure resulting from the carbon-carbon bond

formation, has a similar UV-band. In either case however, we identified a characteristic UV band for the intermediate resulting from the carbon-carbon bond formation.

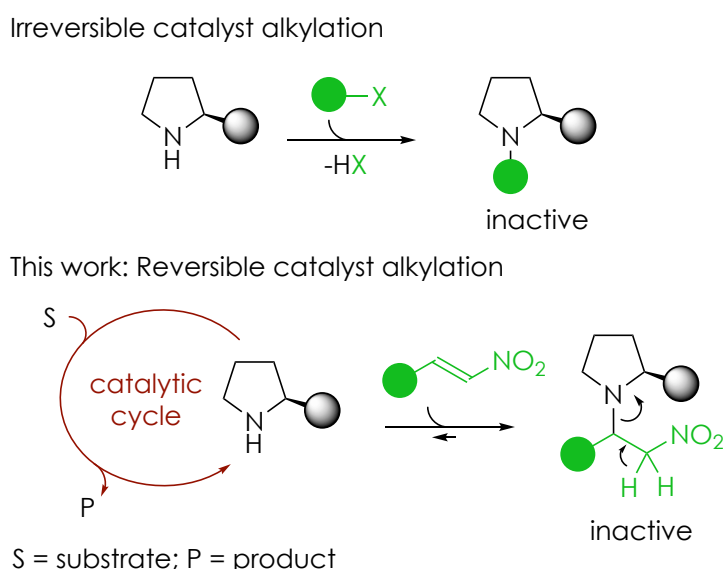
We then identified such a nitronate/oxazine *N*-oxide structure under reaction conditions by UV/Vis stopped-flow measurements and investigated its relative occurrence in the steady-state. Depending on catalyst stabilization, the reaction pathway either is on-cycle (when stabilized by acid containing catalyst) or off-cycle (when insufficiently stabilized by catalyst lacking an acid). Within these measurements, the acid containing peptidic catalyst H-DPro-Pro-Glu-NH₂ (**4a**) provided the highest nitronate concentration compared to the acid lacking peptide congener or to prolinol silyl ethers. The relative stabilization by H-DPro-Pro-Glu-NH₂ (**4a**) is increased in protic solvents and lowered in non-protic ones. These results may further contribute to explain why H-DPro-Pro-Glu-NH₂ is such an exceptional catalyst in protic solvents. Currently, *in silico* studies to determine a reaction profile of the conjugate addition reaction of aldehydes to nitroolefins for the different catalysts are ongoing in our laboratories.

4

Catalyst Deactivation by
Electron Deficient Nitroolefins

4.1 Background

The nucleophilic activation of carbonyl compounds via enamines is a powerful strategy in modern asymmetric synthesis (Chapter 1.2).^[3,11] Yet, despite widespread use, this methodology is challenging with some very highly reactive electrophiles which can deactivate the amine-based catalyst via direct alkylation reaction.^[66,97,98] When the alkylated species contains an acidic β -hydrogen an elimination reaction is facilitated, making the undesired reaction of the catalyst reversible (Scheme 4-1).^[99] Catalyst alkylation limits the development of catalytic reactions and therefore a general mechanistic understanding on its occurrence is highly desirable. In order to contribute to this challenging research area, we have explored the influence of catalyst deactivation pathways on the conjugate addition reaction between aldehydes and nitroacrylates.



Scheme 4-1: Influence of catalyst alkylation on reactivity.

The remarkable reactivity of nitroacrylates towards secondary amines is well-established and has been widely applied in synthesis (Chapter 1.2.2.5).^[90,100-102] Despite the strategic synthetic value of nitroacrylates, such as the elegant total synthesis of the antiviral drug (–)-oseltamvir,^[28,62] this class of substrates have rarely been successfully used as electrophiles in asymmetric aminocatalysis.^[103] Preliminary observations by Hayashi and Seebach have shown that chiral, bulky secondary amine catalysts are also prone to be alkylated under catalytic conditions.^[62,65] Therefore, we envisioned that the

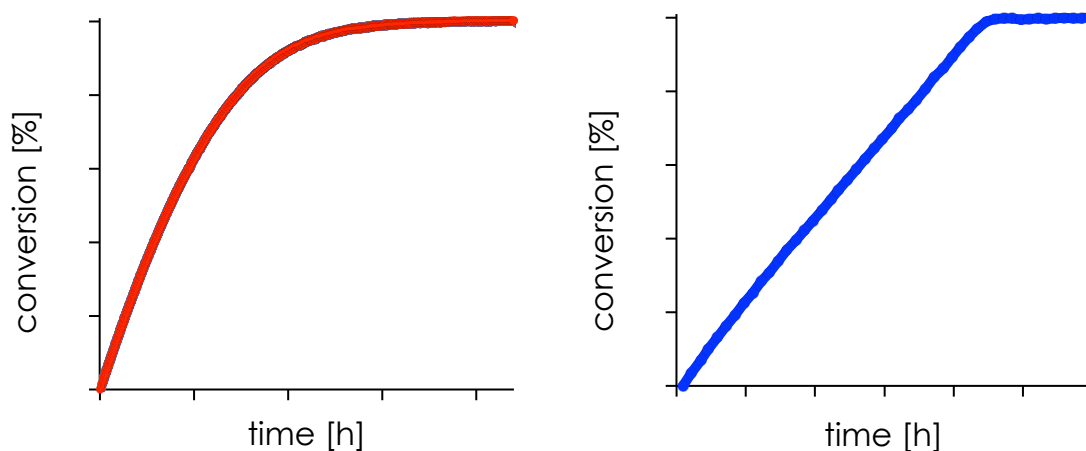
conjugate addition reaction of aldehydes to nitroolefins catalyzed by secondary amines could be a useful model system to explore the impact of competing alkylation on aminocatalysis.

The mechanism of conjugate addition reaction of aldehydes to nitroalkenes has been deeply studied and therefore it represents an optimal ground for the investigations of challenging substrates (see Chapter 1.3).^[45,52,65,70,71,73,78,79] The most effective and selective catalysts are sterically hindered diphenylprolinol derivatives (*i.e.* “Hayashi-Jørgensen catalyst” **3**)^[30,37] as well as the tripeptidic catalyst H-DPro-Pro-Glu-NH₂ **4a** (Chapter 1.2.2).^[45,78,79,104] Previous mechanistic studies allowed the identification of highly reactive catalysts and provided improved conditions for the catalytic process.

Herein, we present our studies on reversible alkylation of secondary aminocatalysts in the presence of electron-deficient nitroalkenes.

4.2 Initial Experiments

At the onset of our investigation, we focused our attention on a kinetic analysis of the conjugate addition of butanal **5a** to methyl nitroacrylate **9a**. As shown in Chapter 1.3, the rate-limiting step depends on the availability of an acid in the catalyst and is either the carbon-carbon bond formation or the protonation. Which one becomes rate limiting depends on the availability of an intramolecular acid within the catalyst. When using the acid bearing H-DPro-Pro-Glu-NH₂ **4a** as a catalyst the rate limiting carbon-carbon bond formation leads to an exponentially decreasing reaction rate (Scheme 4-2, left). With secondary amine-based catalysts that lack a proton donor, the rate limiting step is the protonation. In a direct comparison of a peptidic catalyst bearing a methyl ester instead of a carboxylic acid moiety, a linear reaction profile and slower conversion was observed.^[105] The linear reaction profile shows that neither the aldehyde nor the nitroolefin are involved in the rate-determining step of the reaction.^[52,65,71,79]



Scheme 4-2: Schematic kinetic profiles when using a catalyst with an acid moiety (red) or without an acid (blue).

Using *in situ* IR-spectroscopy, we monitored the reaction progress of the conjugate addition of butanal **5a** to methyl nitroacrylate **9a** (Figure 4-1) in the presence of H-DPro-Pro-Glu-NH₂ **4a** or prolinol-silyl ether **3** with chloroacetic acid as cocatalyst.^[28,63] These experiments showed that despite the potential catalyst alkylation, both catalysts are active and peptidic catalyst **4a** significantly outperforms the prolinol derivative **3** ($\text{TOF}_A = 0.185 \text{ s}^{-1}$; $\text{TOF}_B = 0.032 \text{ s}^{-1}$).^[106] Using 1 mol% of catalyst **4a**, full conversion to the product

10a was observed within 10 min, and the product was isolated in 98% yield with a diastereoselectivity of > 25:1 (syn : anti, for x-ray see Chapter 7.11) and 85% ee. Importantly, an atypical reaction profile (s-shape) was observed for catalyst **4a**: the kinetic profile is not nearly as curved as previously observed for reactions involving e.g. nitrostyrene but flat and s-shaped. This suggests that the reaction path differs when activated nitroolefins are employed.

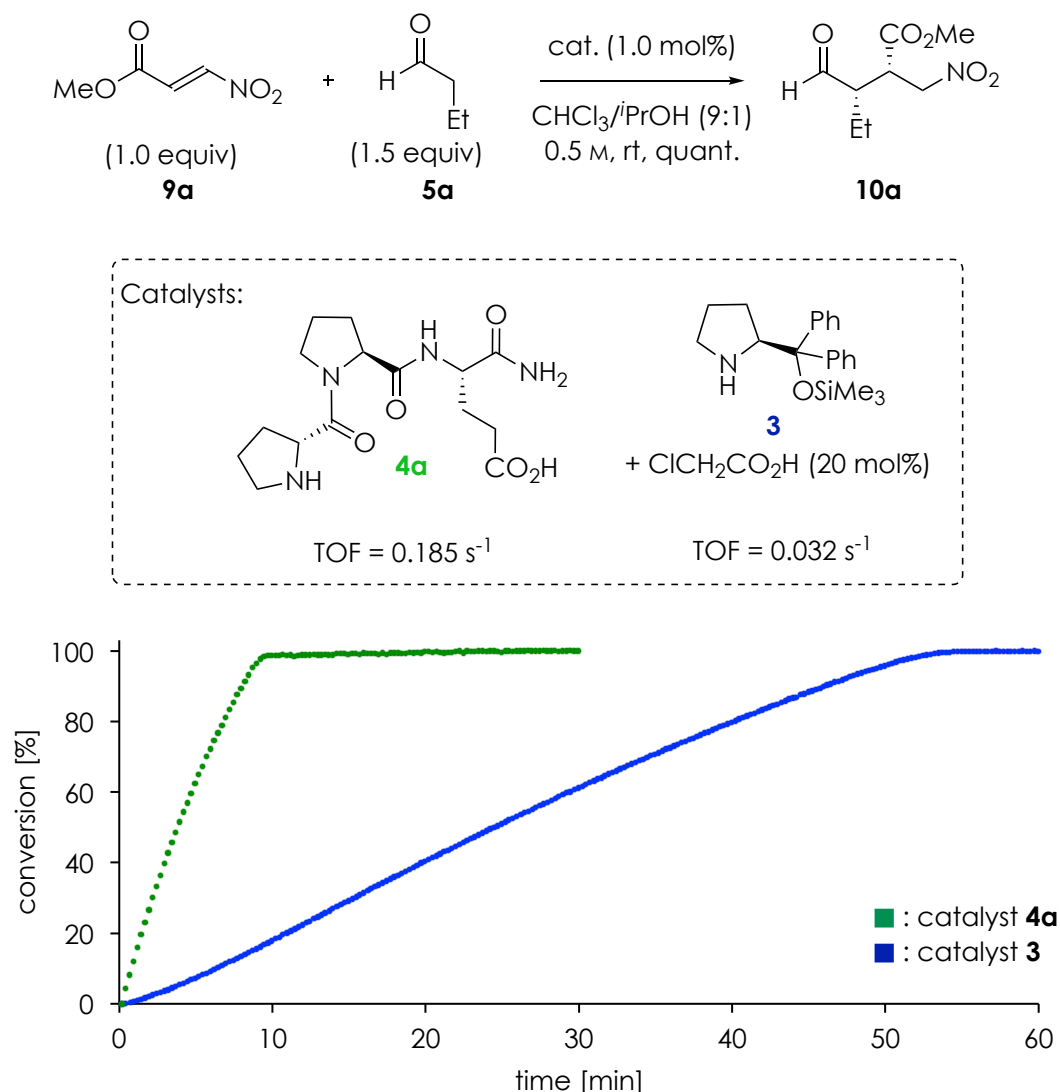
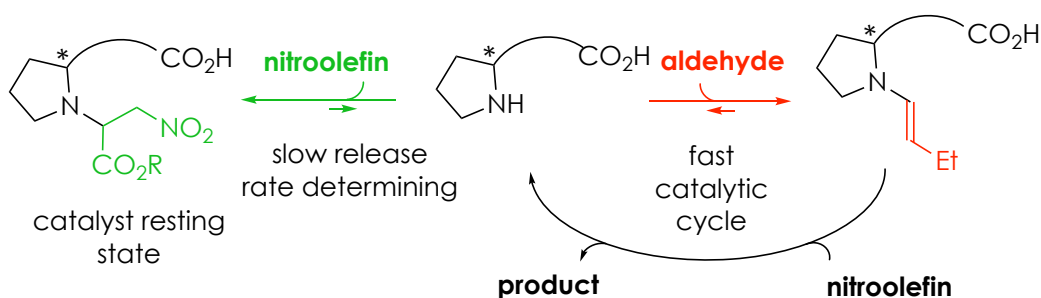


Figure 4-1: Enantioselective secondary amine-catalyzed addition of butanal to methyl nitroacrylate. Product formation monitored by *in situ* IR spectroscopy at 1563 cm⁻¹. The conversion was determined by ¹H-NMR spectroscopy. TOF = turnover frequency.

We hypothesized that the catalyst might react with the nitroacrylate reversibly. As shown in Scheme 4-3, the equilibrium between the reactive enamine and the alkylated catalyst might predominantly lie on the side of this inactive state, thus decelerating the catalytic turnover. In this case the

“adduct” between the catalyst and the nitroacrylate would be the resting state and the release of the catalyst from the adduct would be the rate determining step of the reaction. The reaction rate would not depend on the concentration of the two substrates (**9a** and **5a**) as long as the catalyst is alkylated.

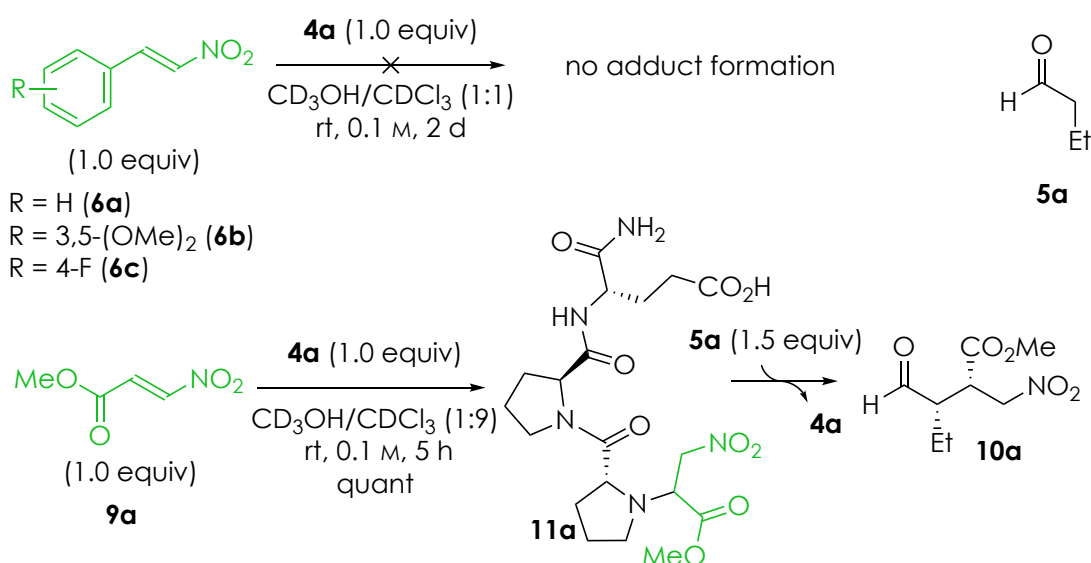


Scheme 4-3: Alkylated catalyst as an off-cycle resting state.

4.3 Reversible Catalyst Alkylation

4.3.1 Alkylation of the Peptidic Catalyst by Different Nitroalkenes

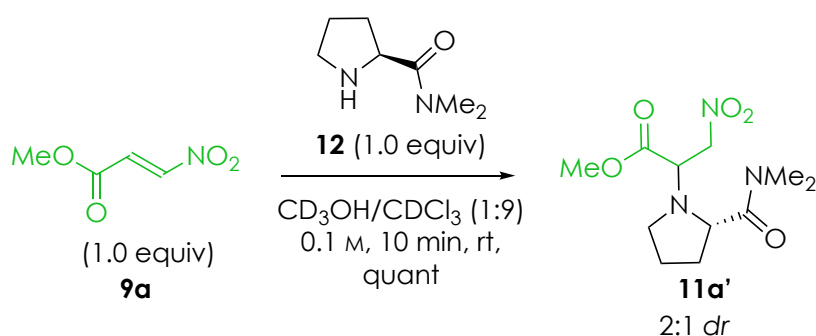
We investigated the formation of the putative “adduct” between the catalyst and the nitroacrylate by reacting the peptidic catalyst with different nitroolefins in stoichiometric amounts. These reactions were monitored by NMR spectroscopy and designed to evaluate the influence of nitroolefins with different electronic properties on the alkylation of the catalyst (Scheme 4-4). The studies showed that peptide **4a** reacts with methyl nitroacrylate **9a**



Scheme 4-4: Alkylation of tripeptidic catalyst **4a** with nitroalkenes monitored by $^1\text{H-NMR}$ spectroscopy (disappearance of olefinic signal between 7.00 ppm and 7.50 ppm).

to adduct **11a** within 5 h (concentration: 0.1 M in CDCl₃/CD₃OH, 9:1) whereas no reaction was observed with any of the evaluated nitrostyrene derivatives **6a**, **6b** or **6c** under the same conditions.

These results support the hypothesis that originated from the kinetic analysis of the catalytic reactions: peptide alkylation does not occur with moderately reactive nitroolefins but with electron-deficient nitroacrylates. Next, we probed the reversibility of the adduct formation. Therefore we added butanal **5a** to the preformed adduct **11a**. This led to the formation of product **10a** (in analogy to the use of prolinol silyl-ether catalysts by Seebach^[65]). Since product formation must occur via the free amine and the nitroacrylate, this experiment confirmed that alkylation is reversible and the active catalyst can be released. Unfortunately, the mixture of diastereoisomers and rotamers of the adduct **11a** was too complex to allow a spectroscopic characterization of the formed adducts. Therefore, the same experiments were performed with H-Pro-NMe₂ **12** as a model system which allowed for the unambiguous assignment of the chemical structure (Scheme 4-5).



Scheme 4-5: Secondary amine alkylation model system.

4.3.2 Tuning the Reactivity by Exploring the Alkylation Process

Before optimizing the catalytic process we aimed to understand the alkylation in the model system. Therefore, we focused on the elucidation of the steric features of the nitroacrylate, which affect the alkylation process. We envisioned that by disfavoring catalyst alkylation, or by favoring the release of the active catalyst from the adduct, the desired conjugate addition reaction could be accelerated. For this reason, nitroacrylates with differently substituted ester moieties (Me, *i*Pr, *t*Bu) were prepared and the corresponding reactions with catalyst **4a** were monitored by ¹H-NMR spectroscopy to evaluate the relative alkylation rates (Figure 4-2).

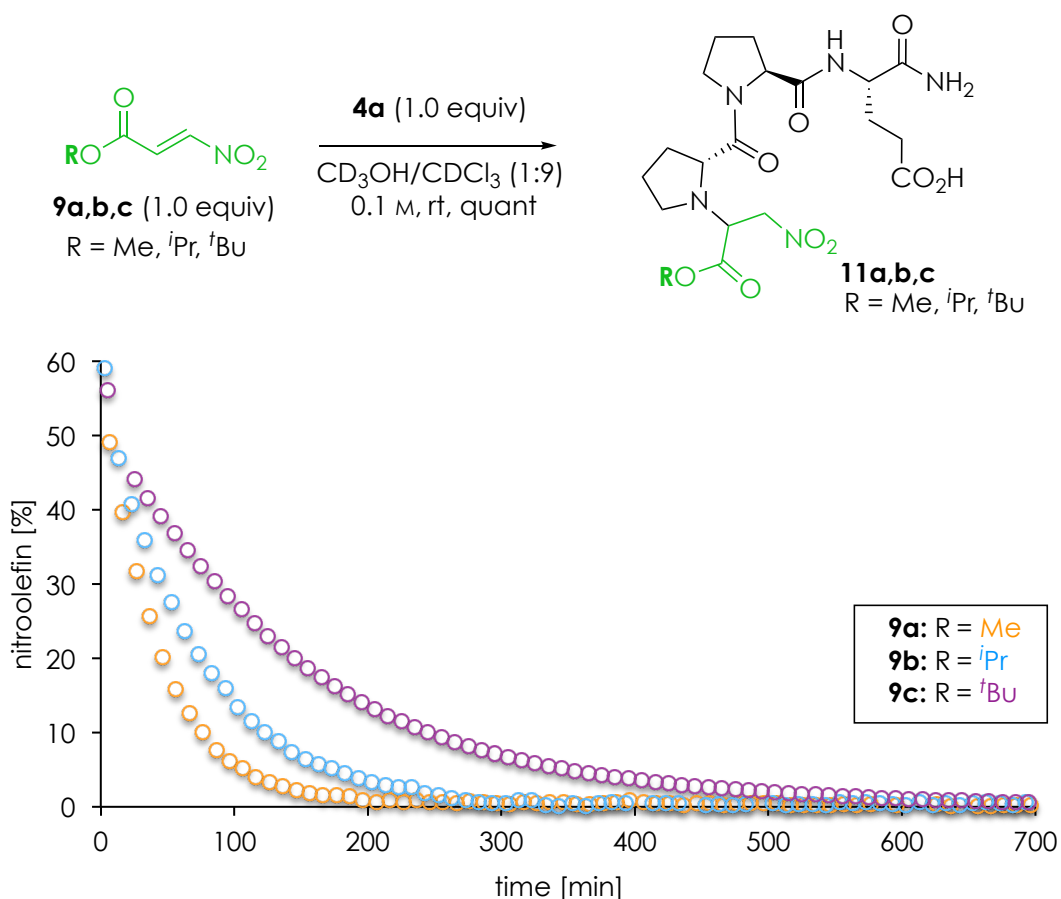


Figure 4-2: Steric influence of the nitroacrylate substrate on the alkylation of catalyst **4a** monitored by *in situ* $^1\text{H-NMR}$ spectroscopy. The remaining nitroolefin content was determined by comparison of the integrated olefinic signal at 7.53 ppm and an external standard ($\text{C}_2\text{H}_2\text{Cl}_4$)

The adduct formed by the nitroacrylate bearing a *tert*-butyl ester formed slowest followed by the *iso*-propyl and methyl derivatives. Thus, these experiments revealed a correlation between the steric bulk of the ester moiety of the nitroacrylate and the reaction rate. In accordance with the *Bell-Evans-Polanyi* principle,^[107,108] this result suggests that adducts bearing bulky residues are thermodynamically less favored. Therefore the corresponding elimination of adducts to the catalyst is a faster kinetic process in comparison to less bulky ester bearing adducts. Hence, the rate of the aminocatalytic reaction should increase by increasing the steric demand of the nitroacrylate. In order to investigate this somewhat counterintuitive hypothesis “*the bulkier, the faster*”, the Michael addition of butanal (**5a**) to nitroacrylate **9a-c** was studied using peptide **4a** as catalyst. Indeed, the size of the ester moiety was found to significantly influence the reaction progress (Figure 4-3). The most sterically hindered substrate **9c** provided an

extraordinary high reactivity (quantitative conversion, 4.5 min, TOF = 0.370 s⁻¹), outperforming less bulky substrates (**9b**, TOF = 0.278 s⁻¹; **9a**, TOF = 0.185 s⁻¹). It is noteworthy that the steric hindrance was also found to have a remarkable influence on the stereoselectivity of the transformation. Product **10c** was obtained with an enantiomeric excess of 93% ee, compared to 85% ee and 82% ee observed for **10a** and **10b** with the methyl and *iso*-propyl residue, respectively.

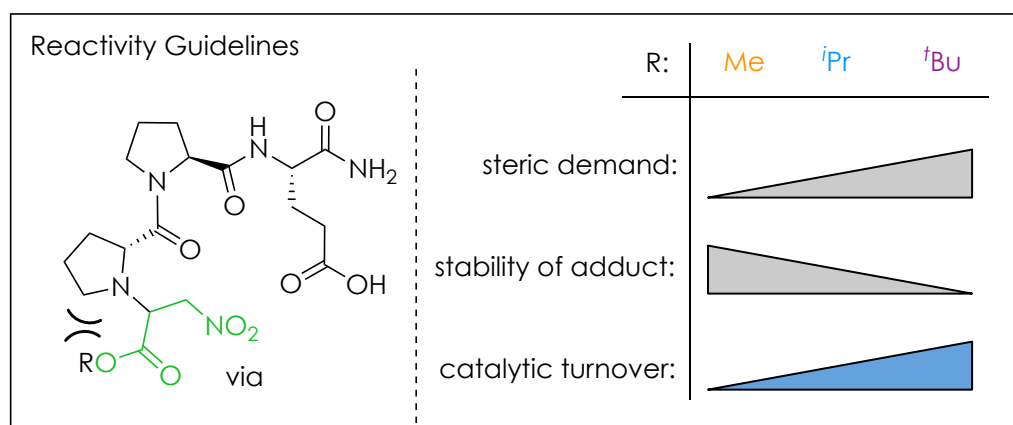
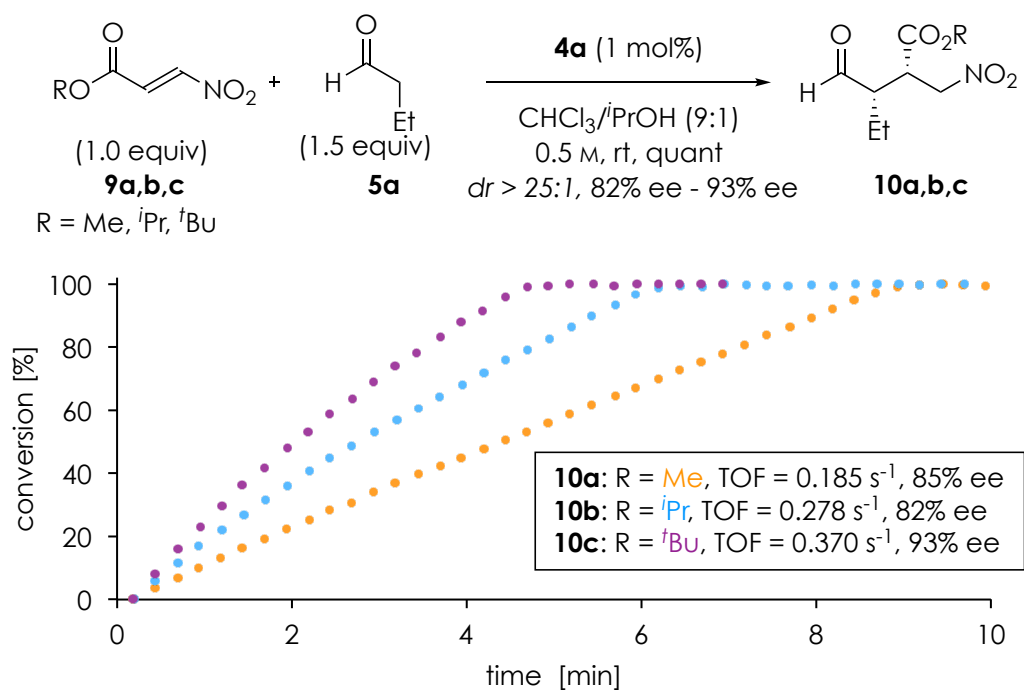
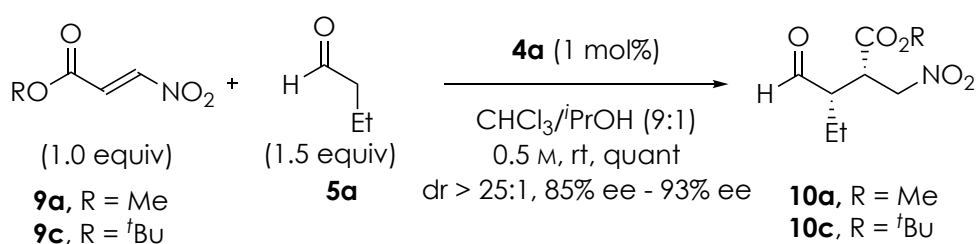


Figure 4-3: Kinetic study on the alkylation of tripeptidic catalyst **4a** with different nitroacrylates. Product formation was monitored by *in situ* IR spectroscopy at 1563 cm⁻¹. The conversion was determined by ¹H-NMR spectroscopy. Additionally reactivity guidelines are provided regarding steric demand and catalytic turnover. TOF = turnover frequency.

4.3.3 Catalytic Cycle: Kinetic vs. Thermodynamic Control

The experiments so far showed that the rate of amine-catalyzed reactions between aldehyde and nitroacrylates is influenced by the alkylation of the catalyst. A competition between enamine formation and catalyst alkylation occurs with both reactions being reversible. As shown in the NMR studies, the deactivation of the catalyst is thermodynamically favored over the free catalyst in the presence of a nitroacrylate (Figure 4-2). We envisioned that a faster catalytic turnover might be obtained by forming the enamine species before adding the nitroacrylate. We therefore explored the influence of the sequence of addition for the reactants and the catalyst on the reaction progress. The catalytic reaction was performed by either adding the aldehyde to the preformed alkylated catalyst (mixture of catalyst and nitroacrylate, "thermodynamic control", Figure 4-4) or by adding the nitroacrylate to a mixture of the preformed enamine (mixture of catalyst and aldehyde, "kinetic control", Figure 4-4).



Different reaction setup:

kinetic control - addition sequence: **5a + 4a** then **9**

thermodynamic control - addition sequence: **9 + 4a** then **5a**

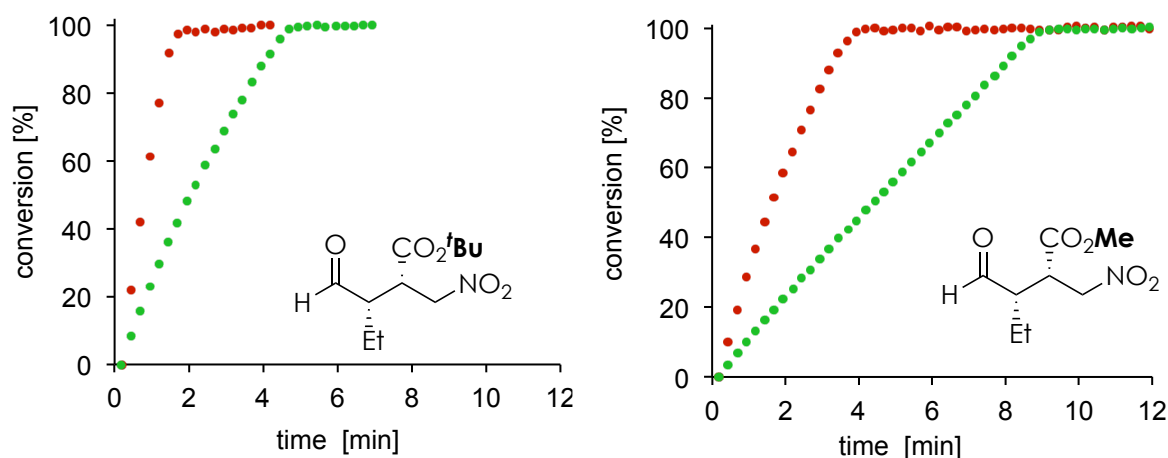


Figure 4-4: Catalytic Michael reaction under "kinetic" (red) and "thermodynamic" (green) control. Product formation was monitored by *in situ* IR spectroscopy at 1563 cm⁻¹. The reaching of full conversion was confirmed by ¹H-NMR spectroscopy.

These experiments showed for all reaction setups a slightly bent reaction curve that differs on the addition sequence. Setting up the reaction under “kinetic control”, the reaction with nitroacrylate **9c** gives the product in quantitative yield, dr > 25:1 and 93% ee within two minutes (TOF = 0.833 s⁻¹) while a reaction setup under “thermodynamic control” the reaction needs almost five minutes until completion (TOF = 0.370 s⁻¹). When using the smaller congener **9a**, the rate was reduced by half (TOF = 0.417 s⁻¹ vs TOF = 0.185 s⁻¹) as compared to the corresponding reaction rate with **9c**. The non-parallel reaction curves suggested that under these conditions the alkylation of the catalyst is diminished and the catalytic cycle experiences a different rate-limiting step.

Since the reaction mechanism should not differ on the addition sequence, we assumed that in prolonged reaction times a shift from the kinetic to the thermodynamic control should be observed. In order to further elucidate this, we investigated how many turnovers the catalyst can perform before reaching the thermodynamic steady state. In order to elucidate this transition, we aimed to increase the turnover number (TON) to give the

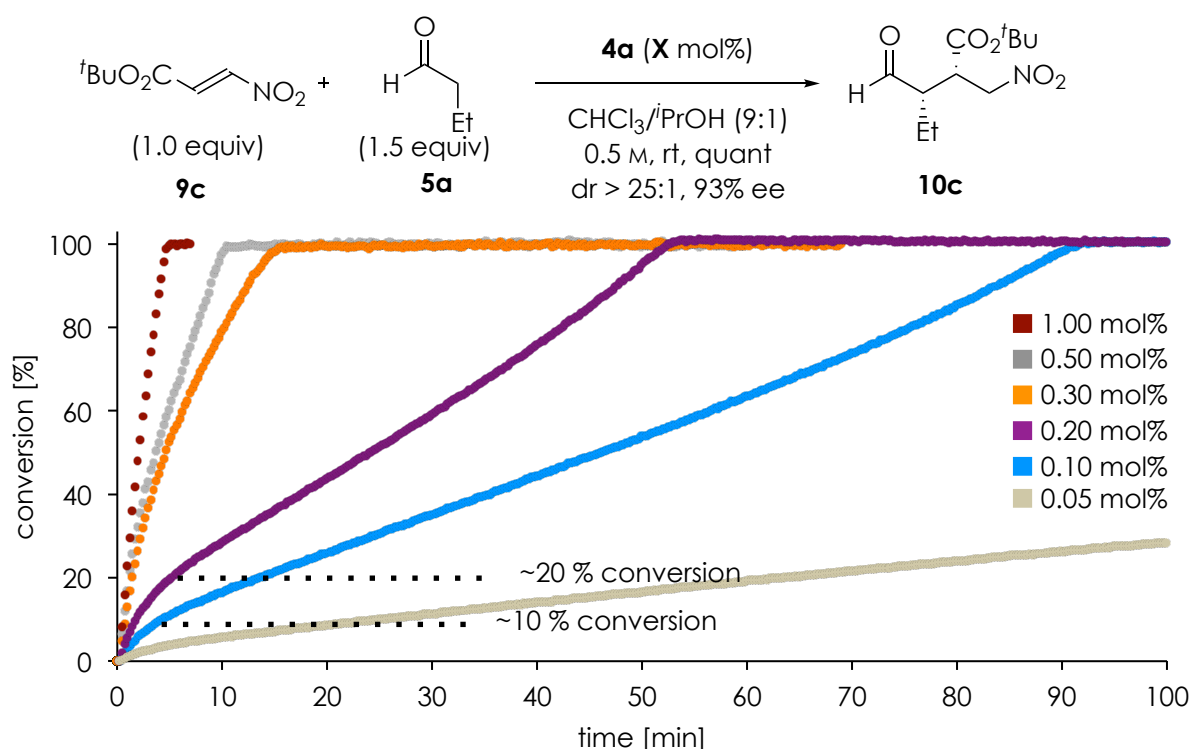


Figure 4-5: Influence of catalyst loading on reaction profile with premixing of **4a** and **5a** for 5 min before addition of **9c**. 0.05 mol% full conversion in 12 h. Product formation was monitored by *in situ* IR spectroscopy at 1563 cm⁻¹. The reaching of full conversion was confirmed by ¹H-NMR spectroscopy.

system more time to equilibrate. Therefore, we explored the reaction at lower catalyst loadings (1.0 to 0.05 mol%, Figure 4-5). The reactions were set up under kinetic control (preformed enamine). The resulting time-conversion plots show an initial accelerated phase followed by a slower and almost linear steady state, thus revealing a change of mechanism during the reaction progress. This result provides a mechanistic scenario in which initially the reaction rate is determined by the productive pathway via the enamine. Later, the rate-limiting step is the release of the alkylated catalyst. In the early stages, the system is under kinetic control and after several catalytic cycle (conversion divided by catalyst loading ~ approximately 100 turnovers) the alkylated catalyst is fully formed and represents an off-cycle resting state.

4.3.4 Steady State and Identification of an Aldol Cocatalyst

In order to further elucidate the steady-state at different addition sequences we used 0.2 mol% of the catalyst **4a** due to its visible steady state and relatively fast reaction time. We applied all of the three possible addition sequences at 0.2 mol% catalyst loading. When performing the alkylated catalyst, the transformation proceeded with a constant rate throughout the reaction time (Figure 4-6, I, green plot). When adding the catalyst at last to the mixture of the two substrates, an initial accelerated phase was observed before a more close to linear reaction rate is reached (Figure 4-6, II, blue plot). The two time-conversion profiles are parallel, which suggests that the two reactions have the same rate-limiting step. In contrast, when adding the nitroacrylate last to a mixture of the aldehyde and the catalyst, a different reaction progress was observed (Figure 4-6, III, red plot). The initial acceleration phase, which represents the reaction under kinetic control, perfectly overlays with the plot previously observed when the catalyst is added last (Figure 4-6, II, blue plot), yet the steady state curve that follows exhibits instead a slightly higher rate. The nearly linear shape suggests that the thermodynamic regime is reached and that also in this experiment the alkylated catalyst is an off-cycle resting state. Nevertheless, the steeper slope indicates an additional, unknown effect on the rate-determining step (*i.e.* faster release of the active catalyst).

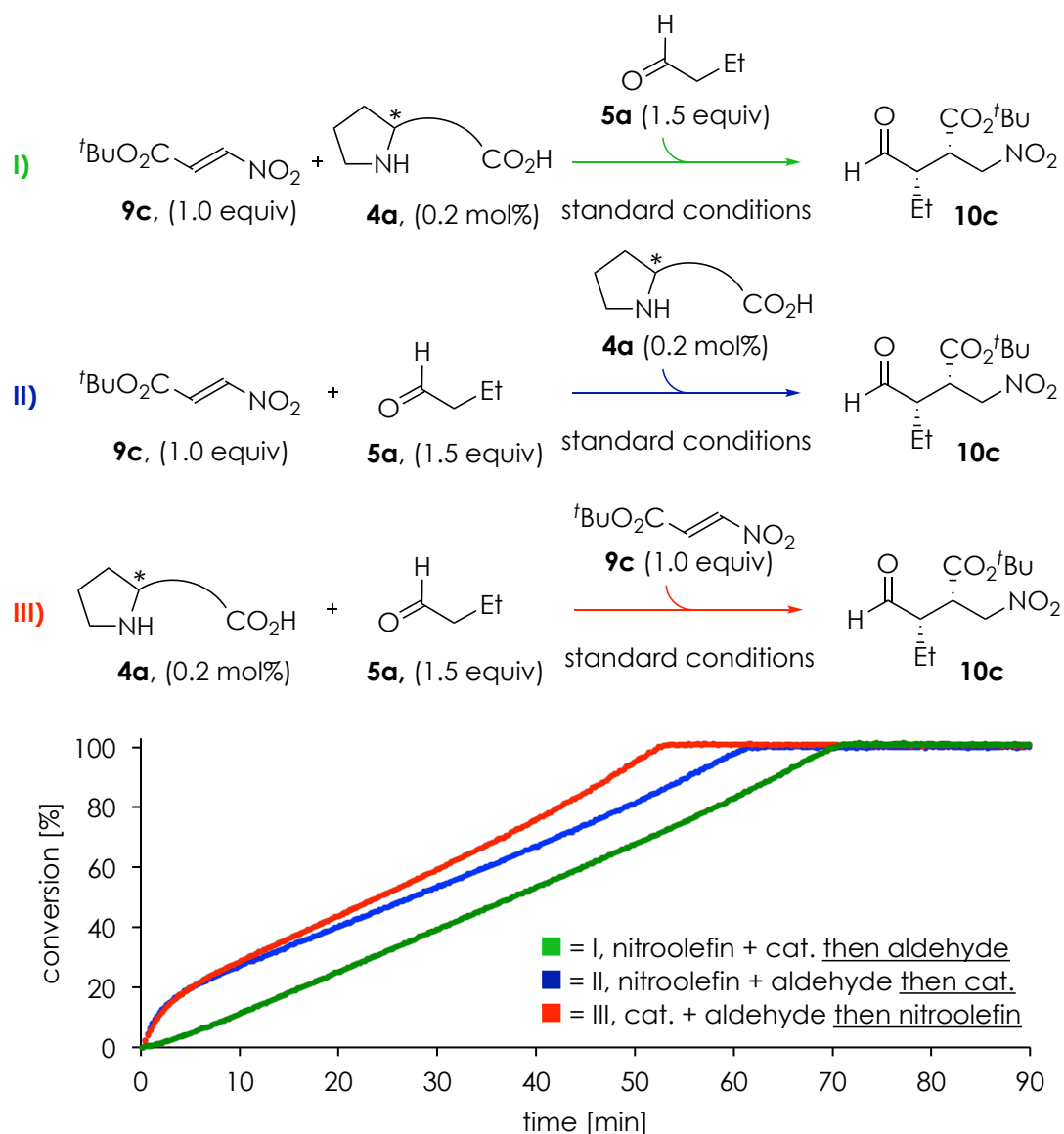
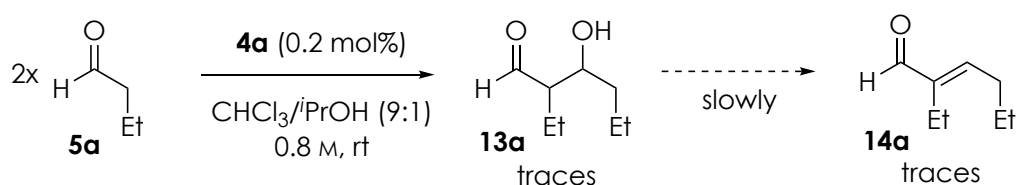


Figure 4-6: Different reaction profiles depending on the order of substrate addition at 0.2 mol% catalyst loading. Product formation was monitored by *in situ* IR spectroscopy at 1563 cm^{-1} . The reaching of full conversion was confirmed by $^1\text{H-NMR}$ spectroscopy. Standard conditions: $\text{CHCl}_3/\text{iPrOH}$ (9:1), 0.5 M, rt.

In order to elucidate the origin of this effect, we explored the reaction between the catalyst and the aldehyde in the absence of the nitroalkene. As previously shown by our group, peptide catalyst **4a** is highly selective for 1,4-addition reactions versus homoaldol byproducts, which can form in trace amounts (Figure 4-7a). Yet, in the absence of a Michael acceptor, peptide **4a** can promote this 1,2-addition, but slowly. In order to elucidate whether a putative homoaldol product is responsible for the change in the reaction rate profile we performed the reaction with different preexposure times (5min,

10min and 30min) of the catalyst **4a** (0.2 mol%) and the aldehyde **5a** (Figure 4-7b). The profiles of the conversion vs. time show that different premixing times of the catalyst and the aldehyde have a significant effect on the rate profile of the reaction. The fastest rate was observed with a premixing time of 10 min. This finding suggests that the homoaldol and/or the aldol condensation product effect the rate of the 1,4 addition reaction. As the homoaldol product forms first, it likely enhances the reaction rate (5 min, 10 min), whereas the condensation product might form a stable α,β -unsaturated iminium catalyst species.

a) Homoaldol side reaction:



b) Enamine preformation:

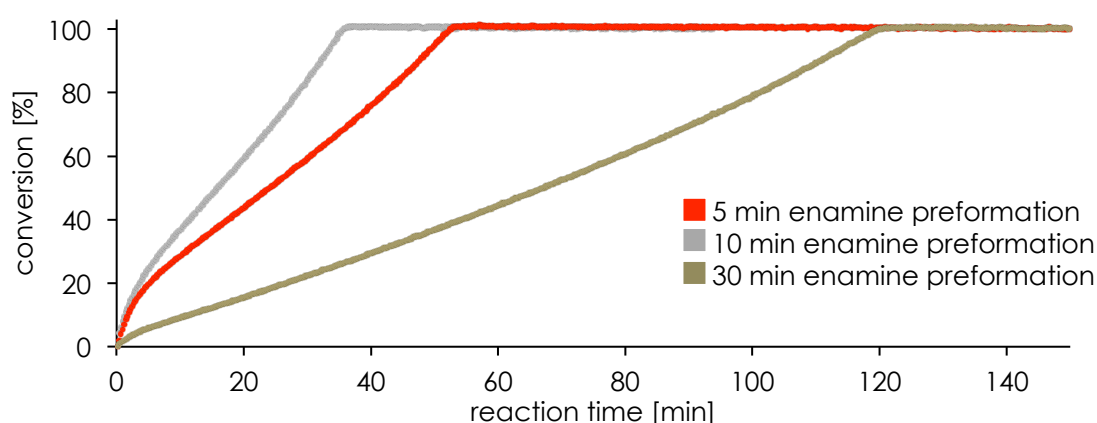
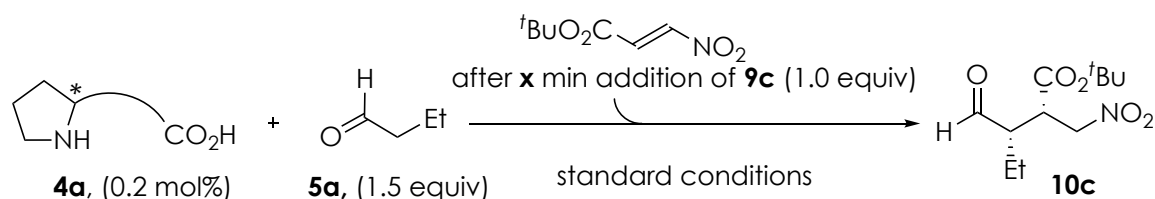


Figure 4-7: Influence of enamine preformation on the overall reaction progress. Product formation was monitored by *in situ* IR spectroscopy at 1563 cm^{-1} . The reaching of full conversion was confirmed by $^1\text{H-NMR}$ spectroscopy. Standard conditions: $\text{CHCl}_3/i\text{PrOH}$ (9:1), 0.5 M, rt.

Previous studies for proline-based aminocatalytic transformations of azodicarboxylates to aldehydes by Blackmond and McQuade have shown a similar effect where additives with an acceptor-donor hydrogen bonding network accelerate the release of an off-cycle catalyst-substrate adduct.^[109,110]

We therefore explored the role of products from aldol reactions and performed the conjugate addition reaction in the presence of catalytic amounts (0.2 mol%) of the aldol model compounds 4-hydroxy-4-methylpentan-2-one (**13b**) and 3-methylbut-2-enal (**14b**) (Figure 4-8). These experiments showed that the aldol product **13b** accelerates the reaction whereas the aldol condensation product **14b** slows the reaction rate down. The latter finding can be rationalized with the formation of a more stable iminium compound by condensation of catalyst **4a** and **14b**. The addition of the achiral aldol **13b** did not affect the stereoselectivity of the reaction. Further experiments are necessary to explore whether enantiomerically enriched aldol products derived from butanal that form in the catalytic

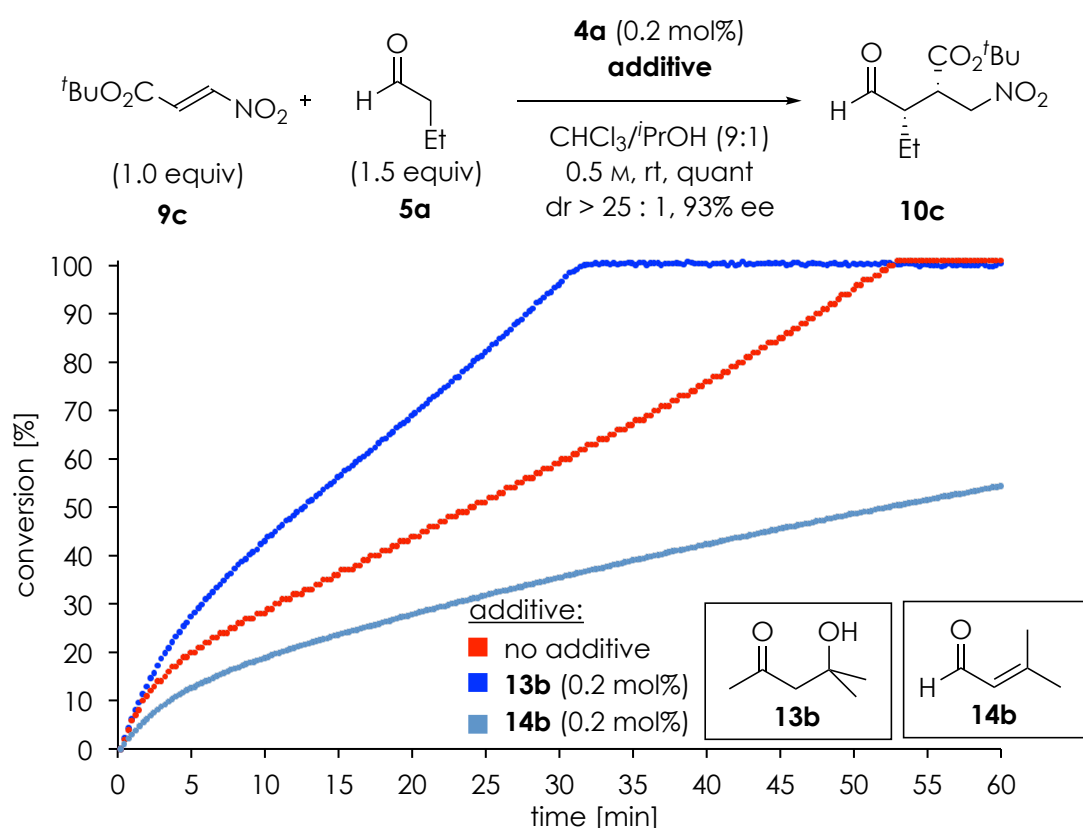
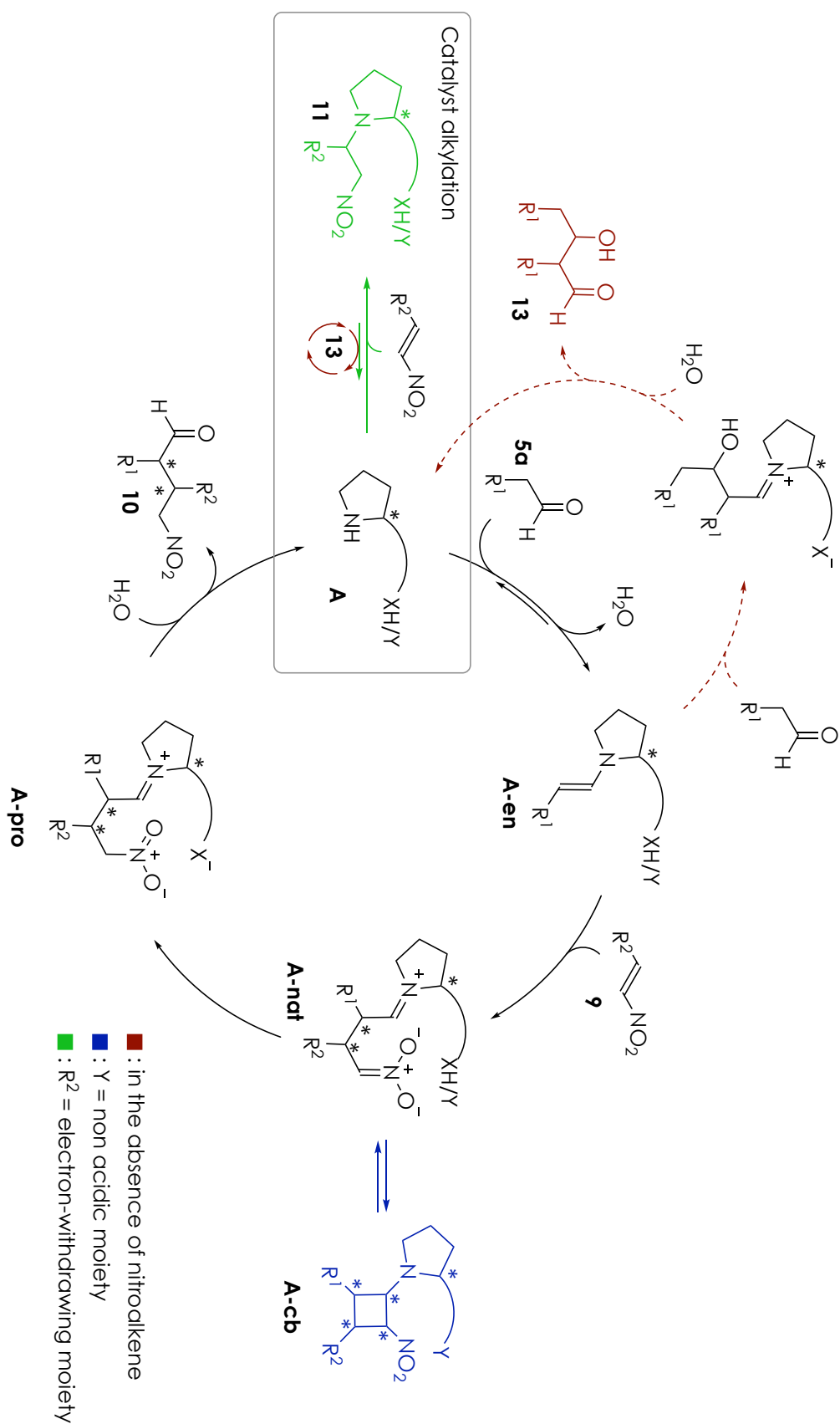


Figure 4-8: Reaction profile depending on additive. Product formation was monitored by *in situ* IR spectroscopy at 1563 cm⁻¹. The conversion was determined by ¹H-NMR spectroscopy.

reaction affect the stereoselectivity. We hypothesize the acceleration occurs through a non-covalent interaction via H-bonding that accelerates the release of the catalyst or an equilibrium between the catalyst and **13b** that prevents the catalyst alkylation.

4.3.5 Revised Catalytic Cycle and ppm-Level Catalysis

Investigations showed that the size of the ester moiety of nitroacrylates, the addition sequence and homoaldol products influence the overall rate of reactions when the secondary amine catalyst is reversibly alkylated by nitroacrylates. The studies allowed a detailed depiction of the catalytic cycle for the aminocatalytic 1,4-addition of aldehydes to nitroalkenes (Scheme 4-6). These insights enabled reactions with 0.2 mol% of catalyst to complete within 32 min. This is an outstanding result for an organocatalytic reaction with chiral amines. The mechanism is governed by a competitive equilibrium between enamine formation and alkylation of the catalyst. Under “thermodynamic conditions” the off-cycle intermediate **11** is the resting-state as the release of the catalyst is slow and rate determining. The steric demand of the nitroacrylate can be used to either favor or disfavor the alkylation of the catalyst and thereby accelerate or decelerate the reaction.



Scheme 4-6: Modified catalytic cycle for the conjugate addition reaction of reversibly alkylating nitroolefins to aldehydes.

As mentioned in Chapter 1.2 catalyst loadings of five to ten mol% are despite large efforts in research typical for the conjugate addition reactions of aldehydes to nitroolefins, and reduction of the loading is an important goal, in particular for industrial applications.^[111-113] Therefore, we probed reduced catalyst loadings for the addition of aldehyde to nitroacrylates. The lowest catalyst loading where full conversion was observed is 0.05 mol% (500 ppm). Further, we probed the reaction rate acceleration upon addition of **13b**. Remarkably, the transformation proceeded smoothly and yielded the desired product in quantitative yield and excellent selectivity in 2.5 hours (Figure 4-9, 12 h without additive). By these experiments, we managed to establish an extremely efficient catalytic system. This result showcases how mechanistic investigations can help to design organocatalytic reactions and to access unprecedented levels of catalytic efficiency.

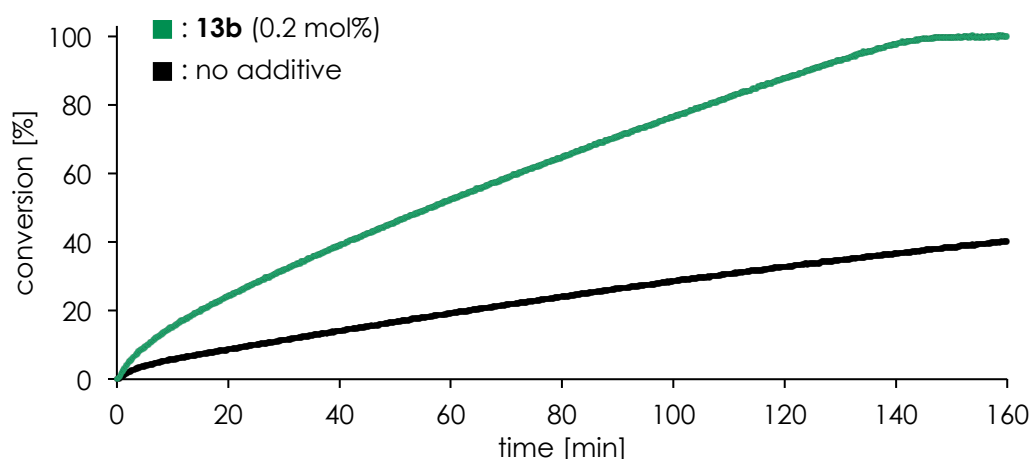
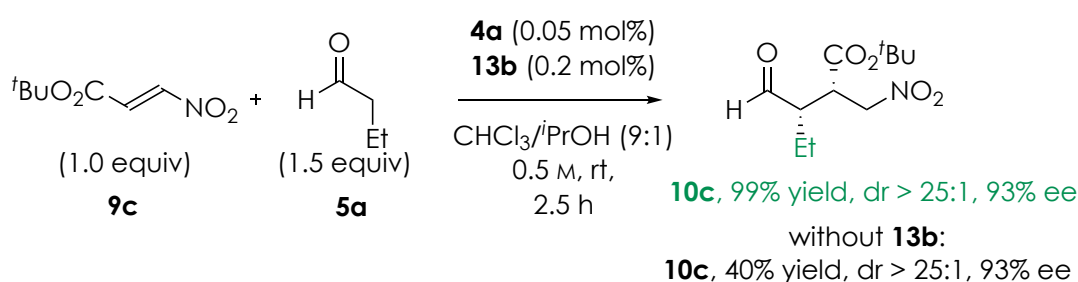
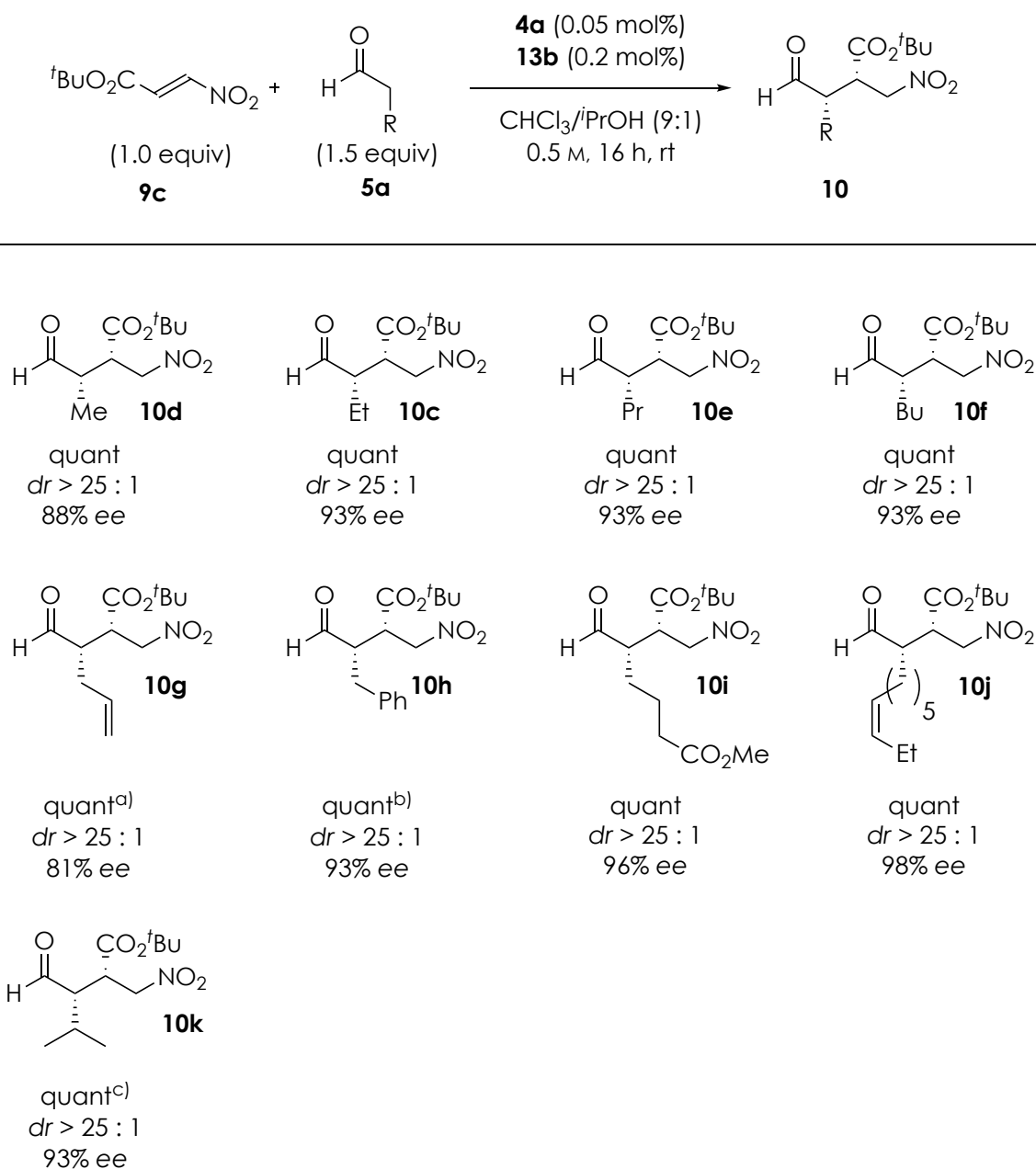


Figure 4-9: Reaction progress when using 0.05 mol% catalyst loading with and without additives. Product formation was monitored by *in situ* IR spectroscopy at 1563 cm^{-1} . The conversion was determined by $^1\text{H-NMR}$ spectroscopy.

4.3.6 Substrate Scope

Having established a catalytic system that allows for an effective transformation using a peptidic catalyst at ppm-level, we further probed its applicability for other substrates. Since the optimal electrophile is the bulky

tert-butyl nitroacrylate (**9c**) we explored reactions of **9c** with different aldehydes (Scheme 4-7). All of the reactions provided the desired product in quantitative yields (isolated > 97%). Products with alkyl substituents of different length (**10c-f**) were obtained with enantioselectivity of 88% - 93% ee. Products with substituents in the γ - or δ -position (**10g, 10h** and **10k**) required longer reaction times but were also isolated with good enantioselectivity (93% ee).



Scheme 4-7: Substrate scope with 0.05 mol% catalyst loading. a) full conversion with 0.2 mol% catalyst, 47% conversion with 0.05 mol% catalyst loading; b) full conversion with 0.2 mol% catalyst loading after 36 h, 15% conversion with 0.05 mol% catalyst loading; c) full conversion with 0.5 mol% catalyst, no conversion with 0.05 mol% catalyst loading.

Other functional groups are tolerated, and γ -nitroaldehydes containing olefinic and ester moieties (**10i** and **10j**) were prepared with enantioselectivities of 96% and 98% ee, respectively.

4.4 Irreversible Catalyst Alkylation

The addition of aldehydes to β -CF₃-substituted nitroolefins in high yields has been challenging.^[26,114,115] We next evaluated whether β -CF₃-substituted nitroolefins also react with the peptidic catalyst under the conditions established for nitroacrylates (Figure 4-10). Using catalyst **4a**, the conjugate addition product of butanal (**5a**) and **15** was obtained in good stereoselectivity (95% ee, 50 : 1 dr) and a yield of 97%. As previously seen for the nitroacrylates, the addition sequence of the reaction pathway plays an important role. Monitoring the reaction progress by *in situ* IR spectroscopy showed a decreasing reaction rate over time for both addition sequences (Figure 4-10).

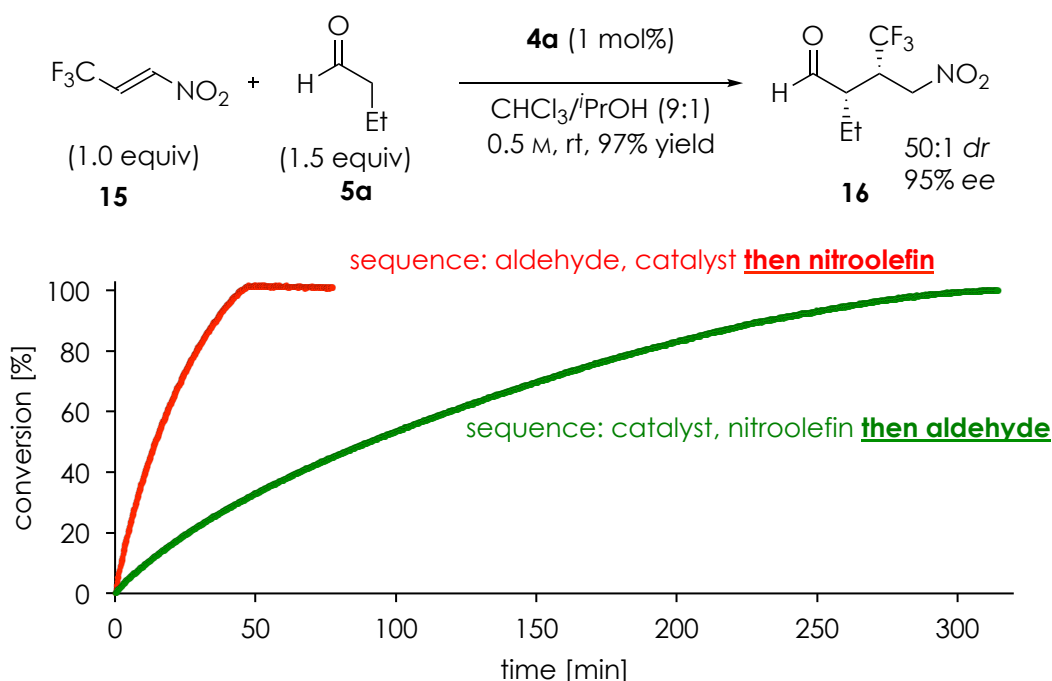
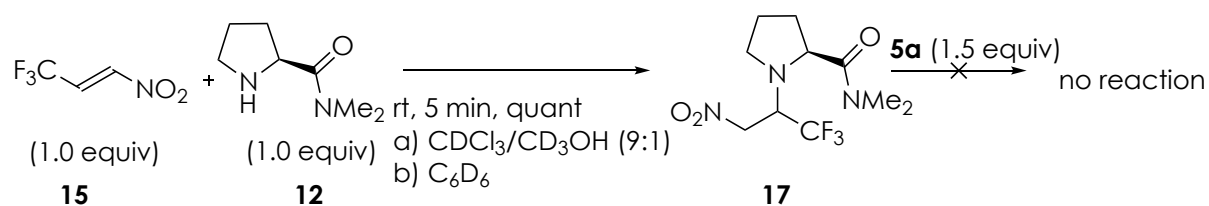


Figure 4-10: Reaction progress of CF₃ substituted nitroolefins depending on the addition sequence of the reactands. Product formation was monitored by *in situ* IR spectroscopy at 1563 cm⁻¹. The conversion was determined by ¹H-NMR spectroscopy. Third component was added after 5 min.

We hypothesized that this decreased rate is related to an irreversible catalyst alkylation. To investigate our hypothesis, secondary amine **12** was alkylated with **15** to adduct **17** which showed no reactivity upon the addition of

aldehyde **5a** (Scheme 4-8). Control experiments revealed that stoichiometric amounts of



Scheme 4-8: Secondary amine alkylation of CF₃ substituted nitroolefin **15**. *N,N*-dimethylproline **12** was used as a catalyst model system. Alkylation was confirmed by ¹H-NMR spectroscopy.

catalyst **12** form product when pre-exposed to the aldehyde. When applying catalyst **4a** in a reaction setting where alkylation is favored (thermodynamic control, Chapter 4.3.3), the decrease of the reaction rate over time was enhanced (Figure 4-10, green). An enhancement of the reaction rate by addition of a β-hydroxy ketone **13b** was not observed (Appendix, Figure 9-4). Therefore we conclude that the very active catalyst **4a** allows a productive catalytic pathway also for this challenging substrate.

4.5 Conclusion

The mechanistic studies on secondary amine catalyzed conjugate addition reaction of aldehydes to nitroacrylates showed that the catalyst forms not only an enamine with the aldehyde but is also alkylated by the nitroacrylate and forms an off-cycle intermediate. NMR-spectroscopic studies revealed that the reaction rate of such adduct formation is sensitive to the steric properties of the nitroacrylate. We showed that the release of alkylated catalyst is rate limiting for the overall reaction. These studies allowed us to optimize the reaction conditions regarding substrate selection and addition sequence of the reactants. By lowering the catalyst loadings we showed the steady-state of the reaction and that the release of the catalyst is rate limiting. Comparison of the steady-state for the different premixing of two of the three reaction partners (nitroolefin, aldehyde and catalyst) followed by addition of the last component allowed us to identify traces of aldol-side products when performing the enamine. This triggered the identification of a β-hydroxyketone cocatalyst that accelerated the reaction rate without affecting the stereoselectivity. The obtained mechanistic understanding allowed us to prepare a substrate scope using the catalyst in only very low

loadings of 500 ppm and provided the corresponding products with high enantio- (up to 98% ee) and diastereoselectivity (> 25 : 1). Further we applied the insights obtained to target challenging CF₃-substituted nitroolefins and show how the peptidic catalyst provides the conjugate addition reaction product in good yields and selectivities.

Since we showed how alkylating substrates could be transformed using low catalyst loadings to conjugate addition reaction products with great yield, diastereoselectivity and enantioselectivity, further projects should investigate applications of alkyl halides, that are known to be challenging substrates.

5

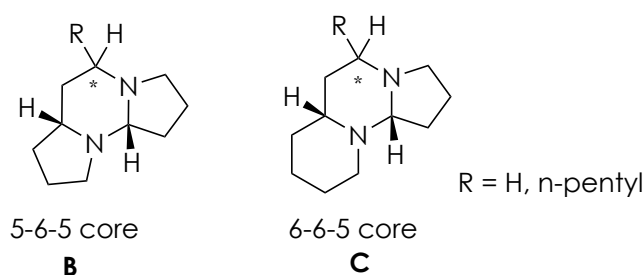
Bioinspired Synthesis of the Tetraponerine Core

Experiments within this chapter have been performed in collaboration with Andreas Kaspar (master thesis) and Marco Emma (visiting PhD student).

5.1 Background

Tetraponerines are alkaloidal venoms found in the Neo Guinean pseudomyrmecine ant *Tetraponera* and serve as strong contact insecticides.^[116,117] Tetraponerines are tricyclic ring systems, where all the rings are annulated via amines. Two subclasses consisting of annulated 5-6-5 (**B**) and 6-6-5 (**C**) ring systems are known (Scheme 5-1). The determination of the relative and absolute configurations of the natural products required an enantioselective total synthesis, which was inspired by the biosynthetic pathway.^[118]

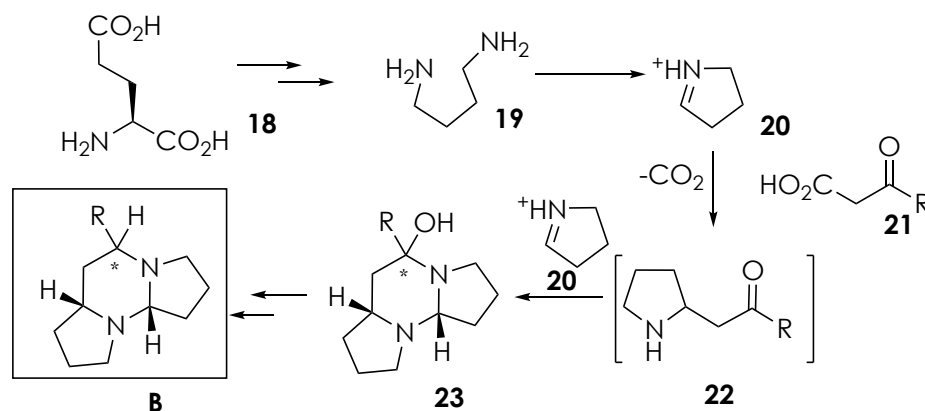
Tetraponerines:



Scheme 5-1: General structure of tetraponerines.

In nature, glutamic acid (**18**) is transformed into diamine **19**, which is subsequently condensed to the cyclic iminium **20** (Scheme 5-2). The cyclic iminium **20** reacts subsequently in the key step, a decarboxylative addition of a β -keto carboxylic acid **21**, to the amine **22**. Amine **22** reacts instantly with a second cyclic iminium **20** to form the annulated tetraponerine core structure **23**. Subsequently, **23** is transformed to natural tetraponerine **B**.^[118]

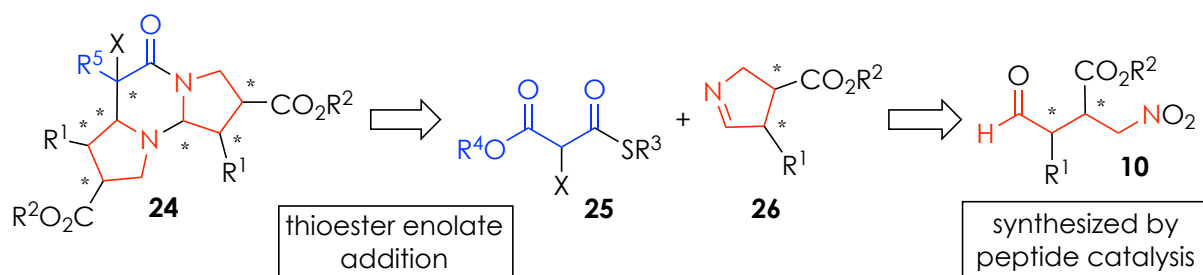
Biosynthesis of the 5-6-5 core:



Scheme 5-2: Biosynthesis of the 5-6-5 tetraponerines.

Besides the natural product synthesis, unnatural derivatives of tetraoponerines bearing different substituents in the six-membered ring were previously synthesized in moderate yields (< 50%).^[119] These syntheses included an addition of malonates and base as enol surrogates to achiral cyclic imines.^[119] The natural products as well as their derivatives showed a non-competitive inhibition of the nicotinic acetylcholine receptor (nAChR) and cytotoxic activity. Structure-activity relationship (SAR) studies revealed that the cytotoxicity depends on the nature of the substituent R, while neither the ring size nor the stereochemistry of the core system showed a significant influence on their activity.^[119,120]

In order to develop an elegant and effective synthesis for tetraoponerine derivatives **24**, we planned to combine two main focuses of our research group: the peptide-catalyzed conjugate addition reaction of aldehydes to nitroolefins, and the cinchona alkaloid catalyzed addition of thioester enolates (Scheme 5-3). Since thioester enolate surrogates **25** are established for the addition to imines,^[121-123] we planned their addition to a chiral cyclic imine building block **26** similarly to the biosynthesis.

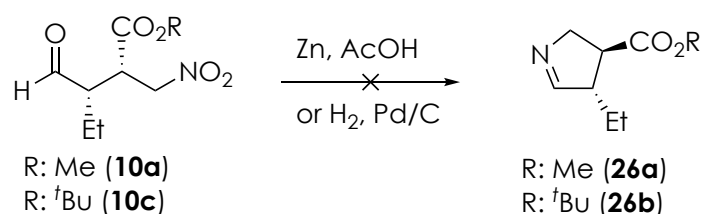


Scheme 5-3: Retrosynthetic analysis of substituted tetraoponerines.

We hypothesized that the key intermediate **26** can be synthesized from γ -nitroaldehyde **10**, which is accessible by a conjugate addition reaction of aldehydes to nitroacrylates (Chapter 4). The modular approach of combining a cyclic imine **26** and with a thioesterenolate surrogate **25** would allow the straightforward incorporation of residues by established methodologies of our group. Differently substituted tetraoponerine derivatives are expected to be of interest for future structure-activity relationship studies.

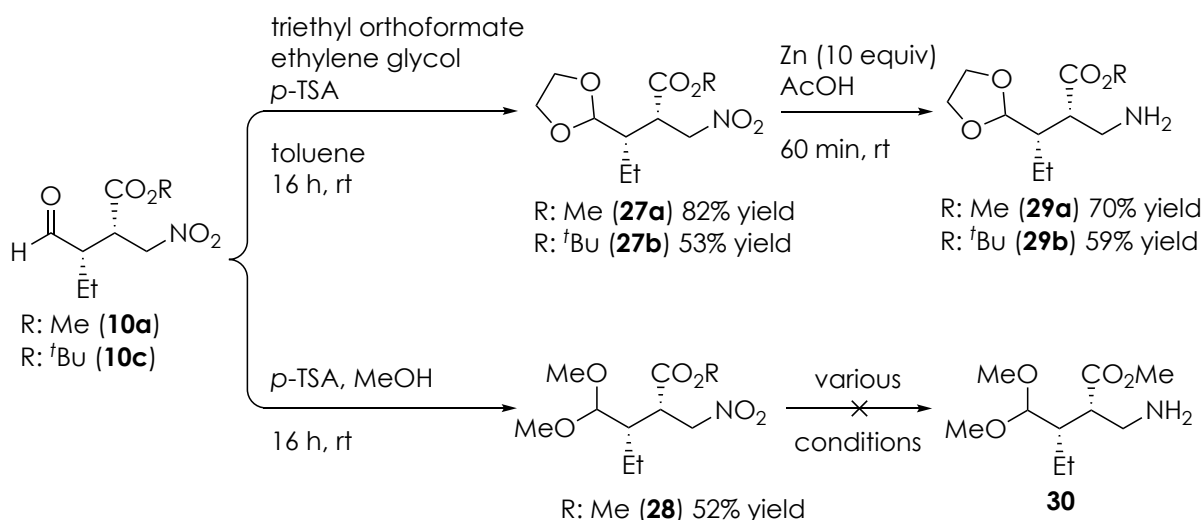
5.2 Synthesis of the Cyclic Imine

We began our investigations with the attempted synthesis of the ester substituted cyclic imines **26a** and **26b**. Reduction of the nitro group of **10a** and **10c** formed by a peptide catalyzed conjugate addition reaction of butanal to a nitroacrylate (Chapter 4), by Zn^[124] only led to decomposition of both reagents (Scheme 5-4). Further, hydrogenation (H₂, Pd/C) of **10** did not lead to the desired cyclic imine.



Scheme 5-4: Attempts for a direct reduction of NO₂ followed by an *in situ* cyclisation.

In order to overcome side reactions we protected the aldehyde moiety of **10a** and **10c** by acetals which were expected to be stable against reductive conditions.^[125] In order to test differently stable acetals regarding reduction and deprotection, we used a dioxolane and a dimethyl acetal as protecting groups.^[125] The syntheses^[61,126] of the corresponding dioxolane acetals **27a** and **27b** as well as the dimethyl acetal **28** were achieved in moderate yields.

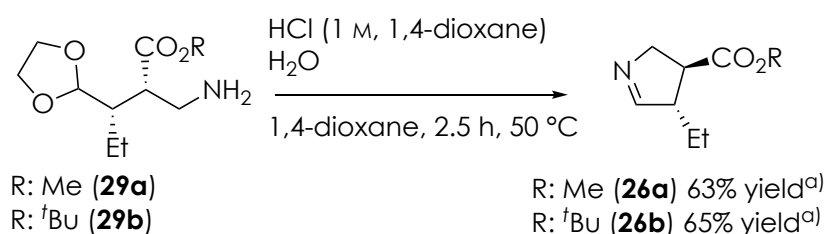


Scheme 5-5: Acetal formation and reduction of the nitro-group of ester substituted γ -nitroaldehydes **10a** and **10c**.

Due to the presence of an adjacent ester group, the reduction of the nitro group to the corresponding primary amine needed a procedure developed

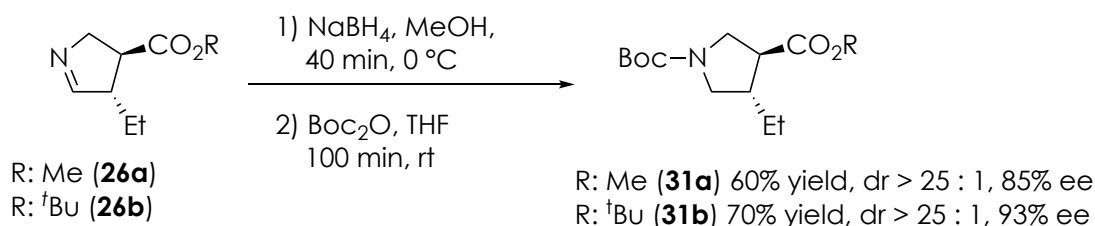
for the nitro reduction in the presence of a thioester^[127] using Zn and glacial acetic acid. Thereby, the dioxolane products **29a** and **29b** were isolated in good yields and the diastereoisomers of **29a** and **29b** could be separated. In contrast to the dioxolane, the dimethyl acetal analogue **28** showed only very low conversion (20% yield max.) where most of the starting material had decomposed.

Subsequent to the nitro reduction, deprotection of **29a** and **29b** to the aldehyde should instantly lead to cyclisation to form the corresponding imine. Different acids and concentrations were tested for the deprotection of **29a** and **29b**. These studies showed that 20 equivalent excess of HCl (1 M, in dioxane) are optimal to obtain **26a** and **26b** in good yields of up to 65%. Following the imine formation of **26a** and **26b**, we observed quantitative conversion (determined by ¹H-NMR), but the yield decreased when products were purified by column chromatography (isolated yield up to 65%). The isolated product is stable during storage in the freezer (-20 °C, > 4 month). Other purification methods such as reversed phase chromatography on a C₁₈-stationary phase or normal phase chromatography on aluminum oxide remained unsuccessful.



Scheme 5-6: Aldehyde deprotection and cyclization towards imines **26a** and **26b**.

Determination of the enantioselectivity of **26a** and **26b** turned out to be difficult due to the reactivity of the imine. To produce a more stable species, we planned to reduce the imine to a β -proline. A reduction towards the



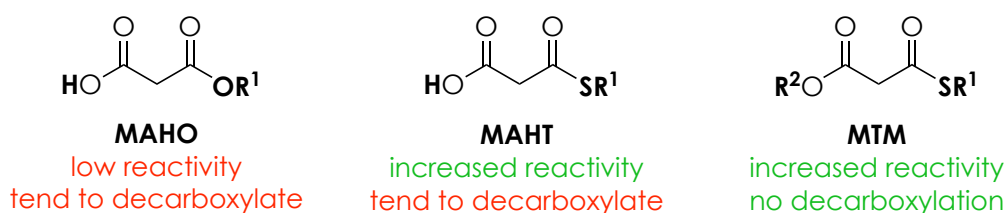
Scheme 5-7: Reduction of the chiral cyclic imine **26a,b** to the Boc-protected β -proline **31a,b**.

unprotected β -proline turned out to be challenging due to decomposition into a large number of unidentified products. However, subsequent Boc-protection^[124] allowed the synthesis of the Boc-protected β -prolines **31a** and **31b** in good yields (Scheme 5-7). Chiral SFC analysis of **31** revealed that the stereogenic centers are retained from the chiral γ -nitroaldehydes **10** and no loss of enantioselectivity was observed. Therefore, intermediates **27** and **29** are expected to have the same enantioselectivity as the corresponding ester substituted γ -nitroaldehydes **10**.

5.3 Tetraponerine Core Structure Synthesis

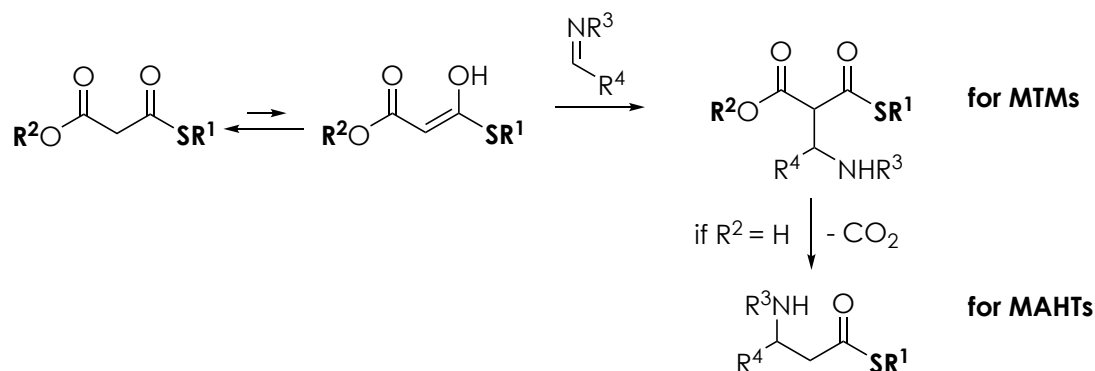
Having the cyclic imine in hand, we planned to probe its transformation into a tetraponerine derivative. Since our group gained deep insights into the addition of thioester enolate surrogates to imines over the last years,^[121-123] we wanted to investigate the formation of tetraponerine derivatives by an addition of a thioester enolate surrogate to the cyclic imine.

Thioester enolates are known as more reactive variants of their malonic acid half oxoester malonate (MAHO, Scheme 5-8) congeners.^[128-132] The main reason for this difference is the poor overlap of the C(2p) and S(3p) orbitals in thioesters, which lead to an increased acidity of the α -protons adjacent to the thioester compared to MAHOs.^[128] Due to the preferred reactivity of malonic acid half thioesters (MAHTs), these compounds were established as enolate surrogates for addition reactions to carbon electrophiles such as aldehydes, imines, and nitroolefins (for examples see^[133-138]). However, decarboxylation prior to the desired addition reaction is an undesired side reaction. To obtain reaction before decarboxylation occurs, catalyst loadings around 20 mol% are commonly used. To address this problem our group introduced monothiomalonates (MTMs) as protected MAHT congeners for non-decarboxylative stereoselective transformations.^[121,123,127,139]



Scheme 5-8: General structures of MAHOs, MAHTs, and MTMs.

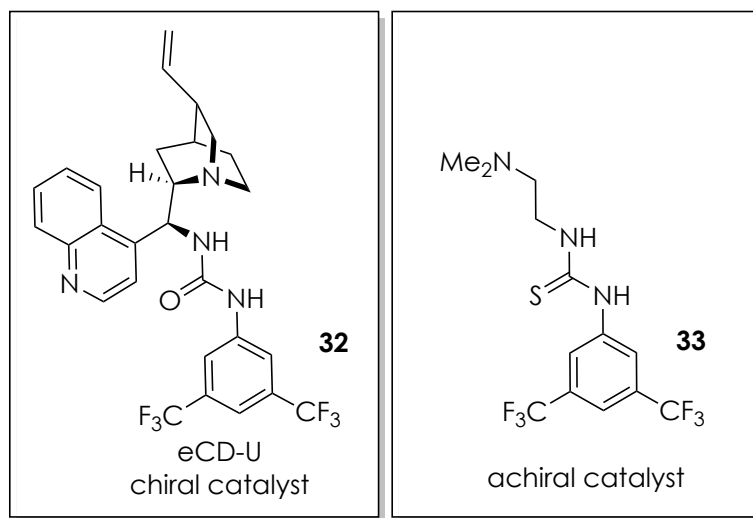
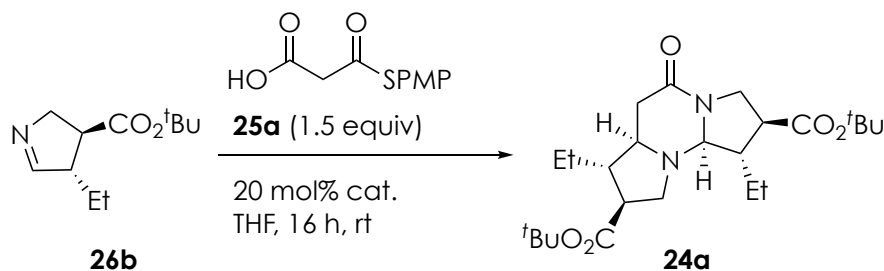
Imines are good electrophiles for the cinchona alkaloid catalyzed addition of thioester enols (Scheme 5-9).^[121-123,139] The reaction is initiated by an enolisation of a thioester, which enables a nucleophilic attack to an imine in order to form a Mannich product. For MTMs this is the final product whereas for MAHTs a spontaneous decarboxylation follows.



Scheme 5-9: Addition of thioester enolates to imines.

We next wanted to probe whether the chiral cyclic imine **26b** forms a tetraponerine core in cinchona alkaloid catalyzed additions of thioenolates. In an initial attempt, we planned the synthesis of a tetraponerine core without a stereogenic center in the six membered ring. Therefore, we intended to produce a decarboxylation after the addition of the enolate and selected a simple MAHT **25a** bearing a *para*-methoxy phenyl (PMP) protected ester moiety as an enolate surrogate. We investigated the cinchona alkaloid-catalyzed addition reaction of this MAHT to the chiral imine **26b** using previously established conditions.^[121,133,138] Within these experiments the MAHT **25a** readily reacted with **26b** affording tetraponerine core **24a** (Table 5-1) in good yield and diastereoselectivity ($dr > 25 : 1$) in the presence of an *epi*-cinchonidine urea catalyst (eCD-U, **32**).

Table 5-1: Synthesis of the tetraponerine core structure via an unsubstituted MAHT addition.

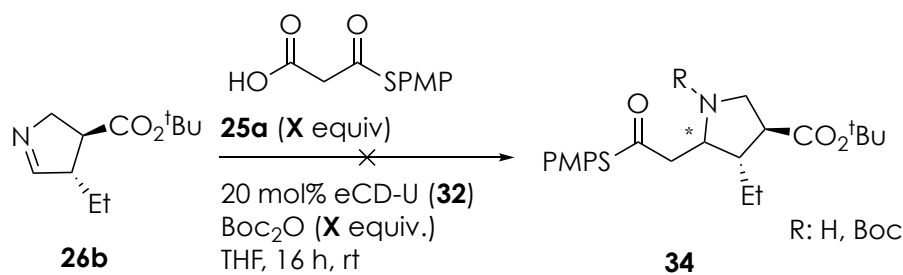


entry	catalyst	yield	dr
1	eCD-U 32	80%	> 25 : 1
2	achiral 33	48%	> 25 : 1
3	none	< 20%	9 : 1

To probe the role of the chiral catalyst for the cyclisation, we investigated the formation of the tetraponerine core in the presence of an achiral catalyst **33**, which bears a thiourea functionalized amine as well as in the absence of any catalyst (Table 5-1). Using eCD-U catalyst **32** we synthesized the tetraponerine **24a** with good yield and diastereoselectivity (entry 1) while the yield dropped significantly with an achiral catalyst **33** (entry 2). In the absence of any catalyst (entry 3), only low yields and a decrease of the diastereomeric ratio to 9:1 were observed. To gain insights into the enantioselectivity, we synthesized a racemic tetraponerine derivative **24a** from a racemic γ -nitroaldehyde **10c**. However, various attempts to separate the racemic sample by chiral normal phase HPLC or SFC failed. Therefore, we assigned

the stereogenic centers in the sample (made with catalyst **32**) by NMR-spectroscopy based on the known configuration of the imine.

Further, we investigated whether the tricyclic tetraponerine core is favored or a mono-adduct species can be synthesized by a similar methodology (Scheme 5-10). We varied the reaction setup and found that when using an eCD-U catalyst, additional equivalents of the imine **26b** (up to 4.0 equiv), reduced temperatures, stepwise addition of the imine **26b** to the MAHT **25a**, or the addition of Boc₂O (1.5 equiv) to trap a free amine^[124] not any mono-adduct species **34** was found. Only conversion to the tricyclic core **24a** was observed. Obviously, a direct formation of a tricyclic product seems to be favored.

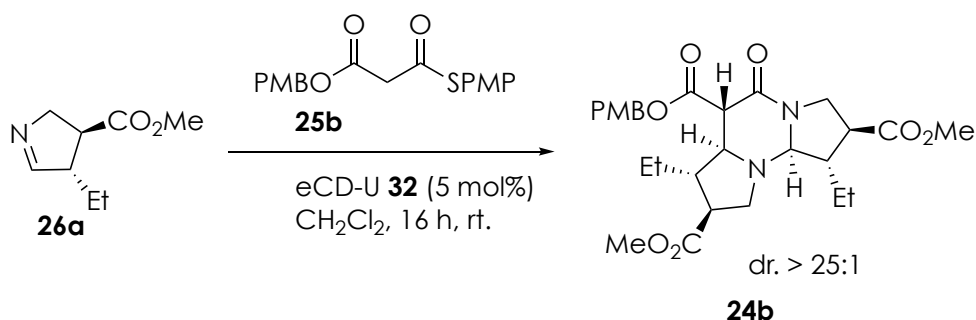


Scheme 5-10: Attempts towards the mono-adduct.

Having established a methodology to synthesize tetraponerines by cyclisation of chiral imines with MAHTs, we next planned to probe whether reactions with MTMs are also applicable as these cyclized tetraponerines would bear an additional stereogenic center in the six-membered ring. Incorporation of different substituents was desired since the bioactivity of tetraponerines was shown to be significantly dependent on the substitution of the six-membered ring of the 5-6-5 core.^[119] We initiated our investigations testing a cinchona alkaloid catalyzed MTM addition to imine **26a**.^[123,140] As a thioester enolate surrogate, we used an orthogonally protected MTM **25b** bearing a *para*-methoxy benzyl (PMB)-protected oxoester and a PMP-protected thioester. In an initial trial we observed the formation of the tetraponerine core structure **24b** with an adjacent ester group in the six-membered ring in low yields (Table 5-2, entry 1). Screening of various reaction conditions revealed that lower concentrations of **26a** and increased concentration of the MTM favor the formation of tetraponerine **24b** and allow a synthesis of **24** in moderate yields of up 43% (entry 4). The configuration of the tetraponerines was determined by 2D NMR using the absolute configuration

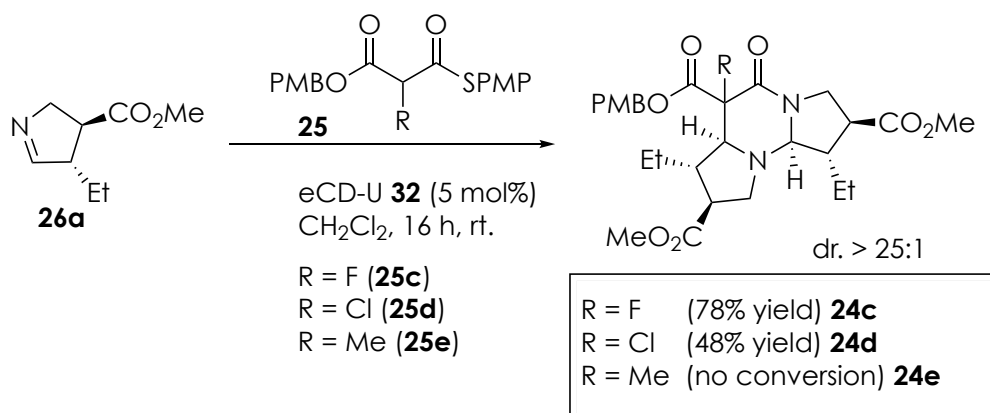
of the protected β -ester γ -nitroaldehyde **10a** obtained in a crystal structure (see appendix 9.1.5). Analysis of the enantioselectivity by chiral normal phase HPLC and SFC turned out to be challenging as no separation of a racemic sample was achieved.

Table 5-2: Formation of tetraponerines by MTM-additions. Yield was determined by isolation.



entry	concentration 26a	MTM equiv	yield
1	0.2 M	1.2	24%
2	0.1 M	1.2	< 10%
3	0.1 M	1.7	26%
4	0.01 M	1.7	43%

Fluorine incorporation in natural products has been shown to be beneficial for improving the bioactivity of pharmaceutically active compounds.^[141,142] Further, our group has shown that incorporation of fluorine via fluorinated MAHTs^[138] and MTMs^[121] can be achieved in good stereoselectivities and yields. Therefore, we aimed to synthesize a fluorinated tetrasubstituted tetraponerine by addition of fluorinated MTM (Scheme 5-11). In these cases, the synthesis of the desired tetraponerine **24c** with α -fluorinated MTM was



Scheme 5-11: Substituted tetraponerine core formation using chiral, cyclic imines and MTMs.

achieved in good yields (78%) and great diastereoselectivity using the previously established conditions. To probe whether other halogen atoms could be introduced, α -chlorinated MTMs were used. This resulted in the synthesis of the chlorinated tetraponerine core **24d** in moderate yields (48%). Expanding the substitution to alkyl residues by using α -methylated MTM, however, did not produce a methylated tetraponerine core **24e**, even with higher catalyst loadings and temperatures.

5.4 Conclusion

In summary, we developed an effective synthesis of a tetraponerine derivative with an annulated 5-6-5 core by combining the expertise of our group in two main areas of research. First, we synthesized a chiral cyclic imine by derivatization of the product of the peptide catalyzed conjugate addition reaction of aldehydes to nitroolefins shown in Chapter 4. Second, this imine was shown to react with thioesters in the presence of a cinchona alkaloid catalyst to form the tetraponerine core. Further, we showed that this modular approach allowed rapid incorporation of residues (ester- or alkyl-groups). The resulting structures are of interest for further biological evaluation. Future studies of tetraponerines should include structure-activity relationship studies of these new compounds.

6

Summary and Outlook

Within this work we investigated secondary amine catalyzed conjugate addition reactions of aldehydes to nitroolefins. We addressed open questions of the reaction mechanism, investigated how challenging substrates can be reacted in a controlled manner, and showcased the value of bifunctional substrates in a synthesis of a natural product derivative.

For the secondary amine catalyzed conjugate addition reaction of aldehydes to nitroolefins, the reaction pathway depends on the availability or absence of an intramolecular acid in the catalyst. The two pathways share a common intermediate before the pathway divides. This intermediate was never observed *in situ* and *ex situ* and *in silico* experiments did not fully answer whether it is of an open iminium nitronate or a cyclized oxazine N-oxide structure. We aimed at its detection and found by UV/Vis spectroscopy a novel characteristic band for nitronates under preparative conditions. Computational studies validated the experimental data and UV/Vis spectroscopic measurements gave insight into the *in situ* absorbance of the reaction intermediate generated in the carbon-carbon bond formation. We showed that acid bearing catalysts stabilize the intermediate compared to lacking an intramolecular acid. Therefore we concluded that a suitably placed acidic group in the catalyst influences the reaction pathway by non-covalent interactions. Future investigations on the reaction mechanism should focus on insights into energy barriers, and therefore include DFT calculations of all the reaction intermediates as well as the transition states.

The application of alkylating substrates in secondary amine catalysis is due to catalyst deactivation a challenge in the field. We investigated the use of nitroacrylates, which are established alkylating agents for amines, for the conjugate addition reaction of aldehydes. We showed that the peptidic H-DPro-Pro-Glu-NH₂ catalyst is alkylated under reaction conditions and its formation rate depended on the steric demand of the nitroacrylate. We showed that this alkylation is reversible and that the release of the catalysts is the rate-limiting step in the catalyzed reaction. Reducing the catalyst loading allowed the identification of a cocatalyst, which triggered the development of a catalytic system with excellent reaction rates at 500 ppm catalyst

loading. We showed the broad applicability of this improved methodology by preparation of a substrate scope in good enantio- (up to 98% ee) and diastereoselectivity (dr > 25 : 1). All these insights allowed us the use of a even more challenging CF₃-substituted nitroolefin, that has been transformed to the corresponding product in good yield and enantio- (95% ee) and diastereoselectivity (dr > 25 : 1). Since we showed that the great reactivity of our catalyst for electron deficient substrates, further studies should include even more challenging substrates that irreversibly alkylate the catalyst as side-reaction (e.g. alkyl halides).

Subsequent transformations of γ -nitroaldehydes often rely on simple achiral modifications. We investigated their subsequent transformation using cinchona alkaloid catalyzed additions of thioester enolates to synthesize a natural product derivative. In these studies we developed a synthesis of a chiral cyclic imine from an ester-substituted γ -nitroaldehyde. Subsequently, by reacting the imine with thioenolates in presence of a cinchona alkaloid catalyst we obtained the tetraponerine core structure bearing seven stereogenic centers. We conclude that combination of peptide catalyzed conjugate addition reactions of aldehydes to nitroolefins followed by cinchona alkaloid catalyzed thioesterenolate additions to imines represent a powerful toolbox for the synthesis of tetraponerine derivatives. Future studies of tetraponerine derivatives might include evaluation of their structure activity relationship, since similar compounds were hypothesized as potential candidates for cancer treatment.

7

Experimental Part

7.1 General Aspects and Materials

Reagents and materials were of the highest commercially available grade and used without further purification. n-Butanal and triethylamine have been freshly distilled before use. Chloroform was neutralized using Al₂O₃ before use. Reactions were monitored by thin layer chromatography using Merck silica gel 60 F254 Glass plates. Visualization of the compounds was achieved by UV or KMnO₄ and DNPH staining. Flash chromatography and plug filtrations were performed using Fluka silica gel 60 (particle size 0.040 – 0.063 mm, 200 – 400 mesh). Solvents for extraction and chromatography were of technical quality and distilled before use. All reactions were performed in oven-dried glassware. Spectra were recorded on a Varian Mercury-VX 300, a Bruker AV 300 (300 MHz/75 MHz), a Bruker DRX 400, a Bruker AV III 400 (400 MHz/100 MHz) or a Bruker AV III 600 (600 MHz/150 MHz). All spectra were recorded at 25 °C, unless stated otherwise. Chemical shifts (δ) are reported in parts per million (ppm) relative to the signal of tetramethylsilane (TMS) using the residual solvent signals or TMS as a reference. HPLC analyses were performed on an analytical Ultimate 3000 HPLC system from Dionex with a diode array detector and chiral stationary phases (Daicel AD-H, Daicel AS-H, AY-H, OD-H or Daicel OJ-H. SFC analyses were performed on an analytical SFC UPC² from waters with a diode array detector ACQUITY-UPLC-PDA from Waters using chiral columns (Trefoil, AS3 SFC, AD3 SFC, IA3 SFC, Whelk, IC3 SFC, OD3 SFC, OJ3 SFC) (150 mm x 30 mm) from Daicel, Regis or Waters under the reported conditions. High-resolution electron ionization (HR-EI) mass spectra were measured on a Waters Micromass AutoSpec Ultima spectrometer. A Bruker maXis (UHR-TOF) was used for high-resolution electrospray ionisation (HR-ESI) mass spectrometry. High-resolution MALDI spectra were acquired on a Bruker solariX94 (ESI/MALDI-FT-ICR) and a Bruker Ultra-Flex II (MALDI-TOF) spectrometer. X-ray structures were measured on a Bruker D8 Advance with Apex II CCD-Detector (Mo). *In situ* FT-IR spectroscopy was carried out on a ReactIR R4000 (SiComb). All measurements were performed at room temperature, collecting spectra every 15 seconds (64 scans).

7.2 General Protocols

Addition of butanal to nitroacrylates catalyzed by a H-DPro-Pro-Glu-NH₂:

Reaction setup for experiments using *in situ* IR-spectroscopy:

Solutions of the nitroolefin (500 μmol , 1.00 equiv), the aldehyde (750 μmol , 1.50 equiv) and the desalted H-DPro-Pro-Glu-NH₂ (5 μmol , 1.0 mol% unless stated otherwise) catalyst were prepared in CHCl₃/*i*PrOH (9:1, 300 μL each). Two of the solutions were combined in a 1.0 mL volumetric flask equipped with a stir bar and stirred for the time indicated as premixture. The stir bar was removed, the third component was added and the solvent filled up to 1.0 mL. The mixture (0.5 M) was poured into a 5 mL round flask attached to the ReactIR and the progress was followed by *in situ* IR spectroscopy at room temperature (125 scans every 15 s). The first spectrum was subtracted from the following ones and the reaction progress was followed in the resulting difference spectra at 1563 cm⁻¹. After completion of the reaction conversion was determined by a crude ¹H-NMR and the mixture was filtered through a small plug of silica, and the solvent and the remaining aldehyde removed under reduced pressure to result in the product. For some of the γ -nitroaldehydes a derivatisation towards the corresponding alcohol was needed to determine the enantioselectivity.

Derivatisation of γ -nitroaldehydes to the corresponding alcohol

In a 5 mL flask the γ -nitroaldehyde (500 μmol , 1.00 equiv) was dissolved in MeOH (1.0 mL) under an argon atmosphere at 0 °C. NaBH₄ (18.9 mg, 500 μmol , 1.00 equiv) was added in one portion and the reaction mixture was stirred for 1.5 h at 0 °C. The solvent was removed under reduced pressure and the orange solid was purified by column chromatography (silica, pentane/ethyl acetate) to result in the corresponding alcohol as a colorless oil.

Zinc activation for nitro group reduction

Zinc powder (1.6 g) was suspended in aqueous HCl (1M, 10 mL) for 6 min. The suspension was decanted without exposing the zinc to air, water (3 x 15 mL) was added and decanted. The zinc powder was suspended in water (15 mL), filtered without letting the residue get dry followed by washing with MeOH (10 mL). The zinc was suspended in acetone (20 mL). After solvent removal, acetone (10 mL) was added, and decanted. After repeating this procedure with MTBE (10 mL) the zinc powder was dried under high vacuum.

Desalting of TFA salts of peptides

A VariPure IPE tube (Varian, Inc.) was used for ion pair extraction. The TFA-salt of the peptide was dissolved in water and loaded on the cartridge (previously activated with MeOH). After elution the cartridge was washed with water/acetonitrile (4:1) and the outcome monitored by TLC (visualized with ninhydrin). When no more peptide was dropping out of the cartridge, the collected fraction was lyophilized and the purity determined by ^{19}F -NMR.

General remarks for chiral analysis

The racemic samples were prepared using a mixture of H-DPro-Pro-Glu-NH₂ and H-Pro-DPro-DGlu-NH₂ as trifluoro acetic acid/NMM salts as catalyst. Some of the racemic samples do not have a proper 1:1 ratio of the catalysts used. This might be due to imprecise mixture of the catalysts or due to different trifluoro acetic acid contents of the catalyst enantiomers. Future studies will require the preparation of racemic products with a 1:1 ratio of the two enantiomers. Further, for most of the samples a diastereomeric ratio > 50:1 was observed. This led to almost undetectable peaks of the second pair of enantiomers in SFC analysis. Using "scratch TLC" for sample preparation the sample was obtained mostly diastereopure.

7.3 Stopped-Flow UV/Vis Measurements

Analysis of kinetics traces for the spectroscopic signature of a nitronate intermediate (experiments in corporation with Dr. Reinhard Kissner)

Because typical UV absorption bands of nitronate, a postulated intermediate, are obscured by other absorptions of components in the reaction mixture, we identified a characteristic band of the nitronate generated by α -deprotonation at the nitro function of (2-nitroethyl)benzene, in the visible region ($\lambda_{\text{max}} \approx 490$ nm). It fortunately has a low extinction coefficient, which is beneficial by not overloading detection at the high concentrations employed in synthesis. We followed absorbance changes in time from 440 to 590 nm with the scanning stopped-flow spectrophotometer. It turned out that static background subtraction by composing the sum spectrum of the reactants at their initial concentrations was not applicable, because at the high concentrations for synthesis, physical interactions produce solvatochromic effects. This was confirmed by variation of a mix of all reactants but one, to avoid reaction start, and recording the according spectra.

Preliminary experiments revealed that absorbance in the wavelength range of observation follows a slow linear time dependence after about 5 or even more seconds, and this remains so for many minutes. We conclude that the concentrations of species contributing to the total absorbance are either constant or their change is limited by saturation of conversion rate. We assumed that short concentration overshoots of initial intermediates, to which the postulated nitronate belongs, might occur. In this case, the total absorbance after 5 seconds would provide the appropriate background to detect an eventual slight nitronate excess during reaction sequence initiation. This feature should be of transient character, rising quickly after reagent mixing and decaying within 5 seconds. Unfortunately, information on the total stationary concentration of nitronate is not available by this approach.

The practical implementation requires to plot time-dependent absorbance traces in the wavelength range of interest (here: at 490 nm) to determine the time at which absorbance becomes stationary or changing in linear fashion.

It also requires averaging, because the spectral changes expected in a range with weak forbidden transitions are small. Therefore, 5 to 9 time resolved spectra sets from independent runs were averaged prior to analysis. The following figure shows this for two catalysts, H-DPro-Pro-Glu-NH₂ which is protic and H-DPro-Pro-Glu(OMe)-NH₂ which is aprotic, in all three solvents examined.

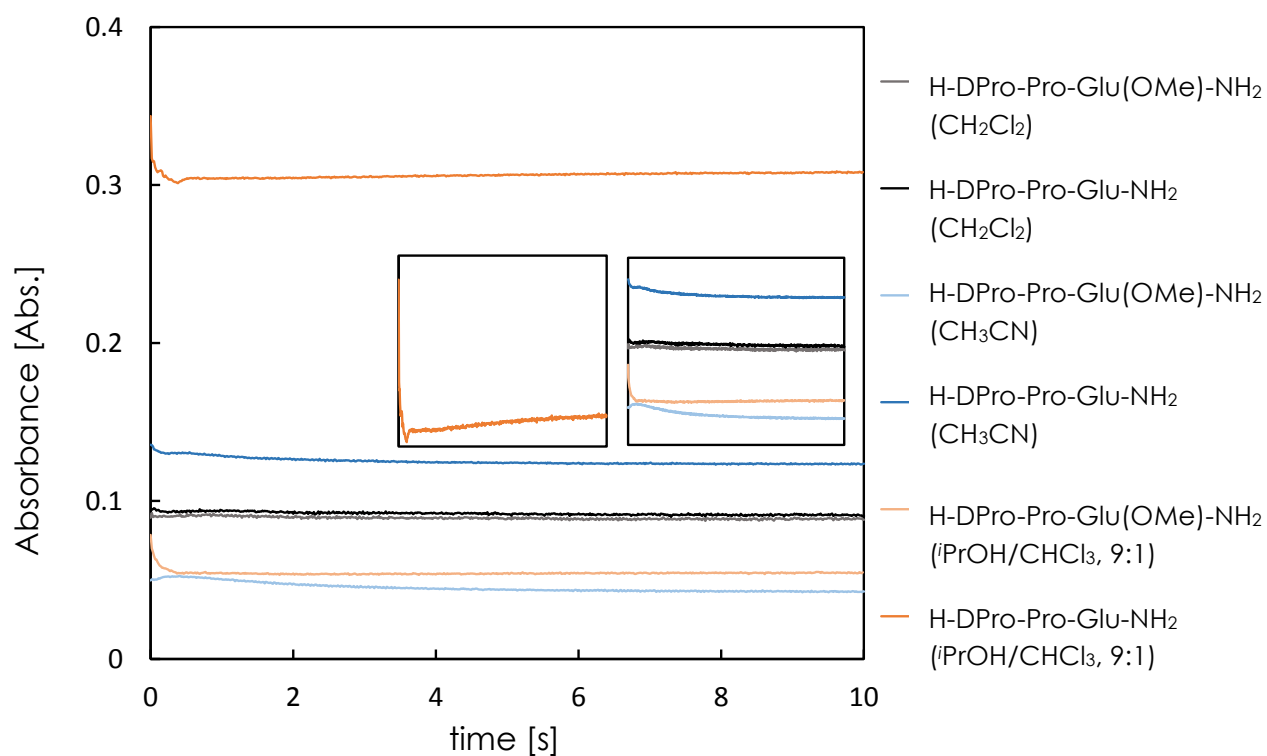


Figure 7-1: Absorbance - time traces for the reaction catalyzed by H-DPro-Pro-Glu-NH₂ or H-DPro-Pro-Glu(OMe)-NH₂ in CH₂Cl₂, CH₃CN and *i*PrOH/CHCl₃ (9:1). Insets are vertically zoomed to reveal details of profiles.

We chose 8 seconds as the time for the extraction of the background spectra, because from this time on all traces have become steady. Subsequently, we extracted spectra at earlier times and subtracted the spectra at 8 seconds from these. Since the position of a possible overshoot maximum in the selected time interval cannot be deduced with initial kinetics unknown, we selected spectra from the 500 collected in the time interval by a bisectional approach, which was directed by recognition of the occurrence of a new band.

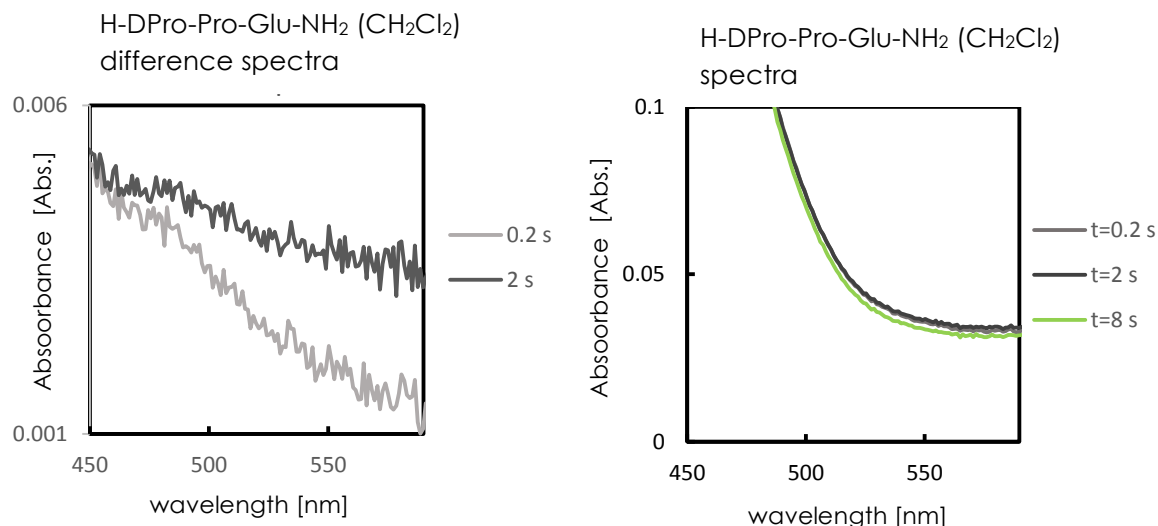


Figure 7-2: Spectra of the reaction catalyzed by pPE (*N*-dodecyl) in CH_2Cl_2 , recorded 0.2 s, 2 s and 8 s after start of reaction. Difference spectra between $t = 0.2$ s, respectively $t = 2$ s, and the spectrum at 8 s. Average of 9 runs.

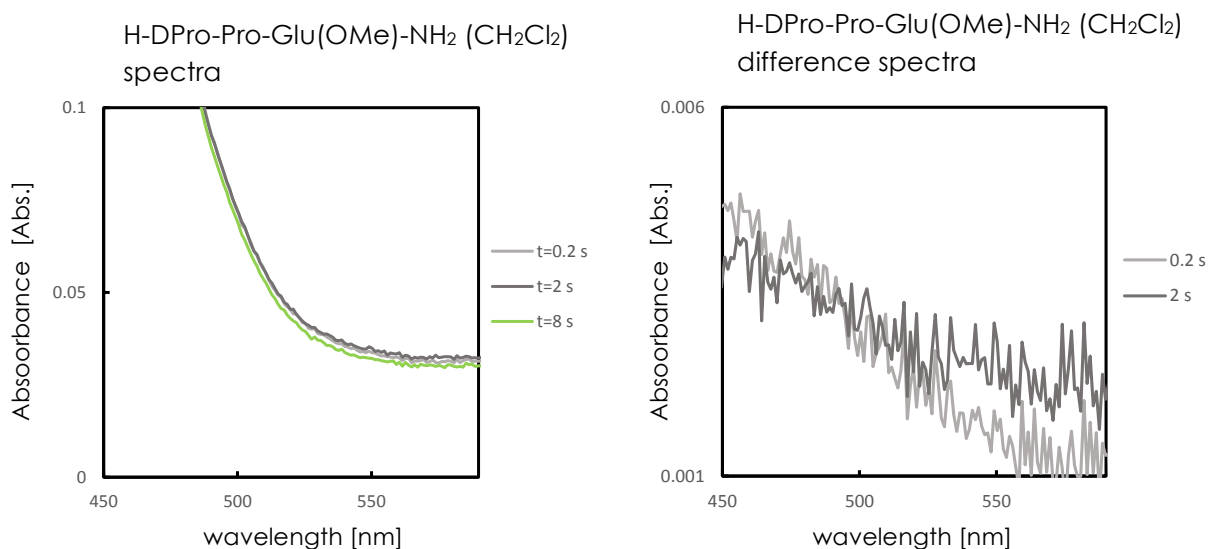


Figure 7-3: Spectra of the reaction catalyzed by pPE(OMe) in CH_2Cl_2 , recorded 0.2 s, 2 s and 8 s after start of reaction. Difference spectra between $t = 0.2$ s, respectively $t = 2$ s, and the spectrum at 8 s. Average of 5 runs.

Comparing the difference spectra obtained with H-DPro-Pro-Glu-NH₂ or H-DPro-Pro-Glu(OMe)-NH₂ catalyst in the aprotic CH_2Cl_2 , we find that they are fairly similar at 0.2 and 2 seconds, respectively. From 0.2 to 2 s, absorbance increases distinctly at $\lambda > 500$ nm. However, in the case of H-DPro-Pro-Glu-NH₂, a weak maximum around 490 nm is superimposed at both times.

The difference between the pPE catalyst that can provide a hydrogen bridge and therefore stabilize a nitronate group, and the H-DPro-Pro-Glu(OMe)-NH₂ which cannot becomes more distinct in the protic

solvent mixture of *i*PrOH/CHCl₃. The nitronate stabilization is quite obvious here. Further, the protic solvent causes a not unexpected shift of the nitronate band towards shorter wavelength, maximum now at 475 nm instead of 490 nm.

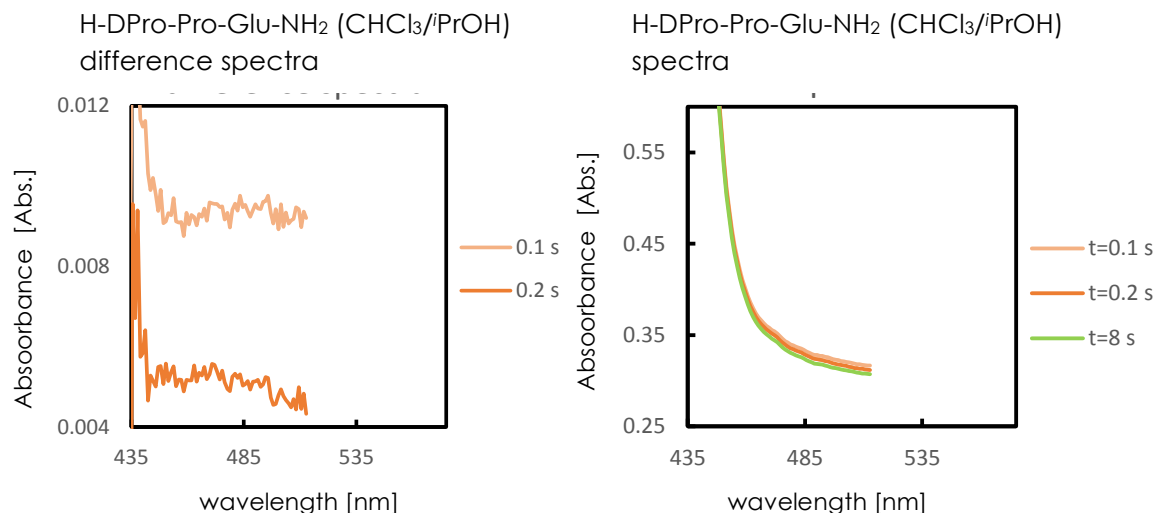


Figure 7-4: Spectra of the reaction catalyzed by H-DPro-Pro-Glu(OMe)-NH₂ in *i*PrOH/CHCl₃, recorded 0.1 s, 0.2 s and 8 s after start of reaction. Difference spectra between $t = 0.1$ s, respectively $t = 0.2$ s, and the spectrum at 8 s. Average of 7 runs.

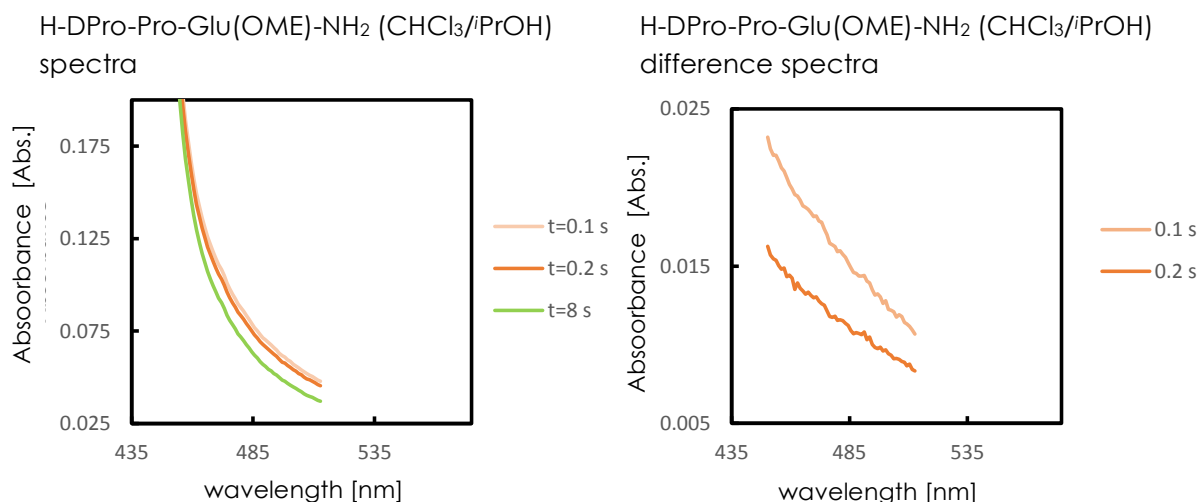


Figure 7-5: Spectra of the reaction catalyzed by H-DPro-Pro-Glu-NH₂ in *i*PrOH/CHCl₃, recorded 0.1 s, 0.2 s and 8 s after start of reaction. Difference spectra between $t = 0.1$ s, respectively $t = 0.2$ s, and the spectrum at 8 s. Average of 9 runs.

7.4 Computational Studies

7.4.1 Structural Analysis

Calculations were performed by Dr. Thomas Weymuth

All initial structures were generated with RDKit as implemented in Adf 2016.107. A total of 600 conformers were generated; of these, only conformers which had a root mean square deviation (RMSD) of at least 0.2 Å to all other conformers were kept. These were subsequently refined with the Uff force field as implemented in RDKit. Of the refined structures, a second RMSD filter of 0.1 Å was applied.

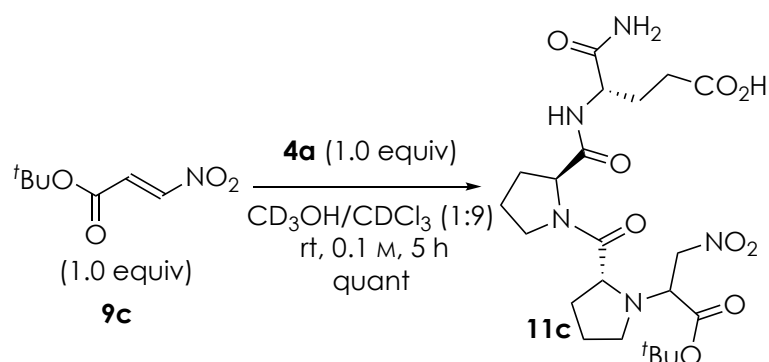
All final conformers were optimized with spin-component scaled second-order Møller–Plesset perturbation theory (SCS-MP2) employing the program package Turbomole 7.0.2 in its shared-memory parallelized implementation. The default scaling parameters for SCS-MP2 were used throughout all calculations. No symmetry constraints were put in place, i.e., all structure optimizations were done in C_1 symmetry. The maximum norm of the Cartesian nuclear gradient was converged to 10^{-4} hartree/bohr, and all electronic energies were converged to 10^{-7} hartree. Ahlrich's triple- ζ basis set with two set of polarization functions and one set of diffuse functions (def2-TZVPPD) was employed at all atoms. For all calculations advantage was taken of the resolution-of-the-identity (RI) approximation for the Coulomb integrals with the corresponding auxiliary basis sets. Solvation effects were taken into account by means of the conductor-like screening model (COSMO), adopting a value of 36.64 for the dielectric constant, corresponding to acetonitrile at room temperature.

For all optimized structures it has been verified that they correspond to minima on the potential energy surface by conducting a vibrational analysis with the same methodology described above. The Hessian matrix was assembled with the Turbomole script NumForce.

Electronic singlet and triplet excitations were calculated with Gaussian 09, revision D.01, by means of time-dependent density functional theory (TD-DFT) employing the CAM-B3LYP exchange–correlation functional. Also for these

calculations, the def2-TZVPPD basis set has been used. All electronic energies were converged to 10^{-6} hartree. Solvation effects have been taken into account with the polarizable continuum model (PCM). Here, a value of 35.688 for the dielectric constant has been adopted.

7.5 NMR Experiments on Catalyst Alkylation:



To monitor the reaction progress of the alkylation of catalyst **4a** we used $^1\text{H-NMR}$ (500 MHz Bruker spectrometer) to monitor the consumption of the nitroolefin. We followed the decrease of the doublet at 7.53 ppm ($J = 13.44$, CH-NO_2) as shown in Figure 7-6. As an external standard $\text{C}_2\text{H}_2\text{Cl}_4$ (2.0 equiv) was used. After dissolving the nitroolefin (1.0 equiv) in $\text{CDCl}_3/\text{CD}_3\text{OH}$ (1 M) at room temperature, we set up the OH-suppression and determined the best parameters for the measurements (AQ = 5 s, D1 = 5 s, PLW9 = 40.15).

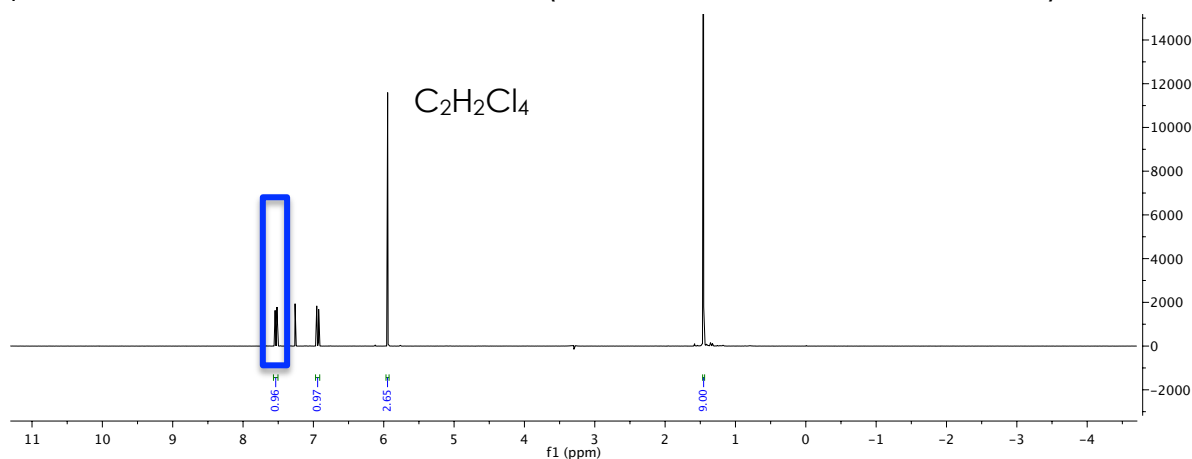


Figure 7-6: $^1\text{H-NMR}$ spectrum of nitroolefin **9c** with $\text{C}_2\text{H}_2\text{Cl}_4$ as external standard.

The catalyst (1.0 equiv) was added to the nitroolefin and $\text{C}_2\text{H}_2\text{Cl}_4$ (1M). After shimming the spectra were recorded (first spectrum, Figure 7-7; then 99 spectra every 10 min with 64 scans, Figure 7-8). The decrease of the signal at 7.53 ppm ($J = 13.44$, CH-NO_2) was monitored (Figure 7-9). The measured

signal intensity was changed to the remaining nitroolefin content using the internal standard and plotted over time (Figure 7-10).

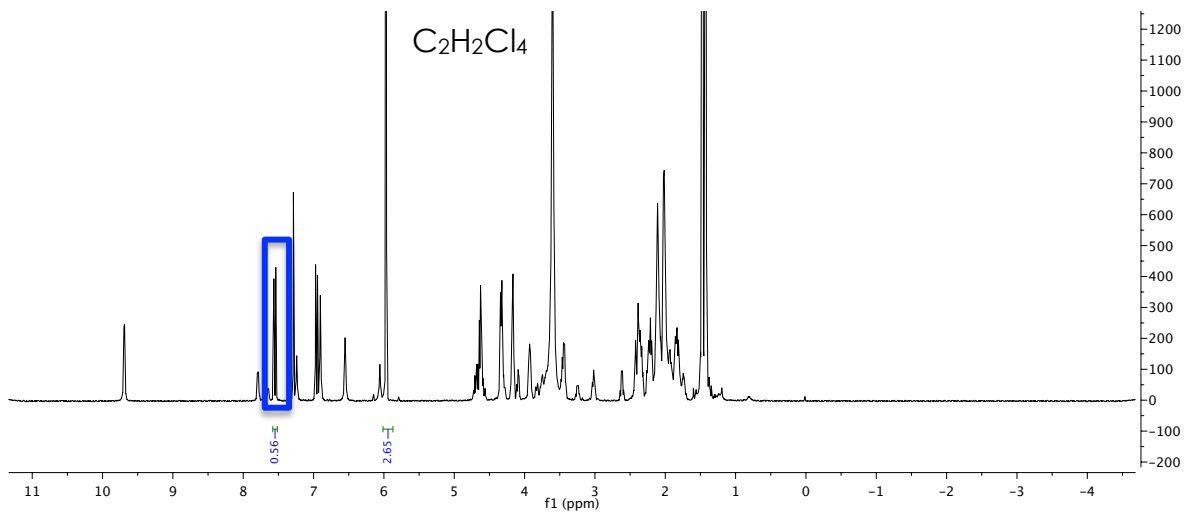


Figure 7-7: ¹H-NMR spectrum of nitroolefin **9c** and catalyst **4a** after 5 min with C₂H₂Cl₄ as external standard.

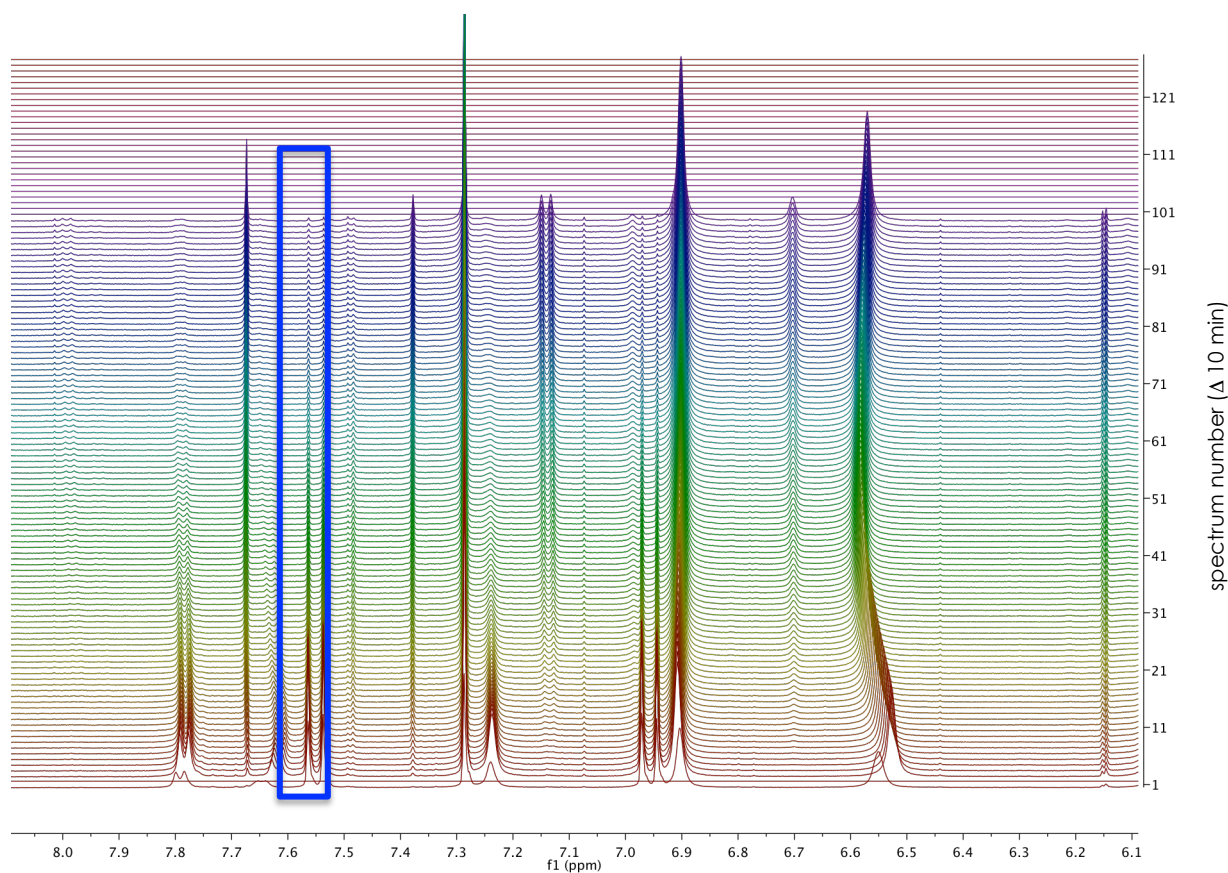


Figure 7-8: Stacked ¹H-NMR spectra of the alkylation of **4a** by **9c** over time (Δ 10 min).

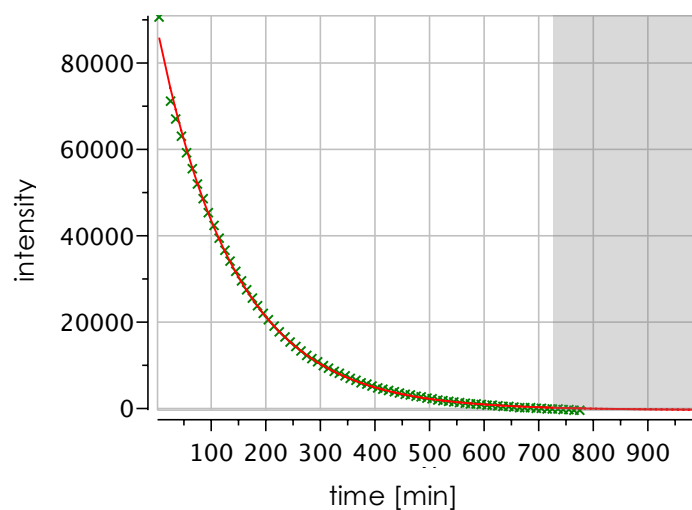


Figure 7-9: Intensity decrease over time of the signal at 7.53 ppm.

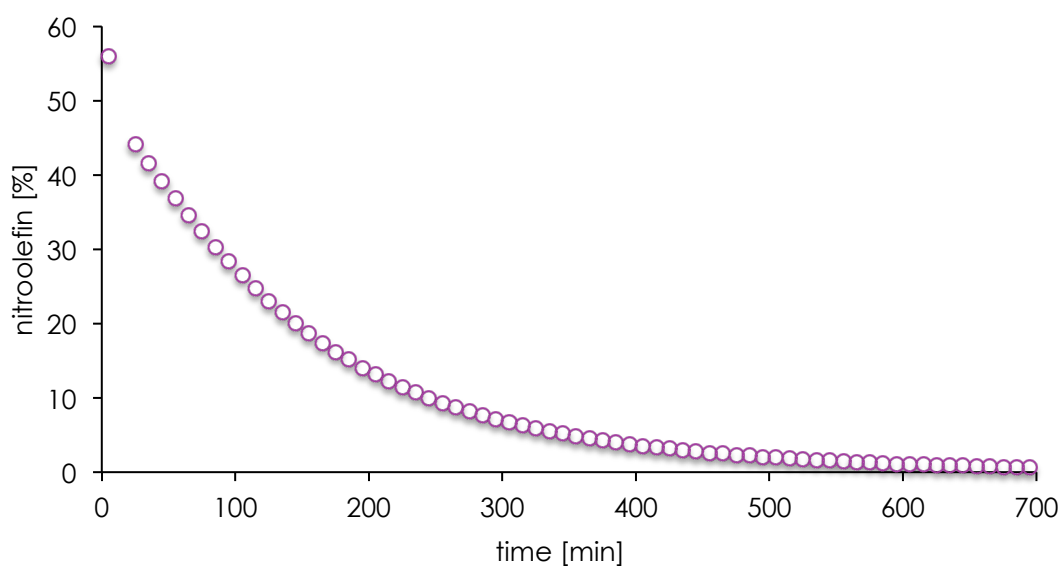
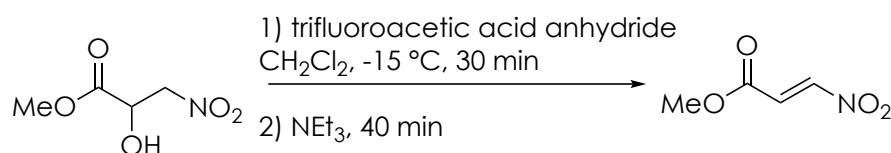


Figure 7-10: Consumption of nitroolefin **9c** by catalyst **4a** over time monitored by $^1\text{H-NMR}$.

7.6 Synthesis of Nitroolefins

Methyl (*E*)-3-nitroacrylate (**9a**)



Methyl 2-hydroxy-3-nitropropanoate^[143] was dissolved in CH₂Cl₂ (100 mL) followed by dropwise addition of trifluoroacetic acid anhydride (3.0 mL, 21.3 mmol, 1.0 equiv) at -15 °C. After 10 min of stirring freshly distilled NEt₃ (6.0 mL, 43.0 mmol, 2.0 equiv) was added dropwise over 30 min using a syringe pump. The reaction mixture was stirred at -15 °C for 40 min CH₂Cl₂ (100 mL) was added and the solution was washed with saturated aqueous NH₄Cl (3 x 100 mL). The organic layer was dried over MgSO₄ and concentrated under reduced pressure. The resulting yellow crude product was purified by flash column chromatography (silica, CH₂Cl₂) to afford the product (2.5 g, 56% yield) as a yellow solid.

¹H-NMR (300 MHz, CDCl₃) δ: 7.68 (d, *J* = 13.5 Hz, 1H), 7.09 (d, *J* = 13.5 Hz), 3.87 (s, 3H).

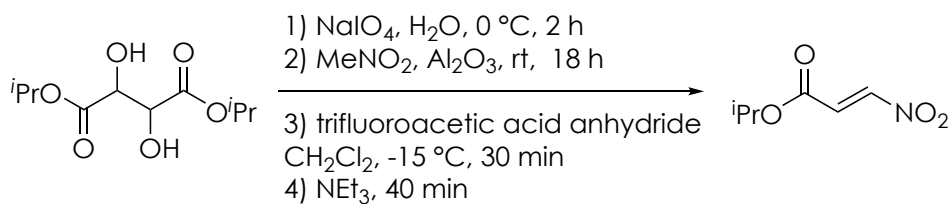
¹³C-NMR (101 MHz, CDCl₃) δ: 163.20, 149.24, 127.35, 53.23.

HRMS: [M+NH₄] calc.: 191.1026 m/z, found: 191.1027 m/z.

R_f = 0.78 (silica, UV, CH₂Cl₂).

Boiling point: 75 °C at 25 mbar.

The data are in agreement with the literature.^[16]

Isopropyl (*E*)-3-nitroacrylate (**9b**)

Isopropyl (*E*)-3-nitroacrylate was synthesized according to a known procedure.^[144]

¹H-NMR (300 MHz, CDCl₃) δ: 7.66 (d, *J* = 13.4 Hz, 1H), 7.06 (d, *J* = 13.5 Hz, 1H), 5.16 (hept, *J* = 6.3 Hz, 1H), 1.33 (d, *J* = 6.3 Hz, 6H).

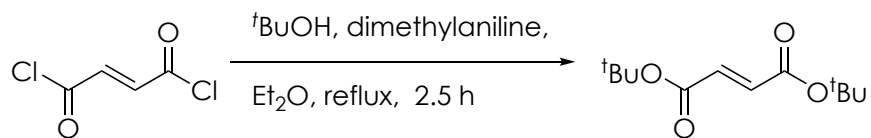
¹³C-NMR (101 MHz, CDCl₃) δ: 162.28, 148.94, 128.32, 70.64, 21.80.

HRMS: ESI [M+NH₄] calculated: 177.0870 m/z, measured: 117.0872 m/z.

R_f = 0.77 (silica, UV, pentane/ethyl acetate, 10:1).

IR [cm⁻¹]: 3111, 2986, 1721, 1535, 1352, 1280, 1249, 1103, 947, 903, 820, 762, 673.

The data are in agreement with the literature.^[144]

Di-*tert*-butyl fumarate

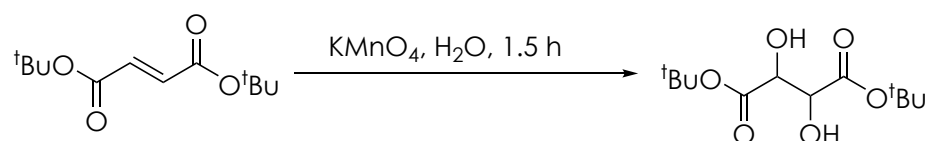
In a three neck flask equipped with a reflux condenser and a dropping funnel *tert*-butanol (130 mL, 1.38 mol, 3.00 equiv) and *N,N*-dimethylaniline (132 mL, 0.92 mol, 2.00 equiv) were dissolved in Et₂O (300 mL) at 0 °C. A solution of fumaryl chloride (50 mL, 0.46 mol, 1.00 equiv) in Et₂O (50 mL) was added dropwise at 0 °C. The mixture was heated to reflux for 2.5 h and the reaction mixture was extracted with aq. H₂SO₄ (6 N, 60 mL). The aqueous layer was extracted with Et₂O (3 x 100 mL) and the combined organic layers were washed with sat. aq. NaHCO₃ (3 x 200 mL) and brine (200 mL). The organic layer was concentrated under reduced pressure to result in the crude product as a brown solid (59 g, 56% yield). The crude product showed a good purity (> 98%) and was used without further purification.

¹H-NMR (300 MHz, CDCl₃) δ: 6.66 (s, 2H), 1.49 (s, 18H).

¹³C-NMR (101 MHz, CDCl₃) δ: 164.58, 134.72, 81.82, 77.16, 28.14.

IR [cm⁻¹]: 2981.3, 1702.6, 1305.6, 1136.4.

The data are in agreement with the literature.^[145]

Di-tert-butyl 2,3-dihydroxysuccinate

Di-*tert*-butyl fumarate (18.6 g, 81.5 mmol, 1.0 equiv) was dissolved in *tert*-butanol (500 mL) and KMnO_4 (38.6 g, 244 mmol, 3.0 equiv) in water (900 mL) was added dropwise over 1.5 h. The brown reaction mixture was extracted with Et_2O (4 x 600 mL) and the combined organic layers were concentrated under reduced pressure. The brown residue was purified by column chromatography (silica, pentane/ethyl acetate 5:1 to 1:1) to result in di-*tert*-butyl 2,3-dihydroxysuccinate as a white solid (9.2 g, 30.9 mmol, 40% yield)

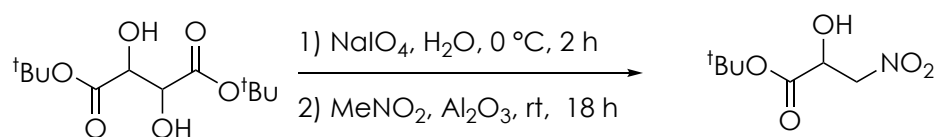
$^1\text{H-NMR}$ (300 MHz, CDCl_3) δ : 4.36 (d, $J = 5.5$ Hz, 2H), 3.13 (d, $J = 6.0$ Hz, 2H), 1.51 (s, 18H).

$^{13}\text{C-NMR}$ (101 MHz, CDCl_3) δ : 171.05, 83.53, 72.43, 28.13.

HRMS: ESI [$\text{M}+\text{NH}_4$] calculated: 280.1755 m/z measured: 280.2757 m/z.

R_f = 0.31 (silica, pentane/ethyl acetate, 5:1).

The data are in agreement with the literature.^[16]

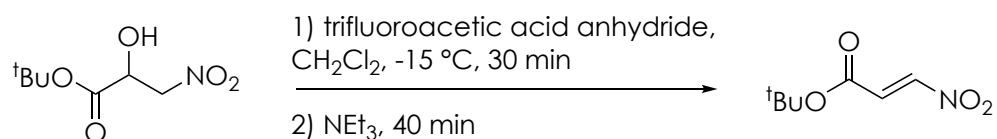
tert-Butyl 2-hydroxy-3-nitropropanoate

Di-tert-butyl 2,3-dihydroxysuccinate (4.0 g, 15.2 mmol, 1.0 equiv) was dissolved in H₂O and THF (1:1, 40 mL). Sodium periodate (4.25 g, 19.8 mmol, 1.3 equiv) dissolved in H₂O (30 mL) was added dropwise at 0 °C over 15 min and the reaction mixture was stirred for 2 h at 0 °C to rt. The crude reaction mixture was extracted with ethyl acetate (4 x 100 mL), the combined organic layers were dried over MgSO₄ and concentrated *under reduced pressure*. The resulting crude *tert*-butyl 2-oxoacetate was obtained as a colorless oily crude product. Due to its tendency to decompose the crude product was directly dissolved in nitromethane (24 mL, 265.7 mmol, 9.1 equiv) and Al₂O₃ (6.5 g, 61.3 mmol, 2.1 equiv) was added. The suspension was stirred overnight at room temperature. The resulting yellow suspension was filtered through celite and washed extensively with ethyl acetate (20 mL). The obtained solution was dried over MgSO₄ and concentrated under reduced pressure. The crude white solid was purified by column chromatography and *tert*-butyl 2-hydroxy-3-nitropropanoate was obtained as colorless solid.

¹H-NMR (300 MHz, CDCl₃) δ: 4.72 (d, *J* = 4.1 Hz, 1H), 4.49 (q, *J* = 4.3 Hz, 1H), 3.35 (d, *J* = 4.5 Hz, 1H), 1.52 (s, 9H).

¹³C-NMR (101 MHz, CDCl₃) δ: 169.85, 84.86, 77.05, 67.81, 28.00.

HRMS: ESI [M+Na] calculated: 214.0686, measured 214.0685.

tert-Butyl (*E*)-3-nitroacrylate (**9c**)

tert-Butyl 2-hydroxy-3-nitropropanoate was dissolved in CH₂Cl₂ (100 mL) followed by dropwise addition of trifluoroacetic acid anhydride (3.0 mL, 21.3 mmol, 1.0 equiv) at -15 °C. After 10 min of stirring freshly distilled NEt₃ (6.0 mL, 43.0 mmol, 2.0 equiv) was added dropwise over 30 min using a syringe pump. The reaction mixture was stirred at -15 °C for 40 min CH₂Cl₂ (100 mL) was added and the solution was washed with saturated aqueous NH₄Cl (3 x 100 mL). The organic layer was dried over MgSO₄ and concentrated under reduced pressure. The resulting yellow crude product was purified by flash column chromatography (silica, CH₂Cl₂) to afford the pure product (3.70 g, 21.4 mmol, 70% yield) as a yellow oil.

¹H-NMR (300 MHz, CDCl₃) δ: 7.57 (d, J = 13.4 Hz, 1H), 6.98 (d, J = 13.4 Hz, 1H), 1.49 (s, 9H).

¹³C-NMR (101 MHz, CDCl₃) δ = 161.75, 148.46, 129.56, 83.86, 27.94.

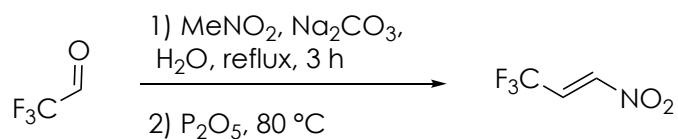
HRMS: ESI [M+NH₄] calculated: 191.1026 m/z, measured: 191.1027 m/z.

R_f = 0.75 (silica, UV, pentane/ethyl acetate, 10:1).

IR [cm⁻¹]: 3110, 2981, 1718, 1535, 1355, 1295, 1259, 1146, 947, 840, 756, 726, 671.

Boiling point: 120 °C at 11 mbar.

The data are in agreement with the literature.^[28]

(E)-3,3,3-Trifluoro-1-nitroprop-1-ene (15)

(E)-3,3,3-Trifluoro-1-nitroprop-1-ene was synthesized according to a known procedure.^[146-148]

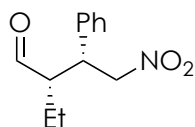
In a 100 mL flask fluoral (75%, 25.0 g, 161 mmol, 1.00 equiv), nitromethane (8.65 mL, 162 mmol, 1.00 equiv) and Na₂CO₃ (1.03 g, 10 mmol, 0.06 equiv) were stirred for 3 h at 60 °C. The reaction mixture was poured in water (15 mL) and extracted with Et₂O (2 x 25 mL). The residue was carefully distilled (boiling point 65 °C). The distillate was placed in a Kugelrohr apparatus and P₂O₅ (24.5 g, 172 mmol, 1.10 equiv) was added. In a continuous distillation for 2.5 h at 90 °C (E)-3,3,3-trifluoro-1-nitroprop-1-ene was isolated (3.37 g, 23.89 mmol, 15% yield).

¹H-NMR (300 MHz, CDCl₃) δ: 7.46 (d, *J* = 13.3 Hz, 1H), 7.21-7.02 (m, 1H).

The data are in agreement with the literature.^[146-148]

7.7 Analytical Data of Catalysis Products

(2*S*,3*R*)-2-Ethyl-4-nitro-3-phenylbutanal (7a)



Butanal (67.6 μ L, 750 μ mol, 1.50 equiv) and H-DPro-Pro-Glu-NH₂ (1.7 mg, 5 μ mol, 1 mol%) were dissolved in CHCl₃/*i*PrOH (9:1, 1.0 mL) and nitrostyrene (500 μ mol, 1.0 equiv) was added. The reaction was stirred for 3 h and the reaction mixture filtered through silica (washed with CH₂Cl₂ 5.0 mL). After removal of the solvents the residue was purified by column chromatography (silica, pentane/ethyl acetate, 10:1). (2*S*,3*R*)-2-ethyl-4-nitro-3-phenylbutanal was isolated as a colorless oil (109 mg, 493 μ mol, 98% yield).

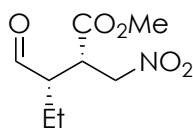
¹H-NMR (300 MHz, CDCl₃) δ : 9.72 (d, *J* = 2.3 Hz, 1H), 7.43-7.10 (m, 8H), 7.07-7.00 (m, 2H), 4.76-4.67 (m, 2H), 3.83 (td, *J* = 8.5, 6.3 Hz, 1H), 3.17-3.03 (m, 1H), 2.82-2.70 (m, 2H).

¹³C-NMR (101 MHz, CDCl₃) δ : 202.91, 137.13, 136.74, 129.22, 128.87, 128.74, 128.34, 128.05, 126.96, 78.03, 55.33, 43.45, 34.26.

Chiral separation: SFC (CO₂), AD-3 SFC, 5% MeOH, 2.0 mL/min, 40 °C

R_{t minor} = 1.003 min, R_{t major} 1.21 min.

The data are in agreement with the literature.^[79]

Methyl (2*S*,3*S*)-3-formyl-2-(nitromethyl)pentanoate (10a)

Butanal (67.6 μL , 750 μmol , 1.50 equiv) and H-DPro-Pro-Glu-NH₂ (1.7 mg, 5 μmol , 1 mol%) were dissolved in CHCl₃/iPrOH (9:1, 1.0 mL) and the methyl-nitroacrylate (65.4 mg, 500 μmol , 1.00 equiv) was added. The reaction was stirred for 3 h and the reaction mixture filtered through silica (washed with CH₂Cl₂ 5.0 mL). After removal of the solvents the residue was purified by column chromatography (silica, pentane/ethyl acetate, 3:1). Methyl (2*S*,3*S*)-3-formyl-2-(nitromethyl)pentanoate was isolated as a colorless oil (99.6 mg, 490 μmol , 98% yield).

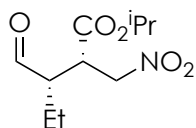
¹H-NMR (300 MHz, CDCl₃) δ : 9.65 (d, J = 0.9 Hz, 1H), 4.91 (dd, J = 14.7, 9.2 Hz, 1H), 4.40 (dd, J = 14.7, 4.0 Hz, 1H), 3.74 (s, 3H), 3.65 (ddd, J = 9.5, 5.9, 4.0 Hz, 1H), 2.80 (dtd, J = 7.2, 6.4, 0.8 Hz, 1H), 1.83 (dq, J = 14.8, 7.4 Hz, 1H), 1.62 -1.48 (m, 1H), 1.07 (t, J = 7.5 Hz, 3H).

¹³C-NMR (101 MHz, CDCl₃) δ : 201.06, 171.15, 72.92, 52.90, 52.39, 41.66, 19.65, 11.74.

HRMS : ESI [M+Na] calculated.: 226.0686, m/z; measured: 226.0688 m/z.

IR [cm⁻¹]: 2968, 2880, 1776, 1733, 1554, 1376.

Chiral separation was achieved by derivatisation to the corresponding alcohol (see Chapter 8.8).

Isopropyl (2*S*,3*S*)-3-formyl-2-(nitromethyl)pentanoate (**10b**)

Butanal (67.6 μL , 750 μmol , 1.50 equiv) and H-DPro-Pro-Glu-NH₂ (1.7 mg, 5 μmol , 1 mol%) were dissolved in CHCl₃/*i*PrOH (9:1, 1.0 mL) and the *iso*-propyl nitroacrylate (72.4 mg, 500 μmol , 1.0 equiv) was added. The reaction was stirred for 3 h and the reaction mixture filtered through silica (washed with CH₂Cl₂ 5.0 mL). After removal of the solvents the residue was purified by column chromatography (silica, pentane/ethyl acetate, 3:1). Isopropyl (2*S*,3*S*)-3-formyl-2-(nitromethyl)pentanoate was isolated as a colorless oil (112.5 mg, 486 μmol , 97% yield).

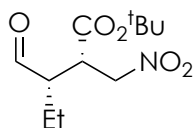
¹H-NMR (300 MHz, CDCl₃) δ : 9.64 (d, J = 0.9 Hz, 1H), 5.04 (hept, J = 6.3 Hz, 1H), 4.87 (dd, J = 14.5, 9.4 Hz, 1H), 4.39 (dd, J = 14.6, 4.1 Hz, 1H), 3.59 (ddd, J = 9.2, 6.0, 4.1 Hz, 1H), 2.75 (dtd, J = 7.5, 6.0, 0.9 Hz, 1H), 1.83 (dt, J = 14.8, 7.4 Hz, 1H), 1.65 – 1.41 (m, 1H), 1.23 (dd, J = 11.3, 6.2 Hz, 6H), 1.05 (t, J = 7.5 Hz, 3H).

¹³C-NMR (101 MHz, CDCl₃) δ : 201.06, 170.04, 73.08, 70.01, 52.32, 41.91, 21.70, 21.59, 19.45, 11.71.

HRMS : ESI [M+Na] calculated: 254.0999, m/z , measured: 254.1003 m/z .

IR [cm⁻¹]: 2979, 1719, 1554, 1376, 1201, 1103.

Chiral separation was achieved by derivatisation to the corresponding alcohol (see Chapter 8.8).

tert-Butyl (2*S*,3*S*)-3-formyl-2-(nitromethyl)pentanoate (**10c**)

Butanal (67.6 μ L, 750 μ mol, 1.50 equiv) and H-DPro-Pro-Glu-NH₂ (1.7 mg, 5 μ mol, 1 mol%) were dissolved in CHCl₃/*i*PrOH (9:1, 1.0 mL) and the *tert*-butyl nitroacrylate (86.5 mg, 500 μ mol, 1.0 equiv) was added. The reaction was stirred for 3 h and the reaction mixture filtered through silica (washed with CH₂Cl₂ 5.0 mL). After removal of the solvents the residue was purified by column chromatography (silica, pentane/ethyl acetate, 5:1). The product was isolated as a colorless oil (120 mg, 489 μ mol, 98% yield).

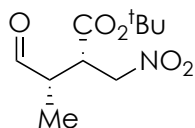
¹H-NMR (400 MHz, CDCl₃) : 4.89 (dd, *J* = 14.6, 10.6 Hz, 1H), 4.38 (dd, *J* = 14.6, 3.8 Hz, 1H), 3.73 (dd, *J* = 11.3, 4.1 Hz, 1H), 3.60 (dd, *J* = 11.3, 7.2 Hz, 1H), 3.41 (dt, *J* = 10.7, 4.0 Hz, 1H), 1.93 (tdd, *J* = 7.2, 4.2, 3.0 Hz, 1H), 1.73 (s, 1H), 1.46 (s, 9H), 1.43-1.33 (m, 2H), 0.99 (t, *J* = 7.4 Hz, 3H).

¹³C-NMR (101 MHz, CDCl₃): 171.25, 82.67, 73.91, 62.98, 45.26, 42.77, 28.05, 21.51, 12.11.

HRMS: ESI [M+Na] calculated: 268.1155 m/z, measured 268.1157 m/z.

IR [cm⁻¹]: 2973, 2879, 1776, 1720, 1555, 1369, 115.

Chiral separation was achieved by derivatisation to the corresponding alcohol (see Chapter 8.8).

tert-Butyl (2*S*,3*S*)-3-methyl-2-(nitromethyl)-4-oxobutanoate (**10d**)

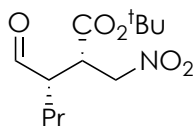
Propionaldehyde (43.3 mg, 750 μ mol, 1.50 equiv), H-DPro-Pro-Glu-NH₂ (85 μ g, 0.25 μ mol, 0.05 mol%) and 4-hydroxy-4-methylpentan-2-one (0.12 μ L, 1.0 μ mol, 0.2 mol%) were dissolved in CHCl₃/iPrOH (9:1, 1.0 mL) and the nitroacrylate (86.5 mg, 500 μ mol, 1.0 equiv) was added. The reaction was stirred for 16 h at room temperature and the reaction mixture filtered through silica (washed with CH₂Cl₂ 5.0 mL). After removal of the solvents the residue was purified by column chromatography (silica, pentane/ethyl acetate, 5:1). *tert*-Butyl (2*S*,3*S*)-3-methyl-2-(nitromethyl)-4-oxobutanoate was isolated as a colorless oil (112 mg, 484 μ mol, 97% yield).

¹H-NMR (400 MHz, CDCl₃) δ : 9.68 (s, 1H), 4.85 (dd, *J* = 14.4, 8.8 Hz, 1H), 4.41 (dd, *J* = 14.4, 5.3 Hz, 1H), 3.70 (ddd, *J* = 8.7, 5.3, 4.7 Hz, 1H), 2.67 (qd, *J* = 7.2, 4.7 Hz, 1H), 1.43 (s, 9H), 1.18 (d, *J* = 7.3 Hz, 3H).

¹³C-NMR (101 MHz, CDCl₃) δ : 200.39, 168.89, 83.64, 73.43, 45.71, 43.81, 27.95, 9.95.

HRMS: ESI [M+Na] calculated: 254.0999 m/z, measured 254.0999 m/z.

Chiral separation was achieved by derivatisation to the corresponding alcohol (see Chapter 8.8).

tert-Butyl (2*S*,3*S*)-3-formyl-2-(nitromethyl)hexanoate (**10e**)

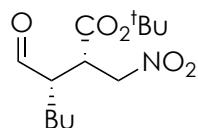
Pentanal (46.6 mg, 750 μmol , 1.50 equiv), H-DPro-Pro-Glu-NH₂ (85 μg , 0.25 μmol , 0.05 mol%) and 4-hydroxy-4-methylpentan-2-one (0.12 μL , 1.0 μmol , 0.2 mol%) were dissolved in CHCl₃/*i*PrOH (9:1, 1.0 mL) and *tert*-butyl nitroacrylate (86.5 mg, 500 μmol , 1.0 equiv) was added. The reaction was stirred for 16 h at room temperature and the reaction mixture filtered through silica (washed with CH₂Cl₂ 5.0 mL). After removal of the solvents the residue was purified by column chromatography (silica, pentane/ethyl acetate, 5:1). *tert*-Butyl (2*S*,3*S*)-3-formyl-2-(nitromethyl)hexanoate was isolated as a colorless oil (126 mg, 484 μmol , 97% yield).

¹H-NMR (400 MHz, CDCl₃) δ : 9.64 (d, J = 1.0 Hz, 1H), 4.85 (ddd, J = 14.5, 9.4, 0.9 Hz, 1H), 4.34 (dd, J = 14.5, 4.3 Hz, 1H), 3.55 (ddd, J = 9.5, 5.5, 4.2 Hz, 1H), 2.86 – 2.48 (m, 1H), 1.87 – 1.70 (m, 1H), 1.55 – 1.33 (m, 12H), 0.96 (dd, J = 7.5, 6.5 Hz, 3H).

¹³C-NMR (101 MHz, CDCl₃) δ : 201.15, 169.46, 83.32, 73.23, 50.85, 42.90, 27.92, 20.65, 14.06.

HRMS: ESI [M+Na] calculated: 282.1312 m/z, measured 282.1316 m/z.

Chiral separation was achieved by derivatisation to the corresponding alcohol (see Chapter 8.8).

tert-Butyl (2*S*,3*S*)-3-formyl-2-(nitromethyl)heptanoate (**10f**)

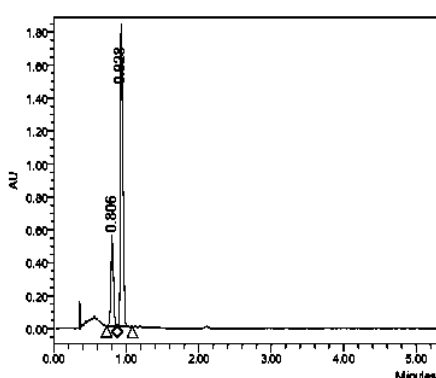
Hexanal (86.6 mg, 750 μmol , 1.50 equiv), H-DPro-Pro-Glu-NH₂ (85 μg , 0.25 μmol , 0.05 mol%) and 4-hydroxy-4-methylpentan-2-one (0.12 μL , 1.0 μmol , 0.2 mol%) were dissolved in CHCl₃/*i*PrOH (9:1, 1.0 mL) and *tert*-butyl nitroacrylate (86.5 mg, 500 μmol , 1.0 equiv) was added. The reaction was stirred for 16 h at room temperature and the reaction mixture filtered through silica (washed with CH₂Cl₂ 5.0 mL). After removal of the solvents the residue was purified by column chromatography (silica, pentane/ethyl acetate, 5:1). *tert*-Butyl (2*S*,3*S*)-3-formyl-2-(nitromethyl)heptanoate was isolated as a colorless oil (136 mg, 496 μmol , 99% yield).

¹H-NMR (400 MHz, CDCl₃) δ : 9.65 (d, J = 0.9 Hz, 1H), 4.85 (dd, J = 14.4, 9.4 Hz, 1H), 4.35 (dd, J = 14.4, 4.2 Hz, 1H), 3.55 (ddd, J = 9.6, 5.6, 4.2 Hz, 1H), 2.75 (dtd, J = 8.0, 5.5, 0.9 Hz, 1H), 1.86 – 1.73 (m, 1H), 1.47 (tt, J = 2.7, 1.2 Hz, 1H), 1.45 (s, 9H), 1.40 – 1.30 (m, 3H), 0.92 (t, J = 7.0 Hz, 3H).

¹³C-NMR (101 MHz, CDCl₃) δ : 201.18, 169.49, 83.33, 77.16, 73.28, 51.05, 42.95, 29.47, 27.95, 25.76, 22.76, 13.90.

Chiral separation: SFC (CO₂), OJ-3 SFC, 1% MeOH, 2.0 mL/min, 40 °C

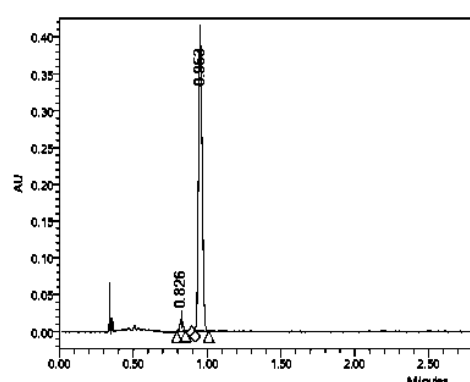
$R_{\text{t minor}}$ = 2.187 min, $R_{\text{t major}}$ = 2.545 min. (see remarks, page 89)



Processed Channel: PDA Ch2
214nm@1.2nm

	Processed Channel	Retention Time (min)	Area	% Area	Height
1	PDA Ch2 214nm@1.2nm	0.806	1339522	22.80	504007
2	PDA Ch2 214nm@1.2nm	0.828	4587655	77.40	1786964

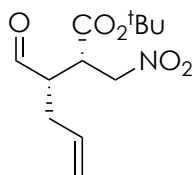
racemic sample



Processed Channel: PDA Ch2
214nm@1.2nm

	Processed Channel	Retention Time (min)	Area	% Area	Height
1	PDA Ch2 214nm@1.2nm	0.826	24581	3.41	16446
2	PDA Ch2 214nm@1.2nm	0.853	697130	86.59	404670

selective sample

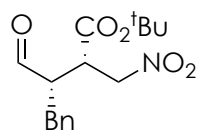
tert-Butyl (2*S*,3*S*)-3-formyl-2-(nitromethyl)hex-5-enoate (**10g**)

Pent-4-enal (62.5 μL , 750 μmol , 1.50 equiv), H-DPro-Pro-Glu-NH₂ (340 μg , 1.00 μmol , 0.2 mol%) and 4-hydroxy-4-methylpentan-2-one (0.12 μL , 1.0 μmol , 0.2 mol%) were dissolved in CHCl₃/iPrOH (9:1, 1.0 mL) and *tert*-butyl nitroacrylate (86.5 mg, 500 μmol , 1.0 equiv) was added. The reaction was stirred for 16 h at room temperature and the reaction mixture filtered through silica (washed with CH₂Cl₂ 5.0 mL). After removal of the solvents the residue was purified by column chromatography (silica, pentane/ethyl acetate, 5:1). *tert*-Butyl (2*S*,3*S*)-3-formyl-2-(nitromethyl)hex-5-enoate was isolated as a colorless oil (125 mg, 486 μmol , 97% yield).

¹H-NMR (400 MHz, CDCl₃) δ : 9.66 (d, J = 0.6 Hz, 1H), 6.01-5.61 (m, 1H), 5.27-5.12 (m, 2H), 4.88 (dd, J = 14.5, 9.2 Hz, 1H), 4.38 (dd, J = 14.5, 4.3 Hz, 1H), 3.61 (ddd, J = 9.3, 5.1, 4.3 Hz, 1H), 2.89 (td, J = 7.1, 5.1 Hz, 1H), 2.71-2.53 (m, 1H), 2.24 (dtt, J = 14.7, 7.2, 1.2 Hz, 1H), 1.44 (s, 9H).

¹³C-NMR (101 MHz, CDCl₃) δ : 200.47, 169.24, 133.64, 83.54, 73.08, 50.47, 42.78, 30.40, 27.94.

Chiral separation was achieved by derivatisation to the corresponding alcohol (see Chapter 8.8).

tert-Butyl (2*S*,3*S*)-3-benzyl-2-(nitromethyl)-4-oxobutanoate (**10h**)

3-Phenylpropanal (100.6 mg, 750 μmol , 1.50 equiv), H-DPro-Pro-Glu-NH₂ (850 μg , 2.5 μmol , 0.5 mol%) and 4-hydroxy-4-methylpentan-2-one (0.12 μL , 1.0 μmol , 0.2 mol%) were dissolved in CHCl₃/iPrOH (9:1, 1.0 mL) and *tert*-butyl nitroacrylate (86.5 mg, 500 μmol , 1.0 equiv) was added. The reaction was stirred for 36 h at room temperature and the reaction mixture filtered through silica (washed with CH₂Cl₂ 5.0 mL). After removal of the solvents the residue was purified by column chromatography (silica, pentane/ethyl acetate, 5:1). *tert*-Butyl (2*S*,3*S*)-3-benzyl-2-(nitromethyl)-4-oxobutanoate was isolated as a colorless oil (151.1 mg, 491 μg , 98% yield).

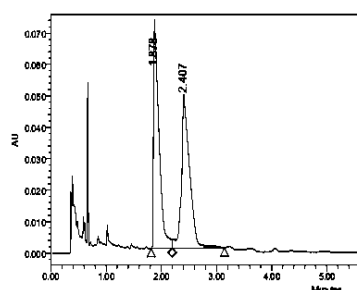
¹H-NMR (400 MHz, CDCl₃) δ : 9.70 (s, 1H), 7.39 – 7.32 (m, 2H), 7.31 – 7.26 (m, 1H), 7.25 – 7.17 (m, 2H), 4.78 (dd, J = 14.5, 9.1 Hz, 1H), 4.27 (dd, J = 14.5, 4.3 Hz, 1H), 3.64 (dt, J = 8.9, 4.3 Hz, 1H), 3.23 (dd, J = 14.0, 7.4 Hz, 1H), 3.14 (td, J = 7.3, 4.4 Hz, 1H), 2.73 (dd, J = 14.0, 7.3 Hz, 1H), 1.48 (s, 9H).

¹³C-NMR (101 MHz, CDCl₃) δ : 200.50, 169.07, 137.36, 129.16, 128.90, 127.32, 83.59, 73.06, 52.82, 43.01, 32.19, 27.91.

HRMS: ESI [M+Na] calculated: 330.1312 m/z, measured 330.1312 m/z.

Chiral separation: SFC (CO₂), OJ-3 SFC, 1% MeOH, 2.0 mL/min, 40 °C

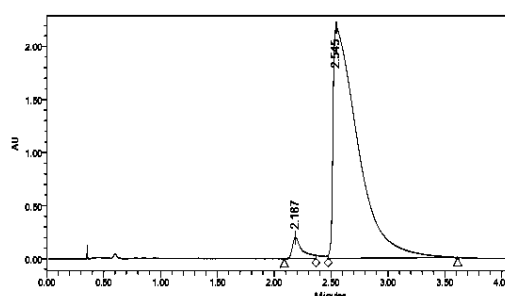
$R_{t \text{ minor}}$ = 2.187 min, $R_{t \text{ major}}$ = 2.254 min. (see remarks, page 89)



Processed Channel: PDA Ch1 254nm@1.2nm
-Compens.

	Processed Channel	Retention Time (min)	Area	% Area	Height
1	PDA Ch1 254nm@1.2nm-Compens.	1.878	495279	49.72	70720
2	PDA Ch1 254nm@1.2nm-Compens.	2.407	909827	50.28	48973

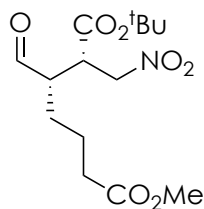
racemic sample



Processed Channel: PDA Ch2 214nm@1.2nm

	Processed Channel	Retention Time (min)	Area	% Area	Height
1	PDA Ch2 214nm@1.2nm	2.187	1187598	3.47	198478
2	PDA Ch2 214nm@1.2nm	2.254	33016270	96.53	2172852

selective sample

1-(*tert*-Butyl) 7-methyl (2*S*,3*S*)-3-formyl-2-(nitromethyl)heptanedioate (**10i**)

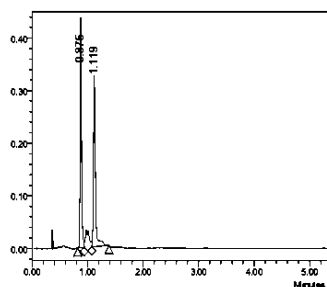
Methyl 6-oxohexanoate (108 mg, 750 μmol , 1.50 equiv), H-DPro-Pro-Glu-NH₂ (85 μg , 0.25 μmol , 0.05 mol%) and 4-hydroxy-4-methylpentan-2-one (0.12 μL , 1.0 μmol , 0.2 mol%) were dissolved in CHCl₃/iPrOH (9:1, 1.0 mL) and *tert*-butyl nitroacrylate (86.5 mg, 500 μmol , 1.0 equiv) was added. The reaction was stirred for 16 h at room temperature and the reaction mixture filtered through silica (washed with CH₂Cl₂ 5.0 mL). After removal of the solvents the residue was purified by column chromatography (silica, pentane/ethyl acetate, 5:1). 1-(*tert*-Butyl) 7-methyl (2*S*,3*S*)-3-formyl-2-(nitromethyl)heptanedioate was isolated as a colorless oil (153 mg, 486 μmol , 97% yield).

¹H-NMR (400 MHz, CDCl₃) δ : 9.66 (d, $J = 0.7$ Hz, 1H), 4.85 (dd, $J = 14.5, 9.2$ Hz, 1H), 4.38 (dd, $J = 14.5, 4.5$ Hz, 1H), 3.67 (s, 3H), 3.59 (ddd, $J = 9.4, 5.2, 4.4$ Hz, 1H), 2.82 – 2.64 (m, 1H), 2.36 (td, $J = 7.0, 1.7$ Hz, 2H), 1.90 – 1.74 (m, 2H), 1.74 – 1.60 (m, 1H), 1.53 – 1.45 (m, 1H), 1.43 (s, 9H).

¹³C-NMR (101 MHz, CDCl₃) δ : 200.53, 173.27, 169.16, 83.56, 73.12, 51.84, 50.85, 42.87, 33.60, 27.92, 25.19, 22.69.

Chiral separation: SFC (CO₂), IC-3 SFC, 8% MeOH, 2.0 mL/min, 40 °C

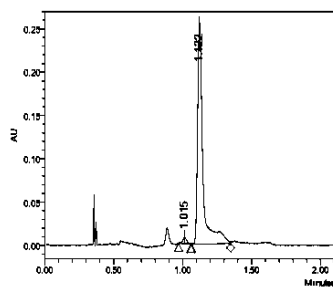
$R_{t \text{ minor}} = 1.015$ min, $R_{t \text{ major}} = 1.122$ min. (see remarks, page 89)



Processed Channel: PDA Ch2
214nm@1.2nm

Processed Channel	Retention Time (min)	Area	% Area	Height
1 PDA Ch2 214nm@1.2nm	0.875	751065	49.49	428758
2 PDA Ch2 214nm@1.2nm	1.119	766578	50.51	311868

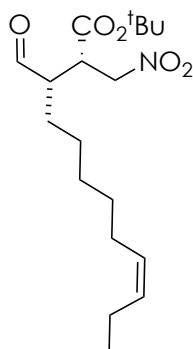
racemic sample



Processed Channel: PDA Ch2
214nm@1.2nm

Processed Channel	Retention Time (min)	Area	% Area	Height
1 PDA Ch2 214nm@1.2nm	1.015	14805	2.07	7722
2 PDA Ch2 214nm@1.2nm	1.122	686683	97.93	255450

selective sample

tert-Butyl (2*S*,3*S*,*Z*)-3-formyl-2-(nitromethyl)dodec-9-enoate (**10j**)

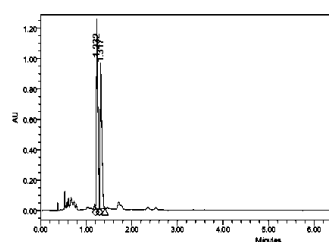
(*Z*)-Undec-8-enal (126.21 mg, 750 μ mol, 1.50 equiv), H-DPro-Pro-Glu-NH₂ (85 μ g, 0.25 μ mol, 0.05 mol%) and 4-hydroxy-4-methylpentan-2-one (0.12 μ L, 1.0 μ mol, 0.2 mol%) were dissolved in CHCl₃/*i*PrOH (9:1, 1.0 mL) and *tert*-butyl nitroacrylate (86.6 mg, 500 μ mol, 1.0 equiv) was added. The reaction was stirred for 16 h at room temperature and the reaction mixture filtered through silica (washed with CH₂Cl₂ 5.0 mL). After removal of the solvents the residue was purified by column chromatography (silica, pentane/ethyl acetate, 5:1). *tert*-Butyl (2*S*,3*S*,*Z*)-3-formyl-2-(nitromethyl)dodec-9-enoate was isolated as a colorless oil (165 mg, 483 μ mol, 97%).

¹H-NMR (400 MHz, CDCl₃) δ : 9.64 (d, *J* = 0.8 Hz, 1H), 5.72 – 5.04 (m, 2H), 4.85 (dd, *J* = 14.4, 9.3 Hz, 1H), 4.34 (dd, *J* = 14.4, 4.3 Hz, 1H), 3.55 (ddd, *J* = 9.5, 5.5, 4.3 Hz, 1H), 2.74 (dddd, *J* = 7.9, 5.4, 4.0, 0.9 Hz, 1H), 2.10 – 1.94 (m, 5H), 1.78 (tdd, *J* = 11.4, 5.9, 3.5 Hz, 1H), 1.43 (s, 9H), 1.40 – 1.29 (m, 6H), 0.95 (t, *J* = 7.5 Hz, 3H).

¹³C-NMR (101 MHz, CDCl₃) δ : 201.11, 169.45, 132.11, 128.83, 83.34, 73.26, 51.06, 42.94, 29.49, 29.23, 27.93, 27.30, 27.00, 26.01, 20.66, 14.50.

Chiral separation: SFC (CO₂), OD-3 SFC, 8% MeOH, 2.0 mL/min, 40 °C

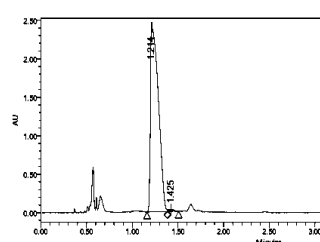
R_{t major} = 1.232 min, R_{t minor} 1.317 min. (see remarks, page 89)



Processed Channel: PDA Ch2
214nm@1.2nm

Processed Channel	Retention Time (min)	Area	% Area	Height
1 PDA.Ch2.214nm@1.2nm	1.232	2790620	50.00	1210270
2 PDA.Ch2.214nm@1.2nm	1.317	2408818	49.99	920090

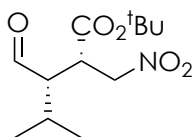
racemic sample



Processed Channel: PDA Ch2 214nm@1.2nm

Processed Channel	Retention Time (min)	Area	% Area	Height
1 PDA.Ch2.214nm@1.2nm	1.234	14644818	99.96	2364907
2 PDA.Ch2.214nm@1.2nm	1.422	94238	0.04	21122

selective sample

tert-Butyl (2*S*,3*S*)-3-formyl-4-methyl-2-(nitromethyl)pentanoate (**10k**)

3-Methylbutanal (80.8 μL , 750 μmol , 1.50 equiv), H-DPro-Pro-Glu-NH₂ (85 μg , 0.25 μmol , 0.05 mol%) and 4-hydroxy-4-methylpentan-2-one (0.12 μL , 1.0 μmol , 0.2 mol%) were dissolved in CHCl₃/*i*PrOH (9:1, 1.0 mL) and *tert*-butyl nitroacrylate (86.5 mg, 500 μmol , 1.0 equiv) was added. The reaction was stirred for 16 h at room temperature and the reaction mixture filtered through silica (washed with CH₂Cl₂ 5.0 mL). After removal of the solvents the residue was purified by column chromatography (silica, pentane/ethyl acetate, 5:1). *tert*-Butyl (2*S*,3*S*)-3-formyl-4-methyl-2-(nitromethyl)pentanoate was isolated as a colorless oil (126.5 mg, 487 μmol , 98% yield).

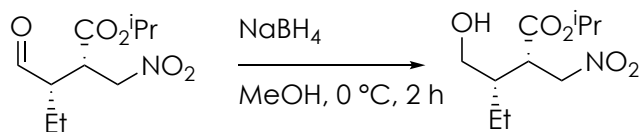
¹H-NMR (400 MHz, CDCl₃) δ : 9.80 (d, J = 1.4 Hz, 1H), 4.81 (dd, J = 14.4, 10.2 Hz, 1H), 4.35 (dd, J = 14.4, 3.1 Hz, 1H), 3.52 (ddd, J = 10.2, 7.0, 3.1 Hz, 1H), 2.78 (td, J = 7.2, 1.4 Hz, 1H), 2.27 – 1.85 (m, 1H), 1.44 (s, 9H), 1.13 (dd, J = 19.0, 6.8 Hz, 6H).

¹³C-NMR (101 MHz, CDCl₃) δ : 202.76, 170.26, 83.12, 73.46, 56.92, 42.48, 27.94, 27.91, 21.49, 19.69.

Chiral separation was achieved by derivatisation to the corresponding alcohol (see Chapter 8.8).

7.8 Analytical Data of Catalysis Product Derivatives

Isopropyl (2*S*,3*S*)-3-(hydroxymethyl)-2-(nitromethyl)pentanoate



In a 5 mL flask isopropyl (2*S*,3*S*)-3-formyl-2-(nitromethyl)pentanoate (**10b**, 115.6 mg, 500 μmol , 1.00 equiv) was dissolved in MeOH (1.0 mL) under argon atmosphere at 0 $^\circ\text{C}$. NaBH₄ (18.9 mg, 500 μmol , 1.00 equiv) was added in one portion and the reaction mixture was stirred for 2 h at 0 $^\circ\text{C}$. The solvents were removed under reduced pressure and the orange solid was purified by column chromatography (silica, pentane/ethyl acetate) to result in isopropyl (2*S*,3*S*)-3-(hydroxymethyl)-2-(nitromethyl)pentanoate as a colorless oil (93 mg, 398.7 μmol , 80% yield).

¹H-NMR (400 MHz, CDCl₃) δ : 5.06 (heptd, $J = 6.3, 1.3$ Hz, 1H), 4.93 (ddd, $J = 14.7, 10.6, 0.9$ Hz, 1H), 4.43 (dd, $J = 14.7, 3.7$ Hz, 1H), 3.80 – 3.65 (m, 1H), 3.58 (ddd, $J = 11.4, 7.0, 1.2$ Hz, 1H), 3.52 – 3.33 (m, 1H), 1.99 – 1.90 (m, 1H), 1.90 – 1.80 (m, 1H), 1.38 (p, $J = 7.5$ Hz, 2H), 1.24 (ddd, $J = 11.5, 6.3, 0.9$ Hz, 6H), 0.97 (td, $J = 7.5, 0.9$ Hz, 3H).

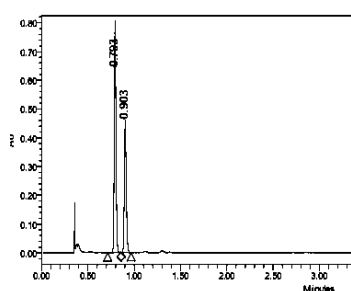
¹³C-NMR (101 MHz, CDCl₃) δ : 171.70, 73.67, 69.42, 62.68, 44.58, 42.75, 21.82, 21.68, 21.57, 12.04.

HRMS : ESI [M+Na] calculated: 256.1155, measured: 256.1160 m/z.

IR [cm⁻¹]: 3512 (broad), 2970, 1722, 1556, 1377, 1105.

Chiral separation: SFC (CO₂), IC-3 SFC, 8% MeOH, 2.0 mL/min, 40 $^\circ\text{C}$

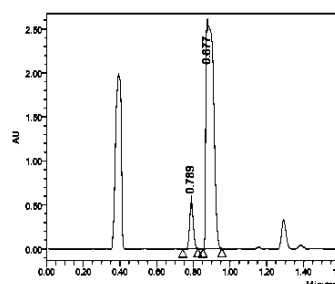
$R_{\text{t minor}} = 0.793$ min, $R_{\text{t major}} = 0.903$ min. (see remarks, page 89)



**Processed Channel: PDA Ch2
214nm@1.2nm**

Processed Channel	Retention Time (min)	Area	% Area	Height
1 PDA Ch2 214nm@1.2nm	0.793	1035120	61.47	783283
2 PDA Ch2 214nm@1.2nm	0.903	648755	38.53	438118

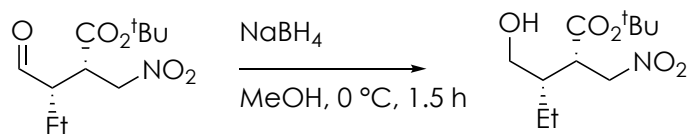
racemic sample



**Processed Channel: PDA Ch2
214nm@1.2nm**

Processed Channel	Retention Time (min)	Area	% Area	Height
1 PDA Ch2 214nm@1.2nm	0.788	738747	8.88	536086
2 PDA Ch2 214nm@1.2nm	0.877	7518870	81.04	2546380

selective sample

tert-Butyl (2*S*,3*S*)-3-(hydroxymethyl)-2-(nitromethyl)pentanoate

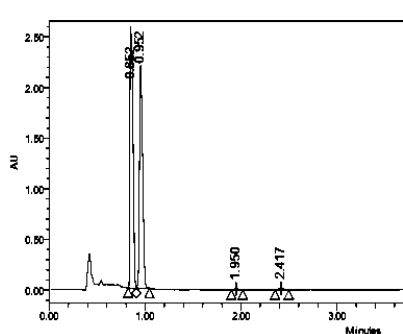
In a 5 mL flask the *tert*-butyl (2*S*,3*S*)-3-formyl-2-(nitromethyl)pentanoate (**10c**, 122 mg, 500 μmol , 1.00 equiv) was dissolved in MeOH (1.0 mL) under argon atmosphere at 0 $^\circ\text{C}$. NaBH₄ (18.9 mg, 500 μmol , 1.00 equiv) was added in one portion and the reaction mixture was stirred for 1.5 h at 0 $^\circ\text{C}$. The solvents were removed under reduced pressure and the orange solid was purified by column chromatography (silica, pentane/ethyl acetate) to result in *tert*-butyl (2*S*,3*S*)-3-(hydroxymethyl)-2-(nitromethyl)pentanoate as a colorless oil (105.3 mg, 426 μmol , 85% yield).

¹H-NMR (400 MHz, CDCl₃) δ : 4.89 (dd, $J = 14.6, 10.6$ Hz, 1H), 4.38 (dd, $J = 14.6, 3.8$ Hz, 1H), 3.73 (dd, $J = 11.3, 4.1$ Hz, 1H), 3.60 (dd, $J = 11.3, 7.2$ Hz, 1H), 3.41 (dt, $J = 10.7, 4.0$ Hz, 1H), 1.93 (tdd, $J = 7.2, 4.2, 3.0$ Hz, 1H), 1.73 (s, 1H), 1.46 (s, 9H), 1.43-1.33 (m, 2H), 0.99 (t, $J = 7.4$ Hz, 3H).

¹³C-NMR (101 MHz, CDCl₃) δ : 171.25, 82.67, 73.91, 62.98, 45.26, 42.77, 28.05, 21.51, 12.11.

Chiral separation: SFC (CO₂), AD-3 SFC, 5% MeOH, 2.0 mL/min, 40 $^\circ\text{C}$

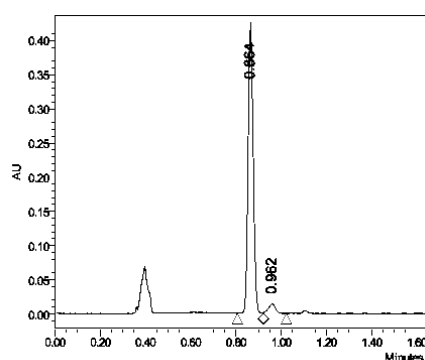
$R_{t \text{ minor}} = 0.852$ min, $R_{t \text{ major}} = 0.952$ min. (see remarks, page 89)



**Processed Channel: PDA Ch2
214nm@1.2nm**

Processed Channel	Retention Time (min)	Area	% Area	Height
1 PDA Ch2 214nm@1.2nm	0.852	5908884	52.51	2509073
2 PDA Ch2 214nm@1.2nm	0.952	4980447	46.63	2133902
3 PDA Ch2 214nm@1.2nm	1.950	34438	0.32	14373
4 PDA Ch2 214nm@1.2nm	2.417	57378	0.54	17381

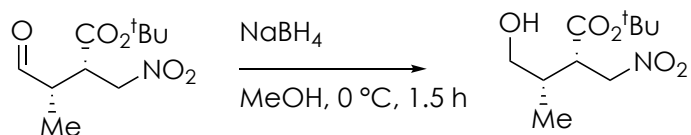
racemic sample



**Processed Channel: PDA Ch2
214nm@1.2nm**

Processed Channel	Retention Time (min)	Area	% Area	Height
1 PDA Ch2 214nm@1.2nm	0.864	663439	95.71	414909
2 PDA Ch2 214nm@1.2nm	0.962	29718	4.29	14261

selective sample

tert-Butyl (2*S*,3*S*)-4-hydroxy-3-methyl-2-(nitromethyl)butanoate

In a 5 mL flask the *tert*-butyl (2*S*,3*S*)-3-methyl-2-(nitromethyl)-4-oxobutanoate (**10d**, 115 mg, 500 μmol , 1.00 equiv) was dissolved in MeOH (1.0 mL) under argon atmosphere at 0 $^\circ\text{C}$. NaBH₄ (18.9 mg, 500 μmol , 1.00 equiv) was added in one portion and the reaction mixture was stirred for 1.5 h at 0 $^\circ\text{C}$. The solvents were removed under reduced pressure and the orange solid was purified by column chromatography (silica, pentane/ethyl acetate) to result in *tert*-butyl (2*S*,3*S*)-4-hydroxy-3-methyl-2-(nitromethyl)butanoate as a colorless oil (81.8 mg, 350 μmol , 70% yield).

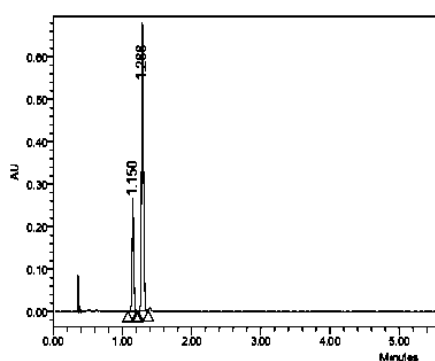
¹H-NMR (400 MHz, CDCl₃) δ : 4.83 (dd, $J = 14.5, 10.5$ Hz, 1H), 4.41 (dd, $J = 14.5, 4.2$ Hz, 1H), 3.73 – 3.47 (m, 2H), 3.35 (dt, $J = 10.6, 4.4$ Hz, 1H), 2.06 (pt, $J = 7.2, 4.8$ Hz, 1H), 1.91 (s, 1H), 1.47 (s, 9H), 0.95 (d, $J = 7.1$ Hz, 3H).

¹³C-NMR (101 MHz, CDCl₃) δ : 170.55, 82.78, 74.46, 65.66, 45.63, 36.09, 28.09, 13.51.

HRMS: ESI [M+Na] calculated: 256.1155 m/z, measured 256.1150 m/z.

Chiral separation: SFC (CO₂), IC-3 SFC, 5% MeOH, 2.0 mL/min, 40 $^\circ\text{C}$

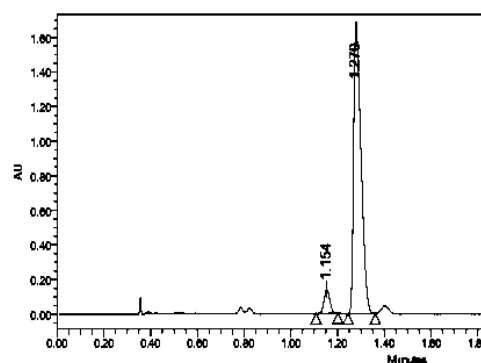
$R_{t \text{ minor}} = 1.150$ min, $R_{t \text{ major}} = 1.288$ min. (see remarks, page 89)



Processed Channel: PDA Ch2
214nm@1.2nm

Processed Channel	Retention Time (min)	Area	% Area	Height
1 PDA Ch2 214nm@1.2nm	1.150	440937	24.94	249425
2 PDA Ch2 214nm@1.2nm	1.288	1327239	75.06	800608

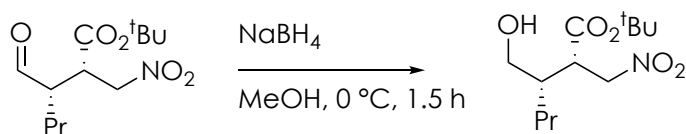
racemic sample



Processed Channel: PDA Ch2
214nm@1.2nm

Processed Channel	Retention Time (min)	Area	% Area	Height
1 PDA Ch2 214nm@1.2nm	1.154	237402	5.09	138018
2 PDA Ch2 214nm@1.2nm	1.279	3963472	93.91	1646526

selective sample

tert-Butyl (2*S*,3*S*)-3-(hydroxymethyl)-2-(nitromethyl)hexanoate

In a 5 mL flask *tert*-butyl (2*S*,3*S*)-3-formyl-2-(nitromethyl)hexanoate (**10e**, 129 mg, 500 μmol , 1.00 equiv) was dissolved in MeOH (1.0 mL) under argon atmosphere at 0 $^\circ\text{C}$. NaBH₄ (18.9 mg, 500 μmol , 1.00 equiv) was added in one portion and the reaction mixture was stirred for 1.5 h at 0 $^\circ\text{C}$. The solvents were removed under reduced pressure and the orange solid was purified by column chromatography (silica, pentane/ethyl acetate) to result in *tert*-butyl (2*S*,3*S*)-3-(hydroxymethyl)-2-(nitromethyl)hexanoate as a colorless oil (65 mg, 248 μmol , 50% yield).

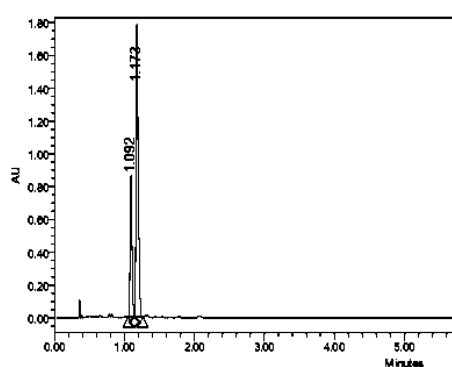
¹H-NMR (400 MHz, CDCl₃) δ : 4.88 (dd, $J = 14.6, 10.6$ Hz, 1H), 4.38 (dd, $J = 14.6, 3.8$ Hz, 1H), 3.70 (dd, $J = 11.3, 4.1$ Hz, 1H), 3.57 (dd, $J = 11.3, 7.3$ Hz, 1H), 3.39 (dt, $J = 10.6, 3.9$ Hz, 1H), 2.11 – 1.94 (m, 1H), 1.81 (s, 1H), 1.46 (s, 9H), 1.44 – 1.20 (m, 4H), 1.05 – 0.83 (m, 3H).

¹³C-NMR (101 MHz, CDCl₃) δ : 171.26, 82.66, 73.90, 63.32, 45.27, 40.81, 30.67, 28.04, 20.64, 14.21.

HRMS: ESI [M+Na] calculated: 284.1468 m/z, measured 284.1472 m/z.

Chiral separation: SFC (CO₂), IC-3 SFC, 8% MeOH, 2.0 mL/min, 40 $^\circ\text{C}$

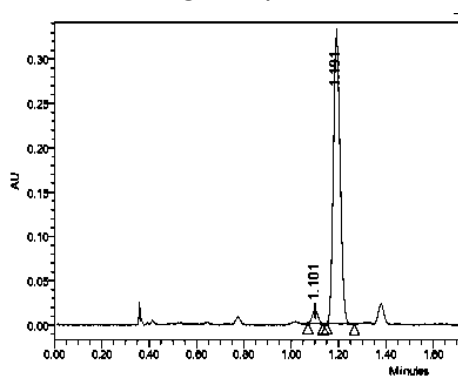
$R_{t \text{ minor}} = 1.101$ min, $R_{t \text{ major}} = 1.191$ min. (see remarks, page 89)



**Processed Channel: PDA Ch2
214nm@1.2nm**

	Processed Channel	Retention Time (min)	Area	% Area	Height
1	PDA Ch2 214nm@1.2nm	1.082	1524408	27.36	817382
2	PDA Ch2 214nm@1.2nm	1.173	4047980	72.64	1738297

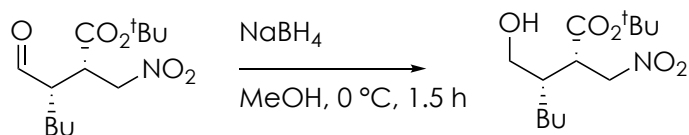
racemic sample



**Processed Channel: PDA Ch2
214nm@1.2nm**

	Processed Channel	Retention Time (min)	Area	% Area	Height
1	PDA Ch2 214nm@1.2nm	1.101	24632	3.88	14575
2	PDA Ch2 214nm@1.2nm	1.191	652871	96.32	324059

selective sample

tert-Butyl (2*S*,3*S*)-3-(hydroxymethyl)-2-(nitromethyl)heptanoate

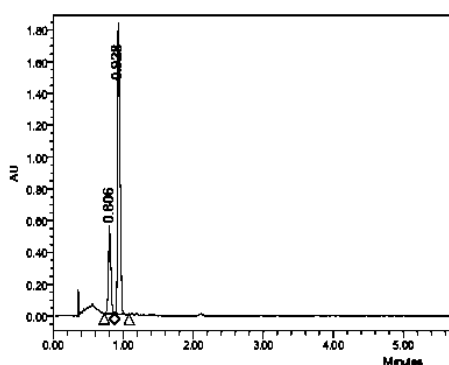
In a 5 mL flask *tert*-butyl (2*S*,3*S*)-3-formyl-2-(nitromethyl)heptanoate (**10f**, 136 mg, 500 μmol , 1.00 equiv) was dissolved in MeOH (1.0 mL) under argon atmosphere at 0 $^\circ\text{C}$. NaBH₄ (18.9 mg, 500 μmol , 1.00 equiv) was added in one portion and the reaction mixture was stirred for 1.5 h at 0 $^\circ\text{C}$. The solvents were removed under reduced pressure and the orange solid was purified by column chromatography (silica, pentane/ethyl acetate) to result in *tert*-butyl (2*S*,3*S*)-3-(hydroxymethyl)-2-(nitromethyl)heptanoate as a colorless oil (99.5 mg, 361 μmol , 72% yield).

¹H-NMR (400 MHz, CDCl₃) δ : 4.88 (dd, $J = 14.6, 10.7$ Hz, 1H), 4.38 (dd, $J = 14.6, 3.8$ Hz, 1H), 3.70 (dd, $J = 11.3, 4.2$ Hz, 1H), 3.57 (dd, $J = 11.3, 7.2$ Hz, 1H), 3.39 (dt, $J = 10.7, 3.9$ Hz, 1H), 2.05 – 1.94 (m, 1H), 1.81 (s, 1H), 1.46 (s, 9H), 1.39 – 1.23 (m, 6H), 0.90 (t, $J = 6.8$ Hz, 3H).

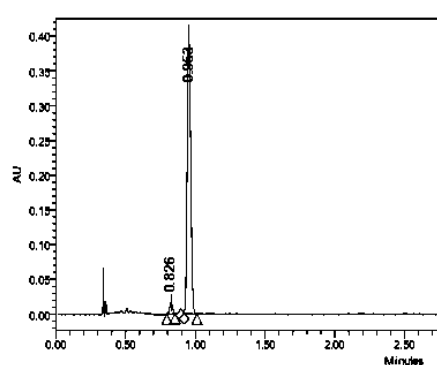
¹³C-NMR (101 MHz, CDCl₃) δ : 171.27, 82.63, 73.90, 63.31, 45.33, 41.08, 29.64, 28.24, 28.04, 22.88, 14.05.

Chiral separation: SFC (CO₂), OJ-3 SFC, 2% MeOH, 2.0 mL/min, 40 $^\circ\text{C}$

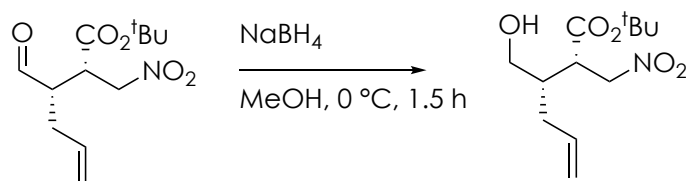
$R_{t \text{ minor}} = 0.826$ min, $R_{t \text{ major}} = 0.953$ min. (see remarks, page 89)



racemic sample



selective sample

tert-Butyl (2*S*,3*S*)-3-(hydroxymethyl)-2-(nitromethyl)hex-5-enoate

In a 5 mL flask *tert*-butyl (2*S*,3*S*)-3-formyl-2-(nitromethyl)hex-5-enoate (**10g**, 128.6 mg, 500 μmol, 1.00 equiv) was dissolved in MeOH (1.0 mL) under argon atmosphere at 0 °C. NaBH₄ (18.9 mg, 500 μmol, 1.00 equiv) was added in one portion and the reaction mixture was stirred for 1.5 h at 0 °C. The solvents were removed under reduced pressure and the orange solid was purified by column chromatography (silica, pentane/ethyl acetate) to result in *tert*-butyl (2*S*,3*S*)-3-(hydroxymethyl)-2-(nitromethyl)hex-5-enoate as a colorless oil (67.6 mmol, 261 μmol, 52% yield).

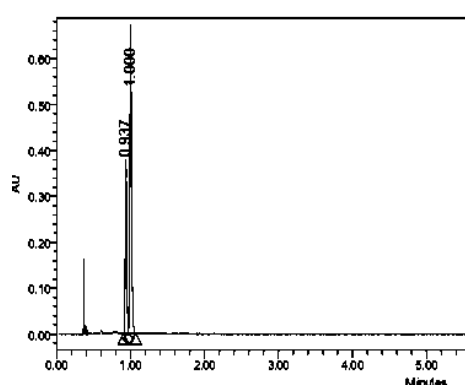
¹H-NMR (400 MHz, CDCl₃) δ: 5.88 – 5.67 (m, 1H), 5.20 – 5.03 (m, 2H), 4.89 (dd, *J* = 14.6, 10.6 Hz, 1H), 4.41 (dd, *J* = 14.6, 3.7 Hz, 1H), 3.76 – 3.54 (m, 2H), 3.40 (dt, *J* = 10.7, 3.7 Hz, 1H), 2.24 – 2.07 (m, 3H), 1.47 (s, 9H).

¹³C-NMR (101 MHz, CDCl₃) δ: 171.09, 135.38, 118.06, 82.75, 73.72, 63.13, 44.99, 40.72, 33.34, 28.06.

HRMS: ESI [M+Na] calculated: 256.1155 m/z, measured 256.1150 m/z.

Chiral separation: SFC (CO₂), OD-3 SFC, 5% MeOH, 2.0 mL/min, 40 °C

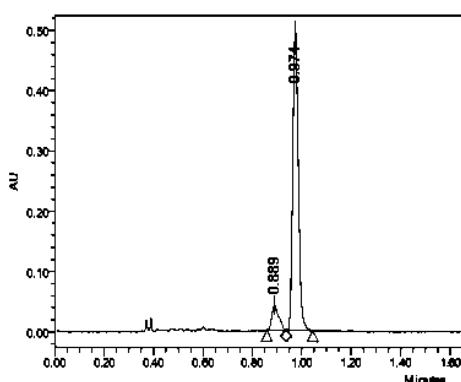
*R*_{t minor} = 0.889 min, *R*_{t major} 0.974 min. (see remarks, page 89)



Processed Channel: PDA Ch2
214nm@1.2nm

Processed Channel	Retention Time (min)	Area	% Area	Height	
1	PDA Ch2 214nm@1.2nm	0.937	528178	33.80	359767
2	PDA Ch2 214nm@1.2nm	1.000	1045827	66.40	654265

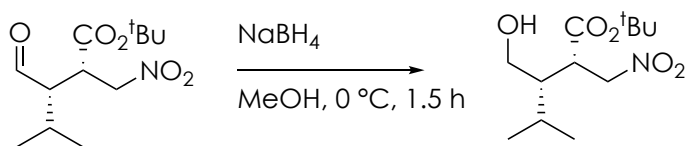
racemic sample



Processed Channel: PDA Ch2
214nm@1.2nm

Processed Channel	Retention Time (min)	Area	% Area	Height	
1	PDA Ch2 214nm@1.2nm	0.889	80085	9.29	41646
2	PDA Ch2 214nm@1.2nm	0.974	781871	90.71	487522

selective sample

tert-Butyl (2*S*,3*S*)-3-(hydroxymethyl)-4-methyl-2-(nitromethyl)pentanoate

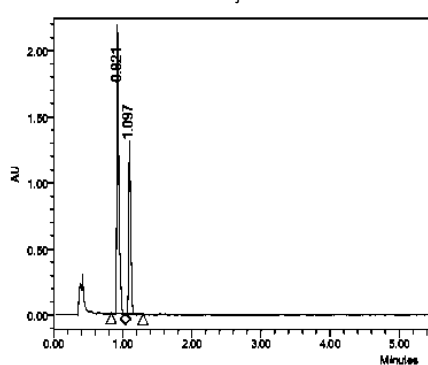
In a 5 mL flask *tert*-butyl (2*S*,3*S*)-3-formyl-4-methyl-2-(nitromethyl)pentanoate (**10k**, 129.6 mg, 500 μmol , 1.00 equiv) was dissolved in MeOH (1.0 mL) under argon atmosphere at 0 $^\circ\text{C}$. NaBH₄ (18.9 mg, 500 μmol , 1.00 equiv) was added in one portion and the reaction mixture was stirred for 1.5 h at 0 $^\circ\text{C}$. The solvents were removed under reduced pressure and the orange solid was purified by column chromatography (silica, pentane/ethyl acetate) to result in *tert*-butyl (2*S*,3*S*)-3-(hydroxymethyl)-4-methyl-2-(nitromethyl)pentanoate as a colorless oil (82.9 mg, 317 μmol , 63% yield).

¹H-NMR (400 MHz, CDCl₃) δ : 4.95 (dd, $J = 14.8, 11.0$ Hz, 1H), 4.43 (dd, $J = 14.8, 3.1$ Hz, 1H), 3.74 (dd, $J = 11.3, 3.4$ Hz, 1H), 3.66 (dd, $J = 11.3, 6.4$ Hz, 1H), 3.48 (ddd, $J = 11.0, 4.6, 3.0$ Hz, 1H), 1.91 – 1.81 (m, 1H), 1.80 – 1.69 (m, 1H), 1.50 (s, 1H), 1.45 (s, 9H), 1.01 (dd, $J = 16.4, 6.6$ Hz, 6H).

¹³C-NMR (101 MHz, CDCl₃) δ : 172.06, 82.39, 73.52, 61.33, 47.29, 44.73, 28.00, 26.81, 21.45, 20.21.

Chiral separation: SFC (CO₂), IC-3 SFC, 5% MeOH, 2.0 mL/min, 40 $^\circ\text{C}$

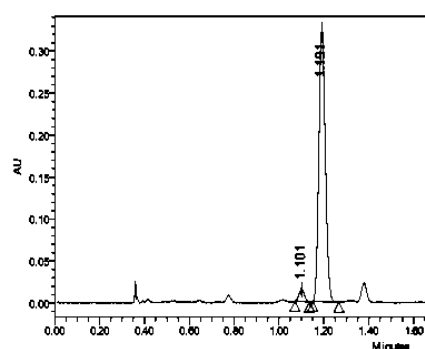
$R_{\text{t minor}} = 0.901$ min, $R_{\text{t major}} = 1.059$ min. (see remarks, page 89)



Processed Channel: PDA Ch2
214nm@1.2nm

	Processed Channel	Retention Time (min)	Area	% Area	Height
1	PDA Ch2 214nm@1.2nm	0.921	4713343	64.60	2128038
2	PDA Ch2 214nm@1.2nm	1.097	2578407	35.34	1243241

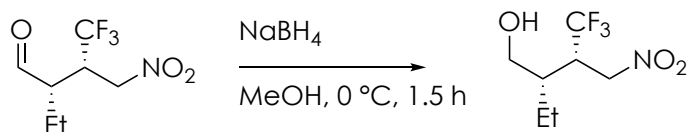
racemic sample



Processed Channel: PDA Ch2
214nm@1.2nm

	Processed Channel	Retention Time (min)	Area	% Area	Height
1	PDA Ch2 214nm@1.2nm	1.101	24632	3.68	14575
2	PDA Ch2 214nm@1.2nm	1.181	652871	96.32	324058

selective sample

(2S,3S)-2-Ethyl-4,4,4-trifluoro-3-(nitromethyl)butan-1-ol

In a 5 mL flask the (2S,3S)-2-ethyl-4,4,4-trifluoro-3-(nitromethyl)butanal (**16**, 106 mg, 500 μmol , 1.00 equiv) was dissolved in MeOH (1.0 mL) under argon atmosphere at 0 $^\circ\text{C}$. NaBH₄ (18.9 mg, 500 μmol , 1.00 equiv) was added in one portion and the reaction mixture was stirred for 1.5 h at 0 $^\circ\text{C}$. The solvents were removed under reduced pressure and the orange solid was purified by column chromatography (silica, pentane/ethyl acetate) to result in (2S,3S)-2-ethyl-4,4,4-trifluoro-3-(nitromethyl)butan-1-ol as a colorless oil (72.2 mg, 335 μmol , 67% yield).

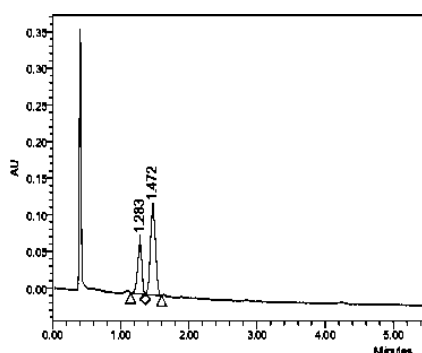
¹H-NMR (400 MHz, CDCl₃) δ : 4.85 – 4.41 (m, 2H), 4.03 – 3.77 (m, 1H), 3.76 – 3.65 (m, 1H), 3.47 (dtd, $J = 9.6, 6.0, 3.3$ Hz, 1H), 1.93 (dddd, $J = 11.5, 6.8, 4.7, 3.5$ Hz, 1H), 1.73 – 1.39 (m, 3H), 1.04 (t, $J = 7.4$ Hz, 3H).

¹³C-NMR (101 MHz, CDCl₃) δ : 71.62, 61.41, 43.31 (q, $J = 26.2$ Hz), 39.75, 29.71, 21.90, 11.90.

¹⁹F-NMR (377 MHz, CDCl₃) δ : -67.84.

Chiral separation: SFC (CO₂), AD-3 SFC, 2% MeOH, 2.0 mL/min, 40 $^\circ\text{C}$

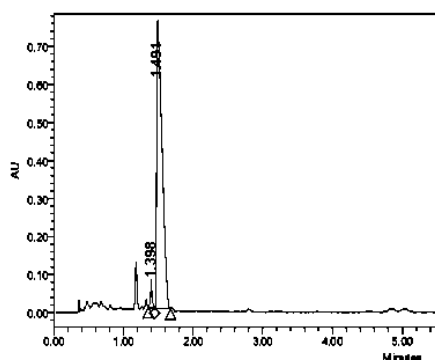
R_{t} minor = 1.398 min, R_{t} major = 1.491 min. (see remarks, page 89)



**Processed Channel: PDA Ch2
214nm@1.2nm**

	Processed Channel	Retention Time (min)	Area	% Area	Height
1	PDA Ch2 214nm@1.2nm	1.283	302825	32.59	68849
2	PDA Ch2 214nm@1.2nm	1.472	626451	67.41	115458

racemic sample



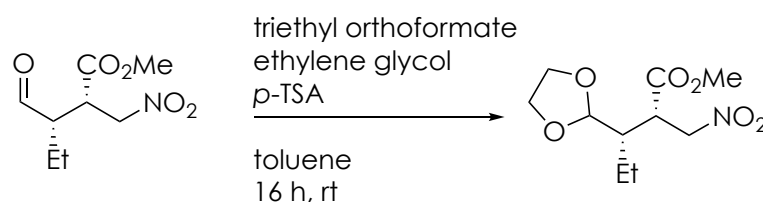
**Processed Channel: PDA Ch2
214nm@1.2nm**

	Processed Channel	Retention Time (min)	Area	% Area	Height
1	PDA Ch2 214nm@1.2nm	1.398	108708	2.02	52743
2	PDA Ch2 214nm@1.2nm	1.491	4042608	97.98	737089

selective sample

7.9 Towards Tetraponerine Structure

Methyl (2*S*,3*S*)-3-(1,3-dioxolan-2-yl)-2-(nitromethyl)pentanoate (**27a**)



Methyl (2*S*,3*S*)-3-formyl-2-(nitromethyl)pentanoate (**10a**, 213 mg, 1.05 mmol, 1.00 equiv) was dissolved in toluene (6 mL) and triethyl orthoformate (192 μ L, 1.15 mmol, 1.10 equiv), ethylene glycol (63 μ L, 1.15 mmol, 1.10 equiv) and *para*-toluenesulfonic acid monohydrate (22 mg, 105 μ mol, 0.10 equiv) were added. The reaction mixture was stirred at room temperature for 16 h and subsequently concentrated under reduced pressure to obtain a colorless oil. After purification by column chromatography (silica, pentane/ethyl acetate, 5:1) methyl (2*S*,3*S*)-3-(1,3-dioxolan-2-yl)-2-(nitromethyl)pentanoate was obtained as a colorless oil (215 mg, 868 μ mol, 53% yield).

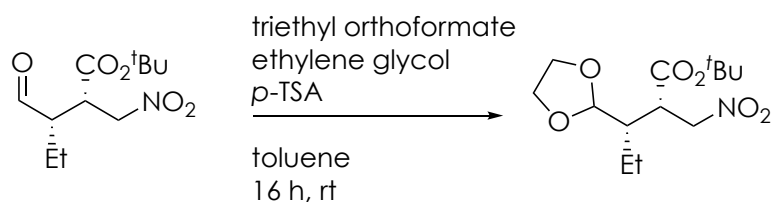
$^1\text{H-NMR}$ (400 MHz, CDCl_3) δ : 4.92 (dd, $J = 15.2, 10.6$ Hz, 1H), 4.78 (d, $J = 3.1$ Hz, 1H), 4.44 (dd, $J = 15.2, 2.8$ Hz, 1H), 4.00 – 3.75 (m, 4H), 3.72 (s, 3H), 3.48 (ddd, $J = 10.6, 4.3, 2.8$ Hz, 1H), 2.42 (dddd, $J = 8.2, 6.4, 4.3, 3.1$ Hz, 1H), 1.72 – 1.59 (m, 1H), 1.49 – 1.33 (m, 1H), 1.03 (t, $J = 7.4$ Hz, 3H).

$^{13}\text{C-NMR}$ (101 MHz, CDCl_3) δ : 172.55, 104.44, 72.41, 65.08, 64.81, 52.42, 43.52, 42.00, 20.91, 12.03.

HRMS: ESI $[M+H]$ calculated: 248.1129 m/z , measured: 248.1133 m/z .

IR [cm^{-1}]: 2894, 1732, 1539, 1378, 1244.

R_f = 0.21 (silica, pentane/ethyl acetate, 5:1).

tert-Butyl (2*S*,3*S*)-3-(1,3-dioxolan-2-yl)-2-(nitromethyl)pentanoate (**27b**)

Tert-butyl (2*S*,3*S*)-3-formyl-2-(nitromethyl) (**10c**, 1.14 g, 5.14 mmol, 1.00 equiv) was dissolved in toluene (14 mL) and triethyl orthoformate (940 μ L, 5.65 mmol, 1.10 equiv), ethylene glycol (315 μ L, 5.65 mmol, 1.10 equiv) and *para*-toluenesulfonic acid monohydrate (97.7 mg, 514 μ mol, 0.10 equiv) were added. The reaction mixture was stirred at room temperature for 16 h and subsequently concentrated under reduced pressure to obtain a colorless oil. After purification by column chromatography (silica, pentane/ethyl acetate, 5:1) *tert*-butyl (2*S*,3*S*)-3-(1,3-dioxolan-2-yl)-2-(nitromethyl)pentanoate was obtained as a colorless oil (1.11 g, 4.19 mmol, 82% yield).

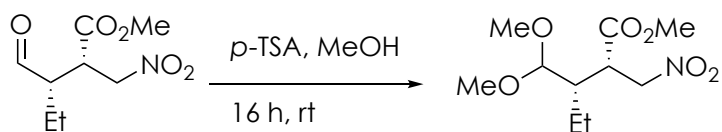
¹H-NMR (400 MHz, CDCl₃) δ : 4.83 (dd, $J = 15.0, 10.9$ Hz, 1H), 4.78 (d, $J = 3.4$ Hz, 1H), 4.38 (dd, $J = 15.0, 2.9$ Hz, 1H), 3.97 – 3.74 (m, 4H), 3.38 (ddd, $J = 10.9, 4.3, 3.0$ Hz, 1H), 2.34 (dddd, $J = 8.0, 6.2, 4.3, 3.4$ Hz, 1H), 1.72 – 1.31 (m, 2H), 1.44 (s, 9H), 1.03 (t, $J = 7.5$ Hz, 3H).

¹³C-NMR (101 MHz, CDCl₃) δ : 170.73, 104.44, 81.86, 72.66, 64.83, 64.57, 43.31, 43.03, 27.81(3C), 20.64, 11.86.

HRMS: ESI [M+Na] calculated: 312.1418 m/z, measured: 312.1420 m/z.

IR [cm⁻¹]: 2972, 1724, 1554, 1368, 1154.

R_f = 0.34 (silica, pentane/ethyl acetate, 2:1).

Methyl (2*S*,3*S*)-3-(dimethoxymethyl)-2-(nitromethyl)pentanoate (**28**)

Methyl (2*S*,3*S*)-3-formyl-2-(nitromethyl)pentanoate (**10a**, 208 mg, 1.02 mmol, 1.00 equiv) was dissolved in methanol (7.5 mL) at room temperature and *para*-toluenesulfonic acid monohydrate (162 mg, 852 μ mol, 0.83 equiv) was added. The reaction mixture was stirred for 16 h followed by concentration under reduced pressure to result in a yellow oil. Saturated aq. NaHCO₃ (5 mL) was added and the aqueous layer was extracted with CH₂Cl₂ (3 x 5 mL). The combined organic layers were dried over MgSO₄, concentrated under reduced pressure and purified by flash column chromatography (silica, pentane/ethyl acetate, 2:1) result in methyl (2*S*,3*S*)-3-(dimethoxymethyl)-2-(nitromethyl)pentanoate as a colorless oil (50.4 mg, 202 μ mol, 20% yield).

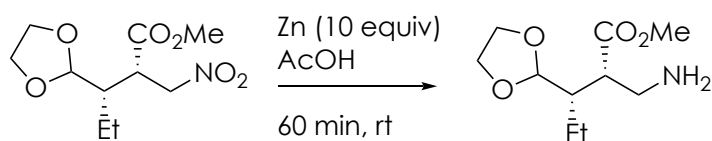
¹H-NMR (400 MHz, CDCl₃) δ : 4.90 (dd, *J* = 15.2, 10.5 Hz, 1H), 4.45 (dd, *J* = 15.2, 3.0 Hz, 1H), 4.14 (d, *J* = 4.4 Hz, 1H), 3.72 (s, 3H), 3.42 (ddd, *J* = 10.5, 4.3, 2.9 Hz, 1H), 3.37 (s, 3H), 3.32 (s, 3H), 2.33 (ddt, *J* = 8.5, 6.2, 4.4 Hz, 1H), 1.66 - 1.47 (m, 1H), 1.41 - 1.25 (m, 1H), 1.00 (t, *J* = 7.4 Hz, 4H).

¹³C-NMR (101 MHz, CDCl₃) δ : 172.74, 107.05, 72.71, 56.57, 55.37, 52.36, 43.67, 42.51, 21.20, 12.08.

HRMS: ESI [M+Na] calculated: 272.1105 m/z, measured: 272.1111 m/z.

IR [cm⁻¹]: 2956, 1735, 1553, 1376, 1200.

R_f = 0.19 (silica, pentane/ethyl acetate, 2:1).

Methyl (2*S*,3*S*)-2-(aminomethyl)-3-(1,3-dioxolan-2-yl)pentanoate (**29a**)

Methyl (2*S*,3*S*)-3-(1,3-dioxolan-2-yl)-2-(nitromethyl)pentanoate (**27a**, 1.30 g, 5.28 mmol, 1.00 equiv) was dissolved in AcOH (105 mL) and freshly activated zinc powder (3.50 g, 53.53 mmol, 10.00 equiv) was added. The grey reaction mixture was stirred at room temperature for 1 h. The suspension was filtered through celite and the residue washed with ethyl acetate (2 x 20 mL). The organic filtrate was partly concentrated under reduced pressure followed by addition of toluene (100 mL). After concentration under reduced pressure, the resulting red oil was redissolved in toluene (2 x 100 mL) concentrated each time under reduced pressure. The slight red solid was purified by column chromatography (silica, CH₂Cl₂/MeOH, 4:1) to yield the acetic acid salt of the product (1.40 g, 5.07 mmol, 96% yield) as a colorless crystalline solid. The residue was redissolved in sat. aq. NH₄Cl (50 mL) and K₂CO₃ was added portionwise until pH 9 was reached. The aqueous layer was extracted with ethyl acetate (9 x 100 mL) and the combined organic layers were dried over MgSO₄. After concentration under reduced pressure methyl (2*S*,3*S*)-2-(aminomethyl)-3-(1,3-dioxolan-2-yl)pentanoate was obtained as colorless oil (677 mg, 3.12 mmol, 59% yield).

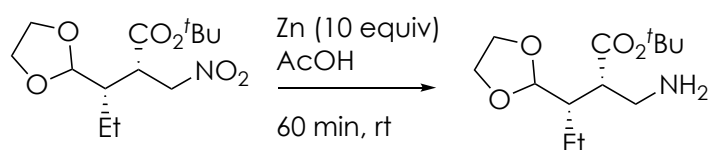
¹H-NMR (400 MHz, CDCl₃) δ: 4.83 (d, *J* = 4.2 Hz, 1H), 3.97 - 3.75 (m, 4H), 3.68 (s, 3H), 3.07 (dd, *J* = 13.0, 9.4 Hz, 1H), 2.79 (dd, *J* = 13.0, 3.8 Hz, 1H), 2.67 (ddd, *J* = 9.1, 5.1, 3.8 Hz, 1H), 2.03 (tdd, *J* = 6.2, 4.8, 4.0 Hz, 1H), 1.59 - 1.35 (m, 2H), 0.95 (t, *J* = 7.5 Hz, 3H).

¹³C-NMR (101 MHz, CDCl₃) δ: 175.22, 105.12, 64.98, 64.83, 51.58, 48.63, 43.87, 41.12, 20.78, 12.43.

HRMS: MALDI [M+H] calculated: 218.1387 m/z, measured: 218.1387 m/z.

IR [cm⁻¹]: 3957, 2879, 1724.

R_f = 0.20 (silica, CH₂Cl₂/MeOH, 4:1).

tert-Butyl (2*S*,3*S*)-2-(aminomethyl)-3-(1,3-dioxolan-2-yl)pentanoate (**29b**)

tert-Butyl (2*S*,3*S*)-3-(1,3-dioxolan-2-yl)-2-(nitromethyl)pentanoate (**27b**, 366 mg, 1.27 mmol, 1.0 equiv) was dissolved in AcOH (25 mL) under argon. Freshly activated zinc powder (830 mg, 12.7 mmol, 10.0 equiv) was added. Reaction was stirred at room temperature for 60 min. The suspension was filtered through celite and washed with ethyl acetate (2 x 10 mL). The resulting solution was partly concentrated under reduced pressure, toluene (20 mL) was added, followed by full evaporation under reduced pressure. The resulting slightly red oil was resuspended in toluene (2 x 20 mL) and concentrated under reduced pressure. The resulting amber crude solid was purified by flash column chromatography (silica, CH₂Cl₂/MeOH, 4:1) to give the acetic acid salt of the product (270.7 mg, 0.85 mmol, 70% yield) as a slightly yellow colorless crystalline solid.

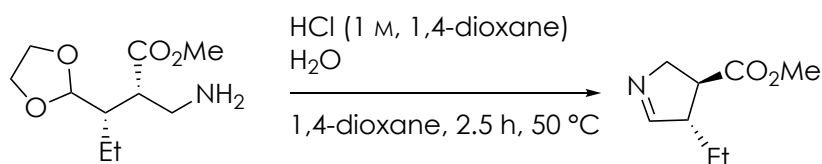
¹H-NMR (300 MHz, DMSO) δ : 4.77 (d, J = 4.4 Hz, 1H), 4.42 (s, 3H), 3.89 - 3.70 (m, 4H), 2.82 (dd, J = 12.8, 9.3 Hz, 1H), 2.67 (dd, J = 12.8, 4.4 Hz, 1H), 2.54 - 2.51 (m, 1H), 1.84 (m, 1H), 1.40 (s, 9H), 1.50 - 1.29 (m, 2H), 0.91 (t, J = 7.5 Hz, 3H).

¹³C-NMR (101 MHz, CDCl₃) δ : 172.79, 104.39, 79.67, 64.36, 64.12, 48.03, 43.37, 40.38, 27.73, 19.83, 12.42.

HRMS: MALDI [M+H] calculated: 260.1856 m/z, measured: 260.1858 m/z.

IR [cm⁻¹]: 2965, 2755, 1720, 1617, 1558, 1393.

R_f = 0.28 (silica, CH₂Cl₂/MeOH, 4:1).

Methyl (3*S*,4*S*)-4-ethyl-3,4-dihydro-2*H*-pyrrole-3-carboxylate (**26a**)

Methyl (2*S*,3*S*)-2-(aminomethyl)-3-(1,3-dioxolan-2-yl)pentanoate (**29a**, 299 mg, 1.38 mmol, 1.00 equiv) was dissolved in 1,4-dioxane (21 mL) and HCl (4 M in 1,4-dioxane 6.9 mL, 27.5 mmol, 20.00 equiv) was added at room temperature. The reaction mixture was heated to 50 °C for 2 h followed by stirring at room temperature for 3 h. MTBE (70 mL) was added and NEt₃ (4.00 mL, 54.5 mmol, 39.00 equiv) was added dropwise. The suspension was filtered through a plug of silica and the silica was flushed with MTBE (25 mL). The reaction mixture was concentrated under reduced pressure and methyl (3*S*,4*S*)-4-ethyl-3,4-dihydro-2*H*-pyrrole-3-carboxylate was obtained as a yellow oil (126 mg, 882 μmol, 60% yield).

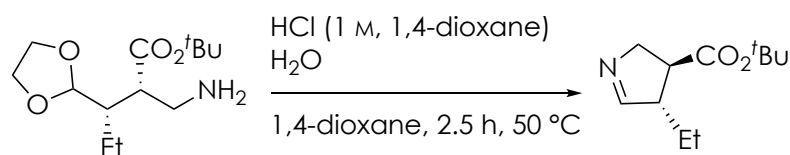
¹H-NMR (400 MHz, CDCl₃) δ: 7.41 (tt, *J* = 2.4, 0.9 Hz, 1H), 4.21 (ddt, *J* = 16.1, 9.3, 2.3 Hz, 1H), 4.00 (dddd, *J* = 16.1, 6.7, 2.6, 1.8 Hz, 1H), 3.71 (s, 3H), 3.16 (dt, *J* = 7.6, 6.5, 2.4 Hz, 1H), 2.73 (dt, *J* = 9.3, 6.8 Hz, 1H), 1.76 – 1.45 (m, 2H), 0.99 (t, *J* = 7.4 Hz, 3H)

¹³C-NMR (101 MHz, CDCl₃) δ: 175.17, 168.95, 64.86, 55.89, 52.27, 46.54, 24.97, 11.78.

HRMS: EI [M+H] calculated: 155.0946 m/z, measured: 155.0944 m/z.

IR [cm⁻¹]: 2956, 1730, 1191.

R_f = 0.19 (silica, MTBE); 0.85 (silica, CH₂Cl₂/MeOH, 4:1).

tert-Butyl (3*S*,4*S*)-4-ethyl-3,4-dihydro-2*H*-pyrrole-3-carboxylate (**26b**)

tert-Butyl (2*S*,3*S*)-2-(aminomethyl)-3-(1,3-dioxolan-2-yl)pentanoate (**29b**, 50 mg, 156 μ mol, 1.00 equiv) was put under argon atmosphere, dissolved in dry 1,4-dioxane (21 mL) and water (2,8 μ L, 156 μ mol, 1.00 equiv), then HCl (in 1,4-dioxane, 4 M, 782 μ L, 3.13 mmol, 20.00 equiv) was added. The reaction was heated to 50 °C for 130 min and allowed to cool to room temperature. MTBE was added followed by dropwise addition of freshly distilled NEt₃ (1 mL) during vigorous stirring. The resulting suspension was filtered through silica and was thoroughly washed with MTBE. The solvent was evaporated under reduced pressure and the crude was purified by flash column chromatography (silica, Et₂O/pentane, 2:1) to yield in *tert*-butyl (3*S*,4*S*)-4-ethyl-3,4-dihydro-2*H*-pyrrole-3-carboxylate (20 mg, 101 μ mol, 65% yield) as a colorless oil.

¹H-NMR (400 MHz, CDCl₃) δ : 7.39 (tt, J = 2.4, 0.9 Hz, 1H), 4.18 (ddt, J = 16.1, 9.3, 2.3 Hz, 1H), 3.96 (dddd, J = 16.1, 6.8, 2.6, 1.8 Hz, 1H), 3.12 – 3.03 (m, 1H), 2.63 (dt, J = 9.3, 6.8 Hz, 1H), 1.68 (dq, J = 13.6, 7.5, 6.1 Hz, 1H), 1.57 – 1.47 (m, 1H), 1.45 (s, 9H), 0.99 (t, J = 7.4 Hz, 3H).

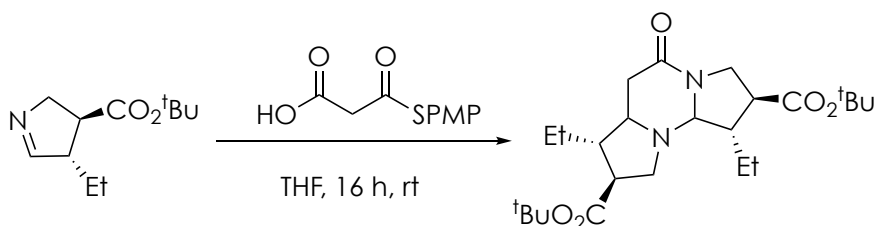
¹³C-NMR (101 MHz, CDCl₃) δ : 173.95, 169.10, 80.98, 64.96, 55.88, 47.84, 28.20(3H), 25.07, 11.90.

HRMS: ESI [M+H] calculated: 198.1494 m/z, measured: 198.1489 m/z.

IR [cm⁻¹]: 2956, 1723, 1365, 1144.

R_f = 0.85 (silica, CH₂Cl₂/MeOH, 4:1).

Di-*tert*-butyl (1*S*,2*S*,7*S*,8*S*)-1,7-diethyl-5-oxodecahydrodipyrrolo[1,2- α :1',2'- c]pyrimidine-2,8-dicarboxylate (**24a**)



tert-Butyl (3*S*,4*S*)-4-ethyl-3,4-dihydro-2*H*-pyrrole-3-carboxylate (12 mg, 61 μ mol 1.00 equiv) was dissolved in dry THF (300 μ L), then catalyst **32** and MATH (20.6 mg, 91 μ mol 1.50 equiv) were added. The reaction was stirred at r.t. for 1 hour. The reaction was fully concentrated under reduced pressure and purified by flash column chromatography (silica, pentane/ethyl acetate, 2:1) to afford di-*tert*-butyl (1*S*,2*S*,7*S*,8*S*)-1,7-diethyl-5-oxodecahydrodipyrrolo[1,2- α :1',2'- c]pyrimidine-2,8-dicarboxylate (7 mg, 29 μ mol, 48% yield) as a white solid.

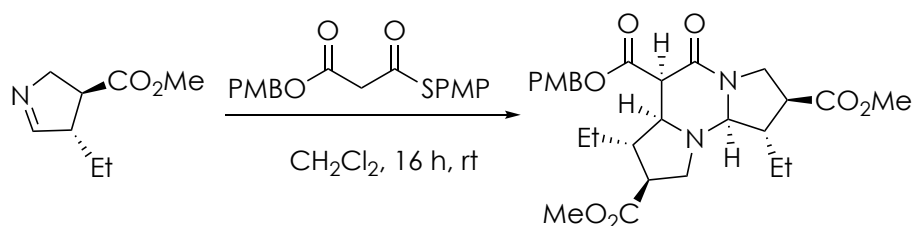
¹H-NMR (400 MHz, CDCl₃) δ : 3.84 – 3.78 (m, 1H), 3.76 – 3.65 (m, 2H), 3.22 (dd, J = 8.9, 5.5 Hz, 1H), 2.75 (t, J = 8.9 Hz, 1H), 2.70 – 2.55 (m, 3H), 2.49 (dd, J = 17.2, 5.7 Hz, 1H), 2.34 (td, J = 17.4, 14.2, 6.8 Hz, 2H), 1.95 (p, J = 6.8 Hz, 1H), 1.74 (ddd, J = 13.0, 7.4, 4.8 Hz, 1H), 1.53 (dq, J = 10.9, 7.7 Hz, 3H), 1.45 (s, 9H), 1.45 (s, 9H), 0.98 (dt, J = 14.8, 7.5 Hz, 6H).

¹³C-NMR (101 MHz, CDCl₃) δ : 173.51, 172.11, 167.37, 81.58, 81.04, 80.22, 65.58, 50.46, 50.31, 49.04, 47.94, 47.01, 46.38, 36.11, 28.22, 28.12, 26.77, 24.08, 12.23, 11.08.

HRMS: ESI [M+H] calculated: 198.1494 m/z, measured: 198.1489 m/z.

IR [cm⁻¹]: 2974, 1715, 1634, 1363.

6-(4-Methoxybenzyl) 2,8-dimethyl (1*S*,2*S*,6*R*,6*aS*,7*S*,8*S*,10*aS*)-1,7-diethyl-5-oxo decahydrodipyrrolo[1,2-*α*:1',2'-*c*]pyrimidine-2,6,8-tricarboxylate (**24b**)



Methyl (3*S*,4*S*)-4-ethyl-3,4-dihydro-2*H*-pyrrole-3-carboxylate (14.5 mg, 67 μ mol, 1.00 equiv) was dissolved in CH_2Cl_2 (9.3 mL, 0.01 M). 4-Methoxybenzyl 3-((4-methoxyphenyl)thio)-3-oxopropanoate (MTM, 39.1 mg, 113 μ mol 1.70 equiv) was added followed by eCDU (**32**, 2.8 mg, 4.8 μ mol, 0.07 equiv). The reaction was stirred at room temperature for 2 weeks. The solution was then filtered through a plug of silica with ethyl acetate (5 mL), fully concentrated under reduced pressure and purified by flash column chromatography (silica, pentane/ethyl acetate, 2:1) to afford the tertaponerine derivative (7.4 mg, 14.3 μ mol, 43% yield) as a colorless oil.

¹H-NMR (400 MHz, CDCl_3) δ : 7.34-7.28 (m, 2H), 6.90-6.84 (m, 2H), 5.14 (s, 2H), 4.22 (d, $J = 9.5$ Hz, 1H), 3.80 (s, 3H), 3.84-3.66 (m, 2H), 3.72 (s, 3H), 3.69 (s, 3H, C), 3.40 (d, $J = 8.5$ Hz, 1H), 3.25 (dd, $J = 8.6, 3.7$ Hz, 1H), 3.01 (t, $J = 8.7$ Hz, 1H), 2.97-2.92 (m, 1H), 2.76 (dt, $J = 10.6, 9.2$ Hz), 2.72 (td, $J = 8.0, 5.7$ Hz, 1H), 2.33 (tt, $J = 9.6, 6.2$ Hz, 1H), 2.15 (tdd, $J = 7.1, 5.6, 3.7$ Hz, 1H), 1.68-1.51 (m, 2H), 1.45-1.33 (m, 2H), 0.96 (t, $J = 7.5$ Hz, 3H), 0.78 (t, $J = 7.4$ Hz, 3H).

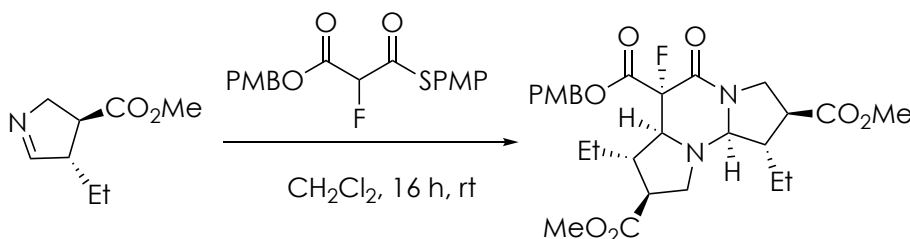
¹³C-NMR (101 MHz, CDCl_3) δ : 174.22, 173.23, 170.06, 163.12, 159.85, 130.44, 127.83, 114.04, 78.31, 67.59, 67.24, 55.44, 52.47, 52.39, 52.28, 50.11, 48.10, 47.95, 47.22, 46.96, 45.02, 27.54, 23.76, 11.90, 10.88.

HRMS: ESI [M+H] calculated: 198.1494 m/z, measured: 198.1489 m/z.

IR [cm^{-1}]: 2956, 1729, 1651, 1244, 1166.

R_f = 0.38 (silica, pentane/ethyl acetate, 2:1).

6-(4-methoxybenzyl) 8-methyl (1*S*,2*S*,7*S*,8*S*)-2-acetyl-1,7-diethyl-6-fluoro-5-oxodecahydrodipyrrolo[1,2-*a*:1',2'-*c*]pyrimidine-6,8-dicarboxylate (**24c**)



Methyl (3*S*,4*S*)-4-ethyl-3,4-dihydro-2H-pyrrole-3-carboxylate (12.0 mg, 77.3 μ mol, 1.00 equiv) was dissolved in CH_2Cl_2 (0.6 mL). 4-methoxybenzyl 2-fluoro-3-((4-methoxyphenyl)thio)-3-oxopropanoate (F-MTM, 31.0 mg, 85 μ mol, 1.10 equiv) was added followed by eCDU (**32**, 2.8 mg, 4.8 μ mol, 0.05 equiv). The reaction was stirred at room temperature for 16 h. The solution was then filtered through a plug of silica with ethyl acetate (3 mL), fully concentrated under reduced pressure and purified by flash column chromatography (silica, pentane/ethyl acetate, 2:1) to afford the teratopenerine derivative (15.4 mg, 29.7 μ mol, 78% yield) as a colorless oil.

$^1\text{H-NMR}$ (400 MHz, CDCl_3) δ : 7.34 – 7.29 (m, 2H), 6.89 – 6.84 (m, 2H), 5.29 – 5.13 (m, 2H), 4.24 – 4.19 (m, 1H), 3.80 (d, J = 1.1 Hz, 4H), 3.77 (d, J = 1.8 Hz, 1H), 3.73 (s, 3H), 3.68 (s, 3H), 3.24 (dd, J = 25.5, 3.6 Hz, 1H), 3.23 – 3.17 (m, 1H), 2.95 (td, J = 8.6, 2.7 Hz, 1H), 2.81 (dt, J = 10.7, 9.3 Hz, 1H), 2.74 – 2.58 (m, 2H), 2.52 – 2.38 (m, 1H), 1.76 – 1.47 (m, 2H), 1.42 – 1.21 (m, 2H), 0.98 (t, J = 7.5 Hz, 3H), 0.73 (t, J = 7.4 Hz, 3H).

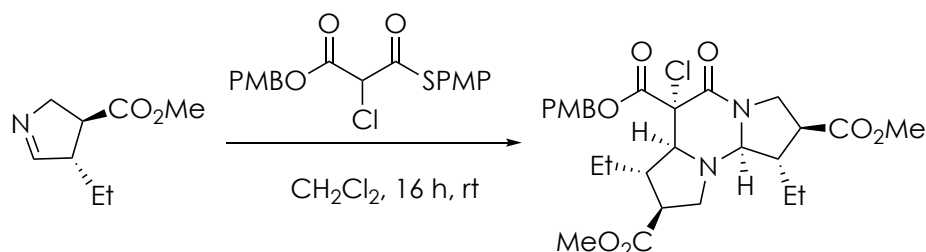
$^{13}\text{C-NMR}$ (101 MHz, CDCl_3) δ : 173.18, 172.80, 160.09, 136.34, 130.80, 126.98, 115.29, 114.09, 78.64, 70.82, 70.63, 68.12, 55.43, 52.55, 52.31, 47.92, 47.69, 47.35, 46.94, 44.79, 42.37, 27.86, 23.54, 11.92, 10.72.

HRMS: ESI [$\text{M}+\text{H}$] calculated: 535.2450 m/z , measured: 535.2448 m/z .

IR [cm^{-1}]: 2957, 1732, 1668, 1244, 1173.

R_f = 0.53 (silica, pentane/ethyl acetate, 2:1).

6-(4-methoxybenzyl) 2,8-dimethyl (1*S*,2*S*,6*S*,6*aS*,7*S*,8*S*,10*aS*)-6-chloro-1,7-diethyl-5-oxodecahydrodipyrrolo[1,2-*a*:1',2'-*c*]pyrimidine-2,6,8-tricarboxylate (24d)



Methyl (3*S*,4*S*)-4-ethyl-3,4-dihydro-2*H*-pyrrole-3-carboxylate (11.0 mg, 70.1 μ mol, 1.00 equiv) was dissolved in CH_2Cl_2 (0.6 mL). 4-methoxybenzyl 2-chloro-3-((4-methoxyphenyl)thio)-3-oxopropanoate (Cl-MTM, 32.0 mg, 84 μ mol, 1.10 equiv) was added followed by eCDU (**32**, 2.8 mg, 4.8 μ mol, 0.05 equiv). The reaction was stirred at room temperature for 16 h. The solution was then filtered through a plug of silica with ethyl acetate (3 mL), fully concentrated under reduced pressure and purified by flash column chromatography (silica, pentane/ethyl acetate, 2:1) to afford the teratopenerine derivative (9.3 mg, 16.9 μ mol, 48% yield) as a colorless oil.

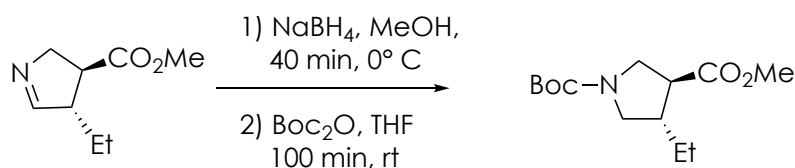
$^1\text{H-NMR}$ (400 MHz, CDCl_3) δ : 7.35 – 7.29 (m, 2H), 6.90 – 6.85 (m, 2H), 5.30 – 5.10 (m, 2H), 3.93 (ddd, $J = 12.8, 7.8, 0.7$ Hz, 1H), 3.83 – 3.76 (m, 3H), 3.74 – 3.68 (m, 6H), 3.68 – 3.58 (m, 2H), 3.04 (d, $J = 6.5$ Hz, 1H), 2.84 – 2.70 (m, 2H), 2.69 – 2.62 (m, 1H), 2.57 – 2.47 (m, 1H), 1.78 (ddt, $J = 14.2, 7.5, 4.0$ Hz, 1H), 1.59 – 1.49 (m, 1H), 1.20 – 1.03 (m, 2H), 0.97 (t, $J = 7.5$ Hz, 3H), 0.74 (t, $J = 7.3$ Hz, 3H).

$^{13}\text{C-NMR}$ (101 MHz, CDCl_3) δ : 173.58, 173.03, 166.63, 162.22, 160.12, 130.97, 126.89, 114.07, 80.63, 73.28, 70.73, 68.93, 55.44, 52.54, 52.45, 50.84, 48.86, 47.31, 47.13, 44.75, 44.28, 26.34, 23.91, 11.54, 10.68.

HRMS: ESI [$\text{M}+\text{H}$] calculated: 551.2155 m/z , measured: 551.2150 m/z .

IR [cm^{-1}]: 2958, 1730, 1664, 1242, 1172.

R_f = 0.10 (silica, pentane/ethyl acetate, 2:1).

1-(*tert*-Butyl) 3-methyl (3*S*,4*S*)-4-ethylpyrrolidine-1,3-dicarboxylate (**31a**)

Methyl (3*R*,4*S*)-4-ethyl-3,4-dihydro-2H-pyrrole-3-carboxylate (15.9 mg, 102 μmol) was dissolved in methanol (2 mL) and cooled to 0 °C. Sodium borohydride (4.9 mg, 122 μmol, 1.20 equiv) was added portionwise. The solution was stirred at 0 °C for 50 min, the solvent was evaporated under reduced pressure and dry THF (2 mL) was added. Boc₂O (51.1 mg, 204 μmol, 2.00 equiv) was added and the reaction was stirred at room temperature for 100 min. The solvent was evaporated under reduced pressure and the resulting crude product was purified by flash column chromatography (silica, CH₂Cl₂/MeOH, 49:1) to afford 1-(*tert*-Butyl) 3-methyl (3*S*,4*S*)-4-ethylpyrrolidine-1,3-dicarboxylate compound (18.2 mg, 70.7 μmol, 69% yield) as a colorless oil.

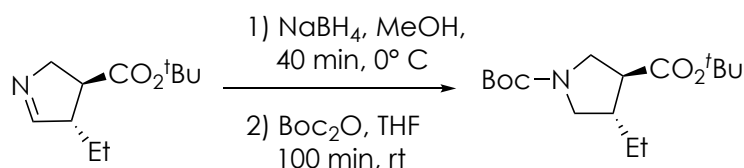
¹H-NMR (400 MHz, CDCl₃) δ: 3.70 (s, 3H), 3.75-3.65 (m, 1H), 3.61 (ddd, *J* = 13.6, 7.6, 4.7 Hz, 1H), 3.48 (q, *J* = 10.6 Hz, 1H), 2.96 (q, *J* = 10.5 Hz, 1H), 2.68 (h, *J* = 8.6, 7.9 Hz, 1H), 2.42-2.24 (m, 1H), 1.61 (dp, *J* = 19.4, 7.0, 6.0 Hz, 1H), 1.45 (s, 9H), 1.42-1.15 (m, 1H), 0.91 (t, *J* = 7.5 Hz, 3H).

¹³C-NMR (101 MHz, CDCl₃) δ: 173.59, 154.35, 79.58, 52.13, 51.08, 50.78, 48.93, 48.90, 48.59, 48.09, 44.24, 43.52, 28.63, 25.62, 12.21.

HRMS: ESI [M+Na] calculated: 280.1519 m/z, measured: 280.1525 m/z.

IR [cm⁻¹]: 2964, 1736, 1693, 1401, 1166.

R_f = 0.61 (silica, CH₂Cl₂/MeOH, 49:1).

di-tert-Butyl (3*S*,4*S*)-4-ethylpyrrolidine-1,3-dicarboxylate (31b)

tert-Butyl (3*S*,4*S*)-4-ethyl-3,4-dihydro-2*H*-pyrrole-3-carboxylate (50 mg, 253 μ mol, 1.00 equiv) was dissolved in dry methanol (5 mL) and cooled to 0 °C. Sodium borohydride (11.5 mg, 304 μ mol, 1.20 equiv) was added portionwise. The solution was stirred at 0 °C for 50 min, the solvent was evaporated under reduced pressure and dry THF (5 mL) was added. Boc₂O (110.6 mg, 507 μ mol, 2.00 equiv) was added and the reaction was stirred at room temperature for 100 min. The solvent was evaporated under reduced pressure and the resulting crude product was purified by flash column chromatography (silica, pentane/ethyl acetate, 5:1) to afford di-tert-butyl (3*S*,4*S*)-4-ethylpyrrolidine-1,3-dicarboxylate (50 mg, 167 μ mol, 65% yield) as a colorless oil.

¹H-NMR (400 MHz, CDCl₃) δ : 3.73 – 3.66 (m, 1H), 3.65 – 3.59 (m, 1H), 3.45 (q, J = 9.7, 8.7 Hz, 1H), 2.96 (dt, J = 14.0, 9.9 Hz, 1H), 2.59 (p, J = 8.9 Hz, 1H), 2.39 – 2.24 (m, 1H), 1.64 (dq, J = 13.5, 7.0 Hz, 1H), 1.50 – 1.44 (m, 18H), 1.41 – 1.30 (m, 1H), 0.95 (t, J = 7.5 Hz, 3H).

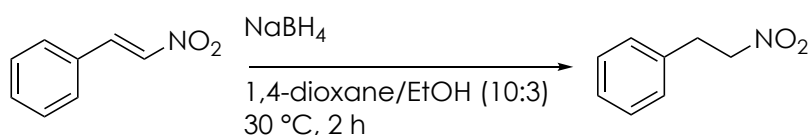
¹³C-NMR (101 MHz, CDCl₃) δ : 172.21, 154.28, 81.00, 79.33, 51.04, 50.70, 49.97, 49.15, 48.81, 48.64, 43.86, 43.41, 28.51, 28.05, 25.52, 12.16.

HRMS: ESI [M+H] calculated: 322.1989 m/z, measured: 322.1993 m/z.

IR [cm⁻¹]: 2970, 1694, 1365, 1143.

7.10 Other Compounds

(2-Nitroethyl)benzene (8b)



(2-Nitroethyl)benzene was synthesized according to a known procedure.^[149]

In a 100 mL flask NaBH₄ (1.07 g, 28.16 mmol, 2.10 equiv) was suspended in 1,4-dioxane/EtOH (10:3, 26 mL) at 30 °C. Nitrostyrene (**6a**, 2.00 g, 13.41 mmol, 1.00 equiv) in 1,4-dioxane (20 mL) was added dropwise. The reaction mixture was stirred at 30 °C for 2 h. The mixture was poured into ice water (200 mL) and extracted with CH₂Cl₂ (4 x 100 mL). The organic layer was dried over MgSO₄ and the solvents removed under reduced pressure. The residue was purified by column chromatography (silica, pentane/ethyl acetate, 5:1) and (2-nitroethyl)benzene was obtained as colorless solid (800 mg, 13.41 mmol, 40% yield).

¹H-NMR (300 MHz, CDCl₃) δ: 7.40 – 7.27 (m, 3H), 7.25 – 7.16 (m, 2H), 4.62 (t, *J* = 7.4 Hz, 2H), 3.33 (t, *J* = 7.4 Hz, 2H).

¹³C-NMR (101 MHz, CDCl₃) δ: 135.75, 129.10, 128.70, 127.58, 76.41, 33.59.

HRMS: ESI [*M*+NH₄] calculated: 151.0633 *m/z*, measured 151.0630 *m/z*.

IR [cm⁻¹]: 3063.2, 3029.7, 2919.1, 1544.5, 1495.1, 1458.1, 1403.2, 1376.6, 1222.1, 1182.5, 1182.5, 1082.5, 1029.7, 969.0, 861.6, 749.5, 696.9.

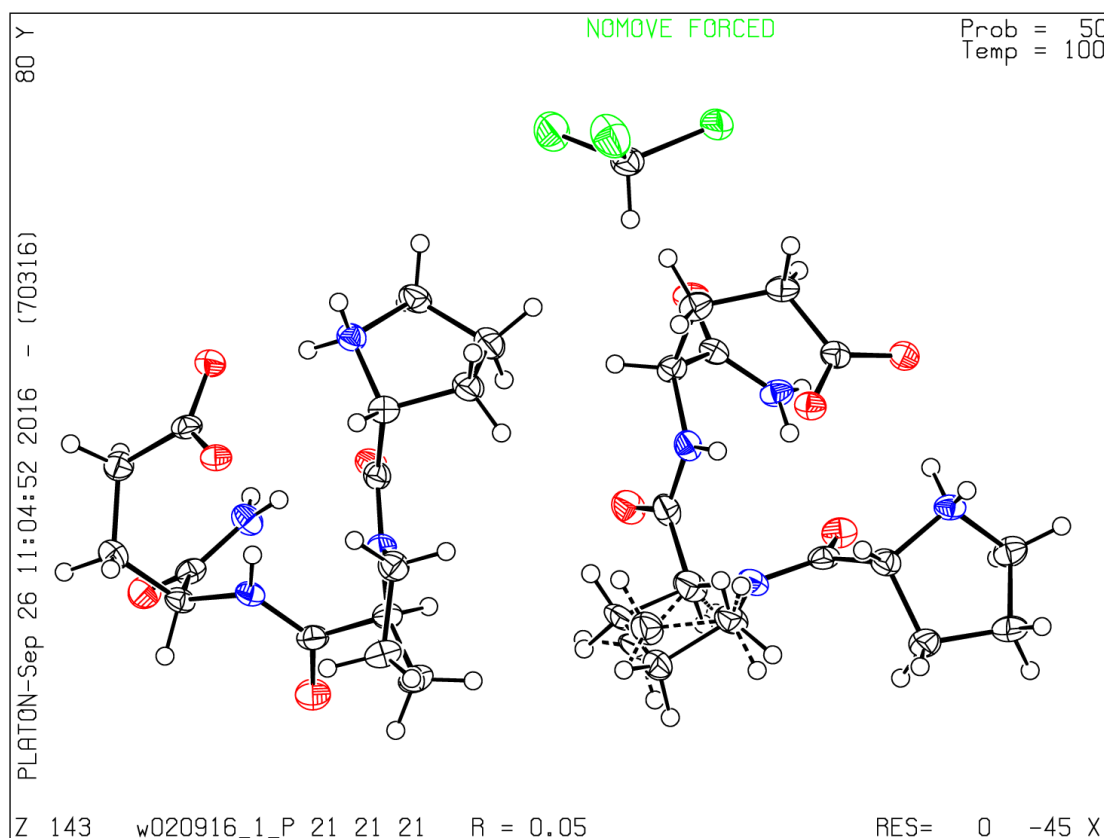
The data are in agreement with the literature.^[149]

7.11 X-Ray Crystal Structures

H-DPro-Pro-Glu-NH₂ (**4a**)

Single crystals of H-DPro-Pro-Glu-NH₂ were obtained by vapour diffusion with CHCl₃/MeOH (9:1) as solvent. A suitable crystal was selected and measured on a Bruker ApexII D8 (Mo) diffractometer at 100 K.

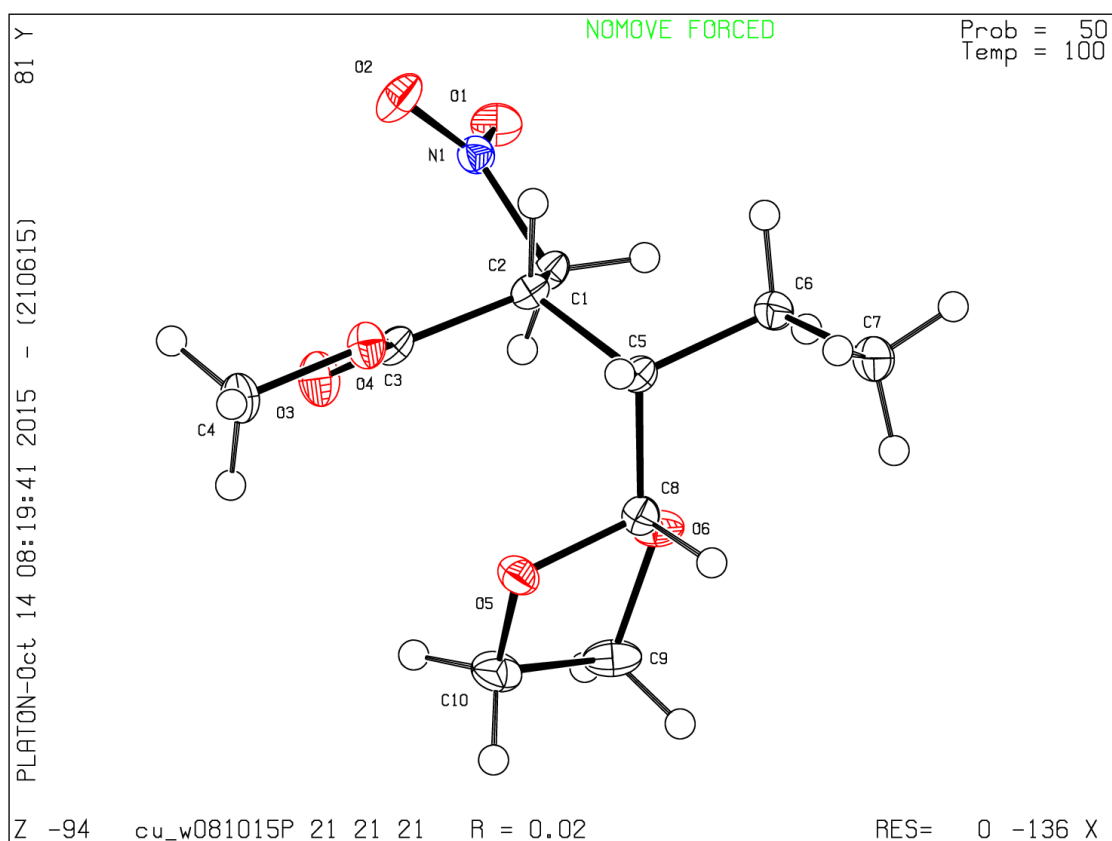
Crystal Data for 2 x (C₁₅H₂₄N₄O₅): space group P2₁2₁2₁, a = 6.30511(13) Å, b = 23.8334(6) Å, c = 24.6841(5) Å, α = β = γ = 90°, V = 3709.32(15) Å³, Z = 8, T = 99.99 K, μ(MoKα) = 2.800 mm⁻¹, D_{calc} = 1.433 g/mm³, 5374 reflections.



Methyl (2S,3S)-2-(aminomethyl)-3-(1,3-dioxolan-2-yl) pentanoate (**27a**)

Single crystals were obtained by vapour diffusion with CHCl_3 as solvent. A suitable crystal was selected and measured on a Bruker ApexII D8 (Mo) diffractometer at 100 K.

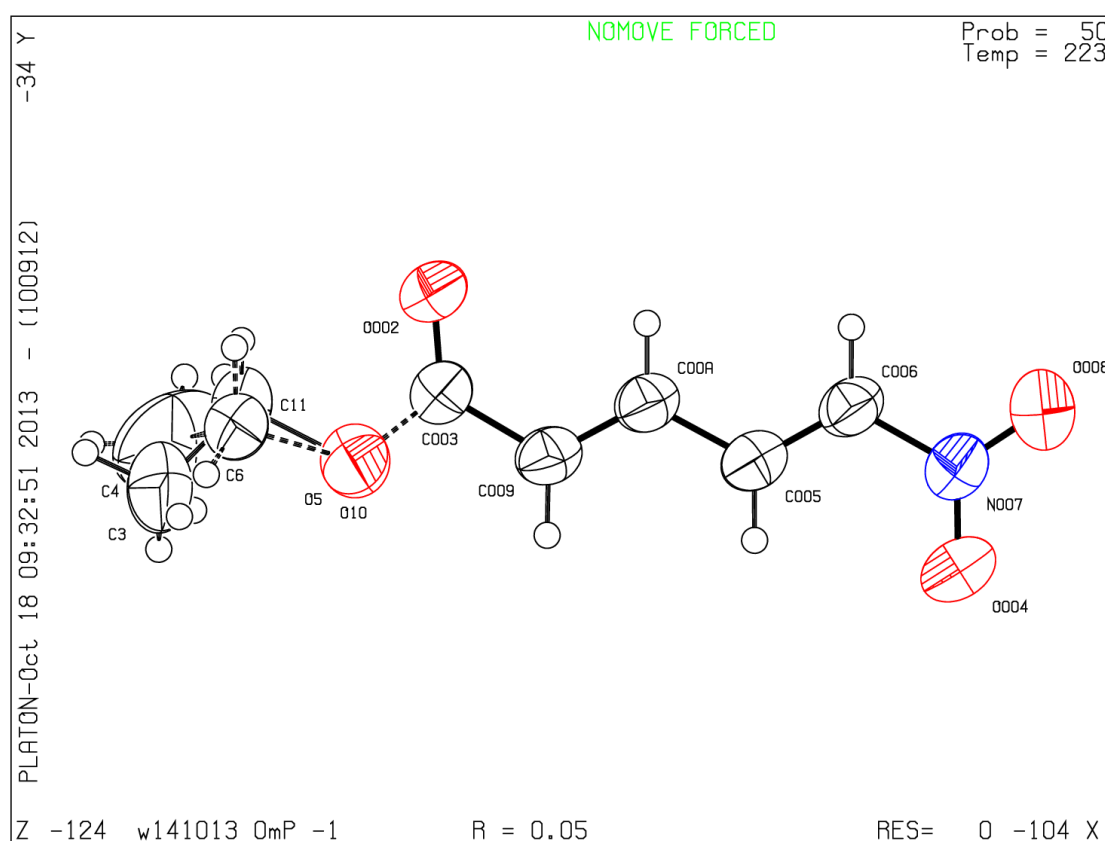
Crystal Data for $\text{C}_{10}\text{H}_{17}\text{NO}_6$: space group $P2_12_12_1$, $a = 5.5560(1) \text{ \AA}$, $b = 14.5067(2) \text{ \AA}$, $c = 14.8131(3) \text{ \AA}$, $\alpha = \beta = \gamma = 90^\circ$, $V = 1193.92(4) \text{ \AA}^3$, $Z = 4$, $T = 99.99 \text{ K}$, $\mu(\text{MoK}\alpha) = 0.974 \text{ mm}^{-1}$, $D_{\text{calc}} = 1.375 \text{ g/mm}^3$, 2021 reflections.



Ethyl (2E,4E)-5-nitropenta-2,4-dienoate (**37a**)

Single crystals were obtained by vapour diffusion with CH₂Cl₂ as solvent. A suitable crystal was selected and measured on a Bruker ApexII D8 (Mo) diffractometer at 100 K.

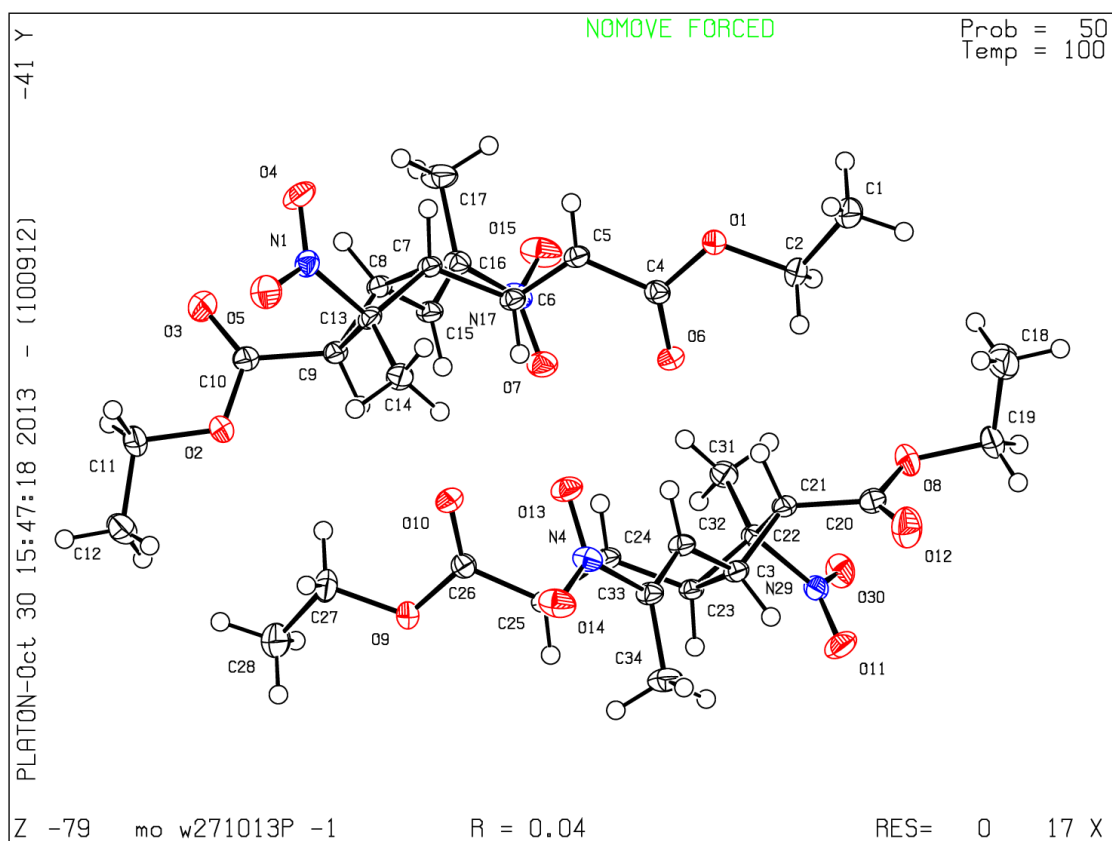
Crystal Data for C₇H₉NO₄: space group P -1, a = 5.0375(6) Å, b = 7.3688(10) Å, c = 12.0999(17) Å, α = 94.528(7)°, β = 98.775(5)°, γ = 101.000(5)°, V = 433.03(10) Å³, Z = 2, T = 99.99 K, μ(MoKα) = 0.109 mm⁻¹, D_{calc} = 1.313 g/mm³, 749s reflections.



Ethyl (2*E*,4*E*)-5-nitropenta-2,4-dienoate dimer (**37b-cb**)

Single crystals of were obtained by vapour diffusion with CH₂Cl₂ as solvent. A suitable crystal was selected and measured on a Bruker ApexII D8 (Mo) diffractometer at 100 K.

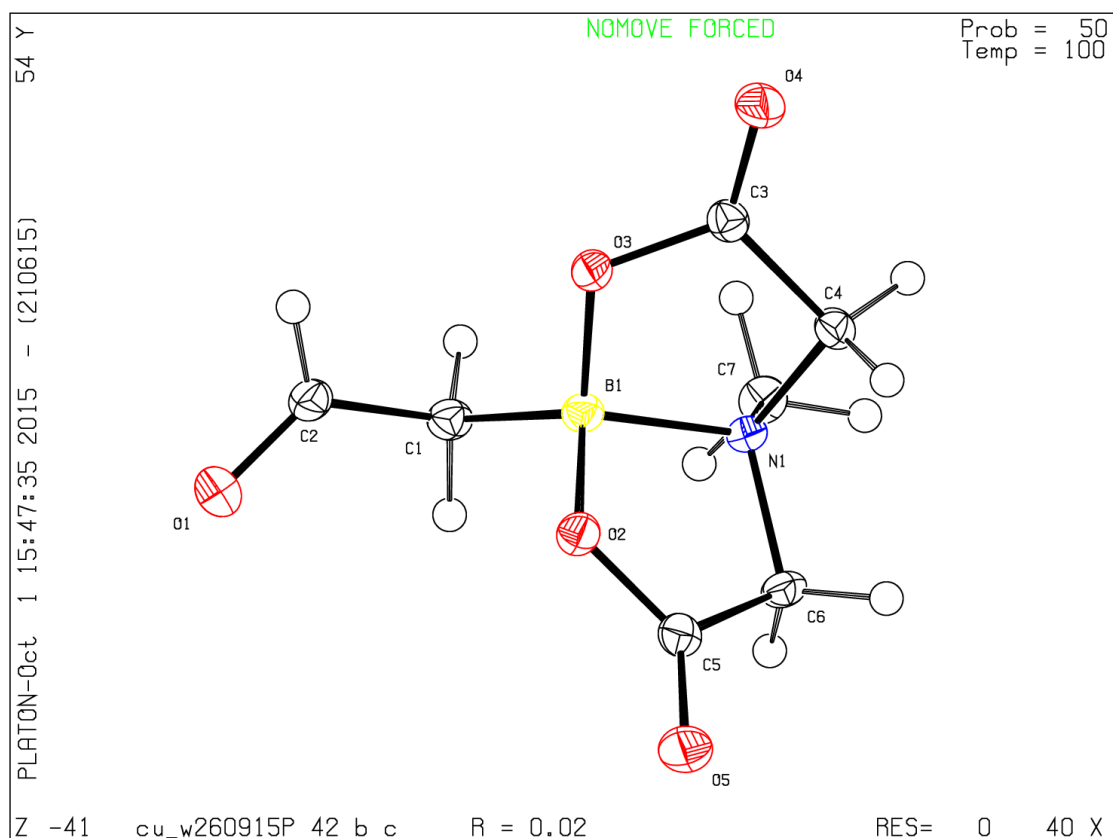
Crystal Data for C₁₆H₂₂N₂O₈: space group P -1, *a* = 9.1609 (10) Å, *b* = 13.6826(15) Å, *c* = 15.0413(17) Å, α = 87.867(2)°, β = 76.382(2)°, γ = 86.581(2)°, *V* = 1828.6(4) Å³, *Z* = 4, *T* = 99.99 K, μ (MoK α) = 0.109 mm⁻¹, *D*_{calc} = 1.345 g/mm³, 6127 reflections.



2-(6-Methyl-4,8-dioxo-1,3,6,2-dioxazaborocan-2-yl)acetaldehyde (**46a**)

Single crystals of **46a** were obtained by vapour diffusion with CHCl_3 as solvent. A suitable crystal was selected and measured on a Bruker ApexII D8 (Mo) diffractometer at 100 K.

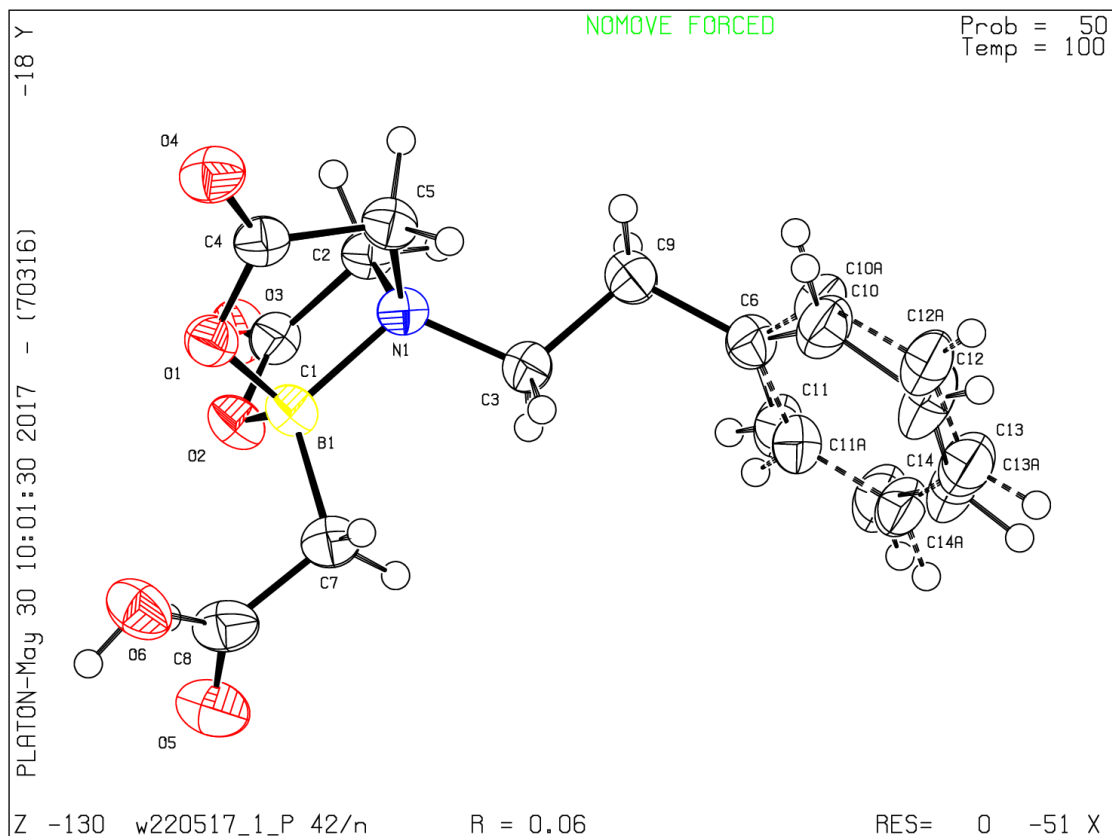
Crystal Data for $\text{C}_7\text{H}_{10}\text{BNO}_5$: space group P 42 b c, $a = 14.2486(3) \text{ \AA}$, $b = 14.2486(3) \text{ \AA}$, $c = 8.5448(3) \text{ \AA}$, $\alpha = \beta = \gamma = 90^\circ$, $V = 1734.79(10) \text{ \AA}^3$, $Z = 8$, $T = 99.99 \text{ K}$, $\mu(\text{MoK}\alpha) = 1.093 \text{ mm}^{-1}$, $D_{\text{calc}} = 1.524 \text{ g/mm}^3$, 858 reflections.



2-(4,8-Dioxo-6-phenethyl-1,3,6,2-dioxazaborocan-2-yl)acetaldehyde (46b)

Single crystals of were obtained by vapour diffusion with CHCl_3 as solvent. A suitable crystal was selected and measured on a Bruker ApexII D8 (Mo) diffractometer at 100 K.

Crystal Data for $\text{C}_{14}\text{H}_{16}\text{BNO}_5$: space group P 42/n, $a = 20.6429(2) \text{ \AA}$, $b = 20.6429(2) \text{ \AA}$, $c = 6.6759(1) \text{ \AA}$, $\alpha = \beta = \gamma = 90^\circ$, $V = 2844.80(7) \text{ \AA}^3$, $Z = 8$, $T = 99.99 \text{ K}$, $\mu(\text{MoK}\alpha) = 0.904 \text{ mm}^{-1}$, $D_{\text{calc}} = 1.402 \text{ g/mm}^3$, 2624 reflections.



8

References

- [1] D. W. C. MacMillan, *Nature* **2008**, *455*, 304-308.
- [2] S. Mukherjee, J. W. Yang, S. Hoffmann, B. List, *Chem. Rev.* **2007**, *107*, 5471-5569.
- [3] B. List, K. Maruoka, *Science of synthesis asymmetric organocatalysis*, Thieme, Stuttgart, **2012**.
- [4] K. A. Ahrendt, C. J. Borths, D. W. C. MacMillan, *J. Am. Chem. Soc.* **2000**, *122*, 4243-4244.
- [5] B. List, R. A. Lerner, C. F. Barbas, *J. Am. Chem. Soc.* **2000**, *122*, 2395-2396.
- [6] G. Stork, S. R. Dowd, *J. Am. Chem. Soc.* **1963**, *85*, 2178-2180.
- [7] M. E. Kuehne, L. Foley, *J. Org. Chem.* **1965**, *30*, 4280-4284.
- [8] I. Zenz, H. Mayr, *J. Org. Chem.* **2011**, *76*, 9370-9378.
- [9] S. J. Blarer, D. Seebach, *Chem. Ber.* **1983**, *116*, 2250-2260.
- [10] S. J. Blarer, W. B. Schweizer, D. Seebach, *Helv. Chim. Acta* **1982**, *65*, 1637-1654.
- [11] E. Vedejs, S. E. Denmark, *Lewis Base Catalysis in Organic Synthesis*, Wiley, Weinheim, **2016**.
- [12] J. M. Betancort, K. Sakthivel, R. Thayumanavan, F. Tanaka, C. F. Barbas III, *Synthesis* **2004**, *2004*, 1509-1521.
- [13] J. M. Betancort, C. F. Barbas, *Org. Lett.* **2001**, *3*, 3737-3740.
- [14] J. Wang, H. Li, B. Lou, L. Zu, H. Guo, W. Wang, *Chem. Eur. J.* **2006**, *12*, 4321-4332.
- [15] S. Zhu, S. Yu, D. Ma, *Angew. Chem. Int. Ed.* **2008**, *47*, 545-548.
- [16] N. Ruiz, E. Reyes, J. L. Vicario, D. Badía, L. Carrillo, U. Uria, *Chem. Eur. J.* **2008**, *14*, 9357-9367.
- [17] C. Palomo, S. Vera, A. Mielgo, E. Gómez-Bengoa, *Angew. Chem. Int. Ed.* **2006**, *45*, 5984-5987.
- [18] Y. Chi, L. Guo, N. A. Kopf, S. H. Gellman, *J. Am. Chem. Soc.* **2008**, *130*, 5608-5609.
- [19] S. Belot, A. Massaro, A. Tenti, A. Mordini, A. Alexakis, *Org. Lett.* **2008**, *10*, 4557-4560.
- [20] P. Melchiorre, *Angew. Chem. Int. Ed.* **2012**, *51*, 9748-9770.
- [21] S. H. McCooey, S. J. Connon, *Org. Lett.* **2007**, *9*, 599-602.
- [22] T. Ishii, S. Fujioka, Y. Sekiguchi, H. Kotsuki, *J. Am. Chem. Soc.* **2004**, *126*, 9558-9559.
- [23] T. C. Nugent, M. Shoaib, A. Shoaib, *Org. Biomol. Chem.* **2011**, *9*, 52-56.
- [24] M. Yoshida, E. Masaki, H. Ikehara, S. Hara, *Org. Biomol. Chem.* **2012**, *10*, 5289-5297.
- [25] J. M. Betancort, C. F. Barbas, *Org. Lett.* **2001**, *3*, 3737-3740.
- [26] O. Andrey, A. Alexakis, A. Tomassini, G. Bernardinelli, *Adv. Synth. Catal.* **2004**, *346*, 1147-1168.
- [27] D. Enders, A. Seki, *Synlett* **2002**, *2002*, 26-28.
- [28] H. Ishikawa, T. Suzuki, Y. Hayashi, *Angew. Chem. Int. Ed.* **2009**, *48*, 1304-1307.
- [29] Y. Hayashi, H. Gotoh, T. Hayashi, M. Shoji, *Angew. Chem. Int. Ed.* **2005**, *44*, 4212-4215.
- [30] Y. Hayashi, H. Gotoh, T. Hayashi, M. Shoji, *Angew. Chem. Int. Ed.* **2005**, *44*, 4212-4215.

- [31] P. García-García, A. Ladépêche, R. Halder, B. List, *Angew. Chem. Int. Ed.* **2008**, *47*, 4719-4721.
- [32] E. A. C. Davie, S. M. Mennen, Y. Xu, S. J. Miller, *Chem. Rev.* **2007**, *107*, 5759-5812.
- [33] M. S. Rasalkar, M. K. Potdar, S. S. Mohile, M. M. Salunkhe, *J. Mol. Catal. A Chem.* **2005**, *235*, 267-270.
- [34] A. Alexakis, O. Andrey, *Org. Lett.* **2002**, *4*, 3611-3614.
- [35] S. Luo, X. Mi, L. Zhang, S. Liu, H. Xu, J. P. Cheng, *Angew. Chem. Int. Ed.* **2006**, *45*, 3093-3097.
- [36] M. Marigo, T. C. Wabnitz, D. Fielenbach, K. A. Jorgensen, *Angew. Chem. Int. Ed.* **2005**, *44*, 794-797.
- [37] K. L. Jensen, G. Dickmeiss, H. Jiang, L. Albrecht, K. A. Jorgensen, *Acc. Chem. Res.* **2012**, *45*, 248-264.
- [38] B. S. Donlund, T. K. Johansen, P. H. Poulsen, K. S. Halskov, K. A. Jorgensen, *Angew. Chem. Int. Ed.* **2015**, *54*, 13860-13874.
- [39] D. Enders, M. R. M. Hüttl, C. Grondal, G. Raabe, *Nature* **2006**, *441*, 861.
- [40] M. Wiesner, J. D. Revell, H. Wennemers, *Angew. Chem. Int. Ed.* **2008**, *47*, 1871-1874.
- [41] M. Wiesner, M. Neuburger, H. Wennemers, *Chem. Eur. J.* **2009**, *15*, 10103-10109.
- [42] M. Wiesner, J. D. Revell, S. Tonazzi, H. Wennemers, *J. Am. Chem. Soc.* **2008**, *130*, 5610-5611.
- [43] M. Wiesner, H. Wennemers, *Synthesis* **2010**, *2010*, 1568-1571.
- [44] M. Wiesner, PhD thesis, University of Basel (Basel), **2009**.
- [45] M. Wiesner, G. Upert, G. Angelici, H. Wennemers, *J. Am. Chem. Soc.* **2009**, *132*, 6-7.
- [46] Y. Arakawa, M. Wiesner, H. Wennemers, *Adv Synth Catal* **2011**, *353*, 1201-1206.
- [47] Y. Arakawa, H. Wennemers, *ChemSusChem* **2013**, *6*, 242-245.
- [48] J. Duschmalé, S. Kohrt, H. Wennemers, *Chem. Commun.* **2014**, *50*, 8109-8112.
- [49] B. Stevenson, W. Lewis, J. Dowden, *Synlett* **2010**, *2010*, 672-674.
- [50] O. Andrey, A. Vidonne, A. Alexakis, *Tetrahedron Lett.* **2003**, *44*, 7901-7904.
- [51] S. Chandrasekhar, K. Mallikarjun, G. Pavankumarreddy, K. V. Rao, B. Jagadeesh, *Chem. Commun.* **2009**, 4985-4987.
- [52] G. Sahoo, H. Rahaman, A. Madarasz, I. Papai, M. Melarto, A. Valkonen, P. M. Pihko, *Angew. Chem. Int. Ed.* **2012**, *51*, 13144-13148.
- [53] L. Wang, X. Zhang, D. Ma, *Tetrahedron* **2012**, *68*, 7675-7679.
- [54] Y. Wang, S. Zhu, D. Ma, *Org. Lett.* **2011**, *13*, 1602-1605.
- [55] L. Guo, Y. Chi, A. M. Almeida, I. A. Guzei, B. K. Parker, S. H. Gellman, *J. Am. Chem. Soc.* **2009**, *131*, 16018-16020.
- [56] J. Duschmalé, H. Wennemers, *Chemistry – A European Journal* **2012**, *18*, 1111-1120.
- [57] R. Kastl, Y. Arakawa, J. Duschmalé, M. Wiesner, H. Wennemers, *CHIMIA* **2013**, *67*, 279-282.
- [58] R. Kastl, PhD thesis, ETH Zurich **2015**.
- [59] R. Ballini, S. Gabrielli, A. Palmieri, *Curr. Org. Chem.* **2010**, *14*, 65-83.

- [60] R. Ballini, N. A. Bazan, G. Bosica, A. Palmieri, *Tetrahedron Lett.* **2008**, *49*, 3865-3867.
- [61] D. Bonne, L. Salat, J.-P. Dulcère, J. Rodriguez, *Org. Lett.* **2008**, *10*, 5409-5412.
- [62] T. Mukaiyama, H. Ishikawa, H. Koshino, Y. Hayashi, *Chem. Eur. J.* **2013**, *19*, 17789-17800.
- [63] H. Ishikawa, T. Suzuki, H. Orita, T. Uchimaru, Y. Hayashi, *Chem. Eur. J.* **2010**, *16*, 12616-12626.
- [64] C. Vaxelaire, P. Winter, M. Christmann, *Angew. Chem. Int. Ed.* **2011**, *50*, 3605-3607.
- [65] D. Seebach, X. Sun, M.-O. Ebert, W. B. Schweizer, N. Purkayastha, A. K. Beck, J. Duschmalé, H. Wennemers, T. Mukaiyama, M. Benohoud, Y. Hayashi, M. Reiher, *Helv. Chim. Acta* **2013**, *96*, 799-852.
- [66] N. Vignola, B. List, *J. Am. Chem. Soc.* **2004**, *126*, 450-451.
- [67] J. Burés, A. Armstrong, D. G. Blackmond, *Acc. Chem. Res.* **2016**, *49*, 214-222.
- [68] J. Bures, A. Armstrong, D. G. Blackmond, *Pure Appl. Chem.* **2013**, *85*, 1919-1934.
- [69] J. Burés, A. Armstrong, D. G. Blackmond, *J. Am. Chem. Soc.* **2012**, *134*, 14264-14264.
- [70] J. Burés, A. Armstrong, D. G. Blackmond, *J. Am. Chem. Soc.* **2012**, *134*, 6741-6750.
- [71] J. Burés, A. Armstrong, D. G. Blackmond, *J. Am. Chem. Soc.* **2011**, *133*, 8822-8825.
- [72] T. Földes, Á. Madarász, Á. Révész, Z. Dobi, S. Varga, A. Hamza, P. R. Nagy, P. M. Pihko, I. Pápai, *J. Am. Chem. Soc.* **2017**, *139*, 17052-17063.
- [73] D. Seebach, X. Sun, C. Sparr, M.-O. Ebert, W. B. Schweizer, A. K. Beck, *Helv. Chim. Acta* **2012**, *95*, 1064-1078.
- [74] K. Patora-Komisarska, M. Benohoud, H. Ishikawa, D. Seebach, Y. Hayashi, *Helv. Chim. Acta* **2011**, *94*, 719-745.
- [75] U. Groselj, W. B. Schweizer, M. O. Ebert, D. Seebach, *Helv. Chim. Acta* **2009**, *92*, 1-13.
- [76] D. Seebach, J. Golinski, *Helv. Chim. Acta* **1981**, *64*, 1413-1423.
- [77] T. Schnitzer, H. Wennemers, *J. Am. Chem. Soc.* **2017**, *139*, 15356-15362.
- [78] F. Bächle, J. Duschmalé, C. Ebner, A. Pfaltz, H. Wennemers, *Angew. Chem. Int. Ed.* **2013**, *52*, 12619-12623.
- [79] J. Duschmalé, J. Wiest, M. Wiesner, H. Wennemers, *Chem. Sci.* **2013**, *4*, 1312-1318.
- [80] H. Gérard, I. Chataigner, *Chem. Eur. J.* **2017**, *23*, 13711-13717.
- [81] A. Castro-Alvarez, H. Carneros, A. M. Costa, J. Vilarrosa, *Synthesis* **2017**, *49*, 5285-5306.
- [82] Y. J. Zhao, Y. Cotelle, A. J. Avestro, N. Sakai, S. Matile, *J. Am. Chem. Soc.* **2015**, *137*, 11582-11585.
- [83] Y. Cotelle, S. Benz, A. J. Avestro, T. R. Ward, N. Sakai, S. Matile, *Angew. Chem. Int. Ed.* **2016**, *55*, 4275-4279.

- [84] M. Cortes-Clerget, J. Jover, J. Dussart, E. Kolodziej, M. Monteil, E. Migianu-Griffoni, O. Gager, J. Deschamp, M. Lecouvey, *Chemistry* **2017**, *23*, 6654-6662.
- [85] M. Cortes-Clerget, O. Gager, M. Monteil, J. L. Pirat, E. Migianu-Griffoni, J. Deschamp, M. Lecouvey, *Adv. Synth. Catal.* **2016**, *358*, 34-40.
- [86] P. Renzi, J. Hioe, R. M. Gschwind, *Acc. Chem. Res.* **2017**.
- [87] D. Seebach, A. K. Beck, D. M. Badine, M. Limbach, A. Eschenmoser, A. M. Treasurywala, R. Hobi, W. Prikoszovich, B. Linder, *Helv. Chim. Acta* **2007**, *90*, 425-471.
- [88] B. List, P. Pojarliev, H. J. Martin, *Org. Lett.* **2001**, *3*, 2423-2425.
- [89] J. L. Vicario, D. Badia, L. Carrillo, E. Reyes, *Organocatalytic Enantioselective Conjugate Addition Reactions A Powerful Tool for the Stereocontrolled Synthesis of Complex Molecules Introduction*, The Royal Society of Chemistry, Cambridge UK, **2010**.
- [90] R. Ballini, G. Bosica, S. Gabrielli, A. Palmieri, *Tetrahedron* **2009**, *65*, 2916-2920.
- [91] Y. Meah, V. Massey, *Proc Natl Acad Sci U S A* **2000**, *97*, 10733-10738.
- [92] T. Kanekiyo, Y. Tamura, S. Tanaka, K. Naruchi, K. Yamada, *Kogakubu Kenkyu Hokoku (Chiba Daigaku)* **1980**, *31*, 307-312.
- [94] A. Zschunke, T. Heyer, R. Szargan, *J. Prakt. Chem.* **1986**, *328*, 656-660.
- [96] M. Hesse, H. Meier, B. Zeeh, *Spektroskopische Methoden in der organischen Chemie*, 7. ed., Thieme, Stuttgart, **2005**.
- [97] A. C. Colgan, H. Müller-Bunz, E. M. McGarrigle, *J. Org. Chem.* **2016**, *81*, 11394-11396.
- [98] B. List, I. Coric, O. O. Grygorenko, P. S. J. Kaib, I. Komarov, A. Lee, M. Leutzsch, S. Chandra Pan, A. V. Tymtsunik, M. van Gemmeren, *Angew. Chem. Int. Ed.* **2014**, *53*, 282-285.
- [99] J. E. Hein, A. Armstrong, D. G. Blackmond, *Org. Lett.* **2011**, *13*, 4300-4303.
- [100] Q. Ma, L. Gong, E. Meggers, *Org. Chem. Front.* **2016**, *3*, 1319-1325.
- [101] A. Palmieri, S. Gabrielli, M. Parlapiano, R. Ballini, *Rsc. Adv.* **2015**, *5*, 4210-4213.
- [102] L. N. Gautam, Q. Wang, N. G. Akhmedov, J. L. Petersen, X. Shi, *Org. Biomol. Chem.* **2013**, *11*, 1917-1920.
- [103] R. Kastl, H. Wennemers, *Angew. Chem. Int. Ed.* **2013**, *52*, 7228-7232.
- [104] H. Wennemers, *Chem. Commun.* **2011**, *47*, 12036-12041.
- [105] D. G. Blackmond, *J. Am. Chem. Soc.* **2015**, *137*, 10852-10866.
- [107] R. P. Bell, *Proceedings of the Royal Society of London. Series A - Mathematical and Physical Sciences* **1936**, *154*, 414-429.
- [108] M. G. Evans, M. Polanyi, *T Faraday Soc* **1938**, *34*, 0011-0023.
- [109] H. Iwamura, D. H. Wells, S. P. Mathew, M. Klussmann, A. Armstrong, D. G. Blackmond, *J. Am. Chem. Soc.* **2004**, *126*, 16312-16313.
- [110] S. L. Poe, A. R. Bogdan, B. P. Mason, J. L. Steinbacher, S. M. Opalka, D. T. McQuade, *J. Org. Chem.* **2009**, *74*, 1574-1580.
- [111] F. Giacalone, M. Gruttadauria, P. Agrigento, R. Noto, *Chem. Soc. Rev.* **2012**, *41*, 2406-2447.
- [112] S. Y. Park, J. W. Lee, C. E. Song, *Nat Commun* **2015**, *6*.

- [113] L. Ratjen, M. van Gemmeren, F. Pesciaioli, B. List, *Angew. Chem. Int. Ed.* **2014**, *53*, 8765-8769.
- [114] M. P. Lalonde, Y. G. Chen, E. N. Jacobsen, *Angew. Chem. Int. Ed.* **2006**, *45*, 6366-6370.
- [115] M. Molteni, R. Consonni, T. Giovenzana, L. Malpezzi, M. Zanda, *J. Fluor. Chem.* **2006**, *127*, 901-908.
- [116] C. Yue, J. Royer, H. P. Husson, *J. Org. Chem.* **1990**, *55*, 1140-1141.
- [117] J. C. Braekman, D. Dalozze, J. M. Pasteels, P. Vanhecke, J. P. Declercq, V. Sinnwell, W. Francke, *Z. Naturforsch.* **1987**, *42*, 627-630.
- [118] C. Devijver, J. C. Braekman, D. Dalozze, J. M. Pasteels, *Chem. Commun.* **1997**, 661-662.
- [119] A. Rouchaud, J.-C. Braekman, *Eur. J. Org. Chem.* **2009**, 2009, 2666-2674.
- [120] W. R. Kem, K. Wildeboer, S. LeFrancois, M. a. Raja, W. Marszalec, J.-C. Braekman, *Cell. Mol. Neurobiol.* **2004**, *24*, 535-551.
- [121] E. Cosimi, O. D. Engl, J. Saadi, M.-O. Ebert, H. Wennemers, *Angew. Chem. Int. Ed.* **2016**, *55*, 13127-13131.
- [122] O. D. Engl, S. P. Fritz, H. Wennemers, *Angew. Chem. Int. Ed.* **2015**, *54*, 8193-8197.
- [123] A. Bahlinger, S. P. Fritz, H. Wennemers, *Angew. Chem. Int. Ed.* **2014**, *53*, 8779-8783.
- [124] B. Han, Y.-C. Xiao, Z.-Q. He, Y.-C. Chen, *Org. Lett.* **2009**, *11*, 4660-4663.
- [125] T. W. Greene, P. G. M. Wuts, *Protective groups in organic synthesis*, Third ed., Wiley, New York, **1999**.
- [126] G. Gros, L. Martinez, A. S. Gimenez, P. Adler, P. Maurin, R. Wolkowicz, P. Falson, J. Hasserodt, *Bioorg. Med. Chem.* **2013**, *21*, 5407-5413.
- [127] A. Kolarovic, A. Käslin, H. Wennemers, *Org. Lett.* **2014**, *16*, 4236-4239.
- [128] N. A. McGrath, R. T. Raines, *Acc. Chem. Res.* **2011**, *44*, 752-761.
- [129] R. Oost, A. Misale, N. Maulide, *Angew. Chem. Int. Ed.* **2016**, *55*, 4587-4590.
- [130] H. Prokopcová, C. O. Kappe, *Angew. Chem. Int. Ed.* **2009**, *48*, 2276-2286.
- [131] B. W. Fausett, L. S. Liebeskind, *J. Org. Chem.* **2005**, *70*, 4851-4853.
- [132] R. Wittenberg, J. Srogl, M. Egi, L. S. Liebeskind, *Org. Lett.* **2003**, *5*, 3033-3035.
- [133] J. Lubkoll, H. Wennemers, *Angew. Chem. Int. Ed.* **2007**, *46*, 6841-6844.
- [134] A. Ricci, D. Pettersen, L. Bernardi, F. Fini, M. Fochi, R. P. Herrera, V. Sgarzani, *Adv. Synth. Catal.* **2007**, *349*, 1037-1040.
- [135] N. Hara, S. Nakamura, M. Sano, R. Tamura, Y. Funahashi, N. Shibata, *Chem. Eur. J.* **2012**, *18*, 9276-9280.
- [136] H. Y. Bae, J. H. Sim, J.-W. Lee, B. List, C. E. Song, *Angew. Chem. Int. Ed.* **2013**, *52*, 12143-12147.
- [137] F. Zhong, C. Jiang, W. Yao, L.-W. Xu, Y. Lu, *Tetrahedron Lett.* **2013**, *54*, 4333-4336.
- [138] J. Saadi, H. Wennemers, *Nat. Chem.* **2016**, *8*, 276-280.
- [139] O. D. Engl, S. P. Fritz, H. Wennemers, *Angew. Chem. Int. Ed.* **2015**, *54*, 8193-8197.

- [140] O. D. Engl, S. P. Fritz, A. Käslin, H. Wennemers, *Org. Lett.* **2014**, *16*, 5454-5457.
- [141] M. C. Walker, M. C. Y. Chang, *Chem. Soc. Rev.* **2014**, *43*, 6527-6536.
- [142] D. M. H. Kern, *J. Am. Chem. Soc.* **1954**, *76*, 1455-1455.
- [143] Y. Yasohara, J. Hasegawa, *Biosci., Biotechnol, Biochem.* **2001**, *65*, 1258-1260.
- [144] S. Mukherjee, E. J. Corey, *Org. Lett.* **2010**, *12*, 1024-1027.
- [145] N. Subasinghe, M. Schulte, M. Y. M. Chan, R. J. Roon, J. F. Koerner, R. L. Johnson, *J. Med. Chem.* **1990**, *33*, 2734-2744.
- [146] M. Molteni, M. C. Bellucci, S. Bigotti, S. Mazzini, A. Volonterio, M. Zanda, *Org. Biomol. Chem.* **2009**, *7*, 2286-2296.
- [147] O. Klenz, R. Evers, R. Miethchen, M. Michalik, *J. Fluor. Chem.* **1997**, *81*, 205-210.
- [148] S. Iwata, Y. Ishiguro, M. Utsugi, K. Mitsuhashi, K. Tanaka, *Bull. Chem. Soc. Jpn.* **1993**, *66*, 2432-2435.
- [149] A. Bhattacharjya, R. Mukhopadhyay, S. C. Pakrashi, *Synthesis* **1985**, 886-887.

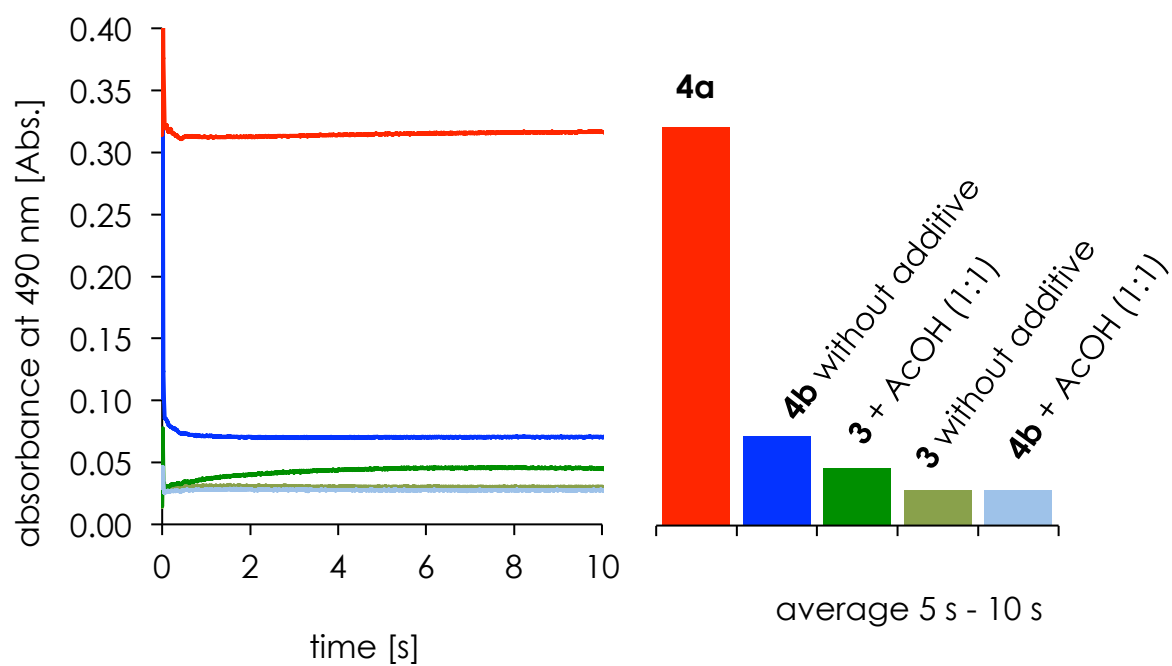
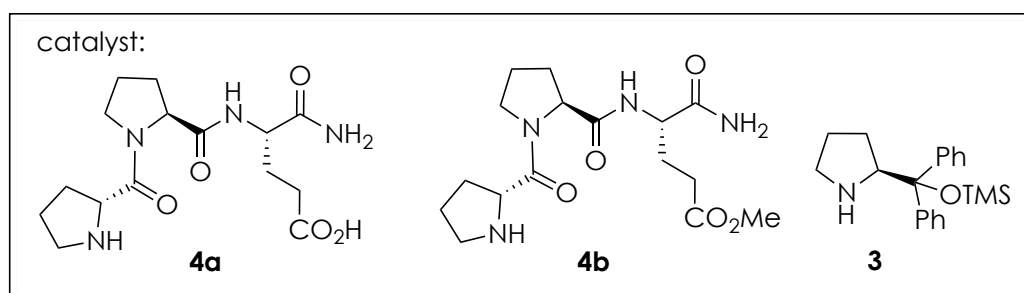
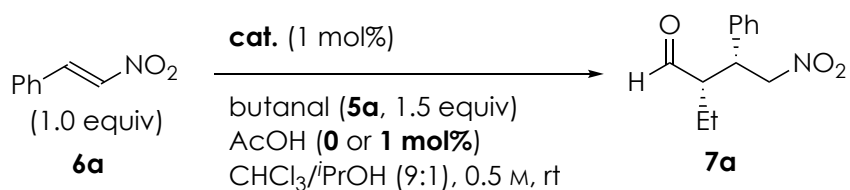
9

Appendix

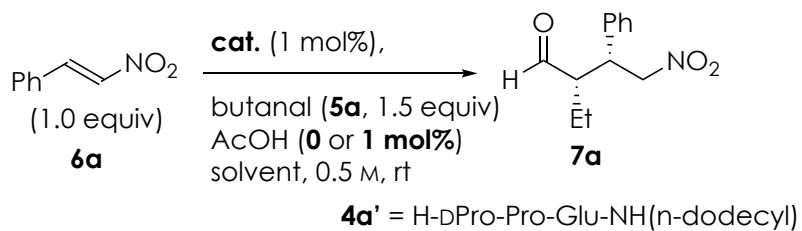
9.1 Additional Experiments

9.1.1 Stopped-Flow Experiments Using Acetic Acid

For a detailed experimental procedure see chapter 9.1.1.

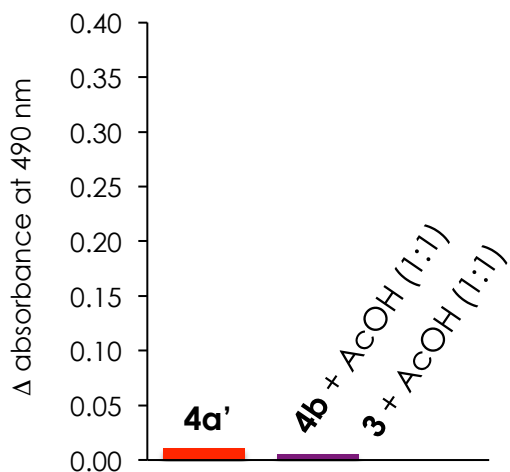
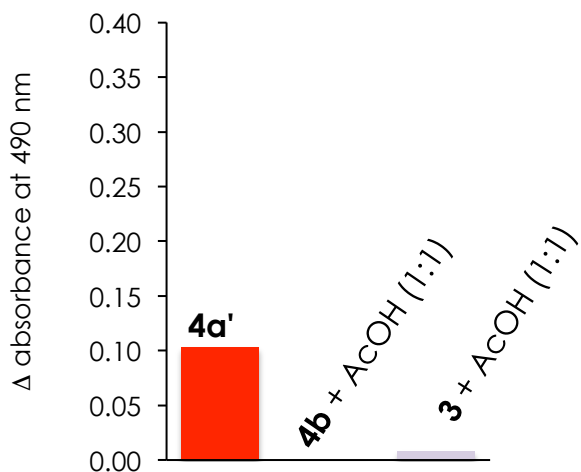
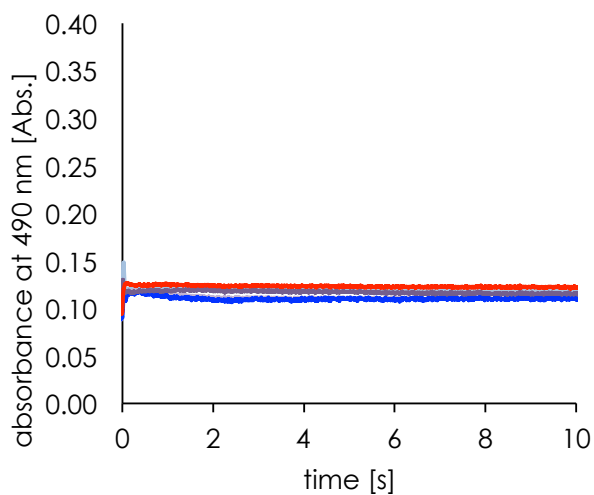
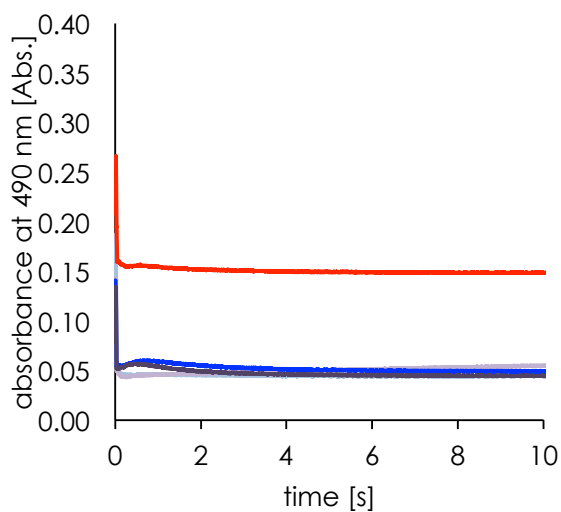


9.1.2



acetonitrile

dichloromethane



9.1.3 Time Dependent Adduct Preformation

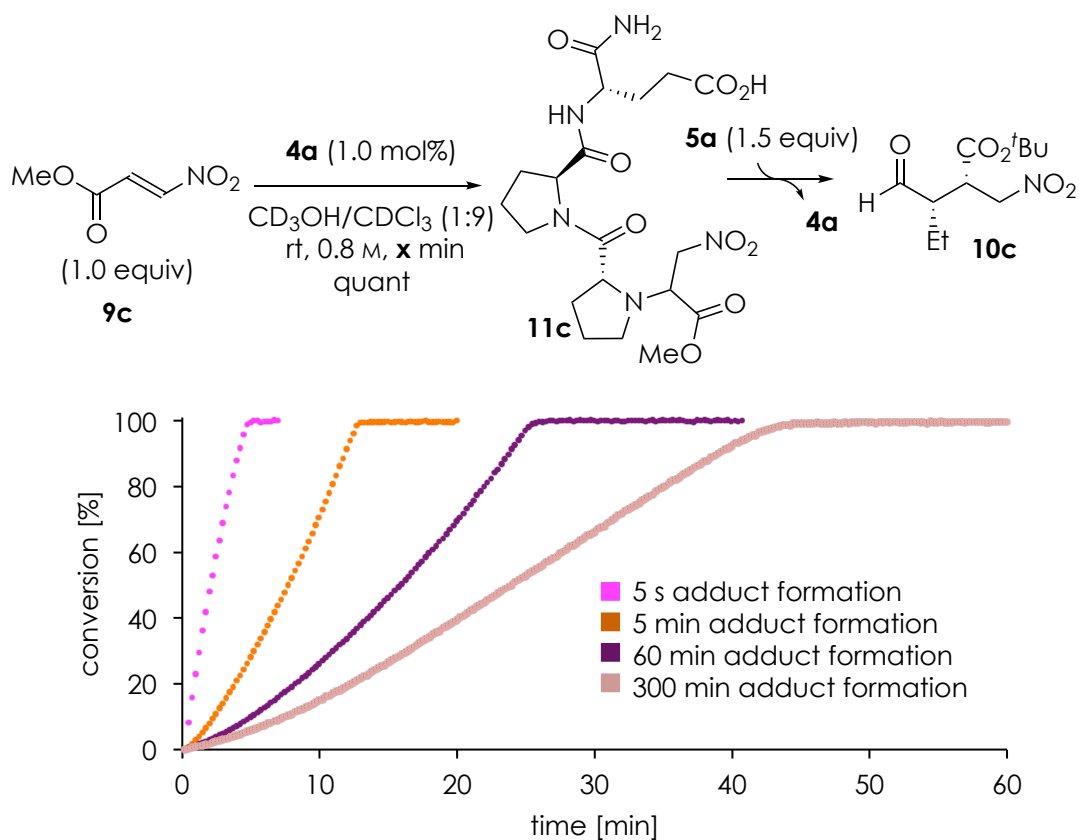


Figure 9-1: Effect by prolonged pre-adduct formation. Product formation was monitored by *in situ* IR spectroscopy at 1563 cm⁻¹. The reaching of full conversion was confirmed by ¹H-NMR spectroscopy.

9.1.4 Time Dependent Enamine Formation

9.1.4.1 Increased Aldehyde Concentration

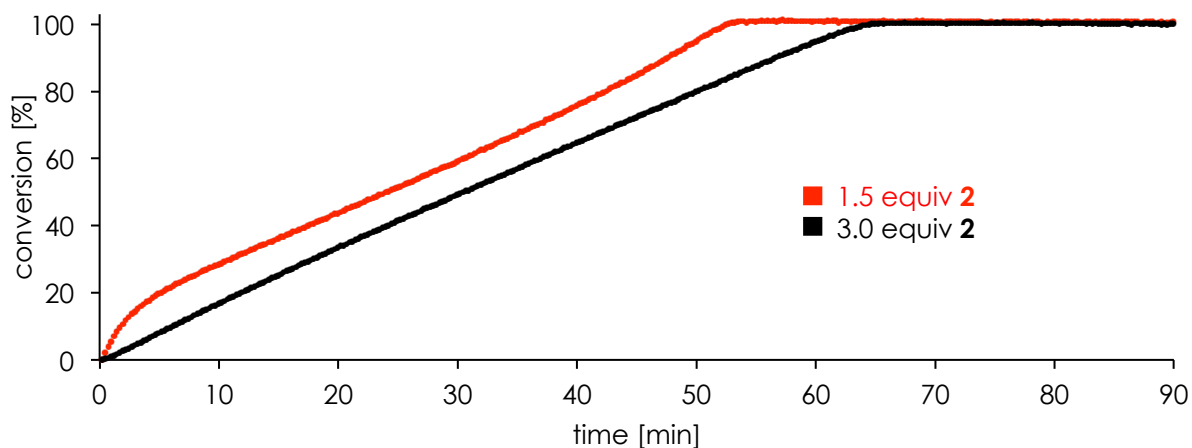
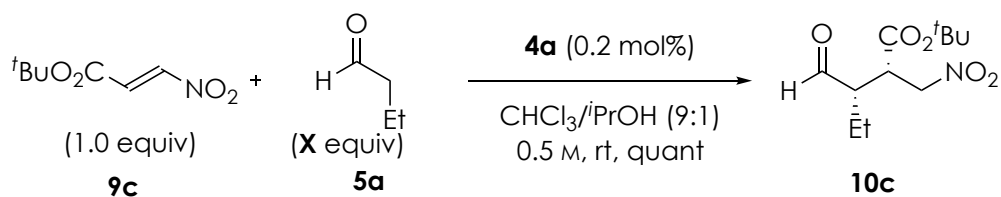


Figure 9-2: Effects of aldehyde concentration. Product formation was monitored by *in situ* IR spectroscopy at 1563 cm^{-1} . The conversion was determined by $^1\text{H-NMR}$ spectroscopy.

9.1.4.2 Aldol Addition Product Additive for Nitrostyrene

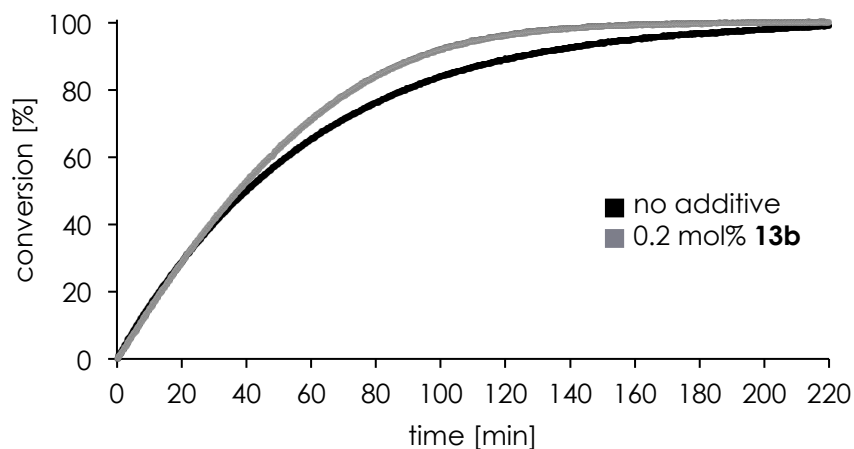
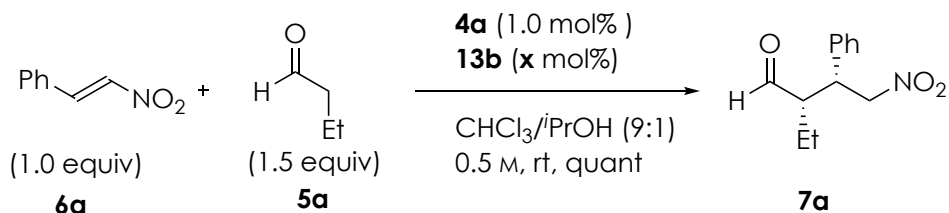


Figure 9-3: Effect of aldol addition product additive. Product formation was monitored by *in situ* IR spectroscopy at 1563 cm^{-1} . The conversion was determined by $^1\text{H-NMR}$.

9.1.4.3 Aldol Addition Additive in Conjugate Additions to CF₃-Nitroolefins

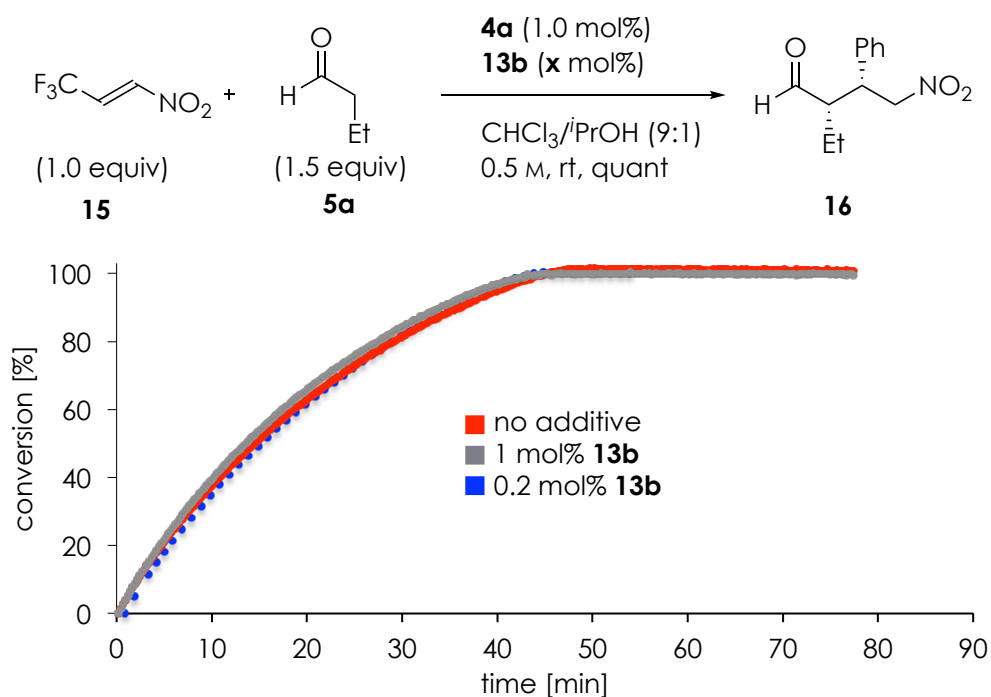
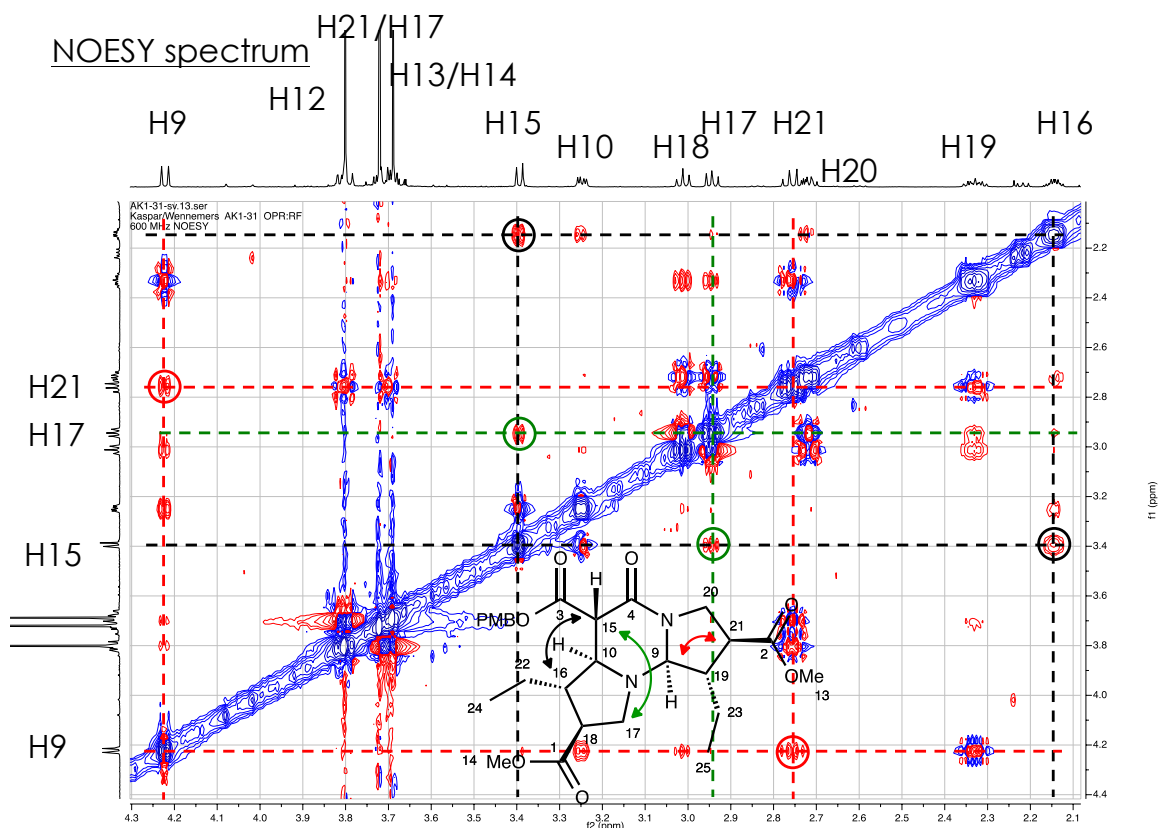
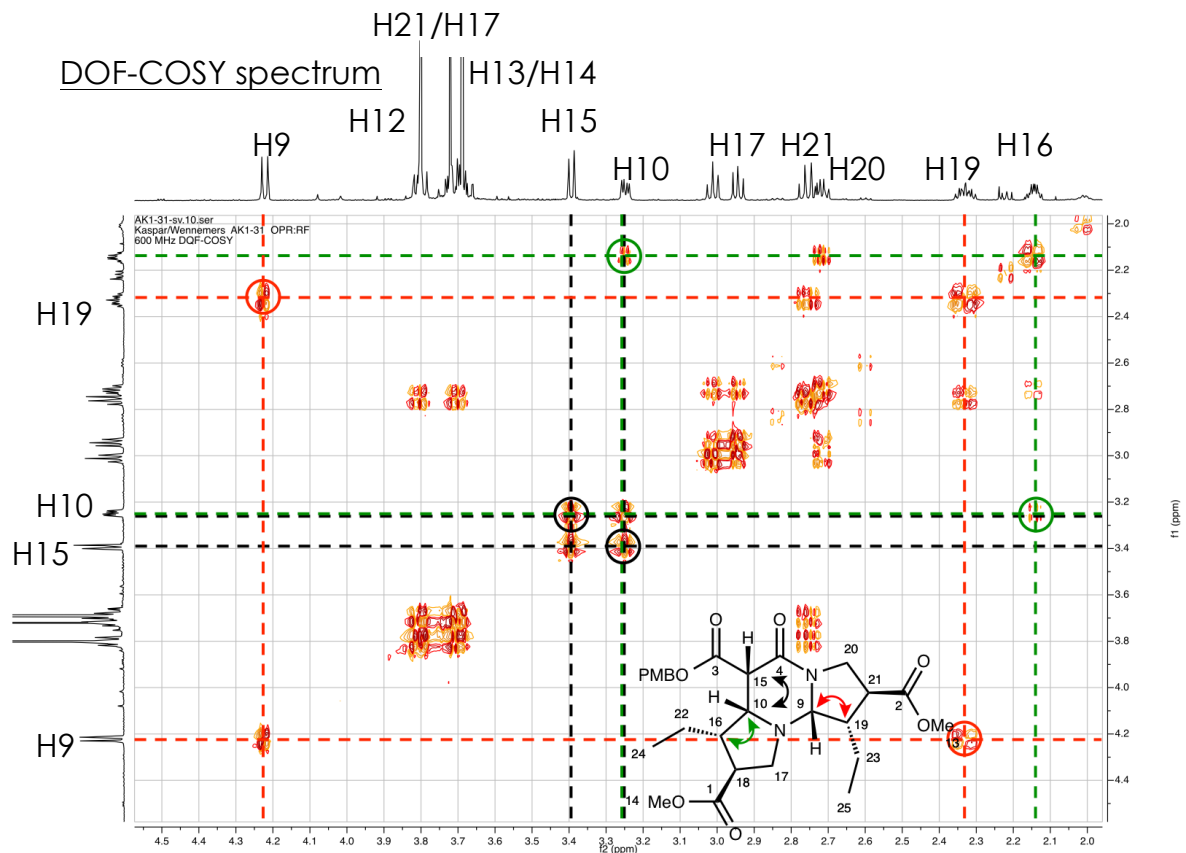
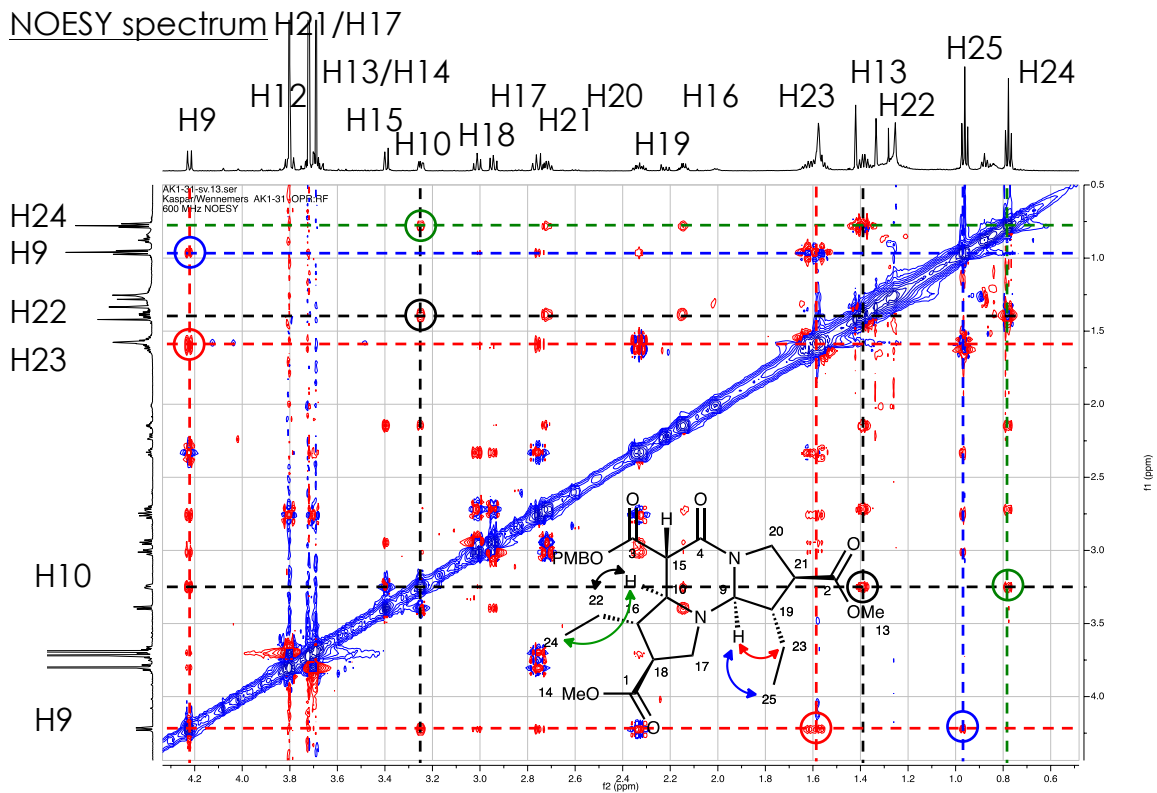
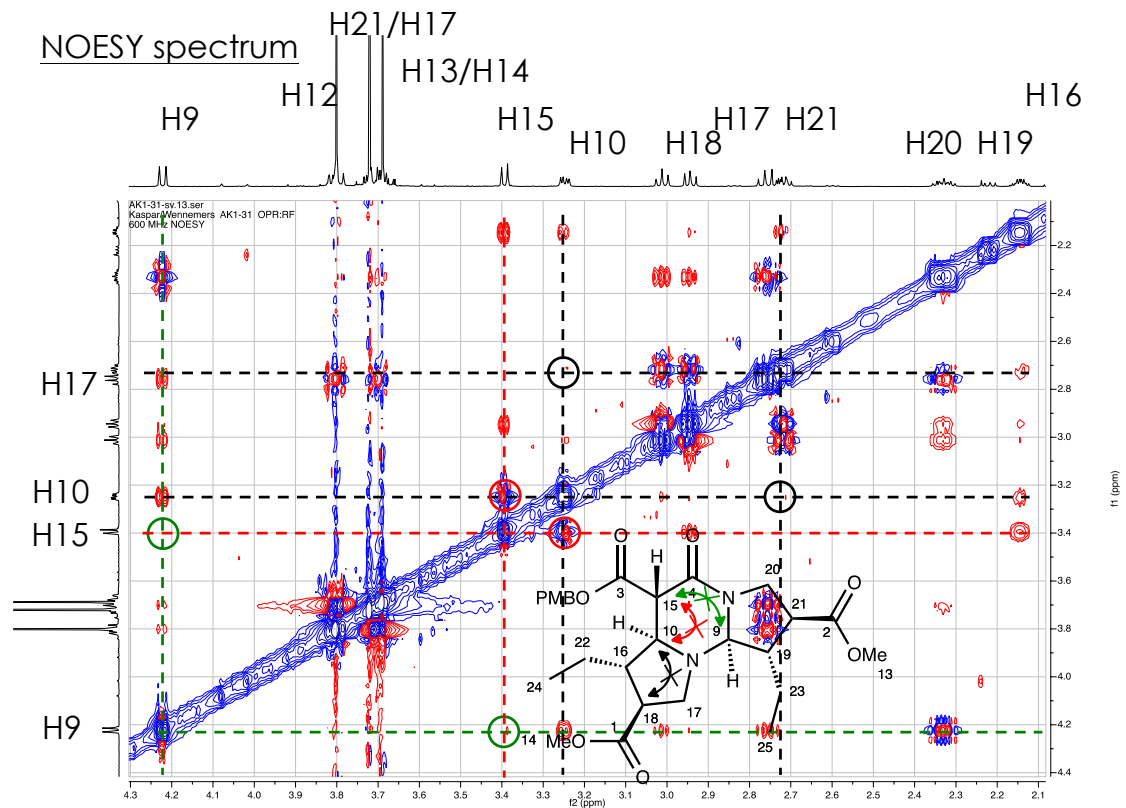
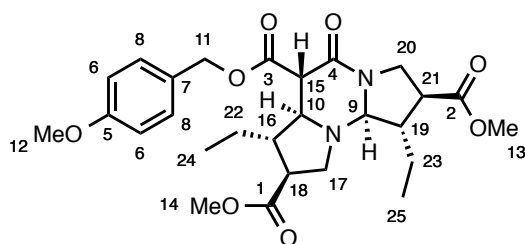


Figure 9-4: Effect of adol addition product additon. Product formation was monitored by *in situ* IR spectroscopy at 1563 cm⁻¹. The reaching of full conversion was confirmed by ¹H-NMR spectroscopy.

9.1.5 Stereochemistry Determination of Tetraponerines by NMR Spectroscopy







¹H-NMR (400 MHz, CDCl₃) δ: 7.34-7.28 (m, 2 H, H₆), 6.90 - 6.84 (m, 2 H, H₈), 5.14 (s, 2 H, H₁₁), 4.22 (d, *J* = 9.5 Hz, 1 H, H₉), 3.80 (s, 3 H, H₁₂), 3.84-3.66 (m, 2 H, H₂₁/H₁₇), 3.72 (s, 3 H, H₁₃/H₁₄), 3.69 (s, 3 H, H₁₃/H₁₄), 3.40 (d, *J* = 8.5 Hz, 1 H, H₁₅), 3.25 (dd, *J* = 8.6, 3.7 Hz, 1 H, H₁₀), 3.01 (t, *J* = 8.7 Hz, 1 H, H₁₈), 2.97-2.92 (m, 1 H, H₁₇), 2.76 (dt, *J* = 10.6, 9.2 Hz, 1 H, H₂₁), 2.72 (td, *J* = 8.0, 5.7 Hz, 1 H, H₂₀), 2.33 (tt, *J* = 9.6, 6.2 Hz, 1 H, H₁₉), 2.21 (m, 1 H, H₁₆), 2.15 (tdd, *J* = 7.1, 5.6, 3.7 Hz, 1 H, H₁₅), 1.68-1.51 (m, 2 H, H₂₃), 1.45-1.33 (m, 2 H, H₂₂), 0.96 (t, *J* = 7.5 Hz, 3 H, H₂₅), 0.78 (t, *J* = 7.4 Hz, 3 H, H₂₄).

¹³C-NMR (101 MHz, CDCl₃) δ: 174.22 (C₂), 173.23 (C₂), 170.06 (C₃), 163.12 (C₄), 159.85 (C₅), 130.44 (C₆), 127.83 (C₇), 114.04 (C₈), 78.31 (C₉), 67.59 (C₁₀), 67.24 (C₁₁), 55.44 (C₁₂), 52.47 (C₁₃), 52.39 (C₁₄), 52.28 (C₁₅), 50.11 (C₁₆), 48.10 (C₁₇), 47.95 (C₁₈), 47.22 (C₁₉), 46.96 (C₂₀), 45.02 (C₂₁), 27.54 (C₂₂), 23.76 (C₂₃), 11.90 (C₂₄), 10.88 (C₂₅).

9.2 Curriculum Vitae

Name: Patrick Hilpert
Date of birth: July 14th, 1988
Nationality : Swiss
Place of origin: Winterthur (ZH)
Adress: Arianestrasse 11,
CH-8052 Zürich, Switzerland
Email: patrick.hilpert@org.chem.ethz.ch

Education

PhD Student with Prof. Dr. Helma Wennemers at ETH Zürich, since 06/2013
Switzerland

Master and Bachelor of Science in Chemistry, University of Basel, Switzerland 09/2008-01/2013

Master thesis with Prof. Dr. Karl Gademann
"TiO₂ supported recyclable organocatalysts using nitrocatechol linkers"

Matura with major in Biology and Chemistry, Gymnasium Oberwil, Switzerland 08/2003-12/2007

Compulsory Education, Hofstetten and Bättwil, Switzerland 08/1995-07/2003

Teaching experience

Practical laboratory course for chemistry and chemical engineers students (spring semester 2014)

Practical laboratory course for pharmaceutical and interdisciplinary sciences students (autumn semester 2014)

Assistant for organic chemistry 1 class from Prof. Dr. Helma Wennemers (autumn semester 2015)

Other activities

Member of the Simon-Behringer committee (2015-2016)

